Analytical Framework for the Performance Analysis of Multiple Antenna Systems

Kyung Kyoon Bae

Dissertation submitted to the Faculty of the Virginia Polytechnic Institute and State University in partial fulfilment of the requirements for the degree of

Doctor of Philosophy
in
Electrical and Computer Engineering

Committee:

Dr. William H. Tranter (Co-Chair)
Dr. Annamalai Annamalai (Co-Chair)
Dr. Jeffrey H. Reed
Dr. Gail F. Gray
Dr. Werner E. Kohler

September, 2005

Blacksburg, Virginia

Keywords: Adaptive Array Processing, Diversity, Null Steering, Capacity

Analytical Framework for the Performance Analysis of Multiple Antenna Systems

Kyung Kyoon Bae

(ABSTRACT)

There has been great interest in antenna array processing (diversity, beamforming, null steering, and spatial multiplexing) to enhance the received signal quality and the capacity of wireless communications systems. However, in order to properly exploit the characteristics of different array processing techniques, understanding trade-offs among different techniques and parametric investigation, which offers an insight as to what parameters determine system performance under different situations is necessary. In this study, we present analytical framework which can facilitate the performance analysis of systems with antenna array.

Five original contributions to the performance analysis of antenna array processing are presented in this study. First, we present theoretical outage probability of a system equipped with an array which suppresses a few dominant interfering signals in TDMA cellular networks when the fading statistics of interfering signals are independent but non-identically distributed. Most of the related previous works assumed either independent and identically distributed fading statistics among cochannel interferences (CCI) or Rayleigh fading when CCI signals are subject to i.n.d. fading statistics. Secondly, the performance of multi-branch predetection equal gain combiner for different modulation techniques in equally correlated Nakagami-m fading is presented through analytical analysis. Specifically, the characteristic function (CHF) and the moment generating function (MGF) of EGC output with $L \geq 3$ correlated inputs are derived and used to evaluate the average symbol error probability (ASEP) and the outage probability performance, respectively. Thirdly, we derived analytical expression which can be used to analyze the performance of different types of diversity techniques in equally correlated Nakagami-m or Rice fading channels. Fourthly, asymptotic analysis on different types of diversity combiners in generalized fading channels is presented in a unifying

way. Finally, we investigate and present the impact of transmit diversity at handsets on the reverse link DS/CDMA systems in terms of capacity and coverage over generalized fading channels through analytical approaches. Then, we validate the analytical results with simulation results and investigate practical issues which are hard to capture through analytical analysis using system level simulator we developed.

Although we have mainly focused on applying the analytical framework we have derived in this work to the performance analysis of physical layer algorithms such as spatial diversity and adaptive null steering, the framework can be extended to assist the analysis and design of wireless communication systems such as, to name a few, distributed multiple input multiple output (MIMO) system in cooperative wireless networks, multipath routing protocol analysis in wireless fading channels, and antenna selection problems in MIMO system.

Dedication

This dissertation is dedicated with love to my heavenly Father, God, my parents, my parents-in-law, my lovely wife, and my two sons.

Acknowledgements

First of all, I would like to give gratitude and praise to my heavenly Father, God, my Savior, Jesus Christ, and my comforter, Holy Spirit for the grace and the love throughout my life. Without God's grace, I could not have come this far. My Lord is the source of my life!

I thank my advisor Dr. William Tranter for his guidance and support to pursue research topics I am interested in. I have greatly benefited from his wisdom and technical insights. Also, my sincere appreciation goes to my co-advisor Dr. A. Annamalai. His technical knowledge, excellent advice, and encouragement have provided me an invaluable experience and allowed me to develop my research capabilities and writing skill. I thank him for being a mentor and a teacher.

I have been honored to have Dr. Jeffrey Reed, Dr. Gail Gray, and Dr. Werner Kohler as my Ph.D. committee. I have learned a lot from Dr. Reed for his leadership and vision. He kindly spared his precious time for students, providing advice and directions not only on academic issues but also on personal matters. I thank Dr. Gray for his kind proof-reading and suggestions on my dissertation. I also thank Dr. Kohler for his support and being on my Ph.D. committee.

My special thanks go to Jong-Han Kim who worked with me on the research topics covered in chapter 7 in this dissertation. Without his excellent programming skill and expertise on DS/CDMA, it would have been hard to imagine to accomplish the work in a relatively short time frame. I am also thankful for the friendship of some members in MPRG: Hae-Soo Kim,

Sudhanshu Gaur, Dr. Jing Jiang, Kyu-Woong Kim, Kye-Hoon Lee, and Jae-Sang Lee. I also acknowledge fellow Korean students at ECE department for their friendship.

I would like to give my special thanks to my pastor, Hyun David Chung, and his family for their prayer and fellowship in God. Thank my sincere brothers and their families of Korean Baptist Church of Blacksburg (KBCB). Especially, I would like to recognize: Dr. Seong-Youp Suh, Dr. Hyung-Seok Oh, Dr. Chang-Hyun Jang, Jin Huh, Kang-Wook Lee, and Dr. Heung-Gweon Shin. My family and I have spent valuable times with them in love and joy.

God has given me special privilege to serve young undergraduate students with His words and love during my studies as a Ph.D. student. I thank all the brothers and sisters in Korea Campus Crusade for Christ (KCCC) at KBCB for their devoted services and fellowship. Dr. Jong-Nam Lee, Jung-Hoon Choi, and Dr. Hwa-Jung Lee, who are my fellow workers at KCCC, have enriched my life in Jesus Christ, our Lord. I would never forget the valuable times and memories we have had together. We have prayed together, and we together have served young souls our Lord loves.

I can't imagine I can be here without my parents' support. I really thank them for their love, care and sacrifices they have made for their children. Their endless and unconditional love has been my biggest support throughout my life. I also thank my parents-in-law for their love, pray, and support. I can't forget my brother, sister-in-law, and brother-in-law for their love and encouragement. I am deeply grateful to my wife, Hee-Jung Kim, who God, my heavenly Father, allowed me to marry. Without her love, pray, patience, and support, I would not have been able to finish my Ph.D. works and spend time in sharing God's words with my beloved KCCC brothers and sisters. Finally, my special thanks go to my two sons, Jae-Sung and Jaehyung, for giving me such a joy during the tough times as a Ph.D. student. Hee-Jung, Jae-Sung, and Jaehyung, I really love you!

Contents

List of Figures

List of Tables

Chapter 1

Introduction

The application of antenna arrays to wireless communications systems has drawn a lot of interests and research efforts since antenna arrays offer improved received signal-to-noise ratio (SNR), which translates to system capacity increase, by suppressing interfering signals or providing diversity mechanisms, and increased data rate through spatial multiplexing. Smart antenna system (which uses antenna array) operations include diversity, beamforming, and null steering where diversity techniques exploit multiple replicas of a signal which might go through different propagation paths, hence fading incoherently, beamforming forms a beam by shaping the antenna radiation pattern toward the desired user in such a way that most of energy is radiated toward or received from the desired user with antenna aperture gain, and null steering shapes the antenna gain pattern by placing deep nulls toward interfering signals while maintaining the power of the desired user at an acceptable level. The distinction between diversity and beamforming/nulling depends on the inter-element spacing of the antenna array. In diversity mode, the spacing must be large enough (within practical limits) to yield uncorrelated signals at the antenna branches, while in beamforming mode, there is an upper limit on the inter-element spacing to restrict generation of grating lobes and to exploit the angle of arrival/departure information to form a beam/nulls. Also, there are performance differences of these techniques under different conditions. Hence, it would

be highly desirable to be able to assess the efficacy of different antenna array structures and to understand the tradeoffs among different techniques so as to help design process in choosing appropriate system structure. However, usually we have to rely on simulations to study system performances, design trade-offs, and system optimization, which can be quite complex and a time-consuming task. Also, even after extensive simulations, it is not easy to get insights as to what parameters determine system performance in different system parameters and fading channels, and the interactions on system parameters. This motivates the efforts to obtain an analytical framework which can provide insights on system behavior and enable parametric investigations in a unifying way. We would like to emphasize, however, that simulation and analytical analysis should compensate and assist each other in achieving the common goal - better understanding of wireless communication system behaviors and optimizing system designs. With this motivation, this work presents an analytical framework to evaluate the performance of a system equipped with an antenna array and provides analyses through analytical solutions and simulations.

1.1 Organization of Dissertation

Chapter 2 includes original derivation of the moment generating function (MGF) of the sum of the N "weakest" interfering signals out of N_I active interfering signals when cochannel interferences (CCI) have independent but non-identically distributed (i.n.d.) fading statistics. Theoretical performance (outage probability, spectral efficiency, and cochannel reuse factor) of a system equipped with an array which suppresses a few dominant interfering signals in TDMA cellular networks is presented using the derived MGF when the i.n.d. fading statistics of interfering signals are subject to Rayleigh, Rice, Nakagami-m, or mixed of those fading distributions.

Chapter 3 presents theoretical performance analysis of multi-branch predetection equal gain combiner (EGC) in equally correlated Nakagami-m fading channels with arbitrary real

values of $m(\geq 0.5)$. The moment generating function (MGF) and the characteristic function (CHF) of EGC output with L correlated inputs are originally derived and used to calculate the average symbol error probability (ASEP) and the outage probability. The mathematical framework presented for the calculation of ASEP utilizing the derived CHF can be used for any digital modulation schemes. Saddle point integration and numerical inversion of Laplace transform of the derived MGF are applied to calculating the outage probability and shown to match each other.

Chapter 4 extends the previous work for an normalized threshold generalized selection combining (NTGSC(μ,L)) scheme by allowing arbitrary real values of m (where $m \geq 0.5$) in the analytical solution. Note that this extension can also be applied to the analysis of generalized selection combining (GSC(N,L)) scheme in equally correlated Nakagami-m fading channels. Also, we exploit the novel transformation of a set of equally correlated complex Gaussian random variables (RVs) into a set of conditionally independent complex Gaussian RVs to tackle the problem from another approach. This second approach allows us to analyze the performance of the NTGSC(μ,L) receiver more efficiently when m is a positive integer value and the diversity order L is large.

Chapter 5 presents analytical analysis which can help understand the effect of branch correlation on different types of diversity combiners such as GSC(N,L), absolute threshold generalized selection combining (ATGSC), and modified absolute threshold generalized selection combining (MATGSC) schemes over equally correlated Rice fading channels. Specifically, we exploit the novel transformation of a set of equally correlated complex Gaussian random variables (RVs) into a set of conditionally independent complex Gaussian RVs to derive the MGF of the combiner output over equally correlated Rice fading channels.

Chapter 6 introduces asymptotic analysis of digital communication systems with diversity technique. The asymptotic analysis offers insights as to what parameter determines system performance with different diversity order and modulation formats in different fading channels in a unifying way. In this chapter, we extend the previous work which deals

with GSC(N,L) to not only GSC(N,L) but also NTGSC(μ,L) and GSEGC(N,L) (which includes EGC as a special case) in a concise, unifying way to facilitate parametric investigation and optimizing system design. Especially, since the analytical solution to GSEGC(N,L) has not been reported in open literature, it is very useful to analytically predict the performance of GSEGC(N,L) receiver in generalized fading channels and do comparison study with GSC(N,L).

Chapter 7 introduces investigation of the impact of transmit diversity techniques on the reverse link DS/CDMA system. The presented analysis incorporates transmit diversity at handsets in conjunction with receive diversity, power control, and soft handoff to assess the impact of transmit diversity on system capacity and coverage of the reverse link DS/CDMA system. The general mathematical framework developed in this chapter enables us to investigate the impact of transmit diversity (open loop and closed loop transmit diversity) on the reverse link DS/CDMA system taking into account the effect of different fading statistics such as Rayleigh, Rice, and Nakagami-m, the effect of correlation between antenna branches, power control, soft handoff, and different user distribution throughout multi-tier cells. Also, to validate the analytical results and investigate some practical issues which couldn't be captured through analytical results, we developed cdma2000 system level simulator. Some system level simulation results will be provided along with a brief description of simulation procedure.

Finally, chapter 8 contains a summary of this work.

1.2 Contributions

To date, the original contributions of this work include:

1. The derivation of the MGF of a sum of the N weakest CCI signals over generalized fading channels including Rayleigh, Nakagami-q, Nakagami-m, and Rice fading channels

when the fading statistics of interfering signals are independent and non-identically distributed and theoretical performance analysis of an array system which suppresses a few dominant interfering signals in TDMA systems, which serves as a performance bound of an actual system in practical situations

2. The original derivation of the CHF (MGF) of the output of predetection equal gain combiner (EGC) with multi-branches ($L > 2$) over equally correlated Nakagami-m fading channels with real values of $m(\geq 0.5)$ and theoretical performance analysis (ASEP and outage probability) of predetection EGC through the use of CHF and MGF which have been derived originally in this work

3. The derivation of the MGF of NTGSC(μ,L) output in equally correlated Nakagami-m fading channel with real values of $m(\geq 0.5)$ and the derivation of NTGSC(μ,L) output MGF when m takes integer values by transforming a set of conditionally independent complex Gaussian RVs

4. Investigation of the performance of different types of diversity combiners (GSC(N,L), ATGSC, MATGSC) over equally correlated Rice fading channels

5. Asymptotic analysis of GSC(N,L), NTGSC(μ,L), and GSEGC(N,L) over generalized fading channels in a unifying way

6. Providing a general mathematical framework for analyzing the impact of diversity techniques associated with power control on system capacity and coverage in the reverse link DS/CDMA systems

7. Investigating the impact of open-loop transmit diversity (space-time block code) and closed-loop transmit diversity at the handset on system capacity and coverage over a general channel model, which includes various fading statistics such as Rayleigh, Nakagami-m and Rice with standard specified multipath power delay profile, in the reverse link DS/CDMA systems

8. Investigating the impact of correlation between diversity branches on the reverse link DS/CDMA system capacity and coverage

9. Building up cdma2000 system level simulator which can facilitate to investigate system level performance with transmit diversity technique at handset and the analysis with practical issues which are hard to capture through analytical solutions

Chapter 2

Adaptive Nulling

The detrimental effects of fading and cochannel interference can be mitigated through the use of diversity mechanisms and CCI (co-channel interference) suppression techniques. However, in an interference-limited environment, CCI suppression is much more effective than diversity methods [2], [3]. Space-time array processing (smart antennas) may enhance SIR (Signal to Interference Ratio) through adaptive beamforming or adaptive null steering. In the case of beamforming approach, a beam is formed by shaping the antenna radiation pattern towards the desired user in such a way that the energy received from the desired user is maximized, while steering nulls towards the CCI signals. On the other hand, in the null steering approach, the antenna gain pattern is shaped by placing deep nulls toward the CCI signals without significantly reducing the power of the desired user signal. In general, an adaptive array with D elements can only effectively suppress $(D-1)$ CCI signals. However, often times, in a practical operating environment, the number of CCI signals may exceed the number of elements in an adaptive array. If the number of antenna elements is less than the number CCI signals that impinge on the antenna array, linear array processing technique for suppressing CCI signals break down. In such an overloaded array scenario, partial cancellation of CCI signals via adaptive null steering can be very effective in enhancing SIR [4]-[9].

In this chapter, we study the theoretical outage probability performance of a cellu-

lar TDMA system employing an adaptive array to suppress the strongest $N_I - N (N = 1, 2, \ldots, N_I)$ out of N_I active interferers. The results presented in this chapter can be viewed as a lower bound on the outage probability of any cancellation scheme which cancels a few dominant co-channel interference signals. The assumptions 1) perfect cancellation and 2) perfect resolvability between desired user and a few strongest co-channel interferers make the results a lower bound. The key for our development is the derivation of the MGF of a sum of N remaining (uncancelled) CCI signals from a total of N_I active interfering signals, in which the CCI signals are subject to independent but non-identically distributed (i.n.d.) Rayleigh, Nakagami-m, Rice, or Nakagami-q fading statistics. Most of the previous studies [4]-[8] have assumed independent and identically distributed (i.i.d.) fading statistics among the CCI signals. The only literature which deals with i.n.d. for the CCI signals is [9], but the analysis is restricted to a Rayleigh fading channel.

Since different CCI signals may take completely different propagation paths before arriving at the receiver, it is more reasonable to assume that the signals have dissimilar fading statistics and signal strengths. In such situations, the efficacy of adaptive interference nulling scheme becomes even more pronounced compared to the i.i.d. case. Despite this, neither analysis nor simulation have been claimed to quantify the benefits of partial cancellation of ordered CCI signals over generalized fading channels.

This chapter is organized as follows. The MGF of a sum of the N "weakest" CCI signals, when interferences have i.n.d. fading statistics, is derived in Section 1. In Section 2, a framework for evaluating the outage probability using the MGF is outlined. Section 3 examines the effects of dominant interference cancellation on outage probability, frequency reuse factor, and spectral utilization efficiency. The main points are summarized in Section 4.

2.1 The MGF of The Sum of Uncancelled Weakest Interferers

Suppose the set $\{p_k\}_{k=1}^{N_I}$ denotes the N_I CCI signal powers with i.n.d. fading statistics. Then the order statistics $p_{k:N_I}$ is obtained by arranging the set $\{p_k\}_{k=1}^{N_I}$ in increasing order of magnitude. The joint pdf of order statistics $0 \leq p_{1:N_I} \leq p_{2:N_I} \leq \cdots \leq p_{N_I:N_I}$ can be expressed as [10]:

$$g_{p_{1:N_I},p_{2:N_I},\cdots,p_{N_I:N_I}}(x_1, x_2, \ldots, x_{N_I}) = \sum_{\sigma \in S_{N_I}} \prod_{i=1}^{N_I} g_{\sigma(i)}(x_i) \tag{2.1}$$

where $g_{\sigma(i)}(x)$ corresponds to the probability density function (PDF) of the $\sigma(i)^{th}$ CCI signal power, $\sigma = (\sigma(1), \sigma(2), \ldots, \sigma(N_I))$ denotes the function which permutes the integers $\{1, 2, \ldots, N_I\}$, and S_{N_I} is the set of all permutations of integers $\{1, 2, \ldots, N_I\}$. We can now define the total remaining interference power I after cancellation of $N_I - N$ dominant CCI signals as $I = \sum_{k=1}^{N} p_{k:N_I}$ where N is the number of uncancelled CCI signals, and its MGF as $\phi_I(s) = E[\exp(-s\sum_{k=1}^{N} p_{k:N_I})]$. Since the ordered CCI signal powers $p_{k:N_I}$ are not independent (although $\{p_k\}_{k=1}^{N}$ are independent), the MGF of a sum of uncancelled CCI signals (N weakest CCI signals) may be computed as

$$\begin{aligned} \phi_I(s) &= \sum_{\sigma \in S_N} \int_0^{\infty} \cdots \int_0^{\infty} e^{-s\sum_{i=1}^{N_I} x_i} \\ &\times \prod_{i=1}^{N_I} g_{\sigma(i)}(x_i) dx_{N_I} \cdots dx_1, \, 0 \leq x_1 \leq \cdots \leq x_{N_I} < \infty. \end{aligned} \tag{2.2}$$

(2.2) can be rewritten into two expressions, which involve a product of two separable nested integrals:

$$\begin{aligned} \phi_I(s) &= \sum_{\sigma \in S_{N_I}} \int_0^{\infty} e^{-sx_N} g_{\sigma(N)}(x_N) \\ &\times \Big[\int_0^{x_N} e^{-sx_{N-1}} g_{\sigma(N-1)}(x_{N-1}) \cdots \int_0^{x_2} e^{-sx_1} g_{\sigma(1)}(x_1) dx_1 \cdots dx_{N-1} \Big] \\ &\times \Big[\int_{x_N}^{\infty} g_{\sigma(N+1)}(x_{N+1}) \cdots \int_{x_{N_I-1}}^{\infty} g_{\sigma(N_I)}(x_{N_I}) dx_{N_I} \cdots dx_{N+1} \Big] dx_N \end{aligned} \tag{2.3}$$

$$\begin{aligned}\phi_I(s) &= \sum_{\sigma\in S_{N_I}}\int_0^\infty g_{\sigma(N+1)}(x_{N+1}) \\ &\times \Big[\int_0^{x_{N+1}} e^{-sx_N} g_{\sigma(N)}(x_N)\cdots\int_0^{x_2} e^{-sx_1} g_{\sigma(1)}(x_1)dx_1\cdot dx_N\Big] \\ &\times \Big[\int_{x_{N+1}}^\infty g_{\sigma(N+2)}(x_{N+2})\cdots\int_{x_{N_I-1}}^\infty g_{\sigma(N_I)}(x_{N_I})dx_{N_I}\cdots dx_{N+2}\Big]dx_{N+1} \end{aligned} \tag{2.4}$$

The above two expression, which involves a product of two separable nested integrals, can be simplified with the aid of the following two integral identities:

$$\begin{aligned}&\sum_{\sigma\in S_{N-1}}\int_{x_1}^\infty f_{\sigma(2)}(x_2)\cdots\int_{x_{N-1}}^\infty f_{\sigma(N)}(x_N)dx_N\cdots dx_2 \\ &= \prod_{k=1}^{N-1} F_{\sigma(N-k+1)}(x_1)\end{aligned} \tag{2.5}$$

$$\begin{aligned}&\sum_{\sigma\in S_N}\int_0^{x_{N+1}} f_{\sigma(N)}(x_N)\cdots\int_0^{x_2} f_{\sigma(1)}(x_1)dx_1\cdots dx_N \\ &= \prod_{k=1}^{N} H_{\sigma(k)}(x_{N+1})\end{aligned} \tag{2.6}$$

where $F_{\sigma(k)}(y)=\int_y^\infty f_{\sigma(k)}(x)dx$ and $H_{\sigma(k)}(y)=\int_0^y f_{\sigma(k)}(x)dx$. Using (2.5) and (2.6) in (2.3) and (2.4), the MGF of the sum of N weakest among N_I CCI signals can be given by

$$\begin{aligned}\phi_I(s) &= \sum_{\sigma\in T_{N_I^N}}\int_0^\infty e^{-sx} g_{\sigma(N)}(x)\Big[\prod_{k=1}^{N-1}\phi_{\sigma(k)}(s,x)\Big] \\ &\times \Big[\prod_{i=N+1}^{N_I} G_{\sigma(i)}(x)\Big]dx\end{aligned} \tag{2.7}$$

$$\begin{aligned}\phi_I(s) &= \sum_{\sigma\in T_{N_I^{N+1}}}\int_0^\infty g_{\sigma(N+1)}(x)\left[\prod_{k=1}^{N}\phi_{\sigma(k)}(s,x)\right] \\ &\times \left[\prod_{i=N+2}^{N_I} G_{\sigma(i)}(x)\right]dx\end{aligned} \tag{2.8}$$

where $G_{\sigma(i)}(x)$ denotes the complementary cumulative distribution function (CCDF) defined as $G_{\sigma(i)}(x)=\int_x^\infty g_{\sigma(i)}(t)dt$, $\phi_{\sigma(k)}(s,x)$ is the marginal MGF of $\phi_{\sigma(k)}(x)$ defined as

$\phi_{\sigma(k)}(s,x) = \int_0^x e^{-st} g_{\sigma(k)}(t)dt$, and $\sum_{\sigma \in T_{L,N}} = \sum_{\substack{\sigma \in S_{N_I}, \sigma(1)<\sigma(2)<\cdots<\sigma(N-1) \\ \sigma(N+1)<\cdots<\sigma(N_I)}}$. For the special case of i.i.d. interfering signal statistics, (2.7) reduces to

$$\begin{aligned} \phi_I(s) &= N\binom{N_I}{N} \int_0^\infty e^{-sx} g(x)[\phi(s,x)]^{N-1} \\ &\times [G(x)]^{N_I-N} dx \end{aligned} \tag{2.9}$$

which is identical to [6, Eq. (5)] and [7, Eq. (A2)]. Also, we can get a new expression for the MGF $\phi_I(s)$ from (2.8) when the statistics of CCI are i.i.d.:

$$\begin{aligned} \phi_I(s) &= (N_I - N)\binom{N_I}{N} \int_0^\infty g(x)[\phi(s,x)]^{N} \\ &\times [G(x)]^{N_I-N-1} dx \end{aligned} \tag{2.10}$$

Note that (2.7) through (2.10) involve the computation of a one-dimensional integral whose integrand is composed of tabulated functions (i.e., $G_{\sigma(i)}(x)$ and $\phi_{\sigma(i)}(s,x)$ can be expressed in closed forms for all common fading channel models). The computational complexities associated with (2.7) and (2.8) are $N\binom{N_I}{N}$ and $(N_I - N)\binom{N_I}{N}$ one-dimensional integrals, respectively, because the cardinality of set $T_{N_I,N}$ is equal to $N_I!/[(N_I - N)!(N-1)!]$ and the cardinality of $T_{N_I,N+1}$ is equal to $N_I!/[(N_I - N - 1)!N!]$. Hence, (2.7) is preferred when $1 \leq N \leq \lfloor (N_I/2) \rfloor$ where $\lfloor \cdot \rfloor$ denotes the floor function which gives the largest integer value less than or equal to its argument. On the other hand, (2.8) is computationally more efficient when $\lceil (N_I/2) \rceil \leq N < N_I$ where $\lceil \cdot \rceil$ represents the ceiling function which gives the smallest integer value greater than or equal to its argument. Also, for the special case of Rayleigh fading, (2.7) and (2.8) may be simplified into (2.11) and (2.12), respectively (after considerable algebraic manipulations).

$$\phi_I(s) = \sum_{\sigma \in T_{N_I N}} \sum_{\nu=0}^{N-1} (-1)^\nu \sum_{b_1+b_2+\cdots+b_N=\nu} \left[\frac{\frac{1}{\overline{p}_{\sigma(N)}} \prod_{i=1}^{N-1} \frac{1/\overline{p}_{\sigma(i)}}{s+1/\overline{p}_{\sigma(i)}}}{s + \sum_{k=1}^{N-1} b_k (s + \frac{1}{\overline{p}_{\sigma(k)}}) + \sum_{k=N}^{N_I} \frac{1}{\overline{p}_{\sigma(k)}}} \right] \tag{2.11}$$

$$\phi_I(s) = \sum_{\sigma \in T_{N_I N+1}} \sum_{\nu=0}^{N} (-1)^\nu \sum_{b_1+b_2+\cdots+b_N=\nu} \left[\frac{\frac{1}{\overline{p}_{\sigma(N+1)}} \prod_{i=1}^{N} \frac{1/\overline{p}_{\sigma(i)}}{s+1/\overline{p}_{\sigma(i)}}}{\sum_{k=1}^{N} b_k (s + \frac{1}{\overline{p}_{\sigma(k)}}) + \sum_{k=N+1}^{N_I} \frac{1}{\overline{p}_{\sigma(k)}}} \right] \tag{2.12}$$

where $(b_1, b_2, \ldots, b_N)$ is a binary sequence with each element assuming the value of either 0 or 1, and $\overline{p}_{\sigma(k)}$ denotes the average signal power of the $\sigma(k)^{th}$ CCI signal.

2.2 Unified Outage Analysis with Null Steering of Dominant Interferers

Outage probability is one of the most important criteria in evaluating the performance of wireless communication systems. The outage probability can be defined as the probability that the ratio of the desired signal power to the interference power falls below a given threshold, and can be expressed as follows:

$$P_{out} = Pr\{p_0 < qI\} \tag{2.13}$$

where p_0 is the signal power of the desired user, I is the power of the total interference signal, and q is the CCI power protection ratio. In practice, thermal noise and receiver threshold exists, which may be of concern for large cells (macro cells). Hence, more refined definitions of outage probability take into consideration additive noise level due to receiver thermal noise and minimum signal requirements for receiver threshold due to noise. When thermal noise and receiver threshold are taken into account in outage evaluations, one approach is that noise is treated as CCI, and the other approach is that an additional minimum signal power requirement is imposed besides CCI power protection ratio [11]. In the subsequent subsections, unified mathematical framework for evaluating outage probability is provided.

2.2.1 Minimum Signal Power Constraint

In the presence of receiver noise, satisfactory reception is assumed to be achieved as long as the received signal to interference ratio (SIR) exceeds the CCI power protection ratio q subject to additional minimum power requirement due to receiver noise floor set by Λ. Hence, the outage probability P_{out} can be expressed as [11]

$$\begin{aligned} P_{out} &= 1 - Pr\left\{\left[q\sum_{k=1}^{N} p_{k:N_I} < p_0\right] \cap [p_0 > \Lambda]\right\} \\ &= F_0(\Lambda) + \frac{1}{2\pi}\int_{-\infty}^{\infty} \frac{G_0(c+j\omega,\Lambda)}{c+j\omega}\phi_I(-c-j\omega)d\omega \end{aligned}$$

$$
\begin{aligned}
&= F_0(\Lambda) + \frac{1}{2\pi}\int_0^{\pi} \Phi_\gamma(\theta)d\theta \\
&\simeq F_0(\Lambda) + \frac{1}{2n}\sum_{i=1}^{n} \Phi_\gamma\left[\frac{(2i-1)\pi}{2n}\right] \qquad (2.14)
\end{aligned}
$$

where p_0 and $F_0(\cdot)$ denote the instantaneous signal power of the desired user and its cumulative distribution function (CDF), respectively, coefficient c is chosen such that $0 < c < a_{min} = min\{a_i \mid 1 \leq i \leq N_I\}$ where a_i correspondes to the i^{th} pole of $G_0(c + j\omega, \Lambda)\phi_I(-c - j\omega)$, $\phi_I(s)$ is the MGF of a sum of uncancelled CCI signals (N weakest CCI signals) as in the previous section, $\Phi_\gamma(\theta) = \Re[(1 - j\tan(\theta/2))G_0(c + jc\tan(\theta/2), \Lambda)\phi_I(-c - jc\tan(\theta/2))]$, and $G_0(s, \Lambda)$ is the marginal MGF defined as $G_0(s, \Lambda) = \int_\Lambda^\infty e^{-sp_0/q} g(p_0)dp_0$ where $g_0(\cdot)$ is the PDF of the desired user signal power. The marginal MGF $G_0(s, \Lambda)$ can be expressed in terms of familiar mathematical functions when the desired signal amplitude is Rayleigh, Rician, or Nakagami-m faded. These results for $G_0(s, \Lambda)$ are summarized in [11], and can be used to evaluate (2.14). The last line in (2.14) can be obtained using Gauss-Chebyshev Quadrature (GCQ) formula [12].

2.2.2 Treating Noise as Interference

In certain literature, the effect of received noise is incorporated in the outage calculations by treating receiver noise as cochannel interference. In this case, the outage probability P_{out} can be expressed as [11]

$$
\begin{aligned}
P_{out} &= Pr\{p_0 < qI + \Lambda\} = Pr\left\{\frac{p_0}{q} - \sum_{k=1}^{N} p_{k:N_I} < \frac{\Lambda}{q}\right\} \\
&= \frac{1}{2\pi}\int_0^{\pi} \Psi_\gamma(\theta)d\theta \qquad (2.15)
\end{aligned}
$$

where $\Psi_\gamma(\theta) = \Re[(1 - j\tan(\theta/2))\phi_\gamma(c + jc\tan(\theta/2))\exp\{(1 + j\tan(\theta/2))\Lambda c/q\}]$, $\phi_\gamma(s) = \phi_0(s/q)\phi_I(-s)$. Note that (2.15) is simply a Laplace inversion integral using the relation that Laplace transform of cumulative distribution function (CDF) of γ is $\phi_\gamma(s)/s$. Also, note that the outage probability can be expressed differently by using Gill-Pelaez inversion

theorem (Fourier inversion formula) [13], with which (2.15) can be rewritten as

$$P_{out} = \frac{1}{2} - \frac{1}{\pi}\int_0^\infty \frac{\mathrm{Im}[\phi_\gamma(-jt)e^{-jt\Lambda/q}]}{t}dt. \tag{2.16}$$

The integrals in (2.15) and (2.16) can be evaluated numerically by using numerical integration methods. One method is GCQ formula [12], and the second one is saddle point integration described in chapter 4.

2.2.3 Interference-limited Environment

In picocell and microcell systems, CCI is dominant and the effect of receiver noise can be ignored. This special case can be treated by setting $\Lambda = 0$ in (2.14) or (2.15), viz.,

$$P_{out} = Pr\{\frac{p_0}{q} - \sum_{k=1}^{N} p_{k:N_I} < 0\}. \tag{2.17}$$

2.3 Outage Analysis

2.3.1 Propagation channel models

Throughout this chapter, we consider a cellular radio environment where the desired and interfering signals may have different fading statistics, and also interfering signals have i.n.d. fading statistics among themselves. Both the desired user signal and CCI signals are assumed to be subject to Rayleigh, Rice, Nakagami-m, or Nakagami-q fading statistics. The average signal power of the desired user is denoted as $\bar{p_0}$, and those of CCI signals are denoted as $\{\bar{p_k}\}_{k=1}^{N_I}$, in which the average power and fading statistics may be different among CCI signals.

2.3.2 Fixed Number Interferers

Figure 2.1 compares the outage probability for cellular systems with and without CCI cancellation capabilities as a function of the normalized average SIR defined as $SIR/q = \bar{p_0}/\bar{p_k}q$ where $\bar{p_0}$ and $\bar{p_k}$ denote the mean power of the desired user and the k^{th} interferer, respectively. As seen in the figure, a system with $N_I = 6$ active interferers but with CCI cancellation capabilities suppressing the strongest interference outperforms a system with $N_I = 5$ active interferers but without CCI cancellation capabilities. Also, the outage performance difference between these two systems becomes more pronounced as more dominant interferers are suppressed ($N_I = 6$,$N = 2$) as compared with no interference cancellation ($N_I = 2$, $N = 2$). These illustrate that the total interference is dominated by the strongest interferer power, and partial cancellation of CCI (cancelling a few dominant interferers) can be very effective in terms of outage probability. Note that all the CCI signal powers are assumed to have the same fading statistics and the same mean powers in the figure.

To quantify the benefits of selective nulling of dominant CCI signals with i.n.d. fading statistics, an exponential power decay model is adopted for modeling the power imbalances among N_I CCI signals via a single parameter $\delta > 0$. Suppose the average power of the k^{th} CCI signal is $\bar{p}_k = Ce^{-k\delta}\bar{I}_T$, where $\bar{I}_T$ denotes the sum of all the average interfering signals, then we can express $\bar{p}_k$ in terms of $\bar{I}_T$ as follows:

$$\bar{p}_k = \frac{(1 - e^{-\delta})e^{-k\delta}}{e^{-\delta} - e^{-(N_I+1)\delta}}\bar{I}_T \tag{2.18}$$

with the constraint $\bar{I}_T = \sum_{k=1}^{N_I} \bar{p}_k$. Obviously, $\delta \to 0$ corresponds to the equal mean power case.

Figure 2.2 shows the outage probability with selective interference cancellation in an interference limited environment for a Rayleigh-faded desired user as function of the normalized average SIR/q defined as

$$\text{SIR/q} = \frac{\bar{p}_0}{\bar{I}_T q} \tag{2.19}$$

where $\bar{p}_0$ denotes the average power of the desired user signal. CCI signal amplitudes are subject to Rice fading with Rice factors K_k ={2, 1.5, 1.2, 1, 0.9, 0.3}. The curves with

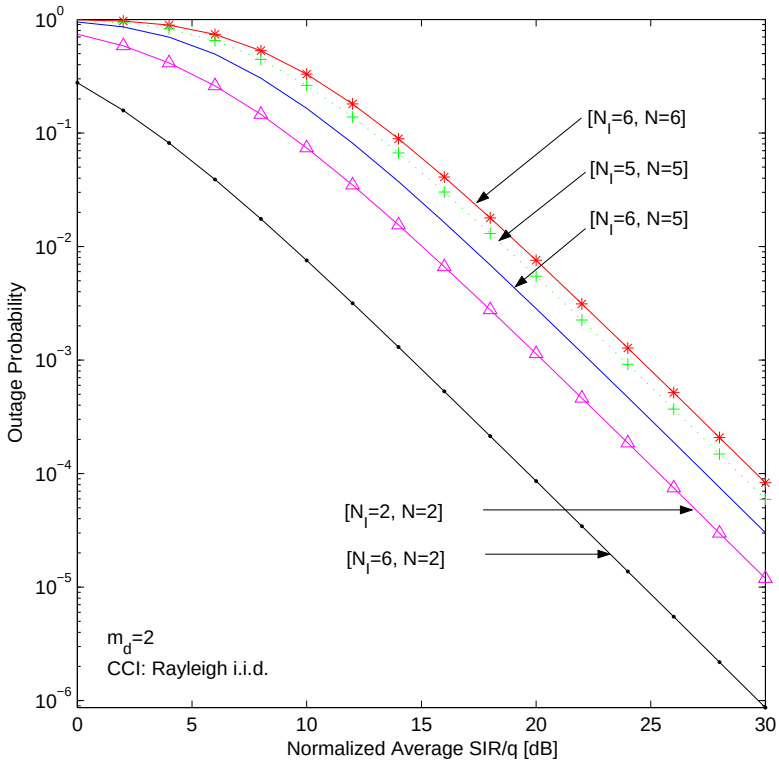

Figure 2.1: Outage probability for a Nakagami-m ($m_d = 2$)/Rayleigh model (N_I: the number of active interferers, and N: the number of uncancelled CCI signals).

asterisks represents the outage probability of selective interference cancellation when CCI signals have equal average power, and the solid lines represent the outage probability when CCI signals have unequal powers $\delta = 0.7$. It is apparent from Figure 2.2 that selective interference nulling of dominant interferers is more effective as the power imbalance among CCI increases. Moreover, the relative improvement is greater when more number of CCI signals are cancelled (because the gap between the equal and unequal mean power cases widens for smaller N). Figure 2.3 compares the outage probability for both Rayleigh and Nakagami-m ($m_d = 2$) faded desired user cases with Rice faded CCI signals when the receiver noise is treated as CCI ($\Lambda = 27$ dB).

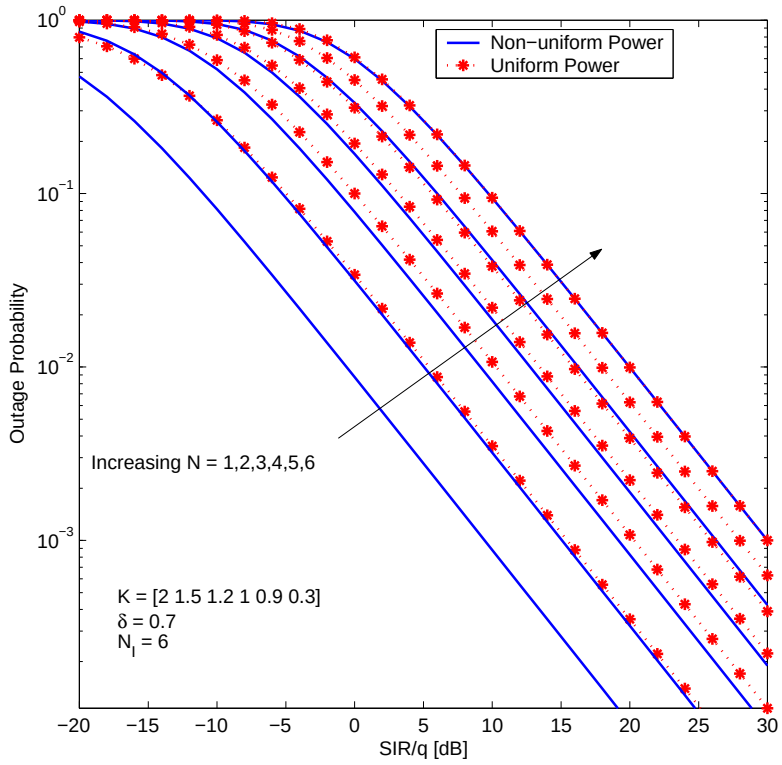

Figure 2.2: Outage probability for a Rayleigh/Rice model: solid lines represent power imbalance among CCI signals while dotted lines with asterisks represent equal power among CCI signals.

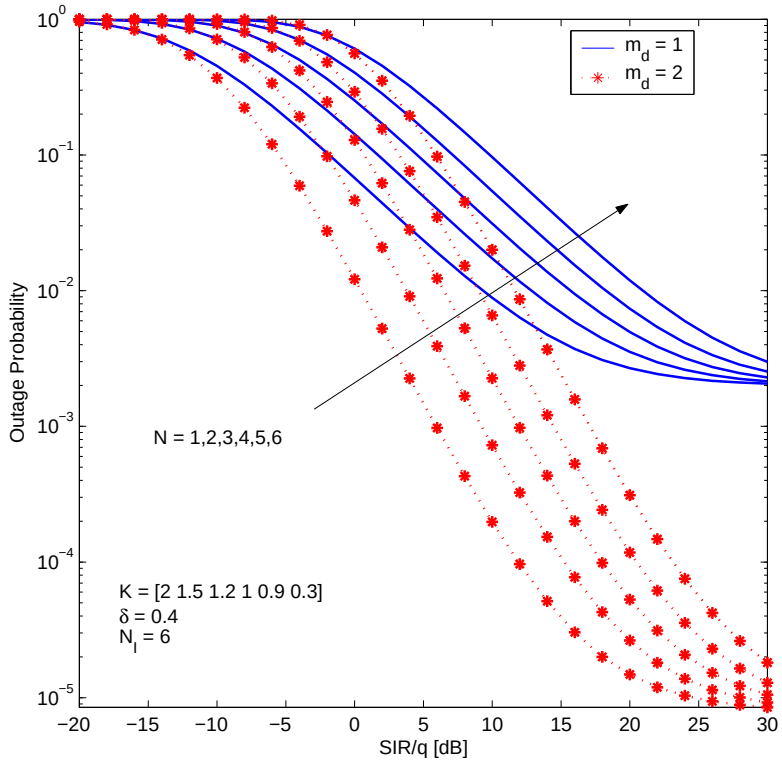

Figure 2.3: Outage probability vs. SIR/q (desired user: Nakagami-m fading with $m_d = 2$ for dotted lines with asterisks and Rayleigh fading for solid lines) when noise is treated as CCI.

2.3.3 Spectral Efficiency

Spectral efficiency is usually measured in terms of the spatial traffic density per unit bandwidth and is defined as [14]

$$\eta = \frac{G_c}{N_c W_c C A_{cell}} \quad \frac{\text{Erlang}}{\text{MHz}\cdot\text{km}^2} \tag{2.20}$$

where G_c is the offered traffic per cell, N_c is the number of channels per cell, W_c is the bandwidth per channel (MHz), C is the cluster size, and A_{cell} is the area per cell (km^2). Assuming a regular hexagonal cell deployment, by using the relationship $A_{cell} = 3\sqrt{3}R^2/2$ and $R_u = D/R = \sqrt{3C}$, we can show that the spectral efficiency defined in (2.20) can be written as

$$\eta = \frac{2G_c}{\sqrt{3}N_c W_c R^2 R_u^2} \quad \frac{\text{Erlang}}{\text{MHz}\cdot\text{km}^2} \tag{2.21}$$

where R_u is the cochannel reuse factor and R is the distance from the center to the corner of a cell. To study the gain obtained from selective interference nulling in terms of spectral efficiency, the outage probability has to be expressed in terms of the reuse distance R_u and the cell radius R. Considering a two-slope two-path model, [14] has shown that the average SIR $\bar{p}_0/\bar{I}_T$ in the worst case scenario (i.e., the desired user is near the edge of its cell and the interfering users are on the cell edges closest to the desired user cell) is given by

$$\begin{aligned} \frac{\bar{p}_0}{\bar{I}_T} &= \left(\frac{D-R}{R}\right)^a \left(\frac{1+\frac{D-R}{g}}{1+\frac{R}{g}}\right)^b \\ &= (R_u - 1)^a \left(\frac{\frac{g}{R} + R_u - 1}{\frac{g}{R} + 1}\right) \end{aligned} \tag{2.22}$$

where a and b are the path loss exponents, g denotes the breakpoint range (typically in the range of 150-300 meters), and D denotes the cochannel reuse distance. Using (2.21) and (2.22) in (2.14)-(2.17), we can study the outage probability as a function of the reuse distance and spectral efficiency, respectively. Figure 2.4 plots the outage probability as a function of spectral efficiency η for Nakagami-m faded desired user signal ($m_d = 2$) and CCI signals with mixed fading statistics. Among total 6 interference signals, three CCI signals are Nakagami-m distributed ($m_1 = 3, m_2 = 2, m_3 = 2$), one CCI signal is Rice distributed

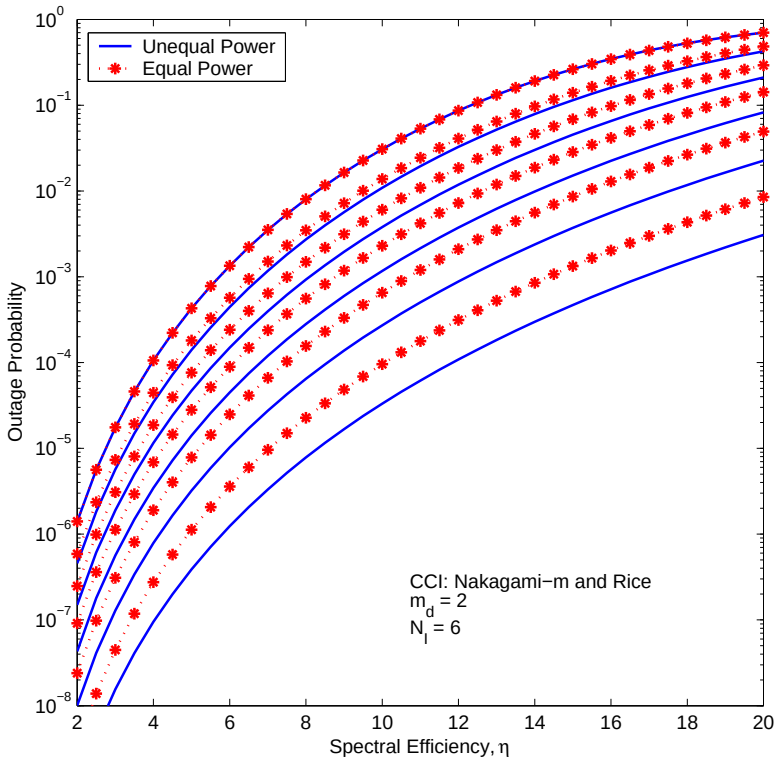

Figure 2.4: Spectral efficiency gain ($m_d = 2$, $m_k \in \{3, 2, 2, 1, 1\}$, $K = 2$, $\delta = 0.4$, $a = 2$, $b = 4$, $R = 200m$, $N_c = 25$, $W = 25$kHz, $g_c = 5$).

with Rice factor $K_4 = 2$, and two CCI signals are Rayleigh distributed ($K_5 = 0, K_6 = 0$). Figure 2.5 presents outage probability curves as a function of reuse distance R_u when the desired user's signal is Nakagami-m distributed with fading severity index $m_d = 2$ and the CCI signal amplitudes are either Rice distributed or subject to Rayleigh fading. For Rayleigh distributed CCI signal amplitudes, only the average power for each CCI signal is different. This plot shows the effect of fading parameters of CCI signals on frequency reuse factor R_u.

2.3.4 Random Number of Interferers

Thus far, we have assumed a fixed number of N_I active cochannel interferers. In practice, however, the number of active interferers is random. This is particulary true if the offered

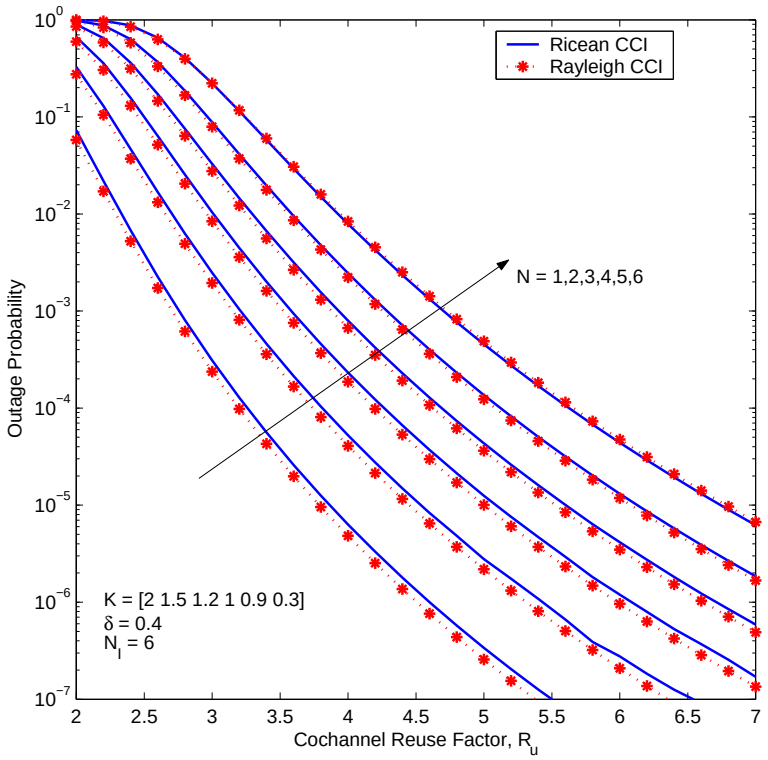

Figure 2.5: Outage probability vs. reuse distance for a Nakagami-m fading desired user signal with $m_d = 2$ and power decay imbalance parameter $\delta = 0.4$ for Rice faded CCI signal amplitudes.

traffic loads in the cochannel cells are not heavy, or when a discontinuous transmission scheme is implemented to improve spectral efficiency. In this scenario, the outage probability may be evaluated by considering all the possibilities for the number of active interferers, viz., [7]

$$P_{out} = \sum_{M=D}^{N_I} \binom{N_I}{M} B^{\frac{1}{N_c}} (1 - B^{\frac{1}{N_c}})^{N_I - M} P_{out}(M - D + 1, M) \tag{2.23}$$

where D denotes the number of antenna elements, N_c is the number of voice channels assigned to each cell, and $P_{out}(M - D + 1, M)$ denotes the outage probability given that $D - 1$ dominant CCI signals among M CCI signals are cancelled. Figure 2.6 shows the outage probability when the desired user signal amplitude experiences Rayleigh fading and CCI signals are subject to Rice fading with $K = 2$ and $\delta = 1$ at two different blocking probabilities $B \in \{0.02, 0.5\}$. The total number of CCI signals N_I is assumed to be 6. Since, the average powers for CCI signals are different, two extreme bounds are provided for each blocking probability and D (the number of smart antenna elements). The optimistic case is when the M active interferers are the M weakest interferers among N_I, and the pessimistic case is when the M active interferers are the M strongest interferers among N_I interferers. The gap between the bounds is larger when $B = 0.02$ than when $B = 0.5$ as one would expect. Although not shown in this figure, we also found that the gap between the bounds diminishes as δ approaches 0.

2.4 Chapter Summary

In this chapter, we extended previous works [4]-[9] by developing a mathematical framework for evaluating the probability of outage for cellular mobile radio systems equipped with smart antennas over generalized fading channels. Our numerical results reveal that the mean power imbalance among CCI signals plays a significant role in the performance assessment of wireless systems employing selective interference nulling algorithm. This observation emphasizes the need to model both the desired user signal and CCI signals accurately for accurate prediction of cellular systems equipped with smart antennas. Although dissimilar

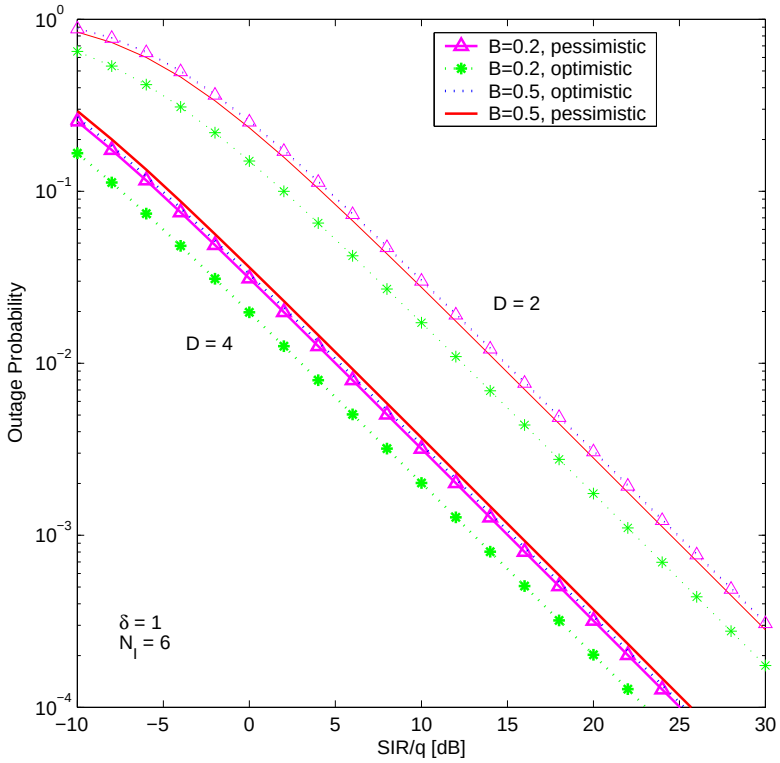

Figure 2.6: Outage probability vs. SIR/q for different blocking probability $B \in \{0.02, 0.5\}$ for an interference limited case in a Rayleigh/Rice fading environment with Rice factor $K = 2$ and $\delta = 1$.

fading severity parameters among CCI signals affect the outage performance, its effect is somewhat marginal unless the number of remaining interferers is small.

Chapter 3

Multi-branch Predetection EGC Performance in Equally Correlated Nakagami-m Fading Channels

Diversity combining techniques have long been used for mitigating the detrimental effects of multipath fading and cochannel interference. Among the various classical diversity combining schemes, predetection EGC diversity receiver is of practical interest because it offers performance comparable to the optimal linear diversity combiner but with greater simplicity (since it does not require accurate estimates of the channel gains). Despite this, the literature on predetection EGC is barren compared to other diversity combining techniques. This stems from the difficulty in computing the probability density function (PDF) of the sum of random fading amplitudes. For example, Brennan [15] has labeled the problem of computing the distribution of the sum of independent Rayleigh random variables (RVs) (i.e., simplest fading distribution) as "frightful". Obviously, the difficulty of the above mathematical problem will be compounded when the diversity paths are correlated. Moreover, as pointed out in [16] the first comprehensive paper giving a precise analysis of EGC with digital modulation did not appear until the early 1990s. In [17], authors developed a unified approach to the

performance evaluation of EGC receivers for L independent but non-identically distributed (i.n.d.) diversity paths. However, [18] reveals that the envelope correlation coefficients of typical diversity implementations may range between 0.1 to 0.8 depending on the antenna configuration and operating environments. Hence, any performance analysis must be revamped to account for the effect of correlation between the combined signals.

A. Relation to Previous Efforts

A number of recent articles [19]-[29] have analyzed the deleterious effects of branch correlation on the performance of digital communications with coherent EGC receivers. With the exception of [27]-[29], all previous studies are restricted to a dual-diversity system. In [27], Karagiannidis utilized the Green's matrix approximation of the multivariate Nakagami-m distribution for computing the moment generating function (MGF) of the EGC output signal-to-noise ratio (SNR) via the Pade approximation technique. Although such an approximation is accurate for an exponential correlation model, it may not be good for the equally correlated model [30]. In [28] and [29], Chen et. al. have utilized a novel transformation of a set of equally correlated branch gains into a set of conditionally independent branch gains to analyze the performance of a L-branch EGC receiver over Rayleigh and Rice channels, respectively. However, their approach does not facilitate EGC receiver analysis over equally correlated Nakagami-m channels when fading index m assumes non-integer values.

B. Our Contributions

In this chapter, we generalize the results in [28] to Nakagami-m channels with arbitrary fading index m. Extensive empirical measurements have confirmed the usefulness of Nakagami-m distribution for modeling radio links [31]-[33]. The Nakagami-m distribution also includes the Rayleigh and the one-sided Gaussian distribution as special cases and can closely approximate the Rice and the Hoyt distributions [34]. Moreover, in contrast to the analytical approaches presented in [27]-[29], we first derive the characteristic function (CHF) of the EGC output statistic and subsequently utilize the frequency domain approach developed in [17] to

analyze a broad range of digital modulation formats in equally correlated[1] Nakagami-m channels. In this chpater, we also derive an exact joint PDF for equally correlated Nakagami-m RVs (instead of Green's matrix approximation for the multivariate Nakagami-m distribution [27, Eq. (9)]). Additionally, our solution for computing the average symbol error probability (ASEP) is much more efficient than the Pade approximation technique employed in [27] (note that [27, Eq. (12)] involves the computational complexity of $(L-1)$ fold infinite sum for calculating each moment [27, Eq. (5)], which is needed for approximating the MGF as an infinite linear sum of moments [27, Eq. (15)] especially for larger diversity order L).

The organization of this chapter is following. Section 1 briefly discusses the frequency domain approach for average symbol error probability (ASEP) analysis and subsequently derive the CHF of the output of an EGC receiver in equally correlated Nakagami-m fading channel starting from the joint CHF of equally correlated Nakagami-m random variables (RV's). Outage probability computation for the EGC output signal-to-noise ratio (SNR) statistic is discussed in Section 2 with numerical inversion of MGF [36]- [37] and saddle point integration [39]- [38]. Selected numerical results and discussions are provided in section 3. Finally, the main points are summarized in chapter summary.

3.1 Error Probability Analysis

3.1.1 Frequency domain analysis

In an EGC receiver, the outputs of the individual diversity branches are first co-phased, equally weighted, and then summed to give the resultant output. The instantaneous SNR

[1]The constant correlation model is appropriate for a set of closely spaced antennas [35] (e.g. mounted on mobile handset) and can be used as a worst-case benchmark or as a rough approximation by replacing every $\rho_{ij}(i\neq j)$ in the correlation matrix with its average value.

at the output of the EGC combiner is $\gamma_{egc} = \nu^2$ where ν is defined as

$$\nu = \sqrt{\frac{E_s}{LN_0}} \sum_{k=1}^{L} \alpha_k \tag{3.1}$$

where E_s/N_0 denotes the energy/symbol/noise spectral density, α_k is a Nakagami-m random variable with the statistical parameters m_k and Ω_k, and L corresponds to the diversity order (the number of diversity branches).

In order to calculate the ASEP of EGC in fading channels, we need to average the conditional error probability (CEP) over the PDF of the signal amplitude at the output of the EGC combiner, viz.,

$$\bar{P}_s = \int_0^\infty P_s(\nu)\, p_\nu(\nu)\, d\nu \tag{3.2}$$

where $P_s(\nu)$ denotes the CEP, and $p_\nu(\cdot)$ corresponds to the PDF of random variable ν. Since a closed-form expression for the PDF of a sum of Nakagami-m distributed RVs does not exist for $L > 2$ (even for the i.n.d. case), [17] suggested the transformation of (3.2) into the frequency domain (using Parseval's theorem) to facilitate the ASEP calculation for EGC receivers. This gives

$$\bar{P}_s = \frac{1}{2\pi} \int_{-\infty}^{\infty} G(\omega)\, \phi_\nu(-\omega)\, d\omega \tag{3.3}$$

where $\phi_\nu(\omega) = \int_0^\infty e^{j\omega\nu} p_\nu(\nu) d\nu$ denotes the CHF of ν and $G(\omega) = \int_0^\infty e^{j\omega\nu} P_s(\nu) d\nu$ denotes the Fourier transform of the CEP $P_s(\nu)$. Although the need to find the PDF of ν is circumvented, we must now determine the CHF of ν and Fourier transform of the CEP instead. Since $G(\omega)$ is available for a broad range of digital modulation formats (see [17, Eqs. (10)-(17)]), only the knowledge of $\phi_\nu(\omega)$ is further required for analyzing the performance of multi-branch predetection EGC receiver with correlated signal inputs. For the special case of coherent binary signaling, the ASEP can be computed as [17],[24]

$$\overline{P}_s = \frac{1}{2} - \frac{1}{2\pi} \int_0^\infty \frac{e^{-t}}{t} \mathrm{Im}\left\{\phi_\nu(\sqrt{2gt})\right\} dt \tag{3.4}$$

where $\mathrm{Im}\{\cdot\}$ denotes the imaginary part of its argument and $g = 1$ for binary phase-shift keying (BPSK). In the following subsection, we will derive the CHF of EGC combiner output in Nakagami-m channels assuming constant correlation model across the diversity branches.

3.1.2 CHF of EGC output statistic

Since an exact expression for the multivariate Nakagami-m distribution for equally correlated cases is not readily available, we will derive this expression starting from the joint CHF of equally correlated Gamma variates. Let $\alpha_k (k \in \{1, 2, \ldots, L\})$ denote the set of Nakagami-m fading RVs where L is the diversity order. Then, the joint CHF of $\underline{\alpha}^2 = [\alpha_1^2, \alpha_2^2, \ldots, \alpha_L^2]^T$ is given by [35],[63],

$$\phi_{\underline{\alpha}^2}(\omega_1, \omega_2, \ldots, \omega_L) = \{det(\underline{I}_L - j\underline{\Lambda}\underline{K})\}^{-m} \tag{3.5}$$

where $[\cdot]^T$ denotes the matrix transpose, $\underline{I}_L$ is a $L \times L$ identity matrix, real $m \geq 0.5$ represents the fading severity index, $\underline{\Lambda}$ represents a $L \times L$ diagonal matrix defined as $\underline{\Lambda} = diag(\omega_1, \omega_2, \ldots, \omega_L)$, and $\underline{K}$ is a $L \times L$ symmetric matrix with elements in the k^{th} row and the l^{th} column expressed as

$$(\underline{K})_{kl} = \begin{cases} \frac{\Omega}{m} & \text{if } k = l \\ \frac{\rho\Omega}{m} & \text{if } k \neq l \quad k, l = 1, 2, \ldots, L \end{cases} \tag{3.6}$$

In (3.6), $\rho = \sqrt{\rho_\gamma}$ and ρ_γ is the power correlation coefficient defined as

$$\rho_\gamma = \frac{E[(\alpha_k^2 - E[\alpha_k^2])(\alpha_l^2 - E[\alpha_l^2])]}{\sqrt{\text{var}[\alpha_k^2]\text{var}[\alpha_l^2]}} \tag{3.7}$$

where $\Omega = E[\alpha_k^2]$ and $E[\cdot]$ denotes the statistical average of its argument. The joint CHF of equally correlated Gamma variates depicted in (3.5) can be rewritten as

$$\phi_{\underline{\alpha}^2}(\omega) = \{det(\underline{K})\}^{-m} \{det(\underline{K}^{-1} - j\Lambda)\}^{-m} \tag{3.8}$$

After a considerable matrix and algebraic manipulations, it can be shown that

$$\{det(\underline{K})\}^{-1} = det(\underline{K}^{-1}) = (A - B)^L \left(1 + \frac{LB}{A - B}\right) \tag{3.9}$$

and

$$det(\underline{K}^{-1} - j\Lambda) = \Big\{ \prod_{k=1}^{L} [(A - B) - j\omega_k] \Big\} \Big\{ 1 + \sum_{l=1}^{L} \frac{B}{(A - B) - j\omega_l} \Big\} \tag{3.10}$$

where $A = \frac{m(1+[L-2]\rho)}{\Omega(1-\rho)(1+[L-1]\rho)}$ and $B = \frac{-m\rho}{\Omega(1-\rho)(1+[L-1]\rho)}$ [41, Eqs. (12) and (13)]. Substituting (3.9) and (3.10) into (3.8) and after some algebraic manipulations, we obtain

$$\phi_{\underline{\alpha}^2}(\omega_1, \omega_2, \cdots, \omega_L) = \frac{\left(1 + \frac{LB}{A-B}\right)^m}{\prod_{k=1}^{L}\left(1 - \frac{j\omega_k}{A-B}\right)^m} \; {}_2F_1\left(m, 1; 1; -\frac{B}{A-B}\sum_{l=1}^{L}\frac{1}{1-\frac{j\omega_l}{A-B}}\right) \tag{3.11}$$

where ${}_2F_1(a, b; c; z)$ is the Gaussian hypergeometric function which is defined as

$${}_2F_1(a, b; c; z) = \sum_{n=1}^{\infty}\frac{(a)_n(b)_n z^n}{(c)_n n!} \tag{3.12}$$

where $(a)_n = a(a+1)\cdots(a+n+1) = \Gamma(a+n)/\Gamma(a)$ is the Pochhammer symbol and $\Gamma(\cdot)$ is Gamma function. Using the identity ${}_2F_1(m, 1; 1; -z) = \sum_{p=0}^{\infty}\frac{\Gamma(m+p)}{\Gamma(m)p!}(-z)^p$ and the multinomial expansion formula $\left(\sum_{l=1}^{L} x_l\right)^p = \sum_{\substack{0\le l_1,\ldots,l_L\le p \\ l_1+\cdots+l_L=p}} \frac{p!}{l_1!\cdots l_L!}\prod_{k=1}^{L} x_k^{l_k}$, (3.11) can be rewritten as

$$\begin{aligned}\phi_{\underline{\alpha}^2}(\omega_1, \omega_2, \ldots, \omega_L) &= \left(1 + \frac{LB}{A-B}\right)^m \sum_{p=0}^{\infty}\frac{\Gamma(m+p)}{\Gamma(m)p!}\left(\frac{-B}{A-B}\right)^p \\ &\quad \times \sum_{\substack{0\le l_1,l_2,\ldots,l_L\le p \\ l_1+l_2+\cdots+l_L=p}} \frac{p!}{l_1!l_2!\cdots l_L!}\prod_{k=1}^{L}\left(\frac{1}{1-\frac{j\omega_l}{A-B}}\right)\end{aligned} \tag{3.13}$$

Note that, unlike [41, Eq. (16)], (3.13) holds for any real $m \geq 0.5$ (not restricted to positive integer m values). For the special case of positive m, (3.13) simplifies into [41, Eq. (18)]. Although (3.13) appears to be more complicated as compared to (3.11), we will show shortly that this step is crucial in the derivation of the joint CHF of equally correlated Nakagami-m RVs (i.e. enables us to convert an L-fold nested integral into a product of L separable integrals). Substituting $A = \frac{m(1+[L-2]\rho)}{\Omega(1-\rho)(1+[L-1]\rho)}$ and $B = \frac{-m\rho}{\Omega(1-\rho)(1+[L-1]\rho)}$ into (3.13) yields

$$\begin{aligned}\phi_{\underline{\alpha}^2}(\omega_1, \omega_2, \ldots, \omega_L) &= \left(\frac{1-\rho}{1+[L-1]\rho}\right)^m \sum_{p=0}^{\infty}\frac{\Gamma(m+p)}{\Gamma(m)p!}\left(\frac{\rho}{1+[L-1]\rho}\right)^p \\ &\quad \times \sum_{\substack{0\le l_1,l_2,\ldots,l_L\le p \\ l_1+l_2+\cdots+l_L=p}} \frac{p!}{l_1!l_2!\cdots l_L!}\prod_{k=1}^{L}\left[\frac{m}{m - j\omega_k\Omega(1-\rho)}\right]^{m+l_k}\end{aligned} \tag{3.14}$$

Taking the inverse Fourier Transform of (3.14) leads to the joint PDF of equally correlated Gamma RVs $\alpha_k^2 (k \in \{1, 2, \ldots, L\})$, where α_k is Nakagami-m distributed, as follows:

$$f_{\underline{\alpha}^2}(x_1, x_2, \ldots, x_L) = \left(\frac{1-\rho}{1+[L-1]\rho}\right)^m \sum_{p=0}^{\infty}\frac{\Gamma(m+p)}{\Gamma(m)p!}\left(\frac{\rho}{1+[L-1]\rho}\right)^p$$

$$\times \sum_{\substack{0\le l_1,l_2,\ldots,l_L\le p\\ l_1+l_2+\cdots+l_L=p}} \frac{p!}{l_1!l_2!\cdots l_L!}\prod_{k=1}^{L} g\left(x_k, m+l_k, \frac{\Omega(1-\rho)}{m}\right) \quad (3.15)$$

where $g(x_k,\nu,\beta)=\frac{x_k^{\nu-1}e^{-x_k/\beta}}{\beta^{\nu}\Gamma(\nu)}$. Since we have obtained the joint PDF of α_k^2, the joint PDF of α_k can be readily derived by exploiting the fact that

$$f_Y(y)=2yf_X(y^2) \quad (3.16)$$

when $f_X(x)$ is known and $y=\sqrt{x}$ for $x\ge 0$, $y\ge 0$. Using (3.15) and (3.16), we obtain

$$\begin{aligned} f_{\underline{\alpha}}(y_1,y_2,\ldots,y_L) &= \left(\frac{1-\rho}{1+[L-1]\rho}\right)^m \sum_{p=0}^{\infty}\frac{\Gamma(m+p)}{\Gamma(m)p!}\left(\frac{\rho}{1+[L-1]\rho}\right)^p \\ &\times \sum_{\substack{0\le l_1,l_2,\ldots,l_L\le p\\ l_1+l_2+\cdots+l_L=p}} \frac{p!}{l_1!l_2!\cdots l_L!}\prod_{k=1}^{L} h\left(y_k, m+l_k, \frac{\Omega(1-\rho)}{m}\right) \end{aligned} \quad (3.17)$$

where $h\left(y_k, m+l_k, \frac{\Omega(1-\rho)}{m}\right)=\frac{2y_k^{2(m+l_K)-1}e^{-y_k^2/[\frac{\Omega(1-\rho)}{m}]}}{[\frac{\Omega(1-\rho}{m}]^{m+l_k}\Gamma(m+l_k)}$. To the best of our knowledge, (3.17) is new and holds for any real $m\ge$0.5. The CHF of ν can be computed as

$$\begin{aligned} \phi_\nu(\omega) &= \left(\frac{1-\rho}{1+[L-1]\rho}\right)^m \sum_{p=0}^{\infty}\frac{\Gamma(m+p)}{\Gamma(m)p!}\left(\frac{\rho}{1+[L-1]\rho}\right)^p \\ &\times \sum_{\substack{0\le l_1,l_2,\ldots,l_L\le p\\ l_1+l_2+\cdots+l_L=p}} \frac{p!}{l_1!\cdots l_L!}\int_0^{\infty}\cdots\int_0^{\infty} e^{\sum_{i=1}^{L}\frac{j\omega y_i}{\sqrt{L}}}\prod_{k=1}^{L}\frac{2y_k^{2(m+l_K)-1}e^{-y_k^2/[\frac{\bar{\gamma}(1-\rho)}{m}]}}{[\frac{\bar{\gamma}(1-\rho}{m}]^{m+l_k}\Gamma(m+l_k)}dy_1\cdots dy_L \end{aligned} \quad (3.18)$$

where $\overline{\gamma}=\Omega(E_s/N_0)$ denote the average SNR/symbol for each diversity branch. The L-fold integral in Eq. (3.18) can be evaluated effectively as a product of L separable integral as

$$\begin{aligned} \phi_\nu(\omega) &= \left(\frac{1-\rho}{1+[L-1]\rho}\right)^m \sum_{p=0}^{\infty}\frac{\Gamma(m+p)}{\Gamma(m)p!}\left(\frac{\rho}{1+[L-1]\rho}\right)^p \\ &\times \sum_{\substack{0\le l_1,l_2,\ldots,l_L\le p\\ l_1+l_2+\cdots+l_L=p}} \frac{p!}{l_1!\cdots l_L!}\prod_{k=1}^{L}\int_0^{\infty} e^{j\omega y_i/\sqrt{L}}\frac{2y_k^{2(m+l_K)-1}e^{-y_k^2/[\frac{\bar{\gamma}(1-\rho)}{m}]}}{[\frac{\bar{\gamma}(1-\rho}{m}]^{m+l_k}\Gamma(m+l_k)}dy_k \end{aligned} \quad (3.19)$$

Recognizing that the definite integral in (3.19) can be expressed in terms of parabolic cylinder function using identity [42, Eq. (3.462.1)], we obtain

$$\phi_\nu(\omega) = \left(\frac{1-\rho}{1+[L-1]\rho}\right)^m \sum_{p=0}^{\infty}\frac{\Gamma(m+p)}{\Gamma(m)p!}\left(\frac{\rho}{1+[L-1]\rho}\right)^p$$

$$\times \sum_{\substack{0\le l_1,l_2,\ldots,l_L\le p \\ l_1+l_2+\cdots+l_L=p}} \frac{p!}{l_1!\cdots l_L!}\prod_{k=1}^{L}\frac{\Gamma(2(m+l_k))}{2^{m+l_k-1}\Gamma(m+l_k)}$$
$$\times \quad e^{\frac{-\bar{\gamma}(1-\rho)\omega^2}{8Lm}} D_{-2(m+l_k)}\left(\frac{-j\omega\sqrt{\bar{\gamma}(1-\rho)}}{\sqrt{2Lm}}\right) \tag{3.20}$$

where $D_\nu(z)$ is the parabolic cylinder function of order ν and argument z. Using identity [42, Eq. (9.240)], (3.20) can be expressed in terms of confluent hypergeometric function ${}_1F_1(a;b;c)$ as

$$\begin{aligned}\phi_\nu(\omega) &= \left(\frac{1-\rho}{1+[L-1]\rho}\right)^m \sum_{p=0}^{\infty}\frac{\Gamma(m+p)}{\Gamma(m)p!}\left(\frac{\rho}{1+[L-1]\rho}\right)^p \\ &\times \sum_{\substack{0\le l_1,l_2,\ldots,l_L\le p \\ l_1+l_2+\cdots+l_L=p}} \frac{p!}{l_1!\cdots l_L!}\prod_{k=1}^{L}\left\{{}_1F_1\left(m+l_k;\frac{1}{2};\frac{-\bar{\gamma}(1-\rho)\omega^2}{4Lm}\right)+j\frac{\Gamma(m+l_k+\frac{1}{2})}{\Gamma(m+l_k)}\right. \\ &\times \quad \left.\sqrt{\frac{\bar{\gamma}(1-\rho)\omega^2}{Lm}}{}_1F_1\left(m+l_k+\frac{1}{2};\frac{3}{2};\frac{-\bar{\gamma}(1-\rho)\omega^2}{4Lm}\right)\right\}. \end{aligned} \tag{3.21}$$

Substituting the appropriate $G(\omega)$ from [17] and (3.21) into (3.3), we obtain an analytical ASEP expression for evaluating the performance of various digital modulation formats with an EGC receiver in equally correlated Nakagami-m channels. It is also important to highlight that for the special case of half-odd integer m values ($m = \frac{1}{2}, 1, \frac{3}{2}, \cdots$), the MGF of ν can be computed much more efficiently via a recursive formula (using the integral identity developed in the Appendix). This development is discussed in the following section (see (3.28)) along with the MGF-based approach for evaluating the CDF of ν.

3.2 Outage Probability

Outage probability is another performance measure of wireless communication systems over fading channels in addition to the average error probability. The outage probability P_{out} is defined as the probability that the instantaneous receiver output SNR falls below a specified

threshold SNR γ_{th} i.e.,

$$P_{out} = Pr\{0 \leq \gamma_{egc} \leq \gamma_{th}\} = \int_0^{\gamma_{th}} p_{\gamma_{egc}}(x)dx = F_\nu\left(\sqrt{\gamma_{th}}\right) \tag{3.22}$$

where γ_{egc} is the instantaneous EGC output SNR, $p_{\gamma_{egc}}(x)$ is the pdf of γ_{egc}, and $F_\nu(\cdot)$ is the cumulative distribution function (CDF) of random variable ν. However, since a closed-form expression for the PDF of γ_{egc} or ν is not known, P_{out} can not be computed directly using (3.22). Nevertheless, we may evaluate the desired P_{out} (using the MGF of ν) based on the numerical Laplace inversion method [36] or the saddle-point integration method [38]-[39].

From the definitions of the MGF of ν ($\mathcal{M}_\nu(s) = E[e^{-s\nu}]$) and the CHF of ν ($\phi_\nu(\omega) = E[e^{j\omega\nu}]$), we can relate the two quantities as $\mathcal{M}_\nu(s) = \phi_\nu(js)$ or $\phi_\nu(\omega) = \mathcal{M}_\nu(-j\omega)$. Both the CHF and the MGF may be used for evaluating the CDF of ν. It is common to invoke the Gil-Palaez inversion theorem for calculating the CDF of ν from its CHF. However, since the numerical integration has the form of $\frac{1}{2}$ minus an integral, many steps of integration of the oscillating integrand $\phi_\nu(\omega)e^{-j\omega\nu}$ are needed to determine the sum accurately when the tails of the distribution are sought. For this reason, outage probability calculations based on the MGF is preferred (leads to improved accuracy, numerical stability, and computational efficiency).

In the subsequent subsections, we derive two expressions for the MGF and present two simple and accurate methods to compute the outage probability (numerical Laplace inversion method discussed by Abate [36] and saddle-point integration method suggested by Helstrom [38] and [39]).

3.2.1 Derivation of the MGF of the EGC output

A. The MGF containing the confluent hypergeometric function

The CHF of ν is defined as $\phi_\nu(\omega) = E[e^{j\omega\nu}]$ and the MGF is $\mathcal{M}_\nu(s) = E[e^{-s\nu}] = \phi_\nu(js)$, where $E[\cdot]$ denotes the statistical average of the argument. From these two definitions and

(3.21), the MGF of ν can be written as follows:

$$\begin{aligned}\mathcal{M}_\nu(s) &= \left(\frac{1-\rho}{1+[L-1]\rho}\right)^m \sum_{p=0}^{\infty} \frac{\Gamma(m+p)}{\Gamma(m)p!}\left(\frac{\rho}{1+[L-1]\rho}\right)^p \\ &\times \sum_{\substack{0\le l_1,l_2,\ldots,l_L\le p \\ l_1+l_2+\cdots+l_L=p}} \frac{p!}{l_1!\cdots l_L!}\prod_{k=1}^{L}\left\{ {}_1F_1\left(m+l_k;\frac{1}{2};\frac{\bar{\gamma}(1-\rho)s^2}{4Lm}\right) - \frac{\Gamma(m+l_k+\frac{1}{2})}{\Gamma(m+l_k)}\right. \\ &\times \left.\sqrt{\frac{\bar{\gamma}(1-\rho)s^2}{Lm}}\,{}_1F_1\left(m+l_k+\frac{1}{2};\frac{3}{2};\frac{\bar{\gamma}(1-\rho)s^2}{4Lm}\right)\right\}. \end{aligned} \tag{3.23}$$

B. EGC output statistic for half-odd integer m values

When fading index m assumes half-odd integer values ($m = \frac{1}{2}, 1, \frac{3}{2}, \cdots$), the MGF of ν, $\mathcal{M}_\nu(s) = E[e^{-s\nu}] = \phi_\nu(js)$, can be computed much more efficiently using (3.28)(as compared to (3.23)). Starting from (3.17), the MGF of ν can be written as

$$\begin{aligned}\mathcal{M}_\nu(s) &= \left(\frac{1-\rho}{1+[L-1]\rho}\right)^m \sum_{p=0}^{\infty} \frac{\Gamma(m+p)}{\Gamma(m)p!}\left(\frac{\rho}{1+[L-1]\rho}\right)^p \\ &\times \sum_{\substack{0\le l_1,l_2,\ldots,l_L\le p \\ l_1+l_2+\cdots+l_L=p}} \frac{p!}{l_1!\cdots l_L!}\int_0^\infty\cdots\int_0^\infty e^{-\sum_{i=1}^{L} sy_i/\sqrt{L}} \\ &\times \prod_{k=1}^{L}\frac{2y_k^{2(m+l_K)-1}e^{-y_k^2/[\frac{\bar{\gamma}(1-\rho)}{m}]}}{[\frac{\bar{\gamma}(1-\rho}{m}]^{m+l_k}\Gamma(m+l_k)}dy_1\cdots dy_L. \end{aligned} \tag{3.24}$$

The L-fold integral in (3.24) can be evaluated as a product of L separable integrals as

$$\begin{aligned}\mathcal{M}_\nu(s) &= \left(\frac{1-\rho}{1+[L-1]\rho}\right)^m \sum_{p=0}^{\infty} \frac{\Gamma(m+p)}{\Gamma(m)p!}\left(\frac{\rho}{1+[L-1]\rho}\right)^p \\ &\times \sum_{\substack{0\le l_1,l_2,\ldots,l_L\le p \\ l_1+l_2+\cdots+l_L=p}} \frac{p!}{l_1!\cdots l_L!}\prod_{k=1}^{L}\frac{2}{\left[\frac{\bar{\gamma}(1-\rho)}{m}\right]^{m+l_k}\Gamma(m+l_k)} \\ &\times \int_0^\infty y_k^{2(m+l_k)-1}e^{-y_k^2/\left[\frac{\bar{\gamma}(1-\rho)}{m}\right]-sy_k/\sqrt{L}}dy_k. \end{aligned} \tag{3.25}$$

Manipulating the exponent of exponential function in the integrand in (3.25) into a complete-squared form gives

$$\mathcal{M}_\nu(s) = \left(\frac{1-\rho}{1+[L-1]\rho}\right)^m \sum_{p=0}^{\infty} \frac{\Gamma(m+p)}{\Gamma(m)p!}\left(\frac{\rho}{1+[L-1]\rho}\right)^p$$

$$\times \sum_{\substack{0\le l_1,l_2,\ldots,l_L\le p\\ l_1+l_2+\cdots+l_L=p}} \frac{p!}{l_1!\cdots l_L!}\prod_{k=1}^{L}\frac{2e^{\bar{\gamma}(1-\rho)s^2/4mL}}{\left[\frac{\bar{\gamma}(1-\rho)}{m}\right]^{m+l_k}\Gamma(m+l_k)}$$
$$\times \int_0^\infty y_k^{2(m+l_k)-1}e^{-\frac{m}{\bar{\gamma}(1-\rho)}\left(y_k+\frac{\bar{\gamma}(1-\rho)s}{2m\sqrt{L}}\right)^2}dy_k \tag{3.26}$$

which can be rewritten using a change of variable in the integrand in (3.26). Let's introduce a new variable u_k and its derivative as follows: $\left(y_k+\frac{\bar{\gamma}(1-\rho)s}{2m\sqrt{L}}\right)\sqrt{\frac{m}{\bar{\gamma}(1-\rho)}}=u_k$, and $dy_k=\sqrt{\frac{\bar{\gamma}(1-\rho)}{m}}du_k$. Then, the MGF can be expressed as

$$\begin{aligned}\mathcal{M}_\nu(s) &= \left(\frac{1-\rho}{1+[L-1]\rho}\right)^m\sum_{p=0}^{\infty}\frac{\Gamma(m+p)}{\Gamma(m)p!}\left(\frac{\rho}{1+[L-1]\rho}\right)^p\\ &\times\sum_{\substack{0\le l_1,l_2,\ldots,l_L\le p\\ l_1+l_2+\cdots+l_L=p}}\frac{p!}{l_1!\cdots l_L!}\prod_{k=1}^{L}\frac{2}{\Gamma(m+l_k)}e^{\bar{\gamma}(1-\rho)s^2/4Lm}\sum_{i=0}^{2(m+l_k)-1}\binom{2(m+l_k)-1}{i}\\ &\times\left(-\sqrt{\frac{\bar{\gamma}(1-\rho)s^2}{4Lm}}\right)^{2(m+l_k)-1}\int_{\sqrt{\bar{\gamma}(1-\rho)s^2/4Lm}}^{\infty}u_k^ie^{-u_k^2}du_k\end{aligned} \tag{3.27}$$

If we define $H_i(z)=(-z)^{2(m+l_k)-1-i}e^{z^2}\int_z^\infty u^ie^{-u^2}du$ in (3.27), then we can arrive at the final expression for the MGF of EGC output ν as follows:

$$\begin{aligned}\mathcal{M}_\nu(s) &= \left(\frac{1-\rho}{1+[L-1]\rho}\right)^m\sum_{p=0}^{\infty}\frac{\Gamma(m+p)}{\Gamma(m)p!}\left(\frac{\rho}{1+[L-1]\rho}\right)^p\\ &\times\sum_{\substack{0\le l_1,l_2,\ldots,l_L\le p\\ l_1+l_2+\cdots+l_L=p}}\frac{p!}{l_1!\cdots l_L!}\prod_{k=1}^{L}\frac{2}{\Gamma(m+l_k)}\\ &\times\sum_{i=0}^{2(m+l_k)-1}\binom{2(m+l_k)-1}{i}H_i\left(\sqrt{\frac{\bar{\gamma}(1-\rho)s^2}{4Lm}}\right).\end{aligned} \tag{3.28}$$

Note that $H_i(z)$ can be obtained by the iteration (see Appendix)

$$H_{i+2}(z)=(-1)^{2(m+l_k)-1-i}\left(\frac{1}{2}\right)z^{2(m+l_k)-2}+\left(\frac{1}{2}\right)(i+1)z^{-2}H_i(z),\qquad i\ge 0 \tag{3.29}$$

where $\begin{cases} H_0(z)=(-1)^{2(m+l_k)-1}z^{2(m+l_k)-1}e^{z^2}\left(\frac{\sqrt{\pi}}{2}\right)\mathrm{erfc}(z), & i=0\\ H_1(z)=(-1)^{2(m+l_k)-2}\left(\frac{1}{2}\right)z^{2(m+l_k)-2}, & i=1\end{cases}$.

3.2.2 Evaluations of CDF at a given threshold to compute the outage probability

Both the CHF and the MGF of a random variable ν can be used when the CDF of ν is evaluated. It is common to use the Gil-Pelaez inversion theorem for calculating the CDF of a random variable from its CHF [38]. Suppose the CHF of a random variable ν is

$$\phi_\nu(\omega) = E[e^{j\omega\nu}] = \int_0^\infty f_\nu(\nu) e^{j\omega\nu} d\nu \tag{3.30}$$

where $f_\nu(\nu)$ is the PDF of the random variable ν. Then the CDF of ν can be calculated by the Gil-Pelaez inversion theorem as

$$F_\nu(\nu) = \frac{1}{2} - \frac{1}{\pi} \int_0^\infty \frac{1}{\omega} \mathrm{Im}[\phi_\nu(\omega) e^{-j\omega\nu}] d\omega \tag{3.31}$$

If the CHF is so complicated that an analytical solution for the integration in (3.31) is not possible, the integration can be evaluated numerically. However, since the numerical integration has the form of $\frac{1}{2}$ minus an integral, many steps of integration of the oscillatory integrand are needed to determine the sum accurately, if the tails of the distribution are sought, when the integration is evaluated by numerical integration [38]. Hence, due to the oscillatory integrand in (3.31), as the random variable ν decreases, the result becomes increasingly inaccurate. Due to this problem, in the subsequent subsections, two different methods, both of which are based on the MGF, for evaluating the CDF of a random variable are used to evaluate the CDF, and ultimately the outage probability. These two methods have shown more accuracy when the tails of distribution are sought as compared with the Gil-Palaez inversion theorem.

A. The numerical inversion of Laplace Transform

The MGF of ν can be interpreted as the Laplace transform of the PDF of ν. Also, since $f_\nu(\nu) = dF_\nu(\nu)/d\nu$ and $F_\nu(0) = 0$, where $f_\nu(\nu)$ and $F_\nu(\nu)$ are the PDF and CDF of ν, respectively, we have $LT[F_\nu(\nu)] = LT[f_\nu(\nu)]/s$ [42, Eq.(17.12.3)], where $LT[\cdot]$ denotes the

Laplace transform operator. Using this relationship between $f_\nu(\nu)$and $F_\nu(\nu)$ for its Laplace transform and applying the numerical inversion method of Laplace transform of probability distribution suggested in [36], we obtain the CDF of ν evaluated at $\nu_{th} = \sqrt{\gamma_{th}}$, which corresponds to the outage probability given a threshold ν_{th}, as

$$\begin{aligned} P_{out} &= P_\nu(0 \le \nu \le \nu_{th}) \\ &= 2^{1-C} e^{A/2} \sum_{k=0}^{C} \binom{C}{k} \sum_{b=0}^{B+k} (-1)^b \alpha_b \Re\left[\mathcal{M}_\nu\left(\frac{A + j2\pi b}{2\nu_{th}}\right)/(A + j2\pi b)\right] \\ &+ E(A) + E(B, C) \end{aligned} \tag{3.32}$$

where $\alpha_b = \begin{cases} 1/2 & b = 0 \\ 1 & b = 1, 2, \ldots \end{cases}$, $\Re[\cdot]$ denotes the real part, $E(A) \le e^{-A}/(1 - e^{-A})$, and

$$E(B, C) \simeq 2^{1-C} e^{A/2} \sum_{k=0}^{C} \binom{C}{k} (-1)^{B+k+1} \Re\left[\mathcal{M}_\nu\left(\frac{A + j2\pi(B + k + 1)}{2\nu_{th}}\right)/[A + j2\pi(B + k + 1)]\right].$$

$E(A)$ and $E(B, C)$ represent a discretization error and an overall truncation error, respectively. A, B, and C can be set to meet the desired error bound.

B. The saddle-point integration method

Since the CDF of ν is the inverse Laplace transform of $\frac{\mathcal{M}_\nu(s)}{s}$, the outage probability (the CDF evaluated at $\nu = \nu_{th}$) can be calculated as

$$P_{out} = F_\nu(\nu_{th}) = \int_{c-j\infty}^{c+j\infty} \frac{\mathcal{M}_\nu(s)}{s} e^{\nu_{th} s} \frac{ds}{2\pi j}, \qquad 0 < c < c_u \tag{3.33}$$

where c_u is the limit of the region of convergence of the Laplace transform. Helstrom [38] suggested a simple method for evaluating (3.33) via saddle point integration technique, viz.,

$$F_\nu(\nu_{th}) = \int_C e^{\Psi(s)} \frac{ds}{2\pi j} \tag{3.34}$$

where C denotes the path of integration that passes through a saddle point s_0 of the integrand on the $\Re[s]$ axis (i.e., $\Psi'(s)|_{s=s_0} = \frac{d\Psi(s)}{ds}|_{s=s_0} = 0, \quad 0 < s_0 < c_u$), and the "phase" is given by

$$\Psi(s) = ln(\mathcal{M}_\nu(s)) + \nu_{th} s - ln(s) \tag{3.35}$$

Thus the numerical evaluation of (3.34) can be approximated as [39]

$$F_\nu(\nu_{th}) \simeq [2\pi\Psi''(s_0)]^{-1/2} e^{\Psi(s_0)} \tag{3.36}$$

3.3 Numerical Results

In this section, we present selected numerical results to illustrate the effects of branch correlations on the performance of EGC receiver in equally correlated Nakagami-m fading channels based on the analytical results derived in the preceding sections. These plots were obtained with Gauss-Chebychev quadrature (GCQ) approximation of (3.3). Based on our experiments, it was observed that for small m ($m < 2$), small ρ_γ ($\rho_\gamma \leq 0.5$), large $\overline{\gamma}$ (> 4dB), and small/moderate L values, only the first 8 terms of the infinite series (3.21) are needed to achieve a relative error less than 0.2%.

Figure 3.1 illustrates the average bit error probability of binary phase shift keying (BPSK) with a 3-branch EGC for different power correlation coefficients $\rho_\gamma = 0$, 0.5, and 0.8. Simulation results using the technique discussed in [43] were also included for comparison and as a sanity check on the accuracy of our derivations. We observe that the simulation results are in agreement with the curves generated with our analytical expressions. We also observe that, at ASEP 10^{-2}, the penalty over independent fading case is approximately 2.3 dB for $m = 1.5$, 3.2 dB for $m = 1$, and 4.5 dB for $m = 0.5$ when power correlation coefficient $\rho_\gamma = 0.8$. From this, we can conclude that the detrimental effect of branch correlation is much more pronounced when the channel experiences more severe fading. Moreover, different from the performance trend of EGC in equally correlated Rice channels reported in [29], we did not notice any cross-over between the performance curves at high SNR region (i.e. EGC always performs better in a less severely faded channel regardless of the mean branch SNR for a specified ρ_γ. This is because the power correlation coefficient for Nakagami-m fading is given by $\rho_\gamma = \rho^2$ where ρ is the cross-correlation coefficient between the underlying complex Gaussian random variables. On the other hand, $\rho_\gamma = \rho(2K + \rho)/(2K + 1)$ for Rice

fading with Rice factor K).

Figure 3.2 shows the effect of branch correlation on the ASEP performance of QPSK in a Nakagami-m fading channel ($m = 0.5$) for different diversity orders with $\rho_\gamma = \{0, 0.1, 0.25, 0.5, 0.8\}$. Solid lines represent the ASEP with the diversity order $L = 5$ and the dotted lines represent the ASEP with the diversity order $L = 3$. We observe that the penalty over the independent fading case at ASEP 10^{-2} is 4.8 dB for $L = 3$ and 5.8 dB for $L = 5$ when power correlation coefficient $\rho_\gamma = 0.8$. This trend illustrates that the deleterious effect of correlation on EGC receiver increases as the order of diversity increases.

Figure 3.3 shows the comparison between the performance of the maximal ratio combining (MRC) and EGC combiner with diversity order $L = 2$ and 4 for BPSK over Nakagami-m fading channel with $m = 0.5$. Although the performance difference between MRC and EGC receiver increases with the increasing diversity order, the penalty over independent fading case when $\rho_\gamma = 0.6$ and $m = 0.5$ is almost the same for both MRC and EGC. Figure 3.4 shows the performance comparison between MRC and EGC receiver with diversity order $L = 4$ for QPSK over Nakagami-m channels with different fading indices ($m = 0.5$ and 1.2). From this figure, we observed the difference in MRC and EGC performance curves increases as the fading index m decreases. This may be attributed to the ability of MRC to effectively mitigate the deep fades as compared to EGC.

Figure 3.5 shows the impact of branch correlation on the outage probability of EGC receiver with equally correlated inputs in a Nakagami-m fading channel ($m = 2$) for L =2 and $L = 4$. These curves were generated by using Abate's method for evaluating the Bromwich integral with parameters A, B, and C set to 30, 18, and 24, respectively [36]. Mathematical software was used for the numerical evaluation which provides flexibility in numerical precision. From this figure, one may conclude that it may be desirable to equip mobile terminals with four closely spaced antenna elements (even up to $\rho_\gamma = 0.8$) rather than using two antenna elements that are spaced sufficiently far apart. Figure 3.6 shows the outage probability of third order EGC receiver over equally correlated Nakagami-m fading channels for

$m = 1$ and 3. Results generated using numerical inversion of Laplace transform (3.32) and saddle-point integration method (3.27) are in good agreement. Based on our experiments, we suggest the use of the saddle point integration technique owing to its numerical stability (less susceptible to roundoff errors) and computational efficiency.

3.4 Chapter Summary

In this chapter, we have derived a new analytical framework for characterizing the performance of multi-branch coherent EGC receiver with equally correlated inputs over Nakagami-m fading channels. In contrast to [27]-[30], we have utilized a characteristic function method for both ASEP and outage analysis. This facilitates efficient evaluation of a broad class of digital modulation schemes over a myriad of fading environments. Also, we observed that the detrimental effect of correlation on EGC receiver increases as the fading index m decreases and as the diversity order increases.

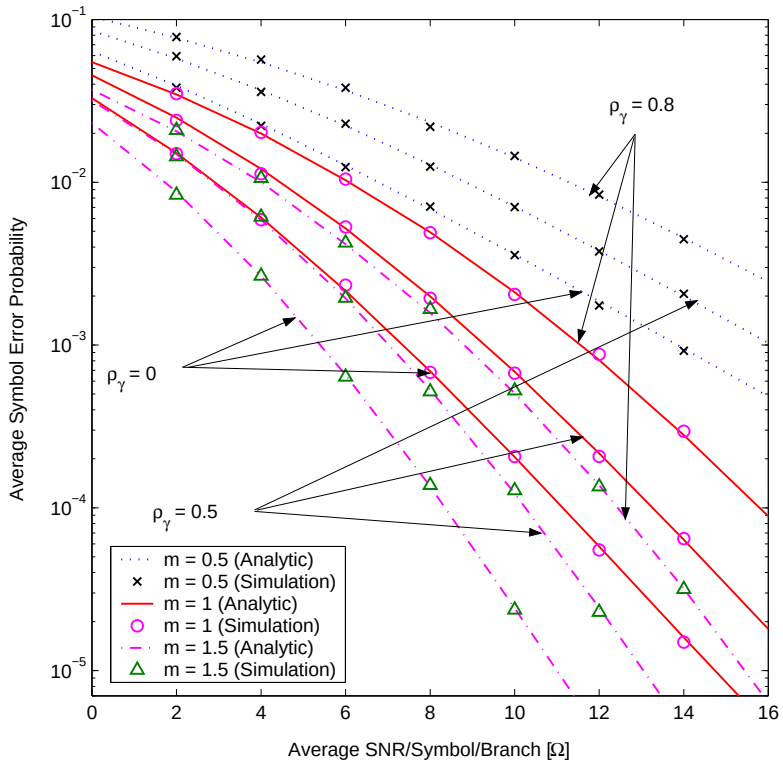

Figure 3.1: Simulation and analytical results for average symbol error probability for coherent BPSK employing third-order ($L = 3$) EGC diversity over equally correlated Nakagami-m fading channels with fading index $m = 0.5$, 1, and 1.5 and different power correlation coefficient ρ_γ.

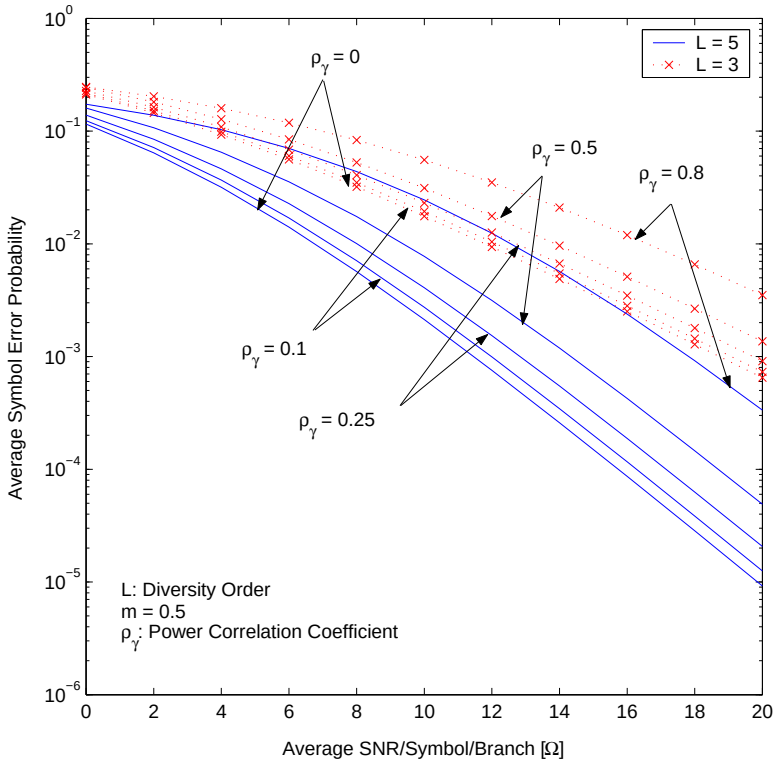

Figure 3.2: Average symbol error probability for coherent QPSK employing third-order ($L = 3$) and fifth-order ($L = 5$) EGC diversity over equally correlated Nakagami-m fading channels with fading index $m = 0.5$ and different power correlation coefficient ρ_γ.

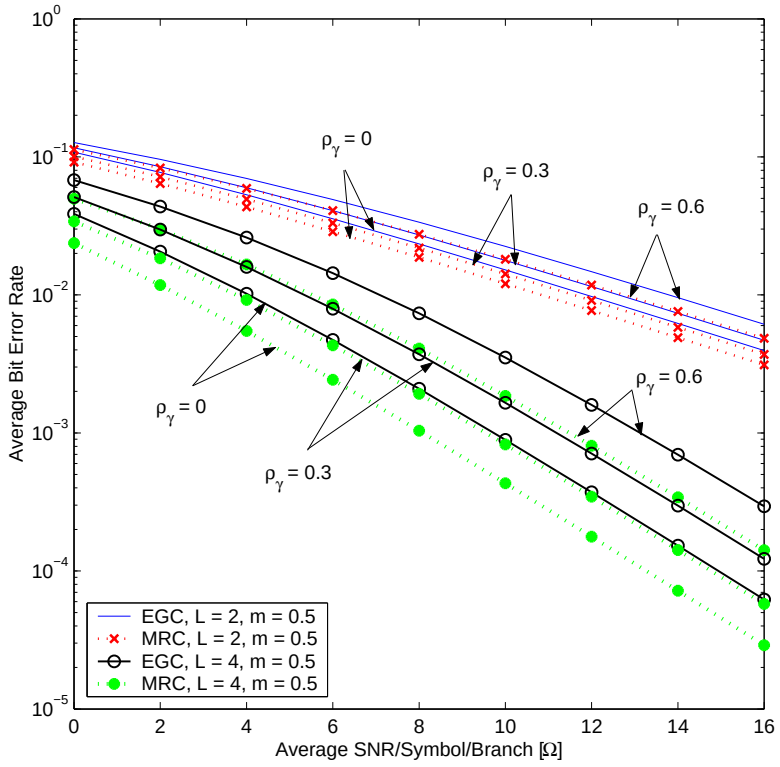

Figure 3.3: Comparison of second-order and forth-order EGC and MRC diversity receiver performance for coherent BPSK over Nakagami-m fading channels with power correlation coefficient $\rho_\gamma = 0, 0.3, 0.6$ and fading index $m = 0.5$.

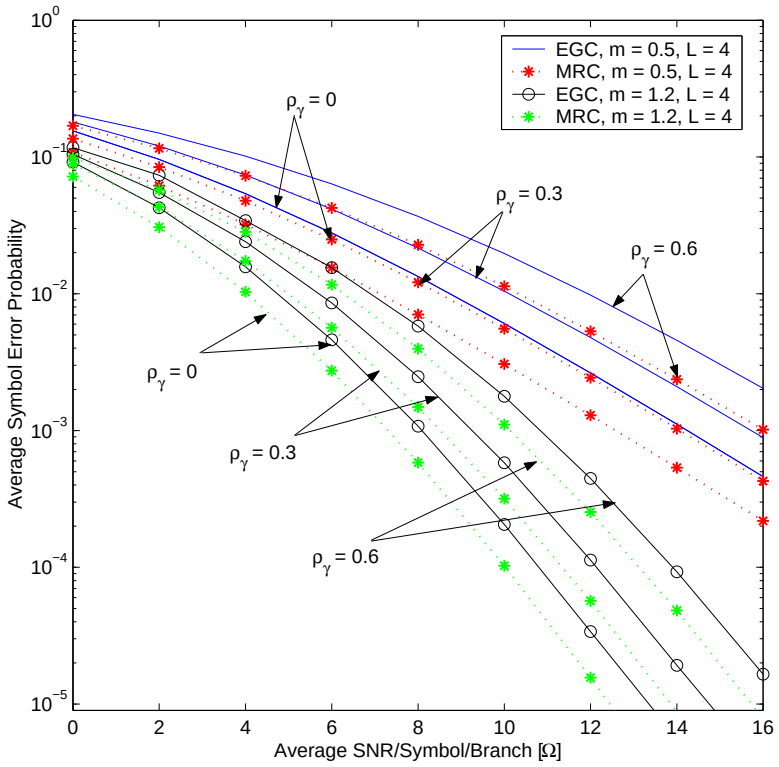

Figure 3.4: Comparison of fourth-order EGC and MRC receiver performance for coherent QPSK over correlated Nakagami-m fading channels with power correlation coefficient $\rho_\gamma = 0, 0.3, 0.6$ and fading index $m = 0.5, 1.2$.

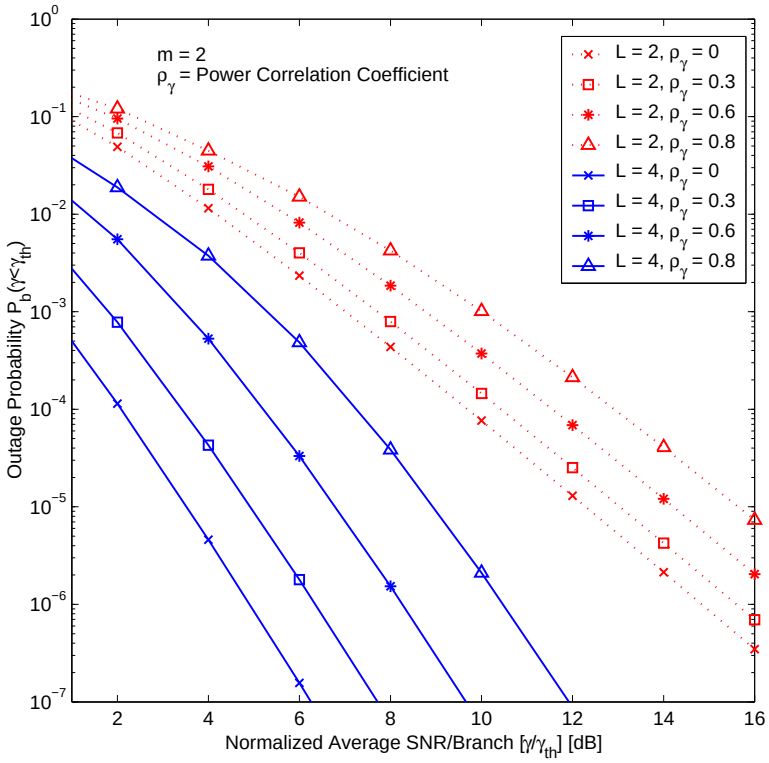

Figure 3.5: Outage probability with second-order and fourth-order EGC versus normalized average SNR γ/γ_{th} over equally correlated Nakagami-m fading channel with fading index $m = 2$.

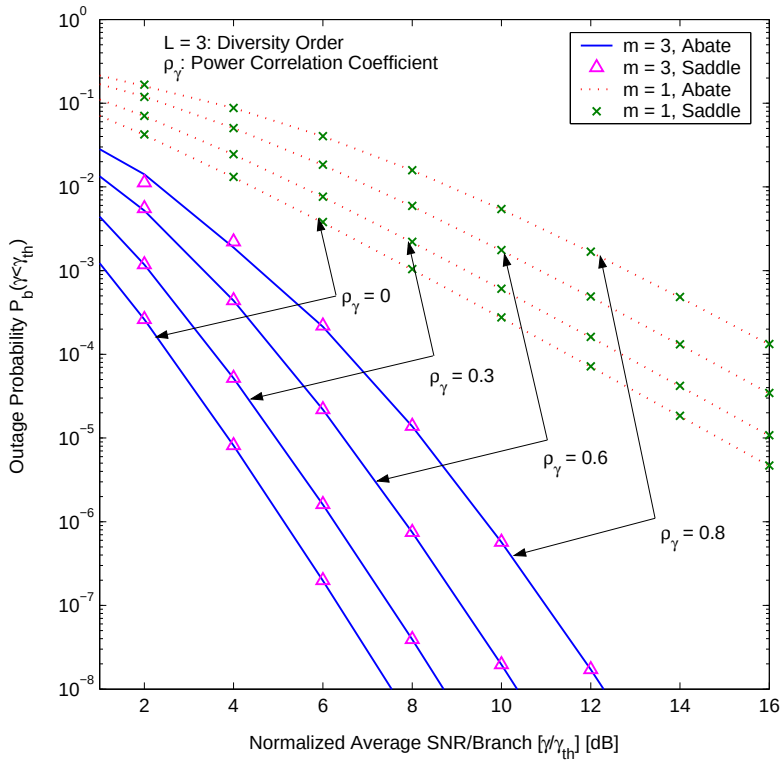

Figure 3.6: Outage probability with third-order EGC versus normalized average SNR γ/γ_{th} over equally correlated Nakagami-m fading channels with fading index $m = 1$ and 3 by using Abate's numerical inversion and saddle-point integration.

Chapter 4

On the Performance Evaluation of Normalized Threshold-Based GSC(μ,L) in Equally Correlated Nakagami Fading

4.1 Introduction

Diversity combining techniques exploit the replicas of transmitted signals to improve transmitted signal fidelity. Therefore, the performance of a system employing diversity combining techniques improves as the number of diversity branches increases. However, the relative diversity improvement diminishes with the increasing diversity order. Also, combining all the available diversity branches might not be appropriate when a large number of diversity paths are available for several obvious reasons. Motivated by these facts, a generalized selection combining technique that combines N branches with the largest instantaneous signal-to-noise ratios (SNRs) out of L available diversity branches (hereafter, referred to it as GSC(N,L) re-

ceiver) has been proposed, aimed at achieving a good design trade-off in terms of performance and implementation complexity (see [44]-[48] and references therein). While the GSC(N,L) scheme has a fixed processing complexity, it suffers from the fact that it potentially discards branches which may improve the receiver performance, or alternatively, includes some weak branches at the expense of processing power consumption [49]-[53]. In [49] and [50] a normalized threshold-based GSC (NT-GSC(μ,L)), which alleviates the above-mentioned problem by combining the branches whose relative branch strength (the ratio of the SNR of each branch to that of the best branch with maximum SNR) exceeds a specified normalized threshold μ (where $0<\mu\leq 1$) was proposed. When the value of μ equals 0 or 1, NT-GSC(μ,L) becomes maximal ratio combining (MRC) or selection combining (SC), respectively.

Analytical studies of NT-GSC(μ,L) have been developed in [51] for independent and identically distributed (i.i.d.) fading statistics, and in [52] and [53] for independent but non-identically distributed fading. These previous studies have been restricted to independent fading statistics among the diversity branches. However, experimental studies in [54]-[18] reveal that the envelope correlation of typical diversity implementations may range between 0.1 to 0.8 depending on the antenna configuration and operating environments. Therefore, any performance analysis must be revamped to account for the effect of correlation between diversity paths. Taking the correlation among branches into account, [41] analyzes the performance of the GSC(N,L) receiver and [56] investigates NT-GSC(μ,L) both in equally correlated Nakagami-m fading channels. However, these results are restricted to positive integer values of m.

In this chapter, we extend the previous work [56] for an NT-GSC(μ,L) combining scheme by allowing arbitrary real values of m (where $m \geq 0.5$) in the analytical solution. Note that this extension can also be applied to the work in [41]. Also, we exploit the novel transformation of a set of equally correlated complex Gaussian random variables (RVs) into a set of conditionally independent complex Gaussian RVs discussed in [30] to tackle the problem from another approach. This second approach allows us to analyze the performance of the NT-GSC(μ,L) receiver more efficiently when m is a positive integer value and the

diversity order L is large.

4.2 System Model

The instantaneous SNR of the k^{th} diversity branch is defined as [41]

$$\gamma_k = \alpha_k^2 \frac{E_s}{N_0},\ k = 1, 2, \ldots, L \tag{4.1}$$

where E_s represents average symbol energy, α_k represents the amplitude of the channel gain which is Nakagami-m distributed, N_0 represents Gaussian thermal noise, and L is the total number of available diversity branches. Let $\gamma_{k:L}$ denote the instantaneous branch SNRs per symbol in decreasing order of magnitude ($\gamma_{1:L} > \gamma_{2:L} > \cdots > \gamma_{L:L}$) and denote the predetermined normalized threshold by μ ($0 \leq \mu \leq 1$). Then, a NT-GSC(μ,L) combiner coherently combines the branches whose instantaneous SNRs per symbol γ_k $(1, 2, \ldots, L)$, equal or exceed the product of the normalized threshold μ and the largest instantaneous SNR per symbol $\gamma_{L:L}$. The output instantaneous SNR per symbol of a NT-GSC(μ,L) combiner is then given by [51]

$$\gamma_{T(N_c)} = \sum_{k=1}^{N_c} \gamma_{k:L},\ N_c = 1, \ldots, L \tag{4.2}$$

where N_c is an integer random variable (RV) that represents the number of branches being combined [51].

Since the NT-GSC(μ,L) combiner outputs corresponding to each integer value of N_c represents disjoint events and form a partition of the probability space, the average symbol error probability (ASEP) of NT-GSC(μ,L), P_e, can be written as [56]

$$P_e = \sum_{N=1}^{L} P\{e, N_c = N\} \tag{4.3}$$

where $P\{e, N_c = N\}$ is the ASEP of NT-GSC(μ,L) corresponding to the event that N branches satisfying $\gamma_{1:L} > \gamma_{2:L} > \cdots > \gamma_{N_c} \geq \mu\gamma_{1:L} > \gamma_{N_c+1} > \cdots > \gamma_{L:L}$ are selected.

The outage probability P_{out} is defined as the probability that the instantaneous receiver output SNR falls below a specified threshold SNR γ_{th}. In a similar way, the outage probability of NT-GSC(μ,L) can be calculated as [56]

$$P_{out}(\gamma_{th}) = \sum_{N=1}^{L} P\{\gamma_{T(N)} < \gamma_{th}, N_c = N\} \tag{4.4}$$

where γ_{th} represents the threshold of the combiner output instantaneous SNR per symbol, $\gamma_{T(N)}$, and $P\{\gamma_{T(N)} < \gamma_{th}, N_c = N\}$ represents the outage probability of the NT-GSC(μ,L) receiver corresponding to the event that N branches are selected.

4.3 MGF of $\gamma_{T(N)}$ for Arbitrary Values of Fading Index m ($\geq$0.5)

Let $\mathcal{M}_{\gamma_{T(N)}}(s)$ denote the moment generating function (MGF) of the combiner output $\gamma_{T(N)} = \sum_{k=1}^{N} \gamma_{k:L}$. The MGF of $\gamma_{T(N)}$ is then given by [56]

$$\begin{aligned}
&\mathcal{M}_{\gamma_{T(N)}}(s) \\
&= \int_0^{\infty} d\gamma_{1:L} \int_{\mu\gamma_{1:L}}^{\gamma_{1:L}} d\gamma_{2:L} \cdots \int_{\mu\gamma_{1:L}}^{\gamma_{N-1:L}} d\gamma_{N:L} \\
&\times \int_0^{\mu\gamma_{1:L}} d\gamma_{N+1:L} \cdots \int_0^{\gamma_{L-1:L}} e^{-s\sum_{i=1}^{N}\gamma_{i:L}} \\
&\times f_{\gamma_{1:L},\ldots,\gamma_{L:L}}(\gamma_{1:L}, \ldots, \gamma_{L:L}) d\gamma_{1:L}
\end{aligned} \tag{4.5}$$

where $f_{\gamma_{1:L},\ldots,\gamma_{L:L}}(\gamma_{1:L}, \ldots, \gamma_{L:L})$ is the joint probability density function (PDF) of the ordered instantaneous branch SNRs per symbol. Applying the identity, which holds for any arbitrary real values of m,

$$(1+x)^{-m} = {}_2F_1(m, 1; 1; -x) = \sum_{p=0}^{\infty} \frac{\Gamma(m+p)}{\Gamma(m)p!}(-x)^p \tag{4.6}$$

where $\Gamma(\alpha) = \int_0^{\infty} t^{\alpha-1}e^{-t}dt$, to [41, Eq. (14),(18)] and [56, Eq. (6)], we can get the MGF of $\gamma_{T(N)}$ for any real values of m as follows

$$\mathcal{M}_{\gamma_{T(N)}}(s) = \left(\frac{1-\rho}{1+[L-1]\rho}\right)^m \sum_{p=0}^{\infty} \frac{\Gamma(m+p)}{\Gamma(m)p!} \left(\frac{\rho}{1+[L-1]\rho}\right)^p$$

$$\times \sum_{\substack{0\le l_1,l_2,\ldots,l_L\le p \\ l_1+l_2+\cdots+l_L=p}} \frac{p!}{l_1!\cdots l_L!}$$
$$\times \sum_{\sigma\in T_{L,N}} \int_0^\infty e^{-sax} g(x, l_{\sigma(1)}+m, 1) \prod_{i=N+1}^{L} F_{\sigma(i)}(\mu x)$$
$$\times \prod_{k=2}^{N} [\mathcal{M}_{\gamma_{\sigma(k)}}(sa, x) - \mathcal{M}_{\gamma_{\sigma(k)}}(sa, \mu x)] dx \tag{4.7}$$

where the correlation coefficient $\rho = \sqrt{\rho_\gamma}$ is given by [41, Eq. (7)], $g(x, \nu, \beta) = \frac{x^{\nu-1}e^{-x/\beta}}{\beta^\nu \Gamma(\nu)}$, $a = \frac{\overline{\gamma}(1-\rho)}{m}$ ($\overline{\gamma}$ is the average branch SNR per symbol), $T_{L,N}$ is a subset of S_L (the set of all permutations of the integers $\{1, \ldots, L\}$) whose elements $\sigma(i)$ satisfies $\sigma(1) < \sigma(2) < \cdots < \sigma(N)$ and $\sigma(N+2) < \cdots < \sigma(L)$, and $F_{\sigma(k)}(x)$ and $\mathcal{M}_{\gamma_{\sigma(k)}}(s, x)$ is the cumulative density function (CDF) and the marginal MGF of the random variable $\gamma_{k:L}$, respectively, defined by

$$\begin{aligned} F_{\sigma(k)}(x) &= \int_0^x g(x, l_{\sigma(k)}+m, 1) dx \\ &= \frac{1}{\Gamma(l_{\sigma(k)}+m)} \gamma(l_{\sigma(k)}+m, x) \end{aligned} \tag{4.8}$$

$$\begin{aligned} \mathcal{M}_{\gamma_{\sigma(k)}}(s, x) &= \int_0^x e^{-sx} g(x, l_{\sigma(k)}+m, 1) dx \\ &= \frac{\gamma(l_{\sigma(k)}+m, (s+1)x)}{\Gamma(l_{\sigma(k)}+m)(s+1)^{l_{\sigma(k)}+m}} \end{aligned} \tag{4.9}$$

where $\gamma(\alpha, x) = \int_0^x t^{\alpha-1}e^{-t}dt$. When m is a positive integer value, (4.8) and (4.9) reduce to

$$F_{\sigma(k)}(x) = 1 - e^{-x} \sum_{k=0}^{l_{\sigma(k)}+m-1} \frac{x^k}{k!} \tag{4.10}$$

and

$$\begin{aligned} \mathcal{M}_{\gamma_{\sigma(k)}}(s, x) = &\frac{1}{(s+1)^{\sigma(k)}+m} \\ &\times \left(1 - e^{-(s+1)x} \sum_{k=0}^{l_{\sigma(k)}+m-1} \frac{(s+1)^k x^k}{k!} \right) \end{aligned} \tag{4.11}$$

respectively. Equations (4.10) and (4.11) are equivalent to [56, Eq. (7)] and [56, Eq. (8)], respectively. Hence, (4.7) extends the previous result for the MGF of $\gamma_{T(N)}$ [56, Eq. (6)] by allowing arbitrary values of fading index m ($m \ge 0.5$).

4.4 MGF of $\gamma_{T(N)}$ for Positive Integer Values of m

Assuming the fading indices m at different L diversity branches are identical and take on integer values, the equally correlated Nakagami-m fading envelopes can be represented by a set of Lm zero-mean complex Gaussian RVs [30]

$$\begin{aligned} G_{kj} = &\left(\sqrt{1-\rho}X_{kj} + \sqrt{\rho}X_{0j}\right) \\ &+i\left(\sqrt{1-\rho}Y_{kj} + \sqrt{\rho}Y_{0j}\right) \end{aligned} \tag{4.12}$$

where $k\in\{1,\ldots,L\}$, $j\in\{1,\ldots,m\}$, and X_{kj}, $Y_{kj} \sim N(0,1/2)$, $k = 0,1,\cdots,L$, and $j = 1,\ldots,m$, are independent. The cross-correlation coefficient between G_{kj} and G_{ln} is given by

$$\rho_g = \frac{E[G_{kj}G_{ln}^*]}{\sqrt{E[|G_{kj}|^2]E[|G_{ln}|^2]}} = \begin{cases} \rho, & \text{if } k\neq l \text{ and } j = n \\ 0, & \text{if } j\neq n \end{cases} \tag{4.13}$$

For any fixed k, $G_{kj}\sim C(0,1/2)$, $j = 1,\ldots,m$, are independent. Hence, the branch power R_k defined by

$$R_k = \sum_{j=1}^{m} |G_{kj}|^2 \tag{4.14}$$

is the sum of squares of m independent Rayleigh envelopes with cross-correlation coefficient

$$\rho_r = \frac{E[R_kR_l]}{\sqrt{E[R_K^2]E[R_l^2]}} = \rho^2,\ k\neq l. \tag{4.15}$$

Therefore, $\sqrt{R_k}$ is a set of equally correlated Nakagami-m fading envelopes with mean-square value $E[R_k] = m$. If we fix $X_{0j} = x_{0j}$ and $Y_{0j} = y_{0j}$, $j = 1,\ldots,m$, the branch power $R_k\sim\chi_{2m}(\sqrt{(}\rho\sum_{j=1}^{m}(x_{0j}^2 + y_{0j}^2),(1-\rho)/2))$ is independent conditioned on $T\sim\chi_{2m}(0,1/2)$, where $T = \sum_{j=1}^{m}(x_{0j}^2 + y_{0j}^2)$. We can now derive the PDF, CDF, and the marginal MGF of γ_k conditioned on T as follows:

$$\begin{aligned} f_{\gamma_k|T}(x) &= \left(\sqrt{\frac{m}{\overline{\gamma}(1-\rho)}}\right)^{m+1}\left(\sqrt{\frac{\rho t}{1-\rho}}\right)^{1-m}(\sqrt{x})^{m-1} \\ &\times \exp\left(-\frac{\rho t}{1-\rho} - \frac{mx}{\overline{\gamma}(1-\rho)}\right) \\ &\times I_{m-1}\left(2\sqrt{\frac{\rho t m x}{\overline{\gamma}(1-\rho)^2}}\right) \end{aligned} \tag{4.16}$$

$$F_{\gamma_k|T}(x) = 1 - Q_m\left(\sqrt{\frac{2\rho t}{1-\rho}}, \sqrt{\frac{2mx}{\overline{\gamma}(1-\rho)}}\right) \tag{4.17}$$

$$\begin{aligned}\mathcal{M}_{\gamma_k|T}(s,x) &= \left(\tfrac{m}{m+s\overline{\gamma}(1-\rho)s}\right)^m \; e^{-\frac{\rho t\overline{\gamma}s}{m+\overline{\gamma}(1-\rho)s}} \\ &\times Q_m\left(\sqrt{\tfrac{2\rho mt}{(1-\rho)(m+\overline{\gamma}(1-\rho)s)}}, \sqrt{\tfrac{2(m+\overline{\gamma}(1-\rho)s)x}{\overline{\gamma}(1-\rho)}}\right)\end{aligned} \tag{4.18}$$

where $I_m(x)$ denotes the m^{th}-order modified Bessel function of the first kind, and

$$\begin{aligned}&Q_m(\sqrt{2a}, \sqrt{2b}) \\ &= \int_b^\infty \left(\sqrt{\frac{x}{a}}\right)^{m-1} \exp(-a-x) I_{m-1}(2\sqrt{ax}) dx\end{aligned} \tag{4.19}$$

is the m^{th}-order Marcum Q-function. Once we obtain the conditional PDF, CDF, and marginal MGF conditioned on T, we can immediately derive the MGF of $\gamma_{k|T}$ and, then, the MGF of $\gamma_{T(N)}$ by averaging the conditional statistics over the distribution of T. The MGF of $\gamma_{k|T}$ can be expressed as

$$\begin{aligned}\mathcal{M}_{\gamma_{T(N)}|T}(s) &= N\binom{L}{N}\int_0^\infty e^{-sx} f_{\gamma_k|T}(x)[F_{\gamma_k|T}(\mu x)]^{L-N} \\ &\times \; [\mathcal{M}_{\gamma_k|T}(s,\mu x) - \mathcal{M}_{\gamma_k|T}(s,x)]^{N-1} dx\end{aligned} \tag{4.20}$$

where $f_{\gamma|T}(x)$, $F_{\gamma|T}(x)$, and $\mathcal{M}_{\gamma|T}(s,x)$ are (4.16), (4.17), and (4.18), respectively. The MGF of the output of NT-GSC(μ,L) receiver over equally correlated Nakagami-m channels with positive integer fading index m can be derived by averaging the conditional MGF $\mathcal{M}_{\gamma_{gsc|T}}(s)$ in (4.20) over the distribution of T. The result is

$$\mathcal{M}_{\gamma_{T(N)}}(s) = \int_0^\infty \mathcal{M}_{\gamma_{T(N)}|T}(s) f_T(t) dt \tag{4.21}$$

where

$$f_T(t) = \frac{1}{\Gamma(m)} t^{m-1} e^{-t}, \; t \geq 0 \tag{4.22}$$

Although (4.21) is restricted to positive integer values of m, when m is a positive integer and the number of diversity branch L increases ($L > 5$), using (4.21) for ASEP and outage calculation is computationally more efficient than using (4.7) due to the summation $\sum_{\substack{0\leq l_1,l_2,\ldots,l_L\leq p \\ l_1+l_2+\cdots+l_L=p}}$ in (4.7) at high correlation ρ values ($\rho > 0.7$).

4.5 ASEP and Outage Probability

4.5.1 ASEP

Since the MGF of NT-GSC(μ,L) receiver over equally correlated Nakagami-m fading channels are derived in the previous section, the MGF approach [58],[62] can be used to investigate the effects of correlation and normalized threshold on the performance of NT-GSC(μ,L) receiver. The ASEP ($Pe, N_c = N$) of M-ary phase-shift-keying (PSK) with coherent NT-GSC(μ,L) receiver is given by

$$P_e = \frac{1}{\pi}\sum_{N=1}^{L}\int_0^{\pi-\frac{\pi}{M}} \mathcal{M}_{\gamma_{T(N)}}\left(\frac{\sin^2(\pi/M)}{\sin^2\theta}\right) d\theta \tag{4.23}$$

where M denotes the alphabet size of M-ary signal constellation (for example, $M = 2$ for binary phase-shift keying and $M = 4$ for quadrature phase-shift keying). Also, the ASEP of M-ary differential phase-shift keying (DPSK) with coherent NT-GSC(μ,L) receiver can be expressed as

$$P_e = \frac{1}{\pi}\sum_{N=1}^{L}\int_0^{\pi-\frac{\pi}{M}} \mathcal{M}_{\gamma_{T(N)}}\left(\frac{\sin^2(\pi/M)}{1+\cos(\pi/M)\cos\theta}\right) d\theta \tag{4.24}$$

4.5.2 Outage Probability

The outage probability $P_{out}\{\gamma_{th}, N_c = N\}$ is defined as the probability that the instantaneous receiver output SNR falls below a specified threshold SNR γ_{th} when N branches are selected for combining i.e.,

$$P_{out}\{\gamma_{th}, N_c = N\} = \int_0^{\gamma_{th}} p_{\gamma_{T(N)}}(x)dx = F_{\gamma_{T(N)}}(\gamma_{th}) \tag{4.25}$$

where $\gamma_{T(N)}$ is the instantaneous NT-GSC(μ,L) output SNR when $N_c = N$, $p_{\gamma_{T(N)}}(x)$ is the PDF of $\gamma_{T(N)}$, and $F_{\gamma_{T(N)}}(\cdot)$ is the CDF of the output SNR of NT-GSC(μ,L) receiver $\gamma_{T(N)}$. However, since the CDF $F_{\gamma_{T(N)}}(x)$ is not available while the MGF $\mathcal{M}_{\gamma_{T(N)}}(s)$ is readily

available, we used Abate's numerical inversion method of Laplace transform of probability distribution [36]. Then, the CDF of $\gamma_{T(N)}$ evaluated at γ_{th} can be computed as

$$\begin{aligned} & P_{out}\{\gamma_{th}, N_c = N\} \\ & \simeq 2^{1-C} e^{A/2} \sum_{k=0}^{C} \binom{C}{k} \sum_{b=0}^{B+k} (-1)^b \alpha_b \\ & \times \Re\left[\mathcal{M}_{\gamma_{T(N)}}\left(\frac{A + j2\pi b}{2\gamma_{th}} \right) / (A + j2\pi b) \right] \end{aligned} \tag{4.26}$$

where $\alpha_b = \begin{cases} 1/2, & b = 0 \\ 1, & b = 1, 2, \ldots \end{cases}$ and $\Re[\cdot]$ denotes the real part. A, B, and C can be set to meet the desired error bound for numerical inversion. The outage probability of NT-GSC(μ,L) receiver is then

$$\begin{aligned} & P_{out}(\gamma_{th}) \\ & \simeq \sum_{N=1}^{L} 2^{1-C} e^{A/2} \sum_{k=0}^{C} \binom{C}{k} \sum_{b=0}^{B+k} (-1)^b \alpha_b \\ & \times \Re\left[\mathcal{M}_{\gamma_{T(N)}}\left(\frac{A + j2\pi b}{2\gamma_{th}} \right) / (A + j2\pi b) \right] \end{aligned} \tag{4.27}$$

4.6 Computational Results and Remarks

In this section, we present selected numerical results to illustrate the effect of branch correlations and normalized threshold on NT-GSC(μ,L) receiver over equally correlated Nakagami-m fading channels with the aid of analytical results derived in the preceding sections.

Figure 4.1 shows the ABEP of DBPSK for NT-GSC(μ,4) over equally correlated Nakagami-m fading channels with fading index $m = 1.3$ as a function of the normalized threshold μ. As expected, the ABEP increases with increasing μ values due to fewer diversity branches combined. However, the performance degradation due to branch correlation is greater at low values of μ, which corresponds to the case that more diversity branches are combined, than higher values of μ. Also, the relative gain by decreasing the value μ diminishes as μ

decreases. This is equivalent to increasing the number of combined branches since $\mu = 1$ corresponds to SC and $\mu = 0$ corresponds to MRC.

Figure 4.2 illustrates the effect of branch correlation and the normalized threshold μ on the ABEP performance of NT-GSC(μ,4) at average SNR per branch $\overline{\gamma}_{gsc} = 7$ dB as a function of the correlation coefficient ρ for DBPSK modulation. From this figure, we observe that NT-GSC(μ,L) receiver is more sensitive to the variation of the normalized threshold μ at low correlation values than at high correlation values as the normalized threshold μ increases.

Figure 4.3 shows that the ASEP of coherent QPSK of NT-GSC(μ,L) versus the average branch SNR per symbol for fading index $m = 2$, the correlation coefficient $\rho = 0.25$, and the normalized threshold $\mu = 0.3$. Results generated using (4.7) in (4.23) and (4.21) in (4.23) are in good agrement. While (4.7) holds for any real values of $m \geq 0.5$ and (4.21) only holds for positive integer values of m, it is more computationally efficient to use (4.21) when m is an integer value and the correlation value is high ($\rho > 0.7$) with diversity order more than 5. However, if m is not an integer value, (4.7) should be used for evaluating the performance of NT-GSC(μ,L) receiver in equally correlated Nakgami-m fading.

Figure 4.4 shows the outage probability of NT-GSC(μ,L) receiver with Nakgami-m fading index $m = 2$, $\rho = 0.3$, and the number diversity branch $L = 3$. As expected, the outage probability increases as the normalized threshold μ increases.

Finally, the outage probability of NT-GSC(μ,L) receiver is shown in Figure 4.5 for Nakgami-m fading index $m = 2$ and the normalized threshold $\mu = 0.3$ for different values of correlation ρ.

4.7 Conclusion

In this chapter, we extend the previous analytical work presented in [56] to arbitrary values of fading index m. While the previous work is restricted to positive integer values of m, the derived solution in this paper works for any real values of m which is greater or equal to 0.5. Also, we exploit the novel transformation discussed in [30] to expedite the evaluation of the performance of NT-GSC(μ,L) receiver. Although, the second method using transformation of a set of Gaussian RVs is restricted to integer values of m, it turns out that it is computationally efficient when the diversity order increases.

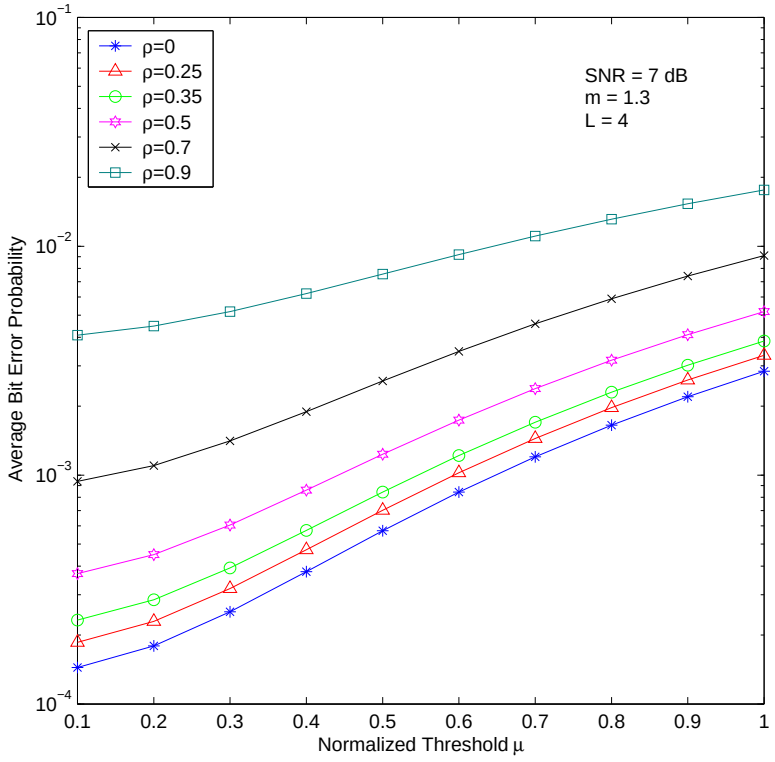

Figure 4.1: Average bit error probability for coherent DBPSK with NT-GSC(μ,4) over equally correlated Nakagami-m fading channels: $\rho = \{0, 0.25, 0.35, 0.5, 0.7, 0.9\}$, $m = 1.3$, and average branch SNR per bit $\overline{\gamma} = 7$ dB.

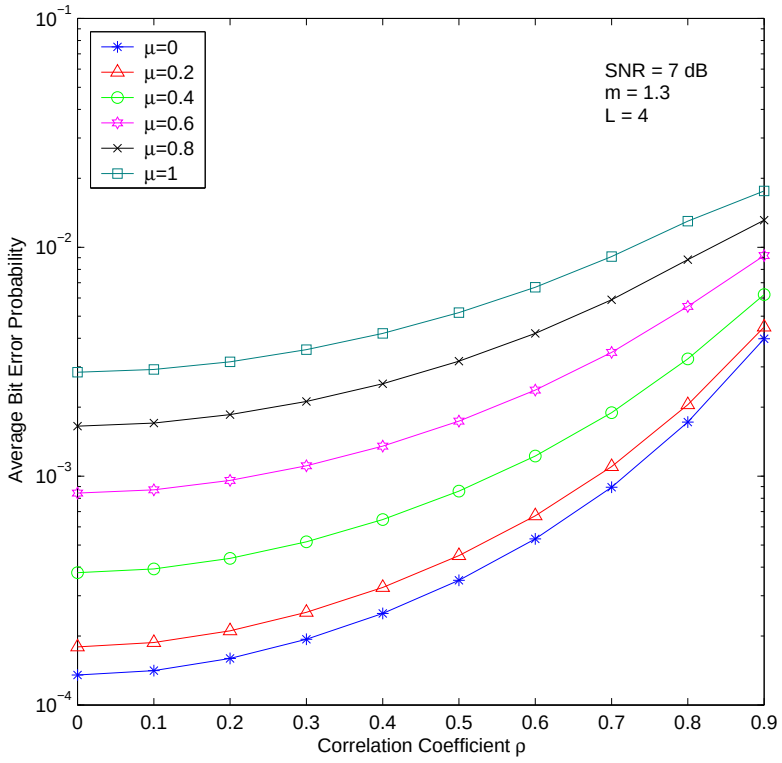

Figure 4.2: Average bit error probability for coherent DBPSK with NT-GSC(μ,4) over equally correlated Nakagami-m fading channels: $\mu = \{0, 0.2, 0.4, 0.6, 0.8, 1\}$, $m = 1.3$, and average branch SNR per bit $\overline{\gamma} = 7$ dB.

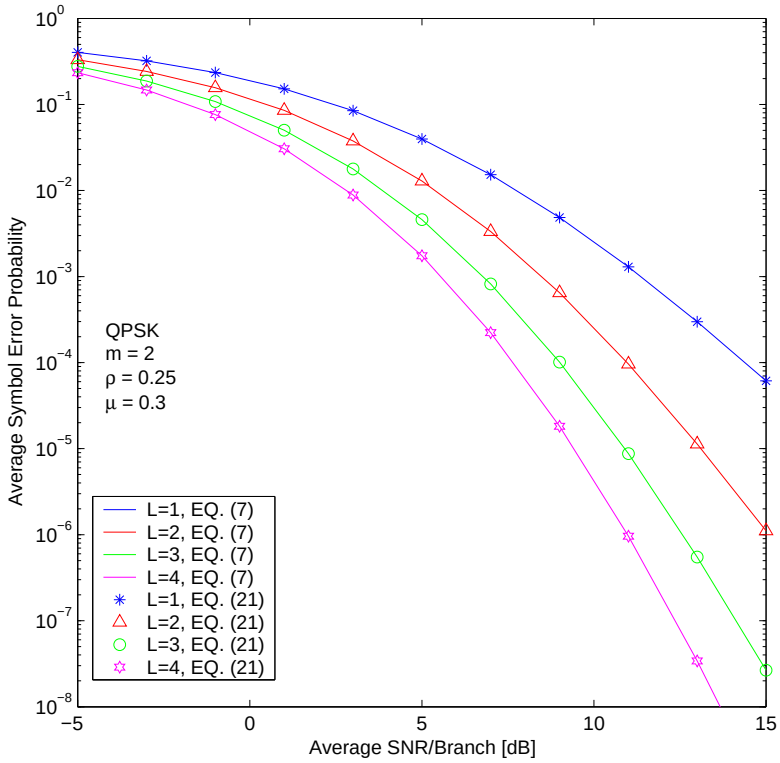

Figure 4.3: the ASEP of coherent QPSK of NT-GSC(μ,L) versus the average branch SNR per symbol for fading index $m = 2$, the correlation coefficient $\rho = 0.25$ and the normalized threshold $\mu = 0.3$.

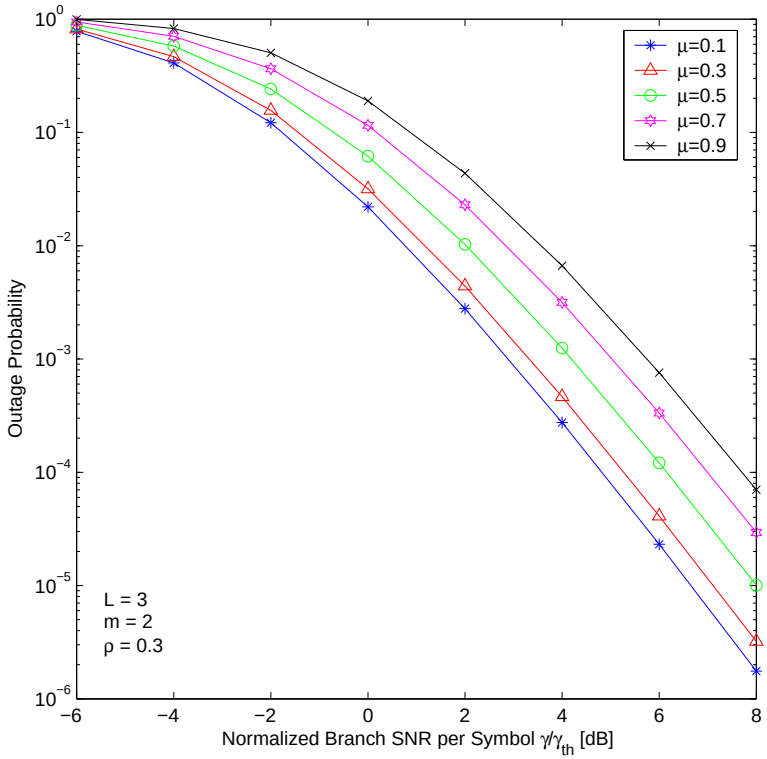

Figure 4.4: The outage probability of NT-GSC(μ,3) over equally correlated Nakagami-m fading with $m = 2$, $\rho = 0.3$, and $\mu = \{0.1, 0.3, 0.5, 0.7, 0.9\}$.

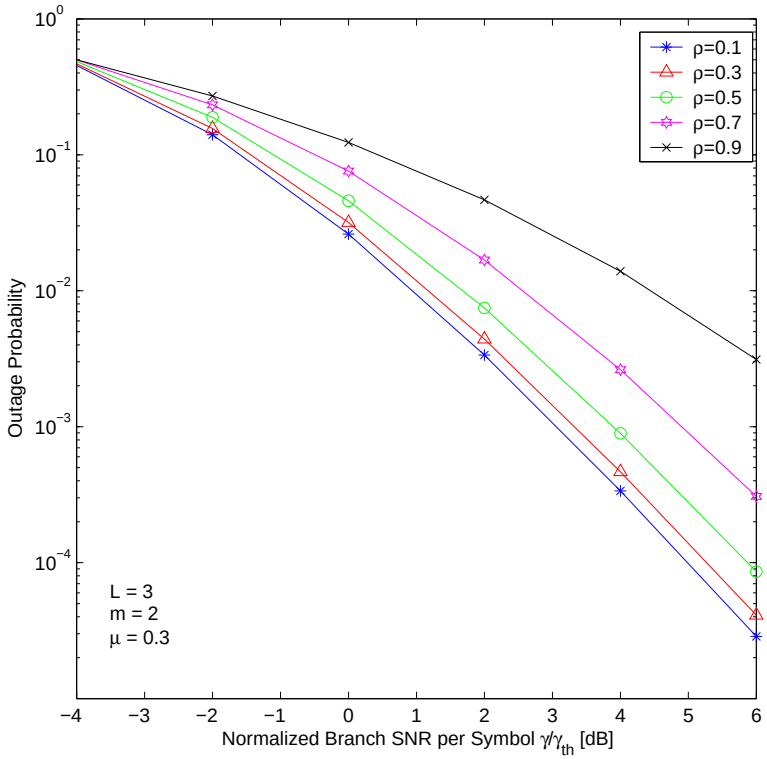

Figure 4.5: The outage probability of NT-GSC(0.3,3) over equally correlated Nakagami-m fading with $m = 2$ and $\rho = \{0.1, 0.3, 0.5, 0.7, 0.9\}$.

Chapter 5

Performance Evaluation of Hybrid Diversity Combining Techniques over Equally Correlated Rice Fading Channels

5.1 Introduction

As pointed out in the previous chapter, classical diversity combining techniques such as maximal ratio combining (MRC), equal gain combining (EGC), and selection combining (SC) may not be appropriate when large number of diversity branches (paths) are available (i.e., ultra-wide bandwidth and millimeter communications) for obvious reasons. In recent years, hybrid diversity combining techniques that process only a subset of available diversity paths have been proposed, aimed at achieving a good design trade-off in terms of performance and implementation complexity (see [44]-[57] and references therein). In [44], a generalized selection combining scheme that combines N branches with the largest instantaneous

signal-to-noise ratios (SNRs) out of L available diversity paths (hereafter, referred to it as GSC(N,L) receiver) was examined. Clearly, GSC(1,L) and GSC(L,L) correspond to the two extremes of SC and MRC receivers, respectively. [49] proposed a normalized threshold GSC (NT-GSC(μ,L)) which combines the branches whose relative branch strength (the ratio of the SNR of each branch to that of the best branch with maximum SNR) exceeds a specified normalized threshold μ (where $0<\mu\leq 1$). The analysis for GSC and NT-GSC has been extended in [45]-[52] for different fading statistics. In [50], Yue proposed and analyzed two variations of hybrid diversity combining schemes, namely NT-GSC(μ,L) and absolute threshold GSC (AT-GSC(μ,L)) which, different from NT-GSC(μ,L), combines all the branches which exceed a fixed absolute threshold. [51] comprehensively analyzed both AT-GSC and NT-GSC over independent fading channels through moment generating function (MGF) approach. [57] proposed a new scheme (modified AT-GSC) where the combiner switches between AT-GSC and selection combining (SC) depending on channel condition.

Note that, however, most of the previous studies have been restricted to independent fading statistics among the diversity branches. Experimental study in [18] reveals that the envelop correlation of typical diversity implementations may range between 0.1 to 0.8 depending on the antenna configuration and operating environments. Turin [54] and Bajwa [55] also showed that correlation coefficients up to 0.6 can exist between adjacent and second adjacent paths in a channel impulse response. Therefore, any performance analysis must be revamped to account for the effect of correlation between diversity paths.

In this chapter, we take a modest step in understanding the effect of branch correlation on the hybrid generalized selection diversity schemes over equally correlated Rice fading channels. Specifically, we exploit the novel transformation of a set of equally correlated complex Gaussian random variables (RVs) into a set of conditionally independent complex Gaussian RVs discussed in [29], [30] to tackle the problem at hand. To the best of our knowledge, only [41], [56] have investigated the effect of branch correlation on GSC(N,L) [41] and NT-GSC(N,L) [56]. However, their analysis is restricted to equally correlated Nakagami-m fading channels. Although one might consider using an approximation for a Rice RV with

Nakgami-m distribution (i.e. $m = (K+1)^2/(2K+1)$), the approximation tends to overestimate receiver performances particulary at high SNRs due to the fact that the tails of the Rice and its Nakgami-m approximation distributions do not fit very closely [46],[60]. Hence, exact performance analysis of hybrid diversity schemes over equally correlated Rice fading channels is desirable.

5.2 Equally Correlated Rice Channel Model

Assuming the Rice factors at different L diversity branches are identical, the equally correlated Rice fading envelopes can be represented by a set of L complex Gaussian RVs [30]

$$\begin{aligned} G_k = &\left(\sqrt{1-\rho}X_k + \sqrt{\rho}X_0 + m_1\right) \\ &+i\left(\sqrt{1-\rho}Y_k + \sqrt{\rho}Y_0 + m_2\right) \end{aligned} \tag{5.1}$$

where $k\in\{1,\ldots,L\}$, $0\leq\rho\leq1$, and X_k, $Y_k \sim N(0,1/2)$, $k=0,1,\cdots,L$, are independent, and m_1+im_2 is the nonzero line of sight (LOS) component. Since $G_k\sim C(m_1+im_2,1/2)$, $|G_k|$ is Rice distributed with the Rice factor and the mean square value given respectively by

$$\begin{aligned} K &= m_1^2+m_2^2 \\ \Omega &= E[|G_k|^2] = 1+K. \end{aligned} \tag{5.2}$$

The cross-correlation coefficient between G_k and G_j ($k\neq j$) is given by

$$\rho = \frac{E\{[G_k - E[G_k]][G_j^* - E[G_j^*]]\}}{\sqrt{E[|G_k-E[G_k]|^2]E[|G_j-E[G_j]|^2]}} \tag{5.3}$$

Letting $T = \left(X_0 + m_1/\sqrt{\rho}\right)^2 + \left(Y_0 + m_2/\sqrt{\rho}\right)^2$ in (5.1), we have

$$|G_k|^2\sim\chi_2\left(\sqrt{(\sqrt{\rho}x_0+m_1)^2+(\sqrt{\rho}y_0+m_2)}, (1-\rho)/2\right). \tag{5.4}$$

Note that the conditional RVs are independent. Suppose $\gamma_k = |G_k|^2E_s/N_0$ is the instantaneous branch signal to noise ratio (SNR) of the k$^{\text{th}}$ diversity path. We can then derive

the probability density function (PDF), cumulative distribution function (CDF), and the marginal MGF of γ_k conditioned on T as follows:

$$\begin{aligned} f_{\gamma_k|T}(x) &= \frac{1+K}{\overline{\gamma}(1-\rho)}\, e^{-\frac{\rho t}{1-\rho}-\frac{(1+K)x}{\overline{\gamma}(1-\rho)}} \\ &\times I_0\left(2\sqrt{\frac{\rho t(1+K)x}{\overline{\gamma}(1-\rho)^2}}\right) \end{aligned} \tag{5.5}$$

$$F_{\gamma_k|T}(x) = 1 - Q\left(\sqrt{\frac{2\rho t}{1-\rho}}, \sqrt{\frac{2(1+K)x}{\overline{\gamma}(1-\rho)}}\right) \tag{5.6}$$

$$\begin{aligned} \mathcal{M}_{\gamma_k|T}(s,x) &= \tfrac{1+K}{1+K+\overline{\gamma}(1-\rho)s}\, e^{-\frac{\rho t\overline{\gamma}s}{1+K+\overline{\gamma}(1-\rho)s}} \\ &\times Q\left(\sqrt{\tfrac{2\rho t(1+K)}{(1-\rho)(1+K+\overline{\gamma}(1-\rho)s)}}, \sqrt{\tfrac{2(1+K+\overline{\gamma}(1-\rho)s)x}{\overline{\gamma}(1-\rho)}}\right) \end{aligned} \tag{5.7}$$

where $I_0(x)$ denotes zero-order modified Bessel function of the first kind, $Q(\sqrt{2a}, \sqrt{2b}) = \int_b^\infty \exp(-a-t) I_0(2\sqrt{at})dt$ is the first-order Marcum Q-function, and $\overline{\gamma} = E[|G_k|^2]\frac{E_s}{N_0} = (1+K)\frac{E_s}{N_0}$. Once we obtain the conditional PDF, CDF, and marginal MGF conditioned on T, we can immediately derive the MGF of the output of diversity combining schemes by averaging the conditional statistic over the distribution of T.

5.3 MGF of the Combiner Output over Equally Correlated Rice Fading Channels

5.3.1 GSC(N,L)

Consider a diversity receiver containing L branches. GSC(N,L) receiver adaptively combines a subset of N branches with the highest instantaneous SNR out of L available diversity branches. Suppose the set $\{\gamma_{k|T}\}_{k=1}^{L}$ denotes the instantaneous SNRs of L diversity branches with independent and identically distributed (i.i.d.) fading statistics conditioned on $T = \left(X_0 + m_1/\sqrt{\rho}\right)^2 + \left(Y_0 + m_1/\sqrt{\rho}\right)^2$. Then the order statistics $\gamma_{k:L|T}$ ($\gamma_{1:L|T} \geq \gamma_{2:L|T} \geq \cdots \geq \gamma_{L:L|T}$)

is obtained by arranging the set $\{\gamma_{k|T}\}_{k=1}^{L}$ in decreasing order of magnitude.

Let $\gamma_{gsc|T} = \sum_{k=1}^{N} \gamma_{k:L|T}$, then the MGF of $\gamma_{gsc|T}$ can be expressed as [47]-[48]

$$\begin{aligned} \mathcal{M}_{\gamma_{gsc|T}}(s) &= N\binom{L}{N}\int_0^\infty e^{-sx} f_{\gamma|T}(x) \\ &\times \left[F_{\gamma|T}(x)\right]^{L-N}\left[\mathcal{M}_{\gamma|T}(s,x)\right]^{N-1} dx \end{aligned} \tag{5.8}$$

where $f_{\gamma|T}(x)$, $F_{\gamma|T}(x)$, and $\mathcal{M}_{\gamma|T}(s,x)$ are (5.5), (5.6), and (5.7), respectively. The MGF of the output of GSC(N,L) receiver over equally correlated Rice fading channels can be derived by averaging the conditional MGF $\mathcal{M}_{\gamma_{gsc|T}}(s)$ in (5.8) over the distribution of T:

$$\mathcal{M}_{\gamma_{gsc}}(s) = \int_0^\infty \mathcal{M}_{\gamma_{gsc|T}}(s) f_T(t) dt \tag{5.9}$$

where

$$f_T(t) = e^{-\left(\frac{K}{\rho}+t\right)} I_0\left(2\sqrt{\frac{Kt}{\rho}}\right),\ t \geq 0 \tag{5.10}$$

since $T \sim \chi_2(K/\rho, 1/2)$, and its PDF is given by [61, Eq. (2-1-118)].

5.3.2 AT-GSC

Allowing the number of combined branches to be a variable rather than fixing it might be appropriate for diversity combining scenarios such as distributed antenna array in a cooperative sensor network and ultra-wide bandwidth communications where processing complexity and total power consumptions are limited.

In AT-GSC scheme, each branch SNR is tested against a fixed branch threshold (μ_{th}) and all the branches whose instantaneous SNRs exceed the threshold are combined [51], [57]. The output of AT-GSC $\gamma_{at\text{–}gsc|T}$ can be written as

$$\gamma_{at\text{–}gsc|T} = \begin{cases} 0, & \text{if } \gamma_{1:L|T} < \mu_{th} \\ \sum_{\gamma_{k:L|T} \geq \mu_{th}} \gamma_{k:L|T}, & \text{otherwise} \end{cases} \tag{5.11}$$

The conditional MGF of AT-GSC conditioned on T is [51]

$$\begin{aligned} \mathcal{M}_{\gamma_{at\text{–}gsc|T}}(s) &= \left[F_{\gamma|T}(\mu_{th}) + \int_{\mu_{th}}^\infty f_{\gamma|T}(x) e^{-sx} dx\right]^L \\ &= \left[F_{\gamma|T}(\mu_{th}) + \mathcal{M}_{\gamma|T}(s,\mu_{th})\right]^L. \end{aligned} \tag{5.12}$$

Averaging the conditional MGF of the output $\gamma_{at\text{–}gsc|T}$ of AT-GSC over the distribution of T leads to the MGF of $\gamma_{at\text{–}gsc}$ over equally correlated Rice fading channels:

$$\mathcal{M}_{\gamma_{at\text{–}gsc}}(s) = \int_0^\infty \mathcal{M}_{\gamma_{at\text{–}gsc|T}}(s) f_T(t) dt \tag{5.13}$$

5.3.3 MAT-GSC

The average bit error probability (ABEP) of AT-GSC receiver can approach 1/2 in the worst case as the fixed threshold (μ_{th}) increases since the output of AT-GSC is zero when there is no branch SNR which exceeds the μ_{th}. This makes the AT-GSC combiner unstable for practical applications and [57] proposed a modified AT-GSC (MAT-GSC) scheme. In the proposed new scheme, if all the diversity branches fall below the threshold μ_{th}, the branch with the largest SNR is selected for its output. Therefore, the MAT-GSC switches between AT-GSC and selection combining (SC) [57]. The output of MAT-GSC combiner can be written as

$$\gamma_{mat\text{–}gsc|T} = \begin{cases} \gamma_{1:L|T} & \text{if } \gamma_{1:L|T} < \mu_{th} \\ \sum_{\gamma_{k:L|T} \geq \mu_{th}} \gamma_{k:L|T}, & \text{otherwise} \end{cases} \tag{5.14}$$

The MGF of $\gamma_{mat\text{–}gsc|T}$ can be expressed as [57]

$$\begin{aligned} \mathcal{M}_{\gamma_{mat\text{–}gsc|T}}(s) &= L\left[\int_0^{\mu_{th}} e^{-sx} f_{\gamma|T}(x)[F_{\gamma|T}(x)]^{L-1} dx\right] \\ &+ \left[F_{\gamma|T}(\mu_{th}) + \mathcal{M}_{\gamma|T}(s, \mu_{th})\right]^L \\ &- [F_{\gamma|T}(\mu_{th})]^L \end{aligned} \tag{5.15}$$

Finally, the MGF of MAT-GSC scheme over equally correlated Rice fading channels is

$$\mathcal{M}_{\gamma_{mat\text{–}gsc}}(s) = \int_0^\infty \mathcal{M}_{\gamma_{mat\text{–}gsc|T}}(s) f_T(t) dt \tag{5.16}$$

5.4 ASEP and Outage Probability

In this section, the MGF-based evaluation methods for the ASEP, outage probability, and higher order statistics are presented. For brevity, the MGF of GSC combiner is used in all

the expressions. However, the MGFs of the other two diversity combining schemes can be used in the same way to evaluate their performances.

5.4.1 ASEP

Since the MGFs of GSC, AT-GSC, and MAT-GSC schemes over equally correlated Rician fading channels are derived in the previous section, the MGF approach [58],[62] can be used to evaluate the ASEP performance of the three diversity combining schemes for different diversity order and branch correlations. The ASEP of M-ary phase-shift-keying (PSK) with coherent GSC receiver is given by

$$\overline{P}_s = \frac{1}{\pi}\int_0^{\pi-\frac{\pi}{M}} \mathcal{M}_{\gamma_{gsc}}\left(\frac{\sin^2(\pi/M)}{\sin^2\theta}\right) d\theta \tag{5.17}$$

where M denotes the alphabet size of M-ary signal constellation (for example, $M = 2$ for binary phase-shift keying and $M = 4$ for quadrature phase-shift keying). Also, the ASEP of M-ary differential phase-shift keying (DPSK) with coherent GSC receiver can be expressed as

$$\overline{P}_s = \frac{1}{\pi}\int_0^{\pi-\frac{\pi}{M}} \mathcal{M}_{\gamma_{gsc}}\left(\frac{\sin^2(\pi/M)}{1+\cos(\pi/M)\cos\theta}\right) d\theta \tag{5.18}$$

5.4.2 Outage Probability

The outage probability P_{out} is defined as the probability that the instantaneous receiver output SNR falls below a specified threshold SNR γ_{th} i.e.,

$$P_{out} = \int_0^{\gamma_{th}} p_{\gamma_{gsc}}(x)dx = F_{\gamma_{gsc}}(\gamma_{th}) \tag{5.19}$$

where γ_{gsc} is the instantaneous GSC output SNR, $p_{\gamma_{gsc}}(x)$ is the PDF of γ_{gsc}, and $F_{\gamma_{gsc}}(\cdot)$ is the CDF of the output SNR of GSC receiver. However, since the CDF $F_{\gamma_{gsc}}(x)$ is not available while the MGF $\mathcal{M}_{\gamma_{gsc}}(s)$ is readily available, we used Abate's numerical inversion method

of Laplace transform of probability distribution [36]. Then, the CDF of γ_{gsc} evaluated at γ_{th} can be computed as

$$\begin{aligned} P_{out} &\simeq 2^{1-C} e^{A/2} \sum_{k=0}^{C} \binom{C}{k} \sum_{b=0}^{B+k} (-1)^b \alpha_b \\ &\times \Re\left[\mathcal{M}_{\gamma_{gsc}}\left(\frac{A + j2\pi b}{2\gamma_{th}} \right) / (A + j2\pi b) \right] \end{aligned} \tag{5.20}$$

where $\alpha_b = \begin{cases} 1/2, & b = 0 \\ 1, & b = 1, 2, \ldots \end{cases}$ and $\Re[\cdot]$ denotes the real part. A, B, and C can be set to meet the desired error bound for numerical inversion.

5.4.3 Higher Order Statistics

The mean combined SNR is another useful performance measure of diversity systems. Higher order moment can be calculated using the MGF:

$$\eta_n = E[\gamma_{gsc}^n] = (-1)^n \frac{d^n \mathcal{M}_{\gamma_{gsc}}(s)}{ds^n}\Big|_{s=0}. \tag{5.21}$$

Central moments can then be obtained via the following relation

$$\lambda_n = E[(\gamma_{gsc} - \overline{\gamma}_{gsc})^n] = \sum_{i=0}^{n} \binom{n}{i} \eta_i (-\overline{\gamma}_{gsc})^{n-i} \tag{5.22}$$

where $\overline{\gamma}_{gsc} = E[\gamma_{gsc}]$.

5.5 Computational Results and Remarks

In this section, we present selected numerical results to illustrate the effect of branch correlations on the hybrid selection combining schemes over equally correlated Rice channels with the aid of analytical results derived in the preceding sections. In all the figures for AT-GSC and MAT-GSC, $\mu_{th}^* = \mu_{th}/\overline{\gamma}$ is the threshold normalized by the average branch SNR ($\overline{\gamma}$).

Figure 5.1 shows the ASEP of BPSK for GSC(2,4) over equally correlated Rice fading channels with different Rice factors $K = 0$ and $K = 3$ dB ($K = 0$ corresponds to equally correlated Rayleigh fading channel). As expected, GSC(2,4) always performs better in Rice fading channel than in Rayleigh fading channel for independent fading ($\rho = 0$) case. However, for correlated fading cases, we observed that the performance of GSC(2,4) in Rice fading channel ($K = 3$ dB) becomes worse than that in Rayleigh fading as the correlation coefficient ρ increases. This phenomena may be explained by the relationship between the power correlation coefficient and the correlation coefficient (ρ) of the underlying Gaussian RVs G_k and G_j ($k \neq j$) in (5.1). Since the power correlation of Rayleigh fading is $\rho_\gamma = \rho^2$ [63] and that of Rice fading is $\rho_\gamma = \rho\frac{2K+\rho}{2K+1}$ [29], for a given value of ρ, the power correlation of Rice fading is larger than that of Rayleigh fading. Therefore, the diversity branches over correlated Rice fading channel are more highly correlated than those over Rayleigh fading channel for a given correlation coefficient ρ.

Figure 5.2 illustrates the effect of branch correlation on the ABEP performance of GSC(N,L) at average SNR per branch $\overline{\gamma}_{gsc} = 8$ dB as a function of correlation coefficient ρ for BPSK modulation. AS expected, the ABEP in both Rayleigh and Rice fading channels increases as the correlation increases. However, the performance of GSC(N,L) in Rice fading channel degrades more rapidly at the low correlation values but more slowly at the high correlation values than that in Rayleigh fading channel, which can be observed from both Figure 5.1 and Figure 5.2. This suggests that Rice fading is more sensitive to the variation of correlation in the low correlation values and less sensitive in the high correlation values. We also observed that for a given Rice parameter K and diversity order L, although selecting more branches improves the performance of GSC(N,L), the relative gain diminishes as the number of combining branches increases and the correlation coefficient increases.

Figure 5.3 and Figure 5.4 show the ABEP of BPSK with MAT-GSC and AT-GSC scheme, respectively, as a function of the normalized threshold μ_{th}^*. From these figures, we observed that the detrimental effect of correlation is more pronounced when Rice factor K is large and the normalized threshold μ_{th}^* is relatively small as the correlation increases. Also, the

performance of MAT-GSC and AT-GSC degrades more rapidly at low correlation values than at high correlation values as the normalized threshold μ_{th}^* increases. That is, the MAT-GSC and AT-GSC schemes are more sensitive to the variation of the normalized threshold when the correlation between diversity branches is low as compared with the high correlation case. Both MAT-GSC and AT-GSC are highly dependent upon the threshold μ_{th}^* and the correlation value. While the ABEP of MAT-GSC approaches 10^{-2}, that of AT-GSC approaches $1/2$ as the threshold increases. Hence, MAT-GSC is less sensitive to the threshold than AT-GSC.

The outage probability of MAT-GSC is shown in Figure 5.5 for Rice factor $K = 0$ and $K = 3$ dB and the normalized threshold $\mu_{th}^* = -5$ dB. The same performance trend as in Figure 5.1 and Figure 5.2 can be observed in this figure. The outage probability performance of MAT-GSC over equally correlated Rice fading becomes worse than that over equally correlated Rayleigh fading and degrades more rapidly at low correlation values as ρ increases as compared with Rayleigh fading.

5.6 Conclusion

In this chapter, we take a modest step in understanding the impact of branch correlation on the hybrid generalized selection combining schemes (GSC, AT-GSC, and MAT-GSC) over equally correlated Rice fading channels. Unlike independent fading case, where the hybrid generalized selection combining schemes always perform better in Rice fading channel than in Rayleigh fading, it turns out that the performance can be worse in correlated Rice fading channels, and correlated Rice fading is more sensitive to the variation of correlation than correlated Rayleigh fading at low correlation values.

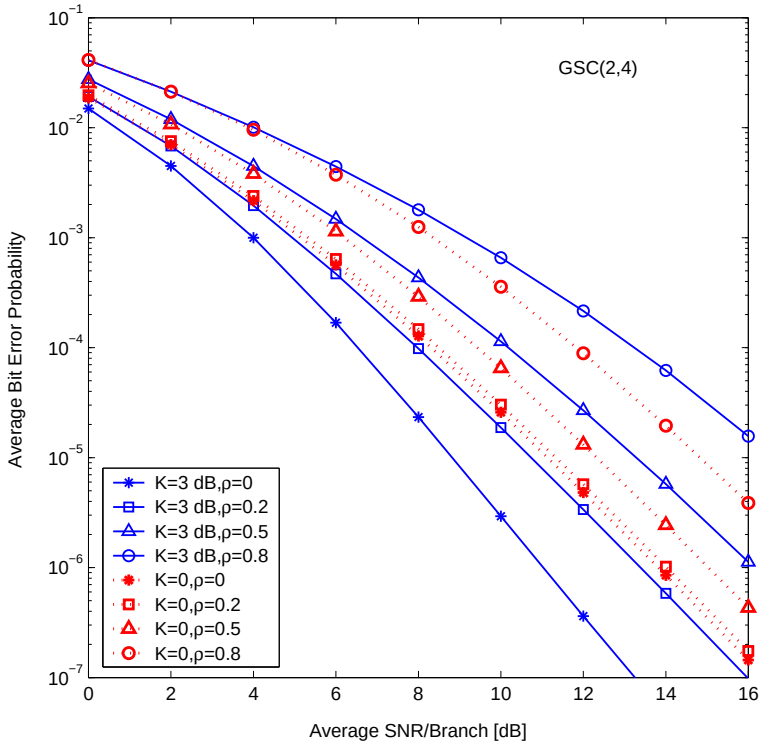

Figure 5.1: Average bit error probability for coherent BPSK with GSC(2,4) over equally correlated Rice fading channels: $\rho = \{0.0.2, 0.5, 0.8\}$ and $K = 0, 3\text{dB}$.

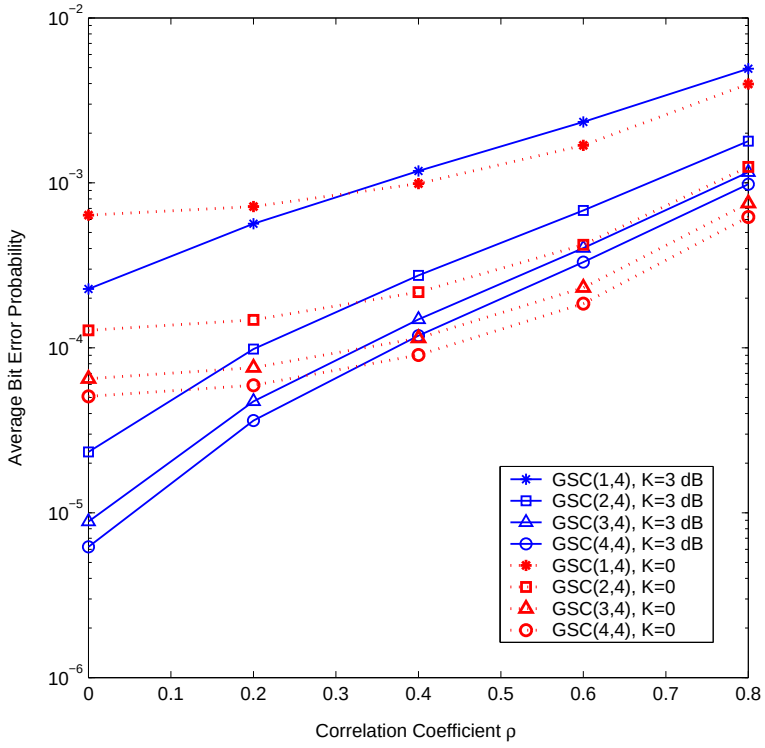

Figure 5.2: Average bit error probability of coherent BPSK for GSC(N,4) with $N = \{1, 2, 3, 4\}$ as a function of correlation coefficient ρ over equally correlated Rice fading channels with $K = \{0, 3\text{dB}\}$ and average branch SNR $\overline{\gamma} = 8\text{dB}$.

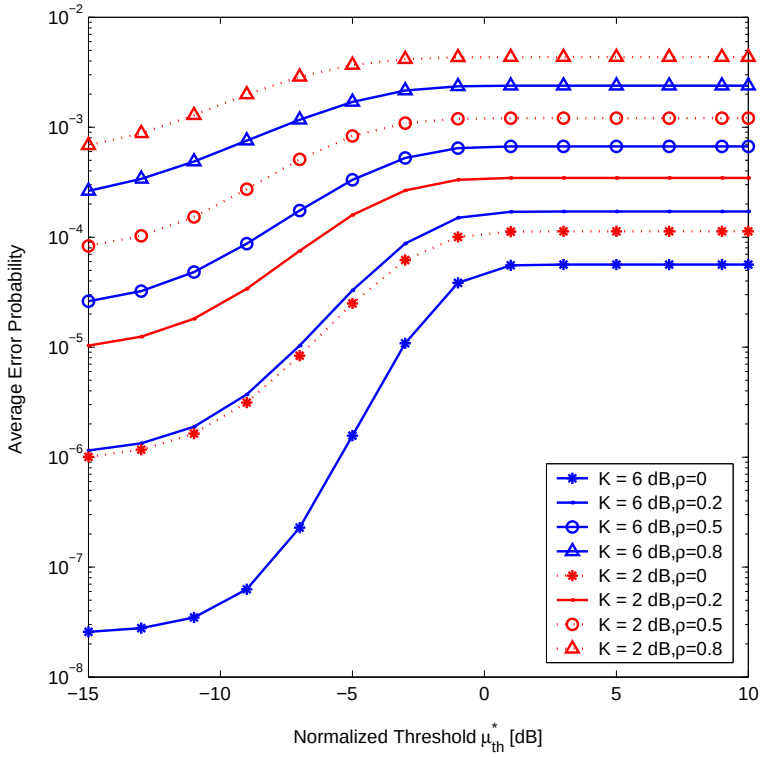

Figure 5.3: The effect of threshold μ_{th}^{*} on the ABEP of MAT-GSC scheme (BPSK) over equally correlated Rice channel with $K = 2$ dB and $K = 6$ dB: diversity order $L = 5$, average SNR per branch $\overline{\gamma} = 8$ dB.

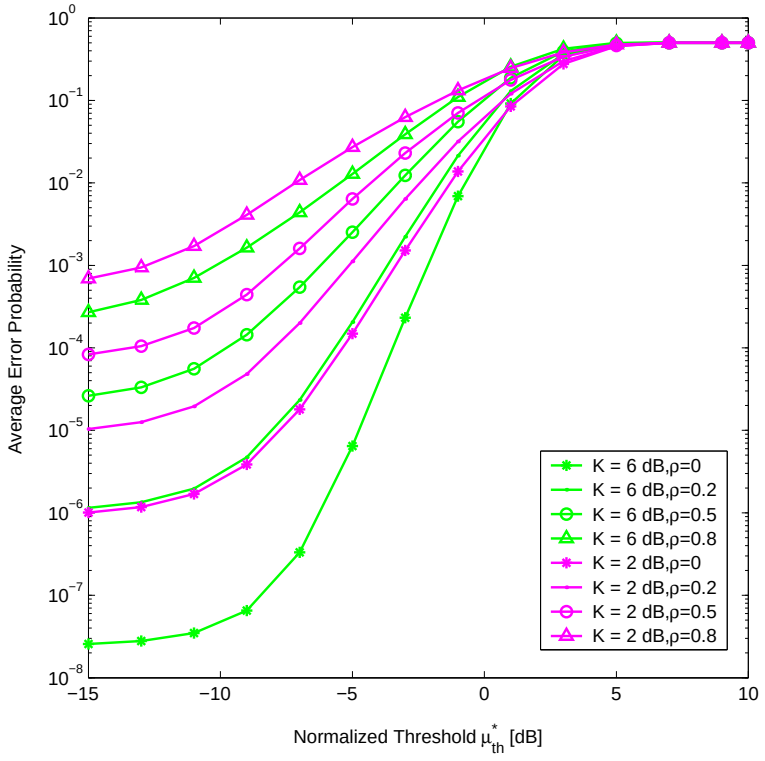

Figure 5.4: The effect of threshold μ_{th}^{*} on the ABEP of AT-GSC scheme (BPSK) over equally correlated Rice channel with $K = 2$ dB and $K = 6$ dB: diversity order $L = 5$, average SNR per branch $\overline{\gamma} = 8$ dB.

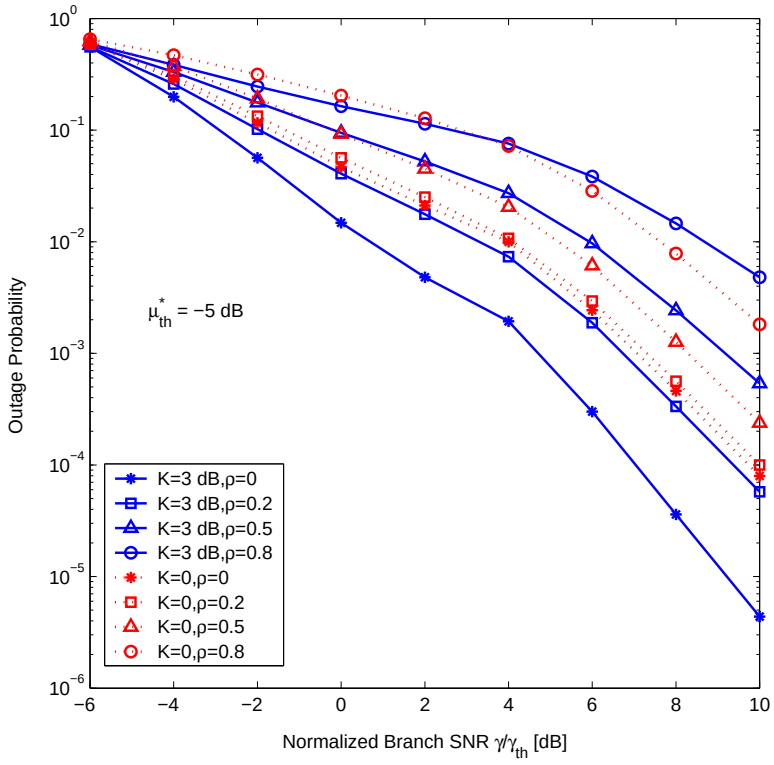

Figure 5.5: Outage probability with MAT-GSC ($L = 4$) versus normalized average SNR γ/γ_{th} over equally correlated Rice fading channel ($K = 0$ and $K = 3$ dB).

Chapter 6

Asymptotic Analysis of Digital Communication Systems with Diversity Techniques

6.1 Introduction

Hybrid diversity combining which selects and combines a subset of available diversity branches achieves a good design trade-off in terms of performance and implementation complexity (see references on hybrid diversity techniques in the previous chapter). In generalized selection combining (GSC(N,L)), N branches with the largest signal-to-noise ratios (SNRs) are selected from a total of L branches, and combined through maximum-ratio combining (this is also called hybrid selection/maximal-ratio combining (HS/MRC)). One variation of this combining scheme is GSEGC(N,L) which selects N branches with largest SNRs out of L branches and combines them through pre-detection equal gain combining (EGC) instead of MRC. Another variation is normalized threshold GSC (NTGSC(μ,L)) which performs maximum-ratio combining on the branches whose relative strength (the ratio of the SNR of

each branch to that of the largest branch with maximum SNR) exceeds a specified normalized threshold μ ($0 \leq \mu \leq 1$). The performance analysis of these techniques (GSC(N,L) and NTGSC(μ,L)) are published in open literatures (see references in the previous chapter).

Along with the previous studies in open literatures, [65] presented asymptotic analysis on GSC(N,L) receiver at high average SNR (ASNR) to approach issues such as performance gaps between Selection diversity (SDC), MRC, and GSC(N,L) in different fading channels and effect of different modulations on the GSC(N,L) performance. The asymptotic analysis offers insights as to what parameter determines system performance with different diversity order and modulation formats in different fading channels in a unifying way. In this chapter, we extend the previous work in [65] to not only GSC(N,L) but also NTGSC(μ,L) and GSEGC(N,L) (which includes EGC as a special case) in a concise, unifying way to facilitate parametric investigation and optimizing system design. Especially, since the analytical solution to GSEGC(N,L) has not been reported in open literature, it is very useful to analytically predict the performance of GSEGC(N,L) receiver in generalized fading channels and do comparison study with GSC(N,L).

6.2 Asymptotic Analysis

For high average signal-to-noise ratios (ASNRs), if the average symbol error probability (ASEP) can be expressed as

$$P_{ASEP}(\bar{\gamma}) = (G_c \bar{\gamma})^{-G_d} + o(\bar{\gamma}^{-G_d}) \tag{6.1}$$

where $\bar{\gamma}$ is the input ASNR per branch at a diversity combiner, and $o(s)$ satisfies that $\lim_{x \to 0} \frac{o(x)}{x} = 0$. Then, G_c represents an improvement (or degradation) factor to the ASNR per branch, and G_d represents the effective diversity order and determines the asymptotic slope of the error probability curves at high ASNRs in a log-log scale. G_c and G_d are defined and called as coding gain and diversity gain of symbol (bit) error probability, respectively [64], [65]. Note that the term 'coding gain' defined here is different from the conventionally

used term which is related to error correcting codes. In a similar manner, if the outage probability of a diversity combiner at predefined SNR threshold γ_{th}, which is defined as $P_{out} = \Pr(\gamma < \gamma_{th})$, can be expressed as

$$P_{out}(\gamma_{th}) = \left(O_c \frac{\bar{\gamma}}{\gamma_{th}}\right)^{-O_d} + o(\bar{\gamma}^{-O_d}) \tag{6.2}$$

then O_c and O_d are called the outage coding gain and outage diversity gain, respectively.

6.2.1 Asymptotic Expression of PDF, CDF, and Incomplete MGF of Random Variables

Let the instantaneous SNR be $\gamma = |\alpha|^2 E_b/N_0 = u\bar{\gamma}$, where α represents the fading envelope, $u = |\alpha|^2$, $E[u] = 1$, and $\bar{\gamma}$ denotes the ASNR. Then, the average bit error probability (ABEP) over fading channel can be calculated

$$P_{ASEP} = \int_0^\infty P_e(u)p(u)du \tag{6.3}$$

where $P_e(u)$ is the conditional error probability which can be expressed for BPSK as

$$P_e(u) = Q(\sqrt{2u\bar{\gamma}}). \tag{6.4}$$

As can be seen in (6.3), the ABEP over fading channel can be calculated by integrating the product of Q function and the probability density function (PDF). Hence, since $Q(\sqrt{2u\bar{\gamma}})$ behaves more and more like a delta function as $\bar{\gamma}\to\infty$, when the ASNR ($\bar{\gamma}$) is high, the system performance (bit (symbol) error probability) will be dominated by the low-probability event that the instantaneous SNR (γ) is small, that is, u is small, in which $\gamma = u\bar{\gamma}$. In the similar way, if we replace Q function with any function which behaves like a delta function as $\bar{\gamma}\to\infty$, the error probability at high ASNR will show the similar trend with Q function case. Therefore, the system performance at high ASNR depends on the behavior of $p(u)$ at small values of u ($u\to 0^+$) [64].

Table 6.1: Asymptotic PDFs and Other Related Parameters

Fading Types	PDF Expression $p_\gamma(\gamma) \simeq a\gamma^t$	a, t, and b
Rayleigh	$\frac{1}{\bar{\gamma}} e^{-\gamma/\bar{\gamma}}$	$t=0$, $a=\frac{1}{\bar{\gamma}}$, $b=1$
Rice	$\frac{1+K}{\bar{\gamma}} e^{-K-\frac{(1+K)\gamma}{\bar{\gamma}}} \times I_0\left(2\sqrt{\frac{K(1+K)\gamma}{\bar{\gamma}}}\right)$	$t=0$, $a=\frac{(1+K)e^{-K}}{\bar{\gamma}}$, $b=(1+K)e^{-K}$
Nakagami-m	$\left(\frac{m}{\bar{\gamma}}\right)^m \frac{\gamma^{m-1}}{\Gamma(m)} e^{-\frac{m}{\bar{\gamma}}\gamma}$	$t=m-1$, $a=\frac{m^m}{\bar{\gamma}\Gamma(m)}$, $b=\frac{m^m}{\Gamma(m)}$
Nakagami-q	$\frac{1+q^2}{2q\bar{\gamma}} e^{-\frac{(1+q^2)^2\gamma}{4q^2\bar{\gamma}}} \times I_o\left(\frac{(1-q^2)\gamma}{4q^2\bar{\gamma}}\right)$	$t=0$, $a=\frac{1+q^2}{2q\bar{\gamma}}$, $b=\frac{1+q^2}{2q}$
Weibull	$\frac{\alpha}{2(\beta\bar{\gamma})^{\frac{\alpha}{2}}} x^{\frac{\alpha}{2}-1} e^{-(\frac{x}{\beta\bar{\gamma}})^{\alpha/2}}$	$t=\frac{\alpha}{2}-1$, $a=\frac{\alpha}{2(\beta\bar{\gamma})^{\alpha/2}}$, $b=\frac{\alpha}{2\beta^{\alpha/2}}$

From the above discussion, in order to derive a closed-form solution for the performance of diversity combiner at high ASNR over different fading channels, the PDF can be approximated by a single polynomial term for $u \rightarrow 0^+$ as $p(u) = au^t + o(u^{t+\epsilon})$, where $\epsilon > 0$. Hence, the asymptotic PDF of instantaneous SNR γ for different fading channels can be expressed as a polynomial for high ASNRs as follows [65]:

$$p(\gamma) \simeq a\gamma^t \tag{6.5}$$

where a and t for different fading environments are tabulated in Table 6.1. Therefore, the incomplete MGF can be expressed as

$$\begin{aligned} \phi(s,x) &\simeq a\int_x^\infty e^{-su}u^t du \\ &= a\int_{sx}^\infty e^{-y}y^t\left(\frac{1}{s}\right)^t\frac{dy}{s} \\ &= \frac{a}{s^{t+1}}\Gamma(t+1,sx) \end{aligned} \tag{6.6}$$

where $\Gamma(\alpha,x) = \int_x^\infty e^{-u}u^{\alpha-1}du$ is the incomplete Gamma function. Also, the asymptotic CDF can be derived from the PDF as

$$\begin{aligned} F(x) &\simeq a\int_0^x u^t du \\ &= \frac{ax^{t+1}}{t+1} \end{aligned} \tag{6.7}$$

6.2.2 Asymptotic PDF, CDF, and MGF of the Outputs of Diversity Combiners

Let $a_l = b_l/\bar{\gamma}_l^{t_l+1}$, $\{l = 1, 2, \ldots, L\}$ where L is the total number of diversity branches and $\bar{\gamma}_l$ is the ASNR per branch. Also, let $g_l = \bar{\gamma}_l/\bar{\gamma}$ where $\bar{\gamma}$ is the total input ASNR for diversity branches divided by L. Then a_l can be expressed as

$$a_l \quad = \quad b_l g_l^{-(t_l+1)} \bar{\gamma}^{-(t_l+1)}. \tag{6.8}$$

Proposition 1 *The asymptotic PDF, CDF, and MGF for the MRC output SNR can be expressed, respectively, as*

$$p_{MRC}(\gamma) \quad \simeq \quad \frac{J_{MRC}(\mathbf{b}, \mathbf{g}, \mathbf{t})}{\Gamma\left(\sum_{k=1}^{L}(t_k+1)\right) \bar{\gamma}^{\sum_{k=1}^{L}(t_k+1)}} \gamma^{-1+\sum_{k=1}^{L}(t_k+1)}, \tag{6.9}$$

$$F_{MRC}(\gamma) \quad \simeq \quad \frac{J_{MRC}(\mathbf{b}, \mathbf{g}, \mathbf{t})}{\Gamma\left(1+\sum_{k=1}^{L}(t_k+1)\right) \bar{\gamma}^{\sum_{k=1}^{L}(t_k+1)}} \gamma^{\sum_{k=1}^{L}(t_k+1)}, \tag{6.10}$$

$$\begin{aligned} \phi_{MRC}(s) \quad &\simeq \quad \prod_{k=1}^{L} \frac{b_k g_k^{-(t_k+1)} \bar{\gamma}^{-(t_k+1)} \Gamma(t_k+1)}{s^{t_k+1}} \\ &= \quad \left(\frac{1}{s\bar{\gamma}}\right)^{\sum_{k=1}^{L}(t_k+1)} J_{MRC}(\mathbf{b}, \mathbf{g}, \mathbf{t}) \end{aligned} \tag{6.11}$$

where

$$J_{MRC}(\mathbf{b}, \mathbf{g}, \mathbf{t}) = \prod_{k=1}^{L} b_k g_k^{-(t_k+1)} \Gamma(t_k+1), \tag{6.12}$$

and $\Gamma(x) = \int_0^\infty u^{x-1} e^{-u} du$.

Proposition 2 *The asymptotic PDF, CDF, and MGF for the SDC output SNR can be expressed, respectively, as*

$$p_{SDC}(\gamma) = F'_{SDC}(\gamma) \quad \simeq \quad J_{SDC}(\mathbf{b}, \mathbf{g}, \mathbf{t}) \bar{\gamma}^{-\sum_{k=1}^{L}(t_k+1)} \left[\sum_{k=1}^{L}(t_k+1)\right] \frac{\gamma^{-1+\sum_{k=1}^{L}(t_k+1)}}{\Gamma\left(1+\sum_{k=1}^{L}(t_k+1)\right)}, \tag{6.13}$$

$$F_{SDC}(\gamma) \simeq J_{SDC}(\mathbf{b},\mathbf{g},\mathbf{t})\bar{\gamma}^{-\sum_{k=1}^{L}(t_k+1)}\frac{\gamma^{\sum_{k=1}^{L}(t_k+1)}}{\Gamma\left(1+\sum_{k=1}^{L}(t_k+1)\right)}, \tag{6.14}$$

$$\phi_{SDC}(s) \simeq J_{SDC}(\mathbf{b},\mathbf{g},\mathbf{t})\bar{\gamma}^{-\sum_{i=1}^{L}(t_i+1)}\left(\frac{1}{s}\right)^{\sum_{k=1}^{L}(t_k+1)}, \tag{6.15}$$

where

$$J_{SDC}(\mathbf{b},\mathbf{g},\mathbf{t}) = \left[\prod_{k=1}^{L}\frac{b_k g_k^{-(t_k+1)}}{t_k+1}\right]\Gamma\left(1+\sum_{k=1}^{L}(t_k+1)\right). \tag{6.16}$$

Proposition 3 *The asymptotic PDF, CDF, and MGF for the GSC(N,L) output SNR can be expressed, respectively, as*

$$p_{GSC}(\gamma) \simeq J_{GSC}(\mathbf{b},\mathbf{g},\mathbf{t})(\bar{\gamma})^{-\sum_{k=1}^{L}(t_k+1)}\frac{\gamma^{-1+\sum_{k=1}^{L}(t_k+1)}}{\Gamma\left(\sum_{k=1}^{L}(t_k+1)\right)}, \tag{6.17}$$

$$F_{GSC}(\gamma) \simeq J_{GSC}(\mathbf{b},\mathbf{g},\mathbf{t})(\bar{\gamma})^{-\sum_{k=1}^{L}(t_k+1)}\frac{\gamma^{\sum_{k=1}^{L}(t_k+1)}}{\Gamma\left(1+\sum_{k=1}^{L}(t_k+1)\right)}, \tag{6.18}$$

$$\phi_{GSC}(s) \simeq J_{GSC}(\mathbf{b},\mathbf{g},\mathbf{t})(s\bar{\gamma})^{-\sum_{k=1}^{L}(t_k+1)}, \tag{6.19}$$

where

$$\begin{aligned} J_{GSC}(\mathbf{b},\mathbf{g},\mathbf{t}) &= \left[\prod_{l=1}^{L} b_l g_l^{-(t_l+1)}\right]\sum_{\sigma\in T_{L,N}}\int_0^\infty e^{-u}\left[\prod_{k=L-N+2}^{L}\Gamma(t_{\sigma(k)}+1,u)\right] \\ &\times \frac{u^{-1+\sum_{i=1}^{L-N+1}(t_{\sigma(i)}+1)}}{\prod_{i=1}^{L-N}(t_{\sigma(i)}+1)}du \end{aligned} \tag{6.20}$$

where $\sum_{\sigma\in T_{LN}} = \sum_{\substack{\sigma\in S_L,\sigma(1)<\sigma(2)<\cdots<\sigma(N-1)\,,\\ \sigma(N+1)<\cdots<\sigma(L)}}$, $\mathbf{b} = [b_1, b_2, \ldots, b_L]^T$, $\mathbf{g} = [\bar{\gamma}_1/\bar{\gamma}, \bar{\gamma}_2/\bar{\gamma}, \ldots, \bar{\gamma}_L/\bar{\gamma}]^T$, and $\mathbf{t} = [t_1, t_2, \ldots, t_L]^T$.

Proposition 4 *The asymptotic PDF, CDF, and MGF for the NTGSC(μ,L) output SNR can be expressed, respectively, as*

$$p_{NTGSC}(\gamma) \simeq J_{NTGSC}(\mathbf{b},\mathbf{g},\mathbf{t},N)\bar{\gamma}^{-\sum_{k=1}^{L}(t_k+1)}\frac{\gamma^{-1+\sum_{k=1}^{L}(t_k+1)}}{\Gamma\left(\sum_{k=1}^{L}(t_k+1)\right)}, \tag{6.21}$$

$$F_{NTGSC}(\gamma) \simeq J_{NTGSC}(\mathbf{b},\mathbf{g},\mathbf{t},N)\bar{\gamma}^{-\sum_{k=1}^{L}(t_k+1)}\frac{\gamma^{\sum_{k=1}^{L}(t_k+1)}}{\Gamma\left(1+\sum_{k=1}^{L}(t_k+1)\right)}, \tag{6.22}$$

$$\phi_{NTGSC}(s) \simeq J_{NTGSC}(\mathbf{b},\mathbf{g},\mathbf{t},N)(s\gamma)^{-\sum_{k=1}^{L}(t_k+1)}, \tag{6.23}$$

where

$$\begin{aligned} J_{NTGSC}(\mathbf{b},\mathbf{g},\mathbf{t},N) &= \left[\prod_{l=1}^{L} b_l g_l^{-(t_l+1)}\right] \sum_{\sigma\in T_{L,N}} \int_0^{\infty} e^{-u} \\ &\times \prod_{k=L-N+1}^{L-1} \left[\Gamma(t_{\sigma(k)}+1,\mu u) - \Gamma(t_{\sigma(k)}+1,u)\right] \\ &\times \frac{u^{-1+\sum_{i=1}^{L-N+1}(t_{\sigma(i)}+1)}}{\prod_{i=1}^{L-N}(t_{\sigma(i)}+1)} du \end{aligned} \tag{6.24}$$

where μ is the normalized threshold $0\leq\mu\leq 1$.

Proposition 5 *The asymptotic PDF, CDF, and MGF for the EGC output envelope can be expressed, respectively, as*

$$p_{EGC}(x) \simeq J_{EGC}(\mathbf{b},\mathbf{g},\mathbf{t}) \times \frac{x^{-1+\sum_{k=1}^{L} 2(t_k+1)}}{\bar{\gamma}^{\sum_{k=1}^{L}(t_k+1)}\Gamma\left(\sum_{k=1}^{L} 2(t_k+1)\right)}, \tag{6.25}$$

$$F_{EGC}(x) \simeq J_{EGC}(\mathbf{b},\mathbf{g},\mathbf{t}) \times \frac{x^{\sum_{k=1}^{L} 2(t_k+1)}}{\bar{\gamma}^{\sum_{k=1}^{L}(t_k+1)}\Gamma\left(1+\sum_{k=1}^{L} 2(t_k+1)\right)}, \tag{6.26}$$

$$\phi_{EGC}(s) \simeq J_{EGC}(\mathbf{b},\mathbf{g},\mathbf{t}) \times \bar{\gamma}^{-\sum_{k=1}^{L}(t_k+1)} \left(\frac{1}{s}\right)^{\sum_{k=1}^{L} 2(t_k+1)}, \tag{6.27}$$

where

$$J_{EGC}(\mathbf{b},\mathbf{g},\mathbf{t}) = 2^L L^{\sum_{k=1}^{L}(t_k+1)} \left[\prod_{k=1}^{L} b_k g_k^{-(t_k+1)} \Gamma(2(t_k+1))\right]. \tag{6.28}$$

Proposition 6 *The asymptotic PDF, CDF, and MGF for the GSEGC(N,L) output envelope can be expressed, respectively, as*

$$p_{GSEGC}(x) \simeq J_{GSEGC}(\mathbf{b},\mathbf{g},\mathbf{t})\bar{\gamma}^{-\sum_{k=1}^{L}(t_k+1)} \frac{x^{-1+\sum_{k=1}^{L} 2(t_k+1)}}{\Gamma\left(\sum_{k=1}^{L} 2(t_k+1)\right)}, \tag{6.29}$$

$$F_{GSEGC}(x) \simeq J_{GSEGC}(\mathbf{b},\mathbf{g},\mathbf{t})\bar{\gamma}^{-\sum_{k=1}^{L}(t_k+1)} \frac{x^{\sum_{k=1}^{L} 2(t_k+1)}}{\Gamma\left(1+\sum_{k=1}^{L} 2(t_k+1)\right)}, \tag{6.30}$$

$$\phi_{GSEGC}(s) \simeq J_{GSEGC}(\mathbf{b},\mathbf{g},\mathbf{t})\bar{\gamma}^{-\sum_{k=1}^{L}(t_k+1)} s^{-\sum_{k=1}^{L} 2(t_k+1)}, \tag{6.31}$$

Table 6.2: Instantaneous Symbol Error Probability (SEP) of Several Common Modulations

Modulation Scheme	Conditional Error Probability $P_e(\gamma)$
CBPSK	$\frac{1}{2}\text{erfc}(\sqrt{\gamma})$
CBFSK	$\frac{1}{2}\text{erfc}(\sqrt{\gamma/2})$
CBDPSK	$\text{erfc}(\sqrt{\gamma}) - \frac{1}{2}\text{erfc}^2(\sqrt{\gamma})$
NCBDPSK	$\frac{1}{2}e^{-\gamma}$
NCBFSK	$\frac{1}{2}e^{-\gamma/2}$
QPSK/MSK	$\text{erfc}(\sqrt{\gamma/2}) - \frac{1}{4}\text{erfc}^2(\sqrt{\gamma/2})$
$\pi/4$-DQPSK	$\frac{1}{2\pi}\int_0^{\pi} \exp\left[\frac{-2\gamma}{2-\sqrt{2}\cos\theta}\right] d\theta$
Square QAM	$2\left[1-\frac{1}{\sqrt{M}}\right]\text{erfc}\left[\sqrt{\frac{3\gamma}{2(M-1)}}\right] - \left[1-\frac{1}{\sqrt{M}}\right]^2 \text{erfc}^2\left[\sqrt{\frac{3\gamma}{2(M-1)}}\right]$
MPSK	$\frac{1}{\pi}\int_0^{(M-1)\pi/M} \exp\left[\frac{-\gamma\sin^2(\pi/M)}{\sin^2\theta}\right] d\theta$
MDPSK	$\frac{1}{\pi}\int_0^{(M-1)\pi/M} \exp\left[\frac{-\gamma\sin^2(\pi/M)}{1+\cos(\pi/M)\cos\theta}\right] d\theta$

where

$$\begin{aligned} J_{GSEGC}(\mathbf{b},\mathbf{g},\mathbf{t}) &= 2^L N^{\sum_{l=1}^{L}(t_l+1)} \left[\prod_{l=1}^{L} b_l g_l^{-(t_l+1)}\right] \sum_{\sigma\in T_{L,N}} \int_0^{\infty} e^{-u} \\ &\times \left[\prod_{k=L-N+2}^{L} \Gamma\left(2(t_{\sigma(k)}+1), u\right)\right] \frac{u^{-1+\sum_{i=1}^{L-N+1} 2(t_{\sigma(i)}+1)}}{\prod_{i=1}^{L-N} 2(t_{\sigma(i)}+1)} du. \end{aligned} \quad (6.32)$$

6.3 Performance Analysis

6.3.1 Average Symbol Error Probability (ASEP) for MRC, SDC, GSC(N,L), and NTGSC(μ,L)

Conventionally, the average error probability over fading channels is obtained by integrating the conditional error probability (CEP), $P_e(\gamma)$, over the PDF of the receiver output. Although the CEPs for different modulation formats (Table 6.2) are well known, it is difficult to

compute the PDFs for certain diversity combiners such as GSC(N,L) and NTGSC(μ,L), so the conventional integration method can not be used. This motivated developing frequency domain approach to analyze the performance of diversity combiners as shown in the previous chapters. However, since the CDFs of different types of diversity combiners are derived in the previous section for asymptotic analysis, we present another method to calculate the average error probability using CDFs. This can readily be done using the integration-by-parts methods:

$$\begin{aligned} \bar{P}_{error} &= \int_0^\infty P_e(\gamma)p(\gamma)d\gamma \\ &= -\int_0^\infty P_e'(\gamma)F(\gamma)d\gamma \end{aligned} \tag{6.33}$$

where $P_e'(\gamma) = \frac{d}{d\gamma}P_e(\gamma)$ denotes the derivative of the CEP. The negative derivative ($-P_e'(\gamma)$) for various modulation formats are summarized in Table 6.3 and $F(\gamma)$ can be obtained using the results in Proposition 1 through 4 [Eqs.(6.10), (6.14), (6.18), and (6.22)].

Since $\gamma^{\sum_{k=1}^{L}(t_k+1)}$ is the only factor in (6.10), (6.14), (6.18), and (6.22), which are involved in the integration in (6.33), we can extract the factor in (6.33) which is directly related to different types of modulation formats. In the following, we will present ASEP(ABEP) for different modulation formats and extract the factor defined as the 'Modulation Factor'.

1) Coherent BPSK (CBPSK):

Using (6.33) and $P_e'(\gamma)$ for CBPSK from Table 6.3, we can get a ABEP expression for MRC, SDC, and GSC(N,L)

$$P_{CBPSK}(\bar{\gamma}) \simeq J_{SNR}(\mathbf{b},\mathbf{g},\mathbf{t})\frac{\bar{\gamma}^{-\sum_{k=1}^{L}(t_k+1)}}{\Gamma\left(1+\sum_{k=1}^{L}(t_k+1)\right)}\int_0^\infty \frac{1}{2\sqrt{\pi}}\gamma^{-\frac{1}{2}+\sum_{k=1}^{L}(t_k+1)}e^{-\gamma}d\gamma, \tag{6.34}$$

Table 6.3: Negative Derivatives of CEPs for Several Common Modulations

Modulation Scheme	Negative Derivative[a] $(-P_e'(\gamma))$
CBPSK	$\frac{e^{-\gamma}}{2\sqrt{\pi\gamma}}$
CBFSK	$\frac{e^{-\gamma/2}}{2\sqrt{\pi\gamma}}$
CBDPSK	$\frac{e^{-\gamma}}{\sqrt{\pi\gamma}} - \text{erfc}(\sqrt{\gamma})\frac{e^{-\gamma}}{\sqrt{\pi\gamma}}$
NCBDPSK	$\frac{1}{2}e^{-\gamma}$
NCBFSK	$\frac{1}{4}e^{-\gamma/2}$
QPSK/MSK	$\frac{e^{-\gamma/2}}{\sqrt{2\pi\gamma}} - \text{erfc}(\sqrt{\gamma/2})\frac{e^{-\gamma/2}}{2\sqrt{2\pi\gamma}}$
$\pi/4$-DQPSK	$\frac{1}{2\pi}\int_0^{\pi}\frac{2}{2-\sqrt{2}\cos\theta}\exp\left[\frac{-2\gamma}{2-\sqrt{2}\cos\theta}\right]d\theta$
Square QAM	$\sqrt{\frac{6}{\pi(M-1)^2}}\left(1-\frac{1}{\sqrt{M}}\right)\frac{\exp\left[-\frac{3\gamma}{2(M-1)}\right]}{\sqrt{\gamma/(M-1)}}$ $-\sqrt{\frac{6}{\pi(M-1)^2}}\left(1-\frac{1}{\sqrt{M}}\right)^2\frac{\exp\left[-\frac{3\gamma}{2(M-1)}\right]}{\sqrt{\gamma/(M-1)}}\text{erfc}\left[\sqrt{\frac{3\gamma}{2(M-1)}}\right]$
MPSK	$\frac{1}{\pi}\int_0^{(M-1)\pi/M}\frac{\sin^2(\pi/M)}{\sin^2\theta}\exp\left[\frac{-\gamma\sin^2(\pi/M)}{\sin^2\theta}\right]d\theta$
MDPSK	$\frac{1}{\pi}\int_0^{(M-1)\pi/M}\frac{\sin^2(\pi/M)}{1+\cos(\pi/M)\cos\theta}\exp\left[\frac{-\gamma\sin^2(\pi/M)}{1+\cos(\pi/M)\cos\theta}\right]d\theta$

[a]Note that γ is instantaneous SNR

where $J_{SNR}(\mathbf{b},\mathbf{g},\mathbf{t})$ represents $J_{MRC}(\mathbf{b},\mathbf{g},\mathbf{t})$, $J_{SDC}(\mathbf{b},\mathbf{g},\mathbf{t})$, or $J_{GSC}(\mathbf{b},\mathbf{g},\mathbf{t})$. For NTGSC($\mu$,$L$), by using (4.3), the ABEP can be expressed as

$$\begin{aligned} P_{CBPSK}(\bar{\gamma}) &\simeq \left[\sum_{N=1}^{L} J_{NTGSC}(\mathbf{b},\mathbf{g},\mathbf{t},N)\right]\frac{\bar{\gamma}^{-\sum_{k=1}^{L}(t_k+1)}}{\Gamma\left(1+\sum_{k=1}^{L}(t_k+1)\right)} \\ &\times \int_0^{\infty}\frac{1}{2\sqrt{\pi}}\gamma^{-\frac{1}{2}+\sum_{k=1}^{L}(t_k+1)}e^{-\gamma}d\gamma \end{aligned} \tag{6.35}$$

Since

$$\int_0^{\infty}\frac{1}{2\sqrt{\pi}}\gamma^{-\frac{1}{2}+\sum_{k=1}^{L}(t_k+1)}e^{-\gamma}d\gamma = \frac{1}{2\sqrt{\pi}}\Gamma\left(\frac{1}{2}+\sum_{k=1}^{L}(t_k+1)\right), \tag{6.36}$$

$P_{CBPSK}(\bar{\gamma})$ for MRC, SDC, and GSC(N,L) can be expressed as

$$P_{CBPSK}(\bar{\gamma}) \simeq J_{SNR}(\mathbf{b},\mathbf{g},\mathbf{t})\bar{\gamma}^{-\sum_{k=1}^{L}(t_k+1)}\frac{\Gamma\left(\frac{1}{2}+\sum_{k=1}^{L}(t_k+1)\right)}{2\sqrt{\pi}\Gamma\left(1+\sum_{k=1}^{L}(t_k+1)\right)}. \tag{6.37}$$

For NTGSC(μ,L), the ABEP is given by

$$P_{CBPSK}(\bar{\gamma}) \simeq \left[\sum_{N=1}^{L} J_{NTGSC}(\mathbf{b},\mathbf{g},\mathbf{t},N)\right] \bar{\gamma}^{-\sum_{k=1}^{L}(t_k+1)} \frac{\Gamma\left(\frac{1}{2}+\sum_{k=1}^{L}(t_k+1)\right)}{2\sqrt{\pi}\Gamma\left(1+\sum_{k=1}^{L}(t_k+1)\right)}. \quad (6.38)$$

In (6.37) and (6.38), we define

$$M_{CBPSK} = \frac{\Gamma\left(\frac{1}{2}+\sum_{k=1}^{L}(t_k+1)\right)}{2\sqrt{\pi}\Gamma\left(1+\sum_{k=1}^{L}(t_k+1)\right)} \quad (6.39)$$

as the *modulation factor* for CBPSK, which is related to CBPSK modulation format and common to $P_{CBPSK}(\bar{\gamma})$ of diversity combiners such as MRC, SDC, GSC(N,L), and NTGSC(μ,L). From (6.37), we can obtain the diversity gain of MRC, SDC, GSC(N,L), and NTGSC(μ,L) as

$$G_d = \sum_{k=1}^{L}(t_k+1), \quad (6.40)$$

and the coding gain for CBPSK is

$$\begin{aligned} G_{c,CBPSK} &= \left(J_{SNR}(\mathbf{b},\mathbf{g},\mathbf{t})\frac{1}{2\sqrt{\pi}}\frac{\Gamma\left(\frac{1}{2}+G_d\right)}{\Gamma(1+G_d)}\right)^{-1/G_d} \\ &= \left(J(\mathbf{b},\mathbf{g},\mathbf{t})M_{CBPSK}\right)^{-1/G_d} \end{aligned} \quad (6.41)$$

for MRC, SDC, and GSC(N,L), and for NTGSC(μ,L)

$$\begin{aligned} G_{c,CBPSK} &= \left[\left(\sum_{N=1}^{L} J_{NTGSC}(\mathbf{b},\mathbf{g},\mathbf{t},N)\right)\frac{1}{2\sqrt{\pi}}\frac{\Gamma\left(\frac{1}{2}+G_d\right)}{\Gamma(1+G_d)}\right]^{-1/G_d} \\ &= \left[\left(\sum_{N=1}^{L} J_{NTGSC}(\mathbf{b},\mathbf{g},\mathbf{t},N)\right)M_{CBPSK}\right]^{-1/G_d}. \end{aligned} \quad (6.42)$$

2) Binary DPSK (BDPSK)

a) Coherent Combiner: In the similar way for ABEP derivation for CBPSK, the ABEP for BDPSK can be expressed as

$$P_{NCBDPSK}(\bar{\gamma}) = J_{SNR}(\mathbf{b},\mathbf{g},\mathbf{t})\frac{\bar{\gamma}^{-\sum_{k=1}^{L}(t_k+1)}}{\Gamma\left(1+\sum_{k=1}^{L}(t_k+1)\right)}\int_0^\infty \frac{1}{2}e^{-\gamma}\gamma^{\sum_{k=1}^{L}(t_k+1)}d\gamma$$

$$= J_{SNR}(\mathbf{b},\mathbf{g},\mathbf{t})\bar{\gamma}^{-\sum_{k=1}^{L}(t_k+1)}\left(\frac{1}{2}\right). \quad (6.43)$$

for coherent MRC, SDC, and GSC(N,L), and

$$P_{NCBDPSK}(\bar{\gamma}) = \left[\sum_{N=1}^{L} J_{NTGSC}(\mathbf{b},\mathbf{g},\mathbf{t},N)\right] \frac{\bar{\gamma}^{-\sum_{k=1}^{L}(t_k+1)}}{\Gamma\left(1+\sum_{k=1}^{L}(t_k+1)\right)} \int_0^\infty \frac{1}{2} e^{-\gamma}\gamma^{\sum_{k=1}^{L}(t_k+1)} d\gamma$$

$$= \left[\sum_{N=1}^{L} J_{NTGSC}(\mathbf{b},\mathbf{g},\mathbf{t},N)\right] \bar{\gamma}^{-\sum_{k=1}^{L}(t_k+1)}\left(\frac{1}{2}\right). \quad (6.44)$$

for coherent NTGSC(μ,L). The modulation factor for BDPSK is

$$M_{BDPSK} = \frac{1}{2}. \quad (6.45)$$

The coding gain for BDPSK is

$$G_{c,BDPSK} = (J_{SNR}(\mathbf{b},\mathbf{g},\mathbf{t})M_{BDPSK})^{-1/G_d}. \quad (6.46)$$

for coherent MRC, SDC, and GSC(N,L), and

$$G_{c,BDPSK} = \left[\left(\sum_{N=1}^{L} J_{NTGSC}(\mathbf{b},\mathbf{g},\mathbf{t},N)\right) M_{BDPSK}\right]^{-1/G_d}. \quad (6.47)$$

for coherent NTGSC(μ,L).

b) Non-coherent Combiner: Since square-law detection (also known as post-detection EGC) circumvents the need to co-phase and weight the diversity branches, it is suitable for use in differentially coherent and non-coherent detection such as BDPSK and non-coherent BFSK. The CEP for multichannel binary orthogonal FSK (BDSK) is given by [61, Eq. (12.1.13)]

$$P_e(\gamma) = \frac{1}{2^{2L-1}} e^{-\xi\gamma} \sum_{k=0}^{L-1} c_k (\xi\gamma)^k, \quad (6.48)$$

where

$$c_k = \frac{1}{k!} \sum_{l=0}^{L-1-k} \binom{2L-1}{l} \quad (6.49)$$

$\xi = 1/2$ for orthogonal binary FSK, and $\xi = 1$ for binary DPSK. Hence, the negative derivative of the CEP can be expressed as

$$-P_e'(\gamma) = \frac{\xi e^{-\xi\gamma}}{2^{2L-1}} \sum_{k=0}^{L-1} c_k (\xi\gamma)^k - \frac{\xi e^{-\xi\gamma}}{2^{2L-1}} \sum_{k=0}^{L-1} c_k k (\xi\gamma)^{k-1}. \tag{6.50}$$

Using (6.50), the ABEP of BDPSK for non-coherent SDC, MRC, and GSC(N,L) can be expressed as

$$\begin{aligned} P_{BDPSK}^{NC} &\simeq J_{SNR}(\mathbf{b},\mathbf{g},\mathbf{t}) \frac{\bar{\gamma}^{-G_d}}{\Gamma(1+G_d)} \\ &\times \int_0^\infty \gamma^{G_d} \left[\frac{e^{-\gamma}}{2^{2N-1}} \sum_{k=0}^{N-1} c_k \gamma^k - \frac{e^{-\gamma}}{2^{2N-1}} \sum_{k=0}^{N-1} c_k k \gamma^{k-1} \right] d\gamma, \end{aligned} \tag{6.51}$$

where $G_d = \sum_{k=1}^{L} (t_k + 1)$. Applying change of variable and using $\Gamma(1+\alpha) = \alpha\Gamma(\alpha)$, we can obtain a closed-form expression for the ABEP of BDPSK with non-coherent SDC, MRC, and GSC(N,L) as

$$\begin{aligned} P_{BDPSK}^{NC} &\simeq J_{SNR}(\mathbf{b},\mathbf{g},\mathbf{t}) \bar{\gamma}^{-G_d} \\ &\times \frac{1}{2^{2N-1}} \sum_{k=0}^{N-1} \frac{c_k \Gamma(G_d + k)}{\Gamma(G_d)}. \end{aligned} \tag{6.52}$$

For non-coherent NTGSC(μ,L), the ABEP can be given by

$$P_{BDPSK}^{NC} \simeq \left[\sum_{N=1}^{L} J_{NTGSC}(\mathbf{b},\mathbf{g},\mathbf{t},N) \frac{1}{2^{2N-1}} \sum_{k=0}^{N-1} \frac{c_k \Gamma(G_d + k)}{\Gamma(G_d)} \right] \bar{\gamma}^{-G_d}. \tag{6.53}$$

The modulation factor for non-coherent SDC, MRC, and GSC(N,L) is

$$M_{BDPSK}^{NC} = \frac{1}{2^{2N-1}} \sum_{k=0}^{N-1} \frac{c_k \Gamma(G_d + k)}{\Gamma(G_d)}. \tag{6.54}$$

The coding gain for non-coherent SDC, MRC, and GSC(N,L) is

$$C_{c,BDPSK}^{NC} = \left(J_{SNR}(\mathbf{b},\mathbf{g},\mathbf{t}) M_{BDPSK}^{NC} \right)^{-1/G_d}, \tag{6.55}$$

and the coding gain for non-coherent NTGSC(μ,L) is

$$C_{c,BDPSK}^{NC} = \left[\sum_{N=1}^{L} J_{NTGSC}(\mathbf{b},\mathbf{g},\mathbf{t},N) \frac{1}{2^{2N-1}} \sum_{k=0}^{N-1} \frac{c_k \Gamma(G_d + k)}{\Gamma(G_d)} \right]^{-1/G_d}. \tag{6.56}$$

3) Binary FSK (BFSK)

a) Coherent Combiner: The ABEP of BFSK for coherent MRC, SDC, and GSC(N,L) can be given by

$$\begin{aligned} P_{BFSK}(\bar{\gamma}) &= J_{SNR}(\mathbf{b},\mathbf{g},\mathbf{t})\frac{\bar{\gamma}^{-\sum_{k=1}^{L}(t_k+1)}}{\Gamma\left(1+\sum_{k=1}^{L}(t_k+1)\right)}\int_0^\infty \frac{1}{4}e^{-\gamma/2}\gamma^{\sum_{k=1}^{L}(t_k+1)}d\gamma \\ &= J_{SNR}(\mathbf{b},\mathbf{g},\mathbf{t})\bar{\gamma}^{-\sum_{k=1}^{L}(t_k+1)}2^{-1+\sum_{k=1}^{L}(t_k+1)}. \end{aligned} \tag{6.57}$$

and

$$\begin{aligned} P_{BFSK}(\bar{\gamma}) &= \left[\sum_{N=1}^{L} J_{NTGSC}(\mathbf{b},\mathbf{g},\mathbf{t},N)\right]\frac{\bar{\gamma}^{-\sum_{k=1}^{L}(t_k+1)}}{\Gamma\left(1+\sum_{k=1}^{L}(t_k+1)\right)}\int_0^\infty \frac{1}{4}e^{-\gamma/2}\gamma^{\sum_{k=1}^{L}(t_k+1)}d\gamma \\ &= \left[\sum_{N=1}^{L} J_{NTGSC}(\mathbf{b},\mathbf{g},\mathbf{t},N)\right]\bar{\gamma}^{-\sum_{k=1}^{L}(t_k+1)}2^{-1+\sum_{k=1}^{L}(t_k+1)}. \end{aligned} \tag{6.58}$$

for coherent NTGSC(μ,L). The modulation factor for BFSK is

$$M_{BFSK} = 2^{-1+G_d}, \tag{6.59}$$

where $G_d = \sum_{k=1}^{L}(t_k+1)$. The coding gain for coherent MRC, SDC, and GSC(N,L) with BFSK is

$$G_{c,FPSK} = (J_{SNR}(\mathbf{b},\mathbf{g},\mathbf{t})M_{BFSK})^{-1/G_d}. \tag{6.60}$$

and

$$G_{c,BFSK} = \left[\left(\sum_{N=1}^{L} J_{NTGSC}(\mathbf{b},\mathbf{g},\mathbf{t},N)\right)M_{BFSK}\right]^{-1/G_d}. \tag{6.61}$$

for coherent NTGSC(μ,L).

b) Non-coherent Combiner: In the same way as we derived a closed-form solution for the ABEP of BDPSK, we can obtain the ABEP of BFSK for non-coherent SDC, MRC, and GSC(N,L)

$$P_{BFSK}^{NC} \simeq J_{SNR}(\mathbf{b},\mathbf{g},\mathbf{t})\frac{\bar{\gamma}^{-G_d}}{\Gamma(1+G_d)}\int_0^\infty \gamma^{G_d}\left[\frac{e^{-\gamma/2}}{2^{2N-1}}\left(\frac{1}{2}\right)^{-G_d}\sum_{k=0}^{N-1} c_k\left(\frac{\gamma}{2}\right)^k\right.$$

$$- \quad \frac{e^{-\gamma/2}}{2^{2N-1}}\left(\frac{1}{2}\right)^{-G_d}\sum_{k=0}^{N-1} c_k k \left(\frac{\gamma}{2}\right)^{k-1}\Bigg] d\gamma$$

$$= \quad J_{SNR}(\mathbf{b},\mathbf{g},\mathbf{t})\bar{\gamma}^{-G_d}\frac{1}{2^{2N-1-G_d}}\sum_{k=0}^{N-1}\frac{c_k\Gamma(G_d+k)}{\Gamma(G_d)} \tag{6.62}$$

where $G_d = \sum_{k=1}^{L}(t_k+1)$ and $c_k = \frac{1}{k!}\sum_{l=0}^{L-1-k}\binom{2L-1}{l}$. For non-coherent NTGSC(μ,L), the ABEP can be given by

$$P_{BFSK}^{NC} \simeq \left[\sum_{N=1}^{L} J_{NTGSC}(\mathbf{b},\mathbf{g},\mathbf{t},N)\frac{1}{2^{2N-1-G_d}}\sum_{k=0}^{N-1}\frac{c_k\Gamma(G_d+k)}{\Gamma(G_d)}\right]\bar{\gamma}^{-G_d}. \tag{6.63}$$

The modulation factor for non-coherent SDC, MRC, and GSC(N,L) is

$$M_{BFSK}^{NC} = \frac{1}{2^{2N-1-G_d}}\sum_{k=0}^{N-1}\frac{c_k\Gamma(G_d+k)}{\Gamma(G_d)}. \tag{6.64}$$

The coding gain for non-coherent SDC, MRC, and GSC(N,L) is

$$C_{c,BFSK}^{NC} = \left(J_{SNR}(\mathbf{b},\mathbf{g},\mathbf{t})M_{BFSK}^{NC}\right)^{-1/G_d}, \tag{6.65}$$

and the coding gain for non-coherent NTGSC(μ,L) is

$$C_{c,BFSK}^{NC} = \left[\sum_{N=1}^{L} J_{NTGSC}(\mathbf{b},\mathbf{g},\mathbf{t},N)\frac{1}{2^{2N-1-G_d}}\sum_{k=0}^{N-1}\frac{c_k\Gamma(G_d+k)}{\Gamma(G_d)}\right]^{-1/G_d}. \tag{6.66}$$

4) QPSK/MSK

The ASEP of QPSK/MSK for MRC, SDC, and GSC(N,L) can be written as

$$P_{QPSK/MSK}(\bar{\gamma}) = J_{SNR}(\mathbf{b},\mathbf{g},\mathbf{t})\frac{\bar{\gamma}^{-\sum_{k=1}^{L}(t_k+1)}}{\Gamma\left(1+\sum_{k=1}^{L}(t_k+1)\right)}$$
$$\times \int_0^{\infty}\gamma^{\sum_{k=1}^{L}(t_k+1)}\left[\frac{e^{-\gamma/2}}{\sqrt{2\pi\gamma}} - \mathrm{erfc}\left(\sqrt{\frac{\gamma}{2}}\right)\frac{e^{-\gamma/2}}{2\sqrt{2\pi\gamma}}\right]d\gamma. \tag{6.67}$$

Since $\mathrm{erfc}(\sqrt{\gamma})$ can be expressed as the incomplete Gamma function, $\mathrm{erfc}(\sqrt{\gamma}) = \frac{1}{\sqrt{\pi}}\Gamma(0.5,\gamma)$, using [42, Eq. (6.455.1)], we can express the integration in (6.67) as

$$\int_0^{\infty}\gamma^{\sum_{k=1}^{L}(t_k+1)}\left[\frac{e^{-\gamma/2}}{\sqrt{2\pi\gamma}} - \mathrm{erfc}\left(\sqrt{\frac{\gamma}{2}}\right)\frac{e^{-\gamma/2}}{2\sqrt{2\pi\gamma}}\right]d\gamma$$

$$
\begin{aligned}
&= \int_0^\infty \frac{1}{\sqrt{2\pi}} \gamma^{-\frac{1}{2}+\sum_{k=1}^{L}(t_k+1)} e^{-\gamma/2} d\gamma \\
&\quad - \int_0^\infty \frac{1}{2\sqrt{2\pi}} \gamma^{-\frac{1}{2}+\sum_{k=1}^{L}(t_k+1)} e^{-\gamma/2} \mathrm{erfc}\left(\sqrt{\frac{\gamma}{2}}\right) d\gamma \\
&= \frac{2^{\sum_{k=1}^{L}(t_k+1)}}{\sqrt{\pi}} \Gamma\left(\frac{1}{2} + \sum_{k=1}^{L}(t_k+1)\right) \\
&\quad - \frac{1}{4\pi} \frac{\Gamma\left(1+\sum_{k=1}^{L}(t_k+1)\right)}{\frac{1}{2}+\sum_{k=1}^{L}(t_k+1)} {}_2F_1\left(1, 1+\sum_{k=1}^{L}(t_k+1); \frac{3}{2}+\sum_{k=1}^{L}(t_k+1); \frac{1}{2}\right), \quad (6.68)
\end{aligned}
$$

where ${}_2F_1(a,b;c;z)$ is the Gauss hypergeometric function defined as

$$
{}_2F_1(a,b;c;z) \quad = \quad \sum_0^\infty \frac{(a)_n (b)_n}{(c)_n} \frac{z^n}{n!}, \quad |z| < 1, \quad (6.69)
$$

where $(a)_n = a(a+1)\cdots(a+n+1) = \Gamma(a+n)/\Gamma(n)$ denotes the Pochhammer symbol. Therefore, the ASEP of QPSK/MSK can be given by

$$
\begin{aligned}
P_{QPSK/MSK}(\bar{\gamma}) &= J_{SNR}(\mathbf{b},\mathbf{g},\mathbf{t}) \bar{\gamma}^{-\sum_{k=1}^{L}(t_k+1)} \left[\frac{2^{\sum_{k=1}^{L}(t_k+1)}}{\sqrt{\pi}} \frac{\Gamma\left(\frac{1}{2}+\sum_{k=1}^{L}(t_k+1)\right)}{\Gamma\left(1+\sum_{k=1}^{L}(t_k+1)\right)} \right. \\
&\quad - \left. \frac{1}{4\pi} \frac{{}_2F_1(1, 1+\sum_{k=1}^{L}(t_k+1); \frac{3}{2}+\sum_{k=1}^{L}(t_k+1); \frac{1}{2})}{\frac{1}{2}+\sum_{k=1}^{L}(t_k+1)} \right]. \quad (6.70)
\end{aligned}
$$

In the similar way, the ASEP for NTGSC(μ,L) can be expressed as

$$
\begin{aligned}
&P_{QPSK/MSK}(\bar{\gamma}) \\
&= \left[\sum_{N=1}^{L} J_{NTGSC}(\mathbf{b},\mathbf{g},\mathbf{t},N) \right] \bar{\gamma}^{-\sum_{k=1}^{L}(t_k+1)} \left[\frac{2^{\sum_{k=1}^{L}(t_k+1)}}{\sqrt{\pi}} \frac{\Gamma\left(\frac{1}{2}+\sum_{k=1}^{L}(t_k+1)\right)}{\Gamma\left(1+\sum_{k=1}^{L}(t_k+1)\right)} \right. \\
&\left. - \frac{1}{4\pi} \frac{{}_2F_1(1, 1+\sum_{k=1}^{L}(t_k+1); \frac{3}{2}+\sum_{k=1}^{L}(t_k+1); \frac{1}{2})}{\frac{1}{2}+\sum_{k=1}^{L}(t_k+1)} \right]. \quad (6.71)
\end{aligned}
$$

The modulation factor for QPSK/MSK is

$$
M_{QPSK/MSK} \quad = \quad \frac{2^{G_d}}{\sqrt{\pi}} \frac{\Gamma(1/2+G_d)}{\Gamma(1+G_d)} - \frac{1}{4\pi} \frac{{}_2F_1(1, 1+G_d; 3/2+G_d; 1/2)}{1/2+G_d}, \quad (6.72)
$$

where $G_d = \sum_{k=1}^{L}(t_k+1)$. The coding gain for MRC, SDC, and GSC(N,L) is

$$
C_{c,QPSK/MSK} \quad = \quad (J_{SNR}(\mathbf{b},\mathbf{g},\mathbf{t}) M_{QPSK/MSK})^{-1/G_d}. \quad (6.73)
$$

$$C_{c,QPSK/MSK} = \left[\left(\sum_{N=1}^{L} J_{NTGSC}(\mathbf{b},\mathbf{g},\mathbf{t},N)\right) M_{QPSK/MSK}\right]^{-1/G_d}. \quad (6.74)$$

for NTGSC(μ,L).

5) MPSK

The ASEP of MPSK for MRC, SDC, and GSC(N,L) can be written as

$$\begin{aligned} P_{MPSK}(\bar{\gamma}) &= J_{SNR}(\mathbf{b},\mathbf{g},\mathbf{t}) \frac{\bar{\gamma}^{-\sum_{k=1}^{L}(t_k+1)}}{\Gamma\left(1+\sum_{k=1}^{L}(t_k+1)\right)} \\ &\times \underbrace{\frac{1}{\pi}\int_0^{\infty}\int_0^{(M-1)\pi/M} \gamma^{\sum_{k=1}^{L}(t_k+1)} \frac{\sin^2(\pi/M)}{\sin^2\theta} e^{-\frac{\sin^2(\pi/M)}{\sin^2\theta}\gamma} d\theta d\gamma}_{INT1}. \end{aligned} \quad (6.75)$$

Recognizing *INT1* is of the form (C.1) with $\theta_U = \frac{(M-1)\pi}{M}$, $\theta_c = \frac{\pi}{M}$, and $\alpha = G_d = \sum_{k=1}^{L}(t_k+1)$ when $h(\theta) = \frac{\sin^2\theta_c}{\sin^2\theta}$ in the appendix, we can obtain

$$\begin{aligned} P_{MPSK}(\bar{\gamma}) &= J_{SNR}(\mathbf{b},\mathbf{g},\mathbf{t})\bar{\gamma}^{-G_d} \\ &\times \frac{1}{\pi\sin^{2G_d}(\pi/M)}\left[\frac{1}{2^{2G_d}}\binom{2G_d}{G_d}\frac{(M-1)\pi}{M}\right. \\ &+ \left.\frac{(-1)^{G_d}}{2^{2G_d-1}}\sum_{k=0}^{G_d-1}(-1)^k\binom{2G_d}{k}\frac{\sin\left(\frac{(2G_d-2k)(M-1)\pi}{M}\right)}{2G_d-2k}\right] \end{aligned} \quad (6.76)$$

for MRC, SDC, and GSC(N,L). Also, the ASEP for NTGSC(μ,L) can be given by

$$\begin{aligned} P_{MPSK}(\bar{\gamma}) &= \left[\sum_{N=1}^{L} J_{NTGSC}(\mathbf{b},\mathbf{g},\mathbf{t},N)\right]\bar{\gamma}^{-G_d} \\ &\times \frac{1}{\pi\sin^{2G_d}(\pi/M)}\left[\frac{1}{2^{2G_d}}\binom{2G_d}{G_d}\frac{(M-1)\pi}{M}\right. \\ &+ \left.\frac{(-1)^{G_d}}{2^{2G_d-1}}\sum_{k=0}^{G_d-1}(-1)^k\binom{2G_d}{k}\frac{\sin\left(\frac{(2G_d-2k)(M-1)\pi}{M}\right)}{2G_d-2k}\right]. \end{aligned} \quad (6.77)$$

The modulation factor for MPSK is

$$M_{MPSK} = \frac{1}{\pi\sin^{2G_d}(\pi/M)}\left[\frac{1}{2^{2G_d}}\binom{2G_d}{G_d}\frac{(M-1)\pi}{M}\right.$$

$$+ \quad \frac{(-1)^{G_d}}{2^{2G_d-1}} \sum_{k=0}^{G_d-1} (-1)^k \binom{2G_d}{k} \frac{\sin\left(\frac{(2G_d-2k)(M-1)\pi}{M}\right)}{2G_d-2k} \Bigg]. \tag{6.78}$$

The coding gain for MPSK with MRC, SDC, and GSC(N,L) is

$$C_{c,MPSK} = (J_{SNR}(\mathbf{b},\mathbf{g},\mathbf{t}) M_{MPSK})^{-1/G_d}, \tag{6.79}$$

and

$$C_{c,MPSK} = \left[\left(\sum_{N=1}^{L} J_{NTGSC}(\mathbf{b},\mathbf{g},\mathbf{t},N) \right) M_{MPSK} \right]^{-1/G_d}. \tag{6.80}$$

with NTGSC(μ,L).

6) MDPSK

The ASEP of MDPSK with coherent with MRC, SDC, and GSC(N,L) can be expressed as

$$\begin{aligned} P_{MDPSK}(\bar{\gamma}) &= J_{SNR}(\mathbf{b},\mathbf{g},\mathbf{t}) \frac{\bar{\gamma}^{-\sum_{k=1}^{L}(t_k+1)}}{\Gamma\left(1+\sum_{k=1}^{L}(t_k+1)\right)} \\ &\times \underbrace{\frac{1}{\pi} \int_0^{\frac{(M-1)\pi}{M}} \int_0^{\infty} \gamma^{\sum_{k=1}^{L}(t_k+1)} \frac{\sin^2\left(\frac{\pi}{M}\right)}{1+\cos\left(\frac{\pi}{M}\right)\cos\theta} e^{-\frac{\sin^2\left(\frac{\pi}{M}\right)}{1+\cos\left(\frac{\pi}{M}\right)\cos\theta}\gamma} d\gamma d\theta}_{INT2} \end{aligned} \tag{6.81}$$

Also, recognizing *INT2* is of the form (C.1) with $\theta_U = \frac{(M-1)\pi}{M}$, $\theta_c = \frac{\pi}{M}$, and $\alpha = G_d = \sum_{k=1}^{L}(t_k+1)$ when $h(\theta) = \frac{\sin^2\theta_c}{1+\cos\theta_c\cos\theta}$ in the appendix, we can obtain

$$\begin{aligned} P_{MDPSK}(\bar{\gamma}) &= J_{SNR}(\mathbf{b},\mathbf{g},\mathbf{t}) \bar{\gamma}^{-G_d} \\ &\times \frac{1}{\pi \sin^{2G_d}(\pi/M)} I_V\left(G_d, \frac{(M-1)\pi}{M}, \frac{\pi}{M}\right) \end{aligned} \tag{6.82}$$

for coherent MRC, SDC, and GSC(N,L) by using (C.17). In (6.82), $I_V\left(G_d, \frac{(M-1)\pi}{M}, \frac{\pi}{M}\right)$ can be calculated by any one of the three formulas given in (C.16) in the appendix. As an illustration, since $0 \le \frac{(M-1)\pi}{2M} \le \frac{\pi}{2}$, we can express $I_V\left(G_d, \frac{(M-1)\pi}{M}, \frac{\pi}{M}\right)$ as one of the three

formulas in (C.16), and it can be given by

$$I_V\left(G_d, \frac{(M-1)\pi}{M}\right) = \sum_{k=0}^{G_d} \binom{G_d}{k} (-1)^k 2^k \cos^k(\pi/M) \left(1+\cos(\pi/M)\right)^{G_d-k} \times B_{\sin^2\left[\frac{(M-1)\pi}{2M}\right]}\left(k+\frac{1}{2}, \frac{1}{2}\right) \quad (6.83)$$

where $B_{\sin^2\left[\frac{(M-1)\pi}{2M}\right]}\left(k+\frac{1}{2}, \frac{1}{2}\right)$ is the incomplete Beta function defined as

$$B_b(t_1, t_2) = \int_0^b y^{t_1-1}(1-y)^{t_2-1} dy. \quad (6.84)$$

The ASEP for MDPSK with coherent NTGSC(μ,L) can also be given by

$$P_{MDPSK}(\bar{\gamma}) = \left[\sum_{N=1}^{L} J_{NTGSC}(\mathbf{b}, \mathbf{g}, \mathbf{t}, N)\right] \bar{\gamma}^{-G_d} \times \frac{1}{\pi \sin^{2G_d}(\pi/M)} I_V\left(G_d, \frac{(M-1)\pi}{M}, \frac{\pi}{M}\right). \quad (6.85)$$

The modulation factor for MDPSK is

$$M_{MDPSK} = \frac{1}{\pi \sin^{2G_d}(\pi/M)} I_V\left(G_d, \frac{(M-1)\pi}{M}, \frac{\pi}{M}\right). \quad (6.86)$$

The coding gain for MDPSK with coherent MRC, SDC, and GSC(N,L) is

$$C_{c,MDPSK} = \left(J_{SNR}(\mathbf{b}, \mathbf{g}, \mathbf{t}) M_{MDPSK}\right)^{-1/G_d}, \quad (6.87)$$

and

$$C_{c,MDPSK} = \left[\left(\sum_{N=1}^{L} J_{NTGSC}(\mathbf{b}, \mathbf{g}, \mathbf{t}, N)\right) M_{MDPSK}\right]^{-1/G_d}. \quad (6.88)$$

with coherent NTGSC(μ,L).

6.3.2 Average Error Probability for EGC and GSEGC(N,L)

The instantaneous SNR at the output of the EGC combiner is $\gamma = \nu^2$ where ν is defined as

$$\nu = \sqrt{\frac{E_s}{LN_0}} \sum_{l=1}^{L} \alpha_l \quad (6.89)$$

Table 6.4: Negative Derivatives of CEPs in Terms of Envelope

Modulation Scheme	Negative Derivative $(-P_e'(x))$
CBPSK	$\frac{e^{-x^2}}{\sqrt{\pi}}$
CBFSK	$\frac{1}{\sqrt{2\pi}}e^{-x^2/2}$
CBDPSK	$\frac{2}{\sqrt{\pi}}e^{-x^2} - \frac{2}{\sqrt{\pi}}e^{-x^2}\text{erfc}(x)$
NCBDPSK	xe^{-x^2}
NCBFSK	$\frac{x}{2}e^{-x^2/2}$
QPSK/MSK	$\sqrt{\frac{2}{\pi}}e^{-x^2/2} - \frac{1}{\sqrt{2\pi}}e^{-x^2/2}\text{erfc}(x/\sqrt{2})$
$\pi/4$-DQPSK	$\frac{1}{\pi}\int_0^{\pi}\frac{2x}{2-\sqrt{2}\cos\theta}\exp\left[\frac{-2x^2}{2-\sqrt{2}\cos\theta}\right]d\theta$
Square QAM	$2\sqrt{\frac{6}{\pi(M-1)}}\left(1-\frac{1}{\sqrt{M}}\right)\exp\left[-\frac{3x^2}{2(M-1)}\right]$ $-2\sqrt{\frac{6}{\pi(M-1)}}\left(1-\frac{1}{\sqrt{M}}\right)^2\exp\left[-\frac{3x^2}{2(M-1)}\right]\text{erfc}\left[\sqrt{\frac{3}{2(M-1)}}x\right]$
MPSK	$\frac{2}{\pi}\int_0^{(M-1)\pi/M}\frac{\sin^2(\pi/M)x}{\sin^2\theta}\exp\left[\frac{-\sin^2(\pi/M)x^2}{\sin^2\theta}\right]d\theta$
MDPSK	$\frac{1}{\pi}\int_0^{(M-1)\pi/M}\frac{\sin^2(\pi/M)x}{1+\cos(\pi/M)\cos\theta}\exp\left[\frac{-\sin^2(\pi/M)x^2}{1+\cos(\pi/M)\cos\theta}\right]d\theta$

for which α_l is the fading amplitude that may be modeled as a Rayleigh, Rice, Nakagami-m, Nakagami-q, or Weibull RV, E_s/N_0 is the SNR per symbol, and L denotes the diversity order. Finding the PDF of the instantaneous SNR γ at the EGC/GSEGC(N,L) combiner can be very tedious and complicated due to the presence of the $\alpha_l\alpha_k$ cross-product terms. Hence, in the pre-detection EGC/GSEGC(N,L) analysis, it is better to use the envelope of EGC/GSEGC(N,L) combiner output in stead of SNR. Because of this reason, we use the CEP $P_e(x)$ where $x = \sqrt{\gamma}$, which is expressed in terms of the envelope of RVs, for the asymptotic error probability analysis. The negative derivatives $-P_e'(x)$ for different modulation formats are summarized in Table 6.4.

1) Coherent BPSK (CBPSK)

The ABEP for CBPSK with EGC and GSEGC(N,L) can be expressed as

$$P_{BPSK}(\bar{\gamma}) \simeq J_{ENV}(\mathbf{b},\mathbf{g},\mathbf{t})\frac{\bar{\gamma}^{-\sum_{k=1}^{L}(t_k+1)}}{\Gamma\left(1+\sum_{k=1}^{L}2(t_k+1)\right)}\int_0^{\infty}\frac{1}{\sqrt{\pi}}e^{-x^2}x^{\sum_{k=1}^{L}2(t_k+1)}dx, \quad (6.90)$$

where $J_{ENV}(\mathbf{b},\mathbf{g},\mathbf{t})$ represents either $J_{EGC}(\mathbf{b},\mathbf{g},\mathbf{t})$ or $J_{GSEGC}(\mathbf{b},\mathbf{g},\mathbf{t})$. Since using (B.6) in the definite integral (6.90) leads to a closed-form expression for the definite integral as follows,

$$\int_0^\infty \frac{1}{\sqrt{\pi}} e^{-x^2} x^{\sum_{k=1}^{L} 2(t_k+1)} dx = \left(\frac{1}{2}\right)^{1+\sum_{k=1}^{L} 2(t_k+1)} \frac{\Gamma(1+\sum_{k=1}^{L} 2(t_k+1))}{\Gamma(1+\sum_{k=1}^{L}(t_k+1))}, \tag{6.91}$$

we can obtain a closed-form expression for (6.90) as

$$P_{BPSK}(\bar{\gamma}) \quad \simeq \quad J_{ENV}(\mathbf{b},\mathbf{g},\mathbf{t}) \bar{\gamma}^{-\sum_{k=1}^{L}(t_k+1)} \frac{2^{-1-\sum_{k=1}^{L} 2(t_k+1)}}{\Gamma(1+\sum_{k=1}^{L}(t_k+1))}. \tag{6.92}$$

The modulation factor for CBPSK is

$$M_{CBPSK} = \frac{2^{-1-\sum_{k=1}^{L} 2(t_k+1)}}{\Gamma(1+\sum_{k=1}^{L}(t_k+1))}. \tag{6.93}$$

The diversity gain for EGC and GSEGC(N,L) is

$$G_d = \sum_{k=1}^{L}(t_k+1), \tag{6.94}$$

and the coding gain for CBPSK is

$$C_{c,CBPSK} = (J_{ENV}(\mathbf{b},\mathbf{g},\mathbf{t}) M_{CBPSK})^{-1/G_d}. \tag{6.95}$$

2) Binary DPSK (BDPSK)

The ABEP for BDPSK can be expressed as

$$\begin{aligned} P_{BDPSK}(\bar{\gamma}) \quad &\simeq \quad J_{ENV}(\mathbf{b},\mathbf{g},\mathbf{t}) \frac{\bar{\gamma}^{-\sum_{k=1}^{L}(t_k+1)}}{\Gamma\left(1+\sum_{k=1}^{L} 2(t_k+1)\right)} \int_0^\infty x^{1+\sum_{k=1}^{L} 2(t_k+1)} e^{-x^2} dx \\ &= \quad J_{ENV}(\mathbf{b},\mathbf{g},\mathbf{t}) \bar{\gamma}^{-\sum_{k=1}^{L}(t_k+1)} \left(\frac{1}{2}\right)^{2+\sum_{k=1}^{L} 2(t_k+1)} \\ &\times \quad \frac{\sqrt{\pi}\Gamma\left(2+\sum_{k=1}^{L} 2(t_k+1)\right)}{\Gamma\left(1+\sum_{k=1}^{L} 2(t_k+1)\right)\Gamma\left(\frac{3}{2}+\sum_{k=1}^{L}(t_k+1)\right)}. \end{aligned} \tag{6.96}$$

The modulation factor is then given by

$$M_{BDPSK} = \left(\frac{1}{2}\right)^{2+\sum_{k=1}^{L} 2(t_k+1)} \frac{\sqrt{\pi}\Gamma\left(2+\sum_{k=1}^{L} 2(t_k+1)\right)}{\Gamma\left(1+\sum_{k=1}^{L} 2(t_k+1)\right)\Gamma\left(\frac{3}{2}+\sum_{k=1}^{L}(t_k+1)\right)}. \quad (6.97)$$

The coding gain is

$$C_{c,BDPSK} = (J_{ENV}(\mathbf{b},\mathbf{g},\mathbf{t})M_{BDPSK})^{-1/G_d}. \quad (6.98)$$

3) Binary FSK (BFSK)

The ABEP for BFSK can be expressed as

$$\begin{aligned} P_{BFSK}(\bar{\gamma}) &\simeq J_{ENV}(\mathbf{b},\mathbf{g},\mathbf{t})\frac{\bar{\gamma}^{-\sum_{k=1}^{L}(t_k+1)}}{\Gamma\left(1+\sum_{k=1}^{L} 2(t_k+1)\right)}\frac{1}{2}\int_0^\infty x^{1+\sum_{k=1}^{L} 2(t_k+1)}e^{-x^2/2}dx \\ &= J_{ENV}(\mathbf{b},\mathbf{g},\mathbf{t})\bar{\gamma}^{-\sum_{k=1}^{L}(t_k+1)}\left(\frac{1}{2}\right)^{1+\sum_{k=1}^{L}(t_k+1)} \\ &\times \frac{\sqrt{\pi}\Gamma\left(2+\sum_{k=1}^{L} 2(t_k+1)\right)}{\Gamma\left(1+\sum_{k=1}^{L} 2(t_k+1)\right)\Gamma\left(\frac{3}{2}+\sum_{k=1}^{L}(t_k+1)\right)}. \end{aligned} \quad (6.99)$$

The modulation factor is then given by

$$M_{BFSK} = \left(\frac{1}{2}\right)^{1+\sum_{k=1}^{L}(t_k+1)} \frac{\sqrt{\pi}\Gamma\left(2+\sum_{k=1}^{L} 2(t_k+1)\right)}{\Gamma\left(1+\sum_{k=1}^{L} 2(t_k+1)\right)\Gamma\left(\frac{3}{2}+\sum_{k=1}^{L}(t_k+1)\right)}. \quad (6.100)$$

The coding gain is

$$C_{c,BFSK} = (J_{ENV}(\mathbf{b},\mathbf{g},\mathbf{t})M_{BFSK})^{-1/G_d}. \quad (6.101)$$

4) QPSK/MSK

The ASEP of QPSK/MSK for EGC and GSEGC(N,L) can be expressed as

$$P_{QPSK/MSK}(\bar{\gamma}) \simeq J_{ENV}(\mathbf{b},\mathbf{g},\mathbf{t})\frac{\bar{\gamma}^{-\sum_{k=1}^{L}(t_k+1)}}{\Gamma\left(1+\sum_{k=1}^{L} 2(t_k+1)\right)}$$

$$\times \quad \Bigg[\underbrace{\sqrt{\frac{2}{\pi}} \int_0^{\infty} x^{\sum_{k=1}^{L} 2(t_k+1)} e^{-x^2/2} dx}_{INT3}$$

$$- \quad \underbrace{\frac{1}{\sqrt{2\pi}} \int_0^{\infty} x^{\sum_{k=1}^{L} 2(t_k+1)} e^{-x^2/2} \mathrm{erfc}(x/\sqrt{2}) dx}_{INT4} \Bigg]. \tag{6.102}$$

Since *INT3* can be expressed as

$$\sqrt{\frac{2}{\pi}} \int_0^{\infty} x^{\sum_{k=1}^{L} 2(t_k+1)} e^{-x^2/2} dx = 2^{-\sum_{k=1}^{L} 2(t_k+1)} \frac{\Gamma\left(1 + \sum_{k=1}^{L} 2(t_k+1)\right)}{\Gamma\left(1 + \sum_{k=1}^{L} (t_k+1)\right)}, \tag{6.103}$$

and from [42, Eq. (6.286.1)], *INT4* can be expressed as

$$\frac{1}{\sqrt{2\pi}} \int_0^{\infty} x^{\sum_{k=1}^{L} 2(t_k+1)} e^{-x^2/2} \mathrm{erfc}(x/\sqrt{2}) dx = \frac{2^{\sum_{k=1}^{L} 2(t_k+1)} \Gamma\left(1 + \sum_{k=1}^{L} (t_k+1)\right)}{\pi \left(1 + \sum_{k=1}^{L} 2(t_k+1)\right)}$$

$$\times {}_2F_1\left(\frac{1}{2} + \sum_{k=1}^{L} (t_k+1), 1 + \sum_{k=1}^{L} (t_k+1); \frac{3}{2} + \sum_{k=1}^{L} (t_k+1); -1\right), \tag{6.104}$$

we can obtain a closed-form expression for the ASEP of QPSK/MSK as follows

$$\begin{aligned} P_{QPSK/MSK}(\bar{\gamma}) \quad &\simeq \quad J_{ENV}(\mathbf{b}, \mathbf{g}, \mathbf{t}) \bar{\gamma}^{-G_d} \left[\frac{2^{-G_d}}{\Gamma(1+G_d)} - \frac{2^{G_d} \Gamma(1+2G_d)}{\pi(1+2G_d)\Gamma(1+2G_d)} \right. \\ &\times \quad \left. {}_2F_1\left(\frac{1}{2} + G_d, 1 + G_d; \frac{3}{2} + G_d; -1\right) \right], \end{aligned} \tag{6.105}$$

where $G_d = \sum_{k=1}^{L} (t_k + 1)$. The modulation factor is

$$\begin{aligned} M_{QPSK/MSK} \quad &= \quad \frac{2^{-G_d}}{\Gamma(1+G_d)} - \frac{2^{G_d} \Gamma(1+2G_d)}{\pi(1+2G_d)\Gamma(1+2G_d)} \\ &\times \quad {}_2F_1\left(\frac{1}{2} + G_d, 1 + G_d; \frac{3}{2} + G_d; -1\right). \end{aligned} \tag{6.106}$$

The coding gain for EGC and GSEGC(N,L) with QPSK/MSK is

$$G_{c,QPSK/MSK} = \left(J_{ENV}(\mathbf{b}, \mathbf{g}, \mathbf{t}) M_{QPSK/MSK}\right)^{-1/G_d}. \tag{6.107}$$

5) MPSK

The ASEP of MPSK for EGC and GSEGC(N,L) can be expressed as

$$\begin{aligned} P_{MPSK}(\bar{\gamma}) &\simeq J_{ENV}(\mathbf{b},\mathbf{g},\mathbf{t})\frac{\bar{\gamma}^{-\sum_{k=1}^{L}(t_k+1)}}{\Gamma\left(1+\sum_{k=1}^{L}2(t_k+1)\right)} \\ &\times \underbrace{\frac{2}{\pi}\int_0^{(M-1)\pi/M}\int_0^{\infty} x^{1+\sum_{k=1}^{L}2(t_k+1)}\frac{\sin^2(\pi/M)}{\sin^2\theta}e^{-\frac{\sin^2(\pi/M)}{\sin^2\theta}x^2}dxd\theta}_{INT5}. \end{aligned} \quad (6.108)$$

Recognizing *INT5* is of the form (C.2) with $\theta_U=\frac{(M-1)\pi}{M}$, $\theta_c=\frac{\pi}{M}$, and $\alpha=G_d=\sum_{k=1}^{L}(t_k+1)$ when $h(\theta)=\frac{\sin^2\theta_c}{\sin^2\theta}$ in the appendix, we can obtain

$$P_{MPSK}(\bar{\gamma}) \simeq J_{ENV}(\mathbf{b},\mathbf{g},\mathbf{t})\bar{\gamma}^{-G_d}\frac{2^{-(2G_d+1)}}{\sqrt{\pi}}\frac{\Gamma(2+2G_d)}{\Gamma\left(\frac{3}{2}+G_d\right)}\frac{I_s(G_d,(M-1)\pi/M)}{\sin^{2G_d}(\pi/M)}, \quad (6.109)$$

where $I_s(G_d,(M-1)\pi/M)$ can be calculated in a closed-form by (C.5) in the appendix. The modulation factor is then given by

$$M_{MPSK}=\frac{2^{-(2G_d+1)}}{\sqrt{\pi}}\frac{\Gamma(2+2G_d)}{\Gamma\left(\frac{3}{2}+G_d\right)}\frac{I_s(G_d,(M-1)\pi/M)}{\sin^{2G_d}(\pi/M)}. \quad (6.110)$$

The coding gain for EGC and GSEGC(N,L) with MPSK is

$$G_{c,MPSK}=(J_{ENV}(\mathbf{b},\mathbf{g},\mathbf{t})M_{MPSK})^{-1/G_d}. \quad (6.111)$$

6) MDPSK

The ASEP of MDPSK for EGC and GSEGC(N,L) can be expressed as

$$\begin{aligned} P_{MDPSK}(\bar{\gamma}) &\simeq J_{ENV}(\mathbf{b},\mathbf{g},\mathbf{t})\frac{\bar{\gamma}^{-\sum_{k=1}^{L}(t_k+1)}}{\Gamma\left(1+\sum_{k=1}^{L}2(t_k+1)\right)} \\ &\times \underbrace{\frac{2}{\pi}\int_0^{\frac{(M-1)\pi}{M}}\int_0^{\infty} x^{1+\sum_{k=1}^{L}2(t_k+1)}\frac{\sin^2\left(\frac{\pi}{M}\right)}{1+\cos\left(\frac{\pi}{M}\right)\cos\theta}e^{-\frac{\sin^2\left(\frac{\pi}{M}\right)}{1+\cos\left(\frac{\pi}{M}\right)\cos\theta}x^2}dxd\theta}_{INT6}. \end{aligned} \quad (6.112)$$

Recognizing *INT6* is of the form (C.2) with $\theta_U = \frac{(M-1)\pi}{M}$, $\theta_c = \frac{\pi}{M}$, and $\alpha = G_d = \sum_{k=1}^{L}(t_k+1)$ when $h(\theta) = \frac{\sin^2\theta_c}{1+\cos\theta_c\cos\theta}$ in the appendix, we can obtain

$$P_{MDPSK}(\bar{\gamma}) \simeq J_{ENV}(\mathbf{b},\mathbf{g},\mathbf{t})\bar{\gamma}^{-G_d}\frac{2^{-(2G_d+1)}}{\sqrt{\pi}}\frac{\Gamma(2+2G_d)}{\Gamma\left(\frac{3}{2}+G_d\right)}\frac{I_V(G_d,(M-1)\pi/M)}{\sin^{2G_d}(\pi/M)} \quad (6.113)$$

where $I_V(G_d,(M-1)\pi/M)$ can be calculated in a closed-form by (C.16) in the appendix. The modulation factor is then given by

$$M_{MDPSK} = \frac{2^{-(2G_d+1)}}{\sqrt{\pi}}\frac{\Gamma(2+2G_d)}{\Gamma\left(\frac{3}{2}+G_d\right)}\frac{I_V(G_d,(M-1)\pi/M)}{\sin^{2G_d}(\pi/M)}. \quad (6.114)$$

The coding gain for EGC and GSEGC(N,L) with MDPSK is

$$G_{c,MDPSK} = (J_{ENV}(\mathbf{b},\mathbf{g},\mathbf{t})M_{MDPSK})^{-1/G_d}. \quad (6.115)$$

6.3.3 Outage Probability

Since the asymptotic CDFs of diversity combiners are derived and available in the previous section, we can obtain the asymptotic outage probability for MRC, SDC, and GSC(N,L) as

$$P_{out}(\gamma_{th}) \simeq \frac{J_{SNR}(\mathbf{b},\mathbf{g},\mathbf{t})}{\Gamma\left(1+\sum_{k=1}^{L}(t_k+1)\right)}\left(\frac{\bar{\gamma}}{\gamma_{th}}\right)^{-\sum_{k=1}^{L}(t_k+1)}, \quad (6.116)$$

where $J_{SNR}(\mathbf{b},\mathbf{g},\mathbf{t})$ represents $J_{MRC}(\mathbf{b},\mathbf{g},\mathbf{t})$, $J_{SDC}(\mathbf{b},\mathbf{g},\mathbf{t})$, or $J_{GSC}(\mathbf{b},\mathbf{g},\mathbf{t})$. For NTGSC($\mu$,$L$), we can obtain

$$P_{out}(\gamma_{th}) \simeq \frac{\sum_{N=1}^{L} J_{NTGSC}(\mathbf{b},\mathbf{g},\mathbf{t},N)}{\Gamma\left(1+\sum_{k=1}^{L}(t_k+1)\right)}\left(\frac{\bar{\gamma}}{\gamma_{th}}\right)^{-\sum_{k=1}^{L}(t_k+1)}. \quad (6.117)$$

For EGC and GSEGC(N,L), we can express as

$$P_{out}(\sqrt{\gamma_{th}}) \simeq \frac{J_{ENV}(\mathbf{b},\mathbf{g},\mathbf{t})}{\Gamma\left(1+\sum_{k=1}^{L}2(t_k+1)\right)}\left(\frac{\bar{\gamma}}{\gamma_{th}}\right)^{-\sum_{k=1}^{L}(t_k+1)}, \quad (6.118)$$

where $J_{ENV}(\mathbf{b},\mathbf{g},\mathbf{t})$ represents $J_{EGC}(\mathbf{b},\mathbf{g},\mathbf{t})$ or $J_{GSEGC}(\mathbf{b},\mathbf{g},\mathbf{t})$. From the above equations, we can also obtain the outage diversity gain and the outage coding gain as we did for the

error probability. The outage diversity gain can be expressed as

$$O_d = G_d = \sum_{k=1}^{L}(t_k + 1), \tag{6.119}$$

which is the same as the error probability diversity gain, and the outage coding gain for MRC, SDC, and GSC(N,L) can be given by

$$O_c = \left(\frac{J_{SNR}(\mathbf{b}, \mathbf{g}, \mathbf{t})}{\Gamma\left[1 + \sum_{k=1}^{L}(t_k + 1)\right]} \right)^{-1/O_d}. \tag{6.120}$$

For NTGSC(μ,L), the outage coding gain is expressed as

$$O_c = \left(\frac{\sum_{N=1}^{L} J_{NTGSC}(\mathbf{b}, \mathbf{g}, \mathbf{t}, N)}{\Gamma\left[1 + \sum_{k=1}^{L}(t_k + 1)\right]} \right)^{-1/O_d}. \tag{6.121}$$

Finally, the outage coding gain for EGC and GSEGC(N,L) is

$$O_c = \left(\frac{J_{ENV}(\mathbf{b}, \mathbf{g}, \mathbf{t})}{\Gamma\left[1 + \sum_{k=1}^{L} 2(t_k + 1)\right]} \right)^{-1/O_d}. \tag{6.122}$$

6.3.4 Loss of Coding Gain

The performance of coherent SDC (or GSC(1,L)), GSC(N,L), and NTGSC(μ,L) is lower-bounded by that of MRC (or GSC(L,L)), and the performance of coherent GSEGC(N,L) is lower-bounded by that of EGC. In this section, we define the loss of the coding gain of GSC(N,L)/NTGSC(μ,L) (GSEGC(N,L)) with respect to MRC (EGC) to investigate the performance gap between these diversity combining schemes. The loss of coding gain can be defined as

$$\zeta_{(N,L)}^{GSC} = \left(\frac{J_{GSC}(\mathbf{b}, \mathbf{g}, \mathbf{t})}{J_{MRC}(\mathbf{b}, \mathbf{g}, \mathbf{t})} \right)^{1/G_d}, \tag{6.123}$$

for GSC(N,L),

$$\zeta_{(\mu,L)}^{NTGSC} = \left(\frac{\sum_{N=1}^{L} J_{NTGSC}(\mathbf{b}, \mathbf{g}, \mathbf{t}, N)}{J_{MRC}(\mathbf{b}, \mathbf{g}, \mathbf{t})} \right)^{1/G_d}, \tag{6.124}$$

for NTGSC(μ,L), and

$$\zeta_{(N,L)}^{GSEGC} = \left(\frac{J_{GSEGC}(\mathbf{b},\mathbf{g},\mathbf{t})}{J_{EGC}(\mathbf{b},\mathbf{g},\mathbf{t})} \right)^{1/G_d}, \tag{6.125}$$

for GSEGC(N,L).

6.3.5 Non-coherent Combining Loss

We define the non-coherent combining loss (NCL) as the coding gain loss of non-coherent GSC(N,L)/NTGSC(μ,L) with respect to coherent GSC(N,L)/NTGSC(μ,L) for BDPSK and BFSK. The non-coherent combining loss for non-coherent GSC(N,L) can be expressed for both BDPSK and NFSK as

$$\begin{aligned} \zeta_{Loss}^{NC} &= \left(\frac{1}{2^{2N-2}} \sum_{k=0}^{N-1} \frac{c_k \Gamma(G_d+k)}{\Gamma(G_d)} \right)^{1/G_d} \\ &= \left(1 + \frac{1}{2^{2N-2}} \sum_{k=1}^{N-1} \frac{c_k \Gamma(G_d+k)}{\Gamma(G_d)} \right)^{1/G_d} \end{aligned} \tag{6.126}$$

by using $c_0 = \sum_{l=0}^{N-1} \binom{2N-1}{l} = 2^{2N-2}$. Since $\sum_{k=1}^{N-1} \frac{c_k \Gamma(G_d+k)}{\Gamma(G_d)} \geq 0$ in (6.126), we can see that $\zeta_{Loss}^{NC} \geq 1$ holds true for generalized fading channels [65]. Also, as G_d increases (that is, the diversity order of GSC(N,L) receiver increases), it can be shown from the figure in the next section that ζ_{Loss}^{NC} decreases. Hence, as the diversity order increases, GSC(N,L) receiver reduces the non-coherent combining loss with respect to MRC receiver. Also, the non-coherent combining loss for non-coherent NTGSC(μ,L) can be expressed for both BDPSK and NFSK as

$$\zeta_{Loss}^{NC} = \left[\frac{\sum_{N=1}^{L} J_{NTGSC}(\mathbf{b},\mathbf{g},\mathbf{t},N) \frac{1}{2^{2N-2}} \sum_{k=0}^{N-1} \frac{c_k \Gamma(G_d+k)}{\Gamma(G_d)}}{\sum_{N=1}^{L} J_{NTGSC}(\mathbf{b},\mathbf{g},\mathbf{t},N)} \right]^{1/G_d}. \tag{6.127}$$

6.4 Numerical Results

In Figure 6.1, we first present exact and asymptotic ABEP results for GSC(N,4) with coherent BPSK modulation on independent but non-identically distributed (i.n.d.) Nakagami-m

channel with fading factor m=[2.4 1.9 1.2 1] from the strongest to the weakest branch and an exponential power decay model for ASNR across diversity branches where the ASNR of the k^{th} diversity branch $\bar{\gamma}_k$ is defined as

$$\bar{\gamma}_k = \frac{\left(1 - e^{-\delta}\right) e^{-\delta(k-1)}}{1 - e^{-L\delta}} \bar{\gamma}_s \tag{6.128}$$

in which $\bar{\gamma}_s$ denotes the ASNR/symbol and δ represents the ASNR difference across the diversity branches. The x-axis is the total input ASNR divided by L, the total number of diversity branches, such as $\bar{\gamma} = \frac{\sum_{k=1}^{L} \bar{\gamma}_k}{L}$. It can be seen that the asymptotic ABEP becomes quite accurate when the ASNR $\bar{\gamma}$ is greater than 15 dB. Figure 6.2 also shows exact and asymptotic ABEP for GSC(N,4) with CBPSK on i.n.d. Rice channel with Rice factor K=[5 3 2 1] dB. In Figure 6.1 and 6.2, the diversity gain for the Nakagami-m channel is $G_d = 6.5$ and that of the Rice channel is $G_d = 4$. From the diversity gain expression $G_d = \sum_{k=1}^{L}(t_k+1)$ for the different types of diversity techniques in this chapter, we can see it depends only on the number of diversity branches and fading channel statistics which determine the value t_k. Hence, the diversity gain of GSC(N,4) for the Nakagami-m channel in Figure 6.1 is higher than that of the Rice channel in Figure 6.2, which can be also observed from the figures. However, the coding gain given by (6.41) for the Rice channel is higher than that of the Nakagami-m channel.

Figure 6.3 shows exact and asymptotic outage probability of GSC(N,4) on i.n.d. Nakagami-m fading channel with m=[1.8 1.5 1.2 0.9]. The x-axis is the normalized ASNR per branch defined as $\bar{\gamma}/\gamma_{th}$. Again, note that from (6.119), (6.120), (6.121), and (6.122) the error probability and outage probability diversity gains for SDC, MRC, GSC(N,L), EGC, and GSEGC(N,L) are identical although the coding gains of those diversity combiners are different.

Figure 6.4 shows exact and asymptotic ABEP of GSC(N,4) and GSEGC(N,4) with coherent BPSK on Nakagami-m fading channel with m=2. It can be seen that the performance difference between GSC(N,4) and GSEGC(N,4) gets smaller when $2 \leq N \leq 3$ and becomes exact same when $N = 1$. From this, we can say GSEGC(N,L) receiver can provide performance

comparable to that of GSC(N,L) but yet simpler receiver structure.

6.5 Chapter Summary

In this chapter, we have presented the asymptotic error and outage probability expression of SDC, MRC, GSC(N,L), EGC, and GSEGC(N,L) in a unifying way. The unifying asymptotic analysis framework can be expressed in terms of the diversity and coding gain, which can provide an insight on the performance differences of the presented different types of diversity combiners over generalized fading channels, and expedite parametric investigations. Along with simulations at low ASNRs, this asymptotic analysis (which becomes quite accurate from moderate to high ASNRs) provide a complete tool to analyze the performance of different types of diversity combiners over generalized fading channels.

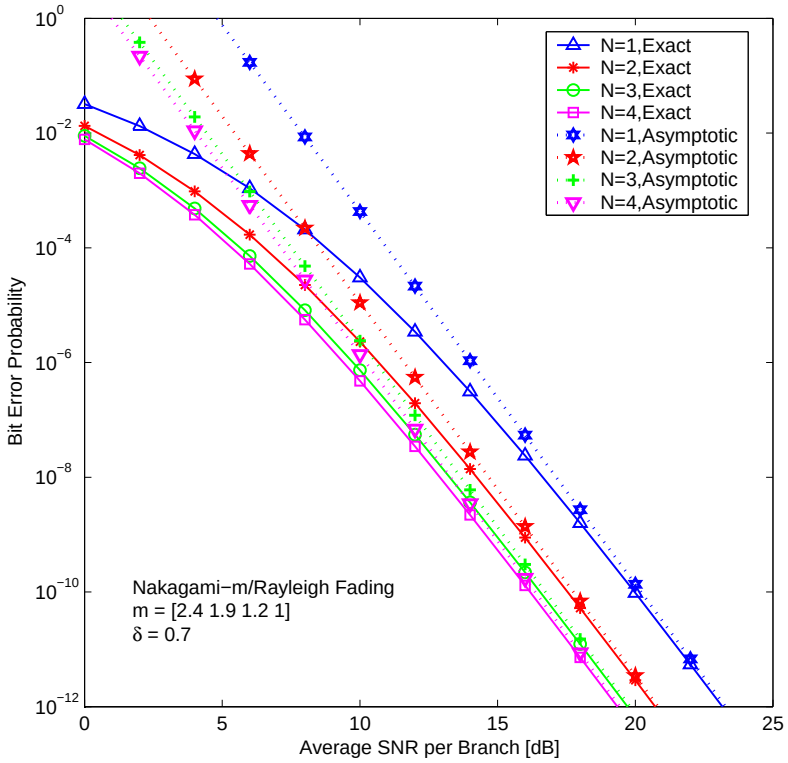

Figure 6.1: Exact and asymptotic ABEP of GSC(N,4) on i.n.d. Nakagami-m fading channel

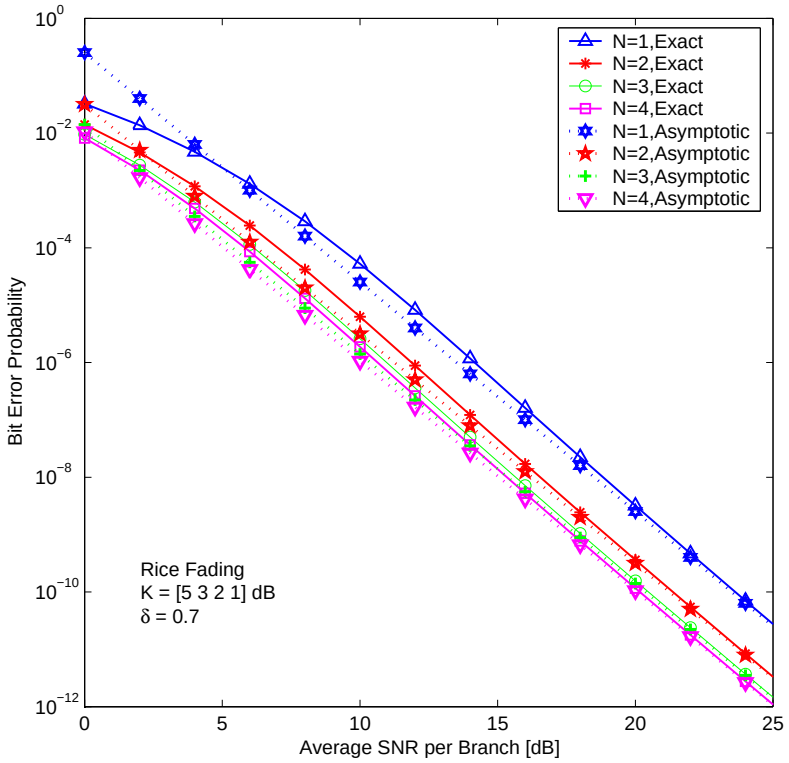

Figure 6.2: Exact and asymptotic ABEP of GSC(N,4) on i.n.d. Rice fading channel

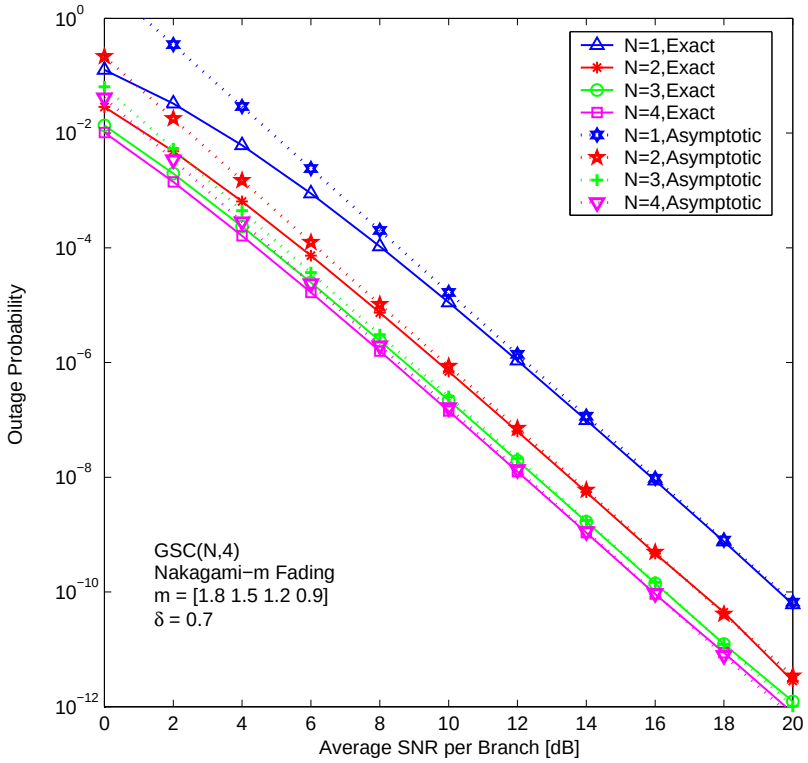

Figure 6.3: Exact and asymptotic outage probability of GSC(N,4) on i.n.d. Nakagami-m fading channel

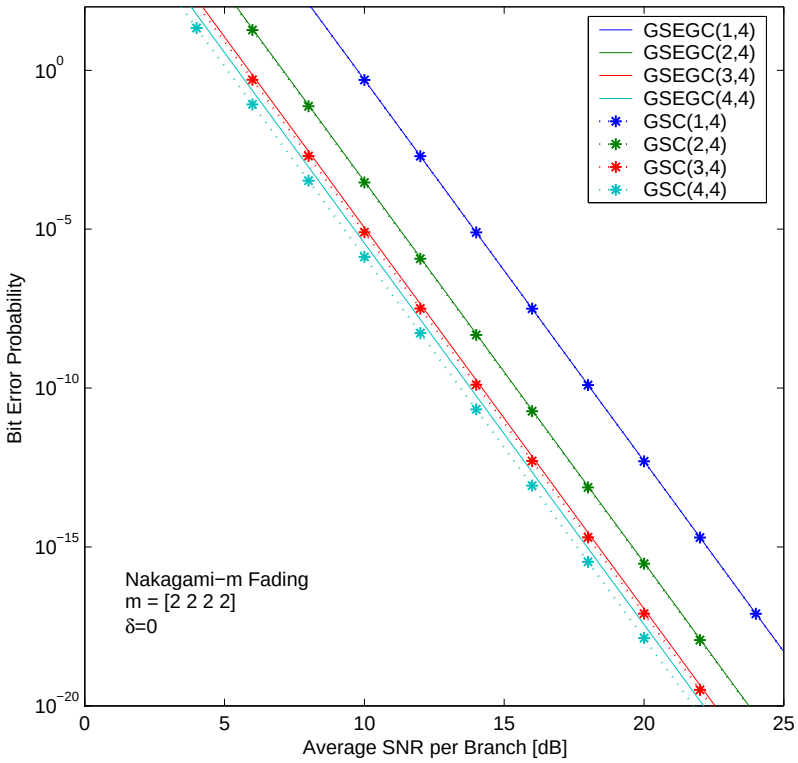

Figure 6.4: Exact and asymptotic ABEP of GSEGC(N,4) and GSC(N,4) on Nakagami-m fading channel

Chapter 7

Capacity and Interference Statistics of Reverse Link DS/CDMA with Transmit Diversity

The capacity of DS/CDMA (Direct Sequence Code-Division Multiple Access) systems is interference limited due to other users in the same frequency band unlike FDMA and TDMA capacities which are primarily bandwidth limited. Hence, any reduction in interference converts directly into an increase in capacity [66]. Especially on the reverse link of a DS/CDMA system, power control is essential to increase system capacity. Gilhousen et al. developed a mathematical model to estimate capacity of a DS/CDMA system and Viterbi et al. theoretically analyzed the impact of soft handoff on such a system. For system capacity analysis and estimation with power control, most previous works [66]-[68] considered only large scale log-normal shadow fading, which varies slowly, neglecting the effect of small scale fading due to multipaths or assuming that the effect of fast fluctuation due to multipaths is mitigated by various receiver techniques such as Rake combining, antenna diversity combining, and error correcting coding techniques for the simplicity of the analysis. However, there exists the effect of multipath on the system capacity interacting with power control. While perfect

power control eliminates fluctuations in the received signal level among intracell users, reducing required signal-to-interference ratio, it increases the intercell interference by tracking fluctuations due to multipaths. Meanwhile, slow power control with relatively slower power control command compared with the channel variations results in fluctuations in the received signal level, increasing outage probability. Therefore, the effect of multipath on system capacity should be taken into account, and [69]-[73] considered the effect of fast fluctuation due to multipaths on the system capacity of the reverse link of DS/CDMA. However, [69], [70] assumed an equal power multipath channel for simplicity, which is not realistic, [71] assumed an exponential power delay profile, which is Rayleigh faded, and [73] investigated the effect of transmit diversity, but assumed only one path. Our work extends and generalizes the previous works by:

1) Providing a general mathematical framework for analyzing the impact of diversity techniques associated with power control on system capacity and coverage;

2) Investigating the impact of open-loop transmit diversity (space-time block code) and closed-loop transmit diversity at the handset on system capacity and coverage as a function of a general channel model;

3) Analyzing the impact of diversity techniques on various fading statistics such as Rayleigh, Nakagami-m and Rice with standard specified multipath channel models;

4) Investigating the impact of different user distributions on system capacity and coverage;

5) Investigating the impact of correlation between diversity branches on system capacity and coverage.

7.1 System Model

In the following subsections, the system model including channel model, cell layout, and handoff region will be described in detail.

7.1.1 Propagation model

Mobile communication channels are generally modeled as consisting of fast fluctuations (also called short term fluctuations) around a slowly varying mean value (also called long term fluctuations). In general, fast fluctuations are caused by multipath fading and slow fluctuations are caused by the distance between two transceivers and shadowing fading effects.

First, large scale propagation loss, which varies slowly, is generally modeled as the product of the power of distance between transceivers and a shadowing component which has a log-normal distribution. That is, for a user at a distance r from a base station, the attenuation is proportional to

$$L_{longterm}(r, \mu) = r^{\mu} 10^{\zeta/10} \tag{7.1}$$

$$L_{longterm}(r, \zeta)_{dB} = 10\mu \log_{10}(r) + \zeta \tag{7.2}$$

where ζ is Gaussian distributed dB attenuation due to shadowing with zero mean and standard deviation σ.

Just as any analysis of other cell interference, our analysis involves a multiple cell system. Therefore, the propagation model must take into account the dependence of the propagation losses from a mobile user to two or more base stations. Taking this into account, the shadowing can be considered to be the sum of two components: a component in the near field of a user, which is common to all base stations, and a component which pertains solely to the receiving base station and is independent from one base station to another [67]. Hence, the random component of the dB loss due to shadowing from the i^{th} mobile to the j^{th} base station ($j = 0, 1, 2, \cdots$) can be expressed as [67]

$$\zeta_{ij} = a\xi + b\xi_j \tag{7.3}$$

where $a^2 + b^2 = 1$ with $E(\zeta_j) = E(\xi) = E(\xi_j) = 0$, $\text{var}(\zeta_j) = \text{var}(\xi) = \text{var}(\xi_j) = \sigma^2$ for all j, $E(\xi\xi_j) = 0$ for all j $E(\xi_i\xi_j) = 0$ for all i and j, $i \neq j$, and $E(\zeta_i\zeta_j)/\sigma^2 = a^2 = 1 - b^2$.

Second, let us consider the fast fluctuation of the signal caused by the multipath fading

channel. In general, the multipath fading channel is modeled as

$$h(t,\tau) = \sum_{l=0}^{L} \alpha_l(t)\delta(\tau - \tau_l) \tag{7.4}$$

where $\alpha_l(t)$ and τ_l are the complex-valued path gain and time delay of the l^{th} path, respectively, and $\alpha_l(t)$ satisfies the following condition:

$$\sum_{l=0}^{L} E[|\alpha_l(t)|^2] = 1. \tag{7.5}$$

In our analysis, it is assumed that $|\alpha_l(t)|$ follows a Nakagami-m distribution since we can evaluate the system capacity and coverage for various fading environment by changing the m factor. For instance, the Nakagami-m distribution is equivalent to a Rayleigh distribution with m equal to 1 and also can approximate a Rice distribution with the following relation of m factor of Nakagami-m distribution and K factor of the Rice distribution [75]:

$$m = \frac{1}{\left(1 - \frac{K^2}{(1+K)^2}\right)} \tag{7.6}$$

$$K = \frac{\sqrt{1-1/m}}{1-\sqrt{1-1/m}}. \tag{7.7}$$

However, our mathematical framework to be presented herein can handle any type of fading distribution including Nakagami-m, Nakagami-q, and Rice. Let us assume that the maximum fading Doppler frequency is very low compared to the data modulation symbol rate (as a matter of fact, in most practical situations it is). Then, the time dependency of the path gain can be dropped for notational simplicity [71]. The Probability Density Function (PDF) for the Nakagami-m distributed random varialbe α is given by

$$f_{\alpha_i}(\alpha) = \frac{2}{\Gamma(m)}\left(\frac{m}{\Omega_i}\right)\alpha^{2m-1}\exp\left(-\frac{m}{\Omega_i}\alpha^2\right) \tag{7.8}$$

where $m = \frac{\Omega_i^2}{E[(\alpha_i - \Omega_i)^2]} \geq \frac{1}{2}$ and $\Omega_i = E[\alpha_i^2]$. Therefore, the total propagation loss from a mobile i to a base station j can be denoted by

$$L_{total} = r_{ij}^{\mu}(x,y)10^{\zeta_{ij}/10}\frac{1}{X_{ij}} \tag{7.9}$$

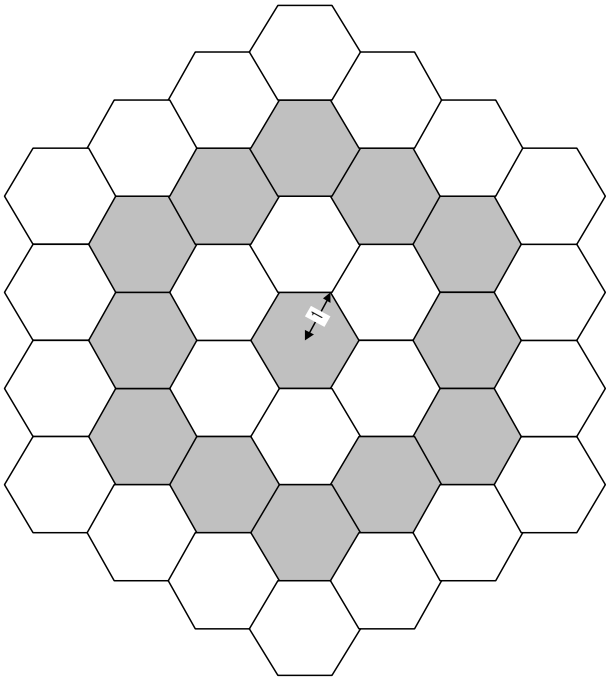

Figure 7.1: Cell layout of the entire system

where the first two terms are the μ^{th} power of distance and a log-normal random variable representing shadowing losses, respectively, and the third term is a random variable modeling short term fading loss due to multipath.

7.1.2 Cell layout

In our analysis, we assume that the cell has hexagonal shape and unity radius, defined as the maximum distance from any point in the cell to the base station at its center. The whole system consists of three rings of hexagonal cells which surround the center cell as shown in the Figure 7.1. We will evaluate the system capacity and coverage based on this center cell because the cell layout is symmetric. It is also assumed that users are uniformly distributed in the whole system and each cell is loaded with an equal number of users.

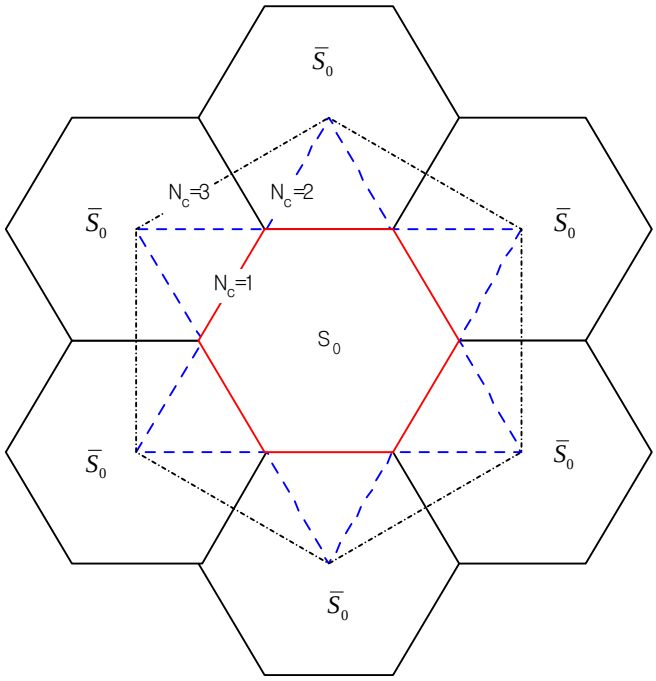

Figure 7.2: S_0 and $\overline{S}_0$ regions for $N_c = 1, 2,$ and3 (within respective boundaries)

7.1.3 Handoff region

In DS/CDMA cellular systems, mobile units in transition between one cell and its neighbor cells can simultaneously communicate with Nc base stations to make a handoff smooth. This technique is called soft handoff. With the given cell layout, the soft handoff region is defined as shown in the Figure 7.2. Since we are mainly interested in the center cell, the handoff region will be divided into two regions: one including the $zero^{th}$ base station (which is denoted by S_0) and another which does not include the $zero^{th}$ base station (denoted by $\overline{S}_0$).

Table 7.1: Space-time transmit diversity

	Antenna 1	Antenna 2
Symbol 1	x_1	x_2
Symbol 2	$-x_2^*$	x_1^*

7.2 Transmit Diversity Techniques

In third generation wideband CDMA systems, such as UMTS, transmit diversity techniques are adopted. In this work, two different transmit diversity schemes are used to investigate the impact of transmit diversity at the handset on system capacity. A theoretical expression is derived in [77], and it is shown that the result matches well with simulation [77].

7.2.1 Open-loop diversity

In the open loop transmit diversity (OLTD), the transmit does not have any information on the channels. To maximize the diversity, a space-time block code is employed as shown in Table 7.1 where x_1 and x_2 belong to a QPSK symbol, which are complex numbers. During symbol duration T, x_1 is transmitted from antenna 1, and $-x_2^*$ from antenna 2. For the next symbol duration, x_2 is transmitted from antenna 1 and x_1^* from antenna 2. In a multipath channel with L resolvable multipaths, the received signal for two consecutive symbol durations will be

$$r_1(t) = \sum_{k=1}^{L}[h_{1,k}x_1 s(t-\tau_k) + h_{2,k}x_2 s(t-\tau_k)] + n_1(t) \tag{7.10}$$

$$r_2(t) = \sum_{k=1}^{L}[-h_{1,k}x_2^* s(t-\tau_k) + h_{2,k}x_1^* s(t-\tau_k)] + n_2(t) \tag{7.11}$$

where $s(t)$ is the spreading sequence. Then, the output of rake finger k will be

$$r_{1,k} = \int_{t_1}^{t_1+T} r_1(t)s^*(t-\tau_k)dt$$

$$= h_{1,k}x_1 + h_{2,k}x_2 + n_{1,k} \tag{7.12}$$

$$\begin{aligned} r_{2,k} &= \int_{t_1+T}^{t_1+2T} r_2(t)s^*(t-\tau_k)dt \\ &= -h_{1,k}x_2^* + h_{2,k}x_1^* + n_{2,k} \end{aligned} \tag{7.13}$$

and the maximum likelihood estimate becomes

$$\begin{aligned} \hat{x}_1 &= \sum_{k=1}^{L} \left(h_{1,k}^* r_{1,k} + h_{2,k} r_{2,k}^*\right) \\ &= \sum_{k=1}^{L} \left(|h_{1,k}|^2 + |h_{2,k}|^2\right) x_1 + \tilde{n}_1 \end{aligned} \tag{7.14}$$

$$\begin{aligned} \hat{x}_2 &= \sum_{k=1}^{L} \left(h_{2,k}^* r_{1,k} + h_{1,k} r_{2,k}^*\right) \\ &= \sum_{k=1}^{L} \left(|h_{1,k}|^2 + |h_{2,k}|^2\right) x_2 + \tilde{n}_2. \end{aligned} \tag{7.15}$$

Hence, open-loop diversity gives $2L$ branch diversity with a 3 dB transmit power penalty.

7.2.2 Closed-loop diversity

In the closed loop transmit diversity (CLTD), the transmitter has knowledge of the channels and transmits on both antennas simultaneously but with weights chosen to optimize the SNR at the receiver. The received signal with weighted transmission is,

$$r(t) = \sum_{k=1}^{L} [w_1 h_{1,k} x s(t-\tau_k) + w_2 h_{2,k} x s(t-\tau_k)] + n(t) \tag{7.16}$$

the k^{th} rake finger output is,

$$r_k = \int_{t_1}^{t_1+T} r(t)s^*(t-\tau_k)dt = w_1 h_{1,k} x + w_2 h_{2,k} x + n_k \tag{7.17}$$

and the maximal ratio combiner (MRC) output is

$$\begin{aligned} \hat{x} &= \sum_{k=1}^{L} \left(w_1 h_{1,k} + w_2 h_{2,k}\right)^* r_k \\ &= \sum_{k=1}^{L} \left\{ ||w_1 h_{1,k} + w_2 h_{2,k}||^2 x_k + (w_1 h_{1,k} + w_2 h_{2,k}) n_k \right\} \end{aligned} \tag{7.18}$$

Hence, the equivalent channel after antenna weights are applied is $\tilde{h}_k = w_1 h_{1,k} + w_2 h_{2,k}$ and the objective is to choose the weights such that this channel has maximum power at the receiver. Let's assume the following channel model to analyze the performance of CLTD

$$h(t,\tau) = \sum_{k=1}^{L} \alpha_k(t)\delta(\tau - \tau_k), \tag{7.19}$$

where the complex-valued path gains $\alpha_k(t)$ exhibit independent fading. Furthermore, the channels for the two antennae are independent with the same average path powers, $E[|\alpha_k|^2]$, and delays, τ_k. In the rake receiver, if perfect dispreading is assumed and any self-interference is ignored, the SNR at the MRC output can be written as

$$\gamma = \frac{||\mathbf{Hw}||^2}{\sigma_n^2} = \frac{\mathbf{w}^H \mathbf{H}^H \mathbf{H}\mathbf{w}}{\sigma_n^2 \mathbf{w}^H \mathbf{w}} \tag{7.20}$$

defining the weight vector and channel matrix as

$$\mathbf{w} = \begin{pmatrix} w_1 \\ w_2 \end{pmatrix}$$

$$\mathbf{H} = (\mathbf{h_1} \quad \mathbf{h_2}) = \begin{pmatrix} h_{1,2} & h_{2,2} \\ \vdots & \vdots \\ h_{1,L} & h_{2,L} \end{pmatrix}$$

The weights are normalized such that $||\mathbf{w}||^2 = |w_1|^2 + |w_2|^2 = 1$ to maintain the same output power. The SNR in (7.20) is a Rayleigh quotient and hence the maximum SNR is proportional to the largest eigenvalue of $\mathbf{H}^H\mathbf{H}$ and the optimal weight $\mathbf{w}$ is the eigenvector corresponding to this eigenvalue. The matrix $\mathbf{H}^H\mathbf{H}$ is

$$\mathbf{H}^H\mathbf{H} = \begin{pmatrix} \sum_{k=1}^{L} |h_{1,k}|^2 & \sum_{k=1}^{L} h_{1,k}h_{2,k}^* \\ \sum_{k=1}^{L} h_{2,k}h_{1,k}^* & \sum_{k=1}^{L} |h_{2,k}|^2 \end{pmatrix}. \tag{7.21}$$

Due to the difficulty of finding the PDF of this matrix, the maximum eigenvalue can be bounded by the fact that the sum of eigenvalues is the trace of the matrix and hence

$$\frac{1}{2\sigma_n^2} \sum_{k=1}^{L} \left(|h_{1,k}|^2 + |h_{2,k}|^2\right) \leq \lambda_{max} \leq \frac{1}{\sigma_n^2} \sum_{k=1}^{L} \left(|h_{1,k}|^2 + |h_{2,k}|^2\right). \tag{7.22}$$

The upper bound and the lower bound have the same PDF with a 3 dB difference in average SNR. Since the diagonal elements of $\mathbf{H}^H\mathbf{H}$ combine coherently while the off-diagonal elements combine incoherently, the matrix can be approximated to be diagonal, and hence

$$\lambda_{max} \simeq \frac{1}{\sigma_n^2}\sum_{k=1}^{L}\left(|h_{1,k}|^2 + |h_{2,k}|^2\right) = \sum_{k=1}^{L}(\gamma_{1,k} + \gamma_{2,k}). \tag{7.23}$$

This gives 2L diversity without the 3 dB transmit power penalty incurred in the uplink open-loop transmit diversity case. It is shown that this theoretical expression matches simulation results well [77].

7.3 Interference Statistics and Capacity Analysis

7.3.1 Intercell interference

Interference consists of intra-cell interference and intercell interference. Suppose we are trying to calculate the interference for the zeroth base station, which is the reference base station BS_0. Then, intra-cell interference is the interference to other users connected to BS_0 caused by the transmitted power of mobile stations which are connected to and power-controlled by BS_0, while inter-cell interference is caused by mobile stations which are connected to and power-controlled by other base stations not including BS_0. If we assume perfect power control in the reverse link, the intra-cell interference is almost constant. On the other hand, the inter-cell interference varies according to the number of users and the amount of power control.

Let us consider the case when a mobile station communicates with the k^{th} base station as shown in Figure 7.3. With the assumption that the transmit power is perfectly power-controlled so as to compensate both slow and fast fluctuation of the channel, the received power at the k^{th} base station from a mobile station can be expressed as

$$P_R = P_T \cdot \frac{1}{r_k^{\mu} 10^{\zeta_k/10}} \cdot X_k = S \tag{7.24}$$

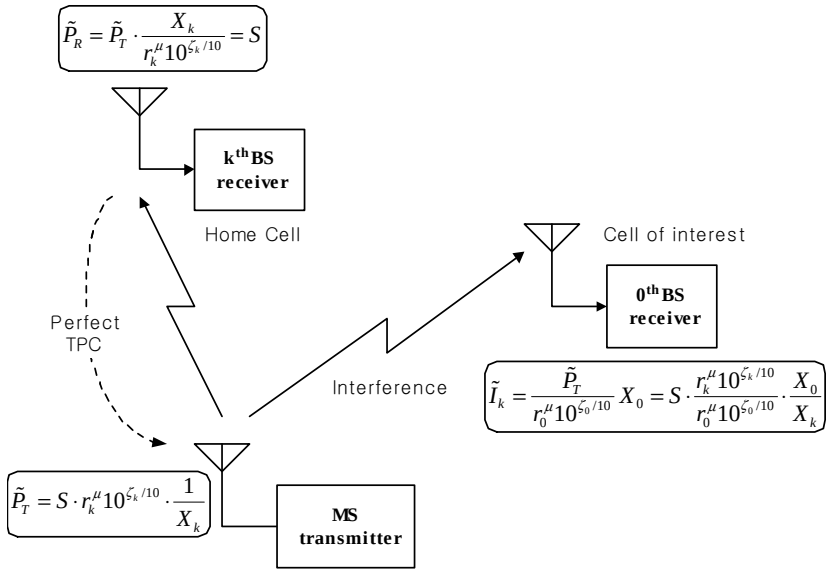

Figure 7.3: Power levels at an MS, home BS, and zeroth BS with perfect power control

where P_T denotes the transmitted power from a mobile station, $r_k^{\mu} 10^{\zeta_k/10}$ represents the propagation loss and long-term fading due to shadowing, X_k is a random variable modeling the effect of multipath fading of the channel, and S is the target E_b/I_0 satisfying the minimum BER (bit error rate) condition. That is, the received power from a mobile station appears as a constant power S to the k^{th} base station by means of the perfect power control. Then, the transmitted power from a mobile station is given by

$$P_T = S \cdot \ r_k^{\mu} 10^{\zeta_k/10} \cdot \frac{1}{X_k} \tag{7.25}$$

Hence, in (7.25), $r_k^{\mu} 10^{\zeta_k/10}$ represents the additional power transmitted due to propagation loss and shadow fading, and $1/X_k$ models the additional power transmitted due to multipath fading. Since the instantaneous transmit power of the mobile station will suffer both propagation loss and multipath fading, the instantaneous interference power I_k to the zeroth base station from a mobile station which is connected to the k^{th} base station, is given by

[67], [70]

$$I_k = \frac{P_T}{r_0^{\mu} 10^{\zeta_0/10}} \cdot X_0 = S \cdot \frac{r_k^{\mu} 10^{\zeta_k/10}}{r_0^{\mu} 10^{\zeta_0/10}} \cdot \frac{X_0}{X_k} \tag{7.26}$$

where X_0 represents the effect of multipath fading to the zeroth base station and is given by

$$X_0 = \sum_{l=1}^{L_m} |\alpha_l|^2 \tag{7.27}$$

where L_m is the number of multipath components between k^{th} mobile and the zeroth base station and α_l is the complex-valued channel gain due to multipath fading. $|\alpha_l|$ can be subject to Rayleigh, Nakagami-m, Rice, or Nakagami-q fading. Here, note that X_0 and X_k are independent, and X_k depends on the fading statistics and the type of diversity techniques used at the mobile station (transmit diversity) and the k^{th} base station (receive diversity). The total inter-cell interference power is the sum of the transmitted power from all mobile stations which are not power-controlled by the zeroth base station. It is known that the statistics of total inter-cell interference can be approximated by a log-normal distribution rather than a Gaussian distribution in the case of perfect power control [69]-[71]. Therefore, we can characterize the distribution function of the total inter-cell interference with only a mean and variance in this case. However, if power control can't track the fast signal fluctuation due to multipath fading, the received signal at the k^{th} basestation has still short-term fading statistics such as Rayleigh, Nakagami-m, or Rice, instead of a constant power S [78]. This can be modeled as a slow power control where only long-term fading is tracked and compensated by the power control. Hence, the slow power control can be considered as a lower bound of a system employing power control algorithm. In the case of slow power control, the instantaneous interference at the zeroth basestation can be expressed as

$$\tilde{I}_k = \widetilde{P}_T \cdot \frac{X_0}{r_0^{\mu} 10^{\zeta_0/10}} = S \cdot \frac{r_k^{\mu} 10^{\zeta_k/10}}{r_0^{\mu} 10^{\zeta_0/10}} \cdot X_0 \tag{7.28}$$

where $\widetilde{P}_T = S \cdot r_k^{\mu} 10^{\zeta_k/10}$ since short-term fading is not compensated.

Now, let's suppose an MS in $\overline{S}_0$ is perfectly power-controlled by the j^{th} basestation and is in soft handoff with multiple base stations where the number of basestations involved in soft handoff is N_c. Then, the normalized instantaneous intercell interference to the zeroth

basestation from the i^{th} MS in $\overline{S}_0$ can be expressed as

$$\left(\frac{I_{oc}^{(i)}}{S}\right)_{\overline{S}_0} = \frac{\min_{j=1}^{N_c}\{r_{ij}^{\mu}10^{\zeta_{ij}/10}\}}{r_{i0}^{\mu}10^{\zeta_{i0}/10}} \cdot \frac{X_{i0}}{X_{ij}}, \tag{7.29}$$

Also, if an MS in S_0 is perfectly power-controlled by the j^{th} basestation, which exclude the zeroth basestation, and is in soft handoff with multiple base stations, the normalized instantaneous intercell interference to the zeroth basestation from the i^{th} MS in S_0 can be expressed as

$$\left(\frac{I_{oc}^{(i)}}{S}\right)_{S_0} = \frac{\min_{j=1}^{N_c-1}\{r_{ij}^{\mu}10^{\zeta_{ij}/10}\}}{r_{i0}^{\mu}10^{\zeta_{i0}/10}} \cdot \frac{X_{i0}}{X_{ij}}, \tag{7.30}$$

where $\min_{j=1}^{N_c-1}\{r_{ij}^{\mu}10^{\zeta_{ij}/10}\} < r_{i0}^{\mu}10^{\zeta_{i0}/10}$.

7.3.2 Intercell Interference statistics under soft handoff

As previously mentioned, since it is known that the statistics of intercell interference can be approximated to be log-normal distribution in the case of perfect power control, the mean and variance of the total interference are the required parameters to evaluate the outage probability of the received signal on the reverse link of DS/CDMA system. The n^{th} moment to obtain the mean and variance of the interference from a mobile station in $\overline{S}_0$ and from a mobile station in S_0 can be calculated as, respectively,

$$E\left[\left(\frac{I_{oc}^{(i)}}{S}\right)_{\overline{S}_0}^{n}\right] = E\left[\frac{\min_{j=1}^{N_c}\{r_{ij}^{n\mu}10^{n\zeta_{ij}/10}\}}{r_{i0}^{n\mu}10^{n\zeta_{i0}/10}}\right] E[X_{i0}^{n}]E\left[\frac{1}{X_{ij}^{n}}\right], \tag{7.31}$$

$$E\left[\left(\frac{I_{oc}^{(i)}}{S}\right)_{S_0}^{n}\right] = E\left[\frac{\min_{j=1}^{N_c-1}\{r_{ij}^{n\mu}10^{n\zeta_{ij}/10}\}}{r_{i0}^{n\mu}10^{n\zeta_{i0}/10}}\right] E[X_{i0}^{n}]E\left[\frac{1}{X_{ij}^{n}}\right]. \tag{7.32}$$

The first expectations of the right hand side (RHS) of (7.31) and (7.32) can be expressed as, respectively, [67], [70]

$$E\left[\frac{\min_{j=1}^{N_c}\{r_{ij}^{n\mu}10^{n\zeta_{ij}/10}\}}{r_{i0}^{n\mu}10^{n\zeta_{i0}/10}}\right]$$

$$= \sum_{j=1}^{N_c} R_{ij}^{n\mu} E[10^{n(\zeta_{ij}-\zeta_{i0})/10}; r_{ij}^{\mu} 10^{\zeta_{ij}/10} < r_{ik}^{\mu} 10^{\zeta_{ik}/10} \quad \text{for all } k \neq j, k > 0]$$

$$= e^{n^2 b^2 (\beta\sigma)^2} \sum_{j=1}^{N_c} R_{ij}^{n\mu} \int_{-\infty}^{\infty} \frac{e^{-z^2/2}}{\sqrt{2\pi}} \prod_{\substack{k=1 \\ k\neq j}}^{N_c} Q\left(z + nb\beta\sigma + \frac{M_{ij} - M_{ik}}{b\sigma}\right) dz, \tag{7.33}$$

and

$$E \left[\frac{\min_{j=1}^{N_c-1}\{r_{ij}^{n\mu} 10^{n\zeta_{ij}/10}\}}{r_{i0}^{n\mu} 10^{n\zeta_{i0}/10}}\right]$$

$$= \sum_{j=1}^{N_c-1} R_{ij}^{n\mu} E[10^{n(\zeta_{ij}-\zeta_{i0})/10}; \min_{k=1}^{N_c-1}\left(r_{ik}^{\mu} 10^{\zeta_{ik}/10}\right) = r_{ij}^{\mu} 10^{\zeta_{ij}/10} < r_{i0}^{\mu} 10^{\zeta_{i0}/10}]$$

$$= e^{n^2 b^2 (\beta\sigma)^2} \sum_{j=1}^{N_c-1} R_{ij}^{n\mu} \int_{-\infty}^{\infty} \frac{e^{-z^2/2}}{\sqrt{2\pi}} Q\left(z + \frac{M_{ij} - M_{i0}}{b\sigma} + 2nb\beta\sigma\right)$$

$$\times \prod_{\substack{k=1 \\ k\neq j}}^{N_c-1} Q\left(z + \frac{M_{ij} - M_{ik}}{b\sigma} + nb\beta\sigma\right) dz, \tag{7.34}$$

where $b = \sqrt{1/2}$, $\beta = \ln(10)/10$, σ is the standard deviation of log-normal shadow fading, $R_{ij} = r_{ij}/r_{i0}$, $M_{ij} = 10\mu\log_{10}(r_{ij})$, and $Q(y) = \int_y^{\infty} e^{-x^2/2}/\sqrt{2\pi}$.

Evaluating the second and third expectations of the RHS of (7.31) and (7.32) for arbitrary mutipath fading channels can be achieved through calculating the PDF (probability density function) of X_{i0} and X_{ij} in (7.31) and (7.32). While X_{i0} represents the effect of multipath fading process from the i^{th} MS to the zeroth basestation, $1/X_{ij}$ models the additional power transmitted by the i^{th} MS to compensate for the multipath fading process to the j^{th} basestation, which power-controls the i^{th} MS, using diversity combining processing. Let us assume that basestation employs the receive diversity of order L_r and rake receiver with maximal ratio combining (MRC) for L_m multipaths, and the MS employs the transmit diversity of order L_t. Then, when closed-loop transmit diversity is employed, the random variable X_{ij} can be expressed as

$$X_{ij} \simeq \sum_{m=1}^{L_t} \sum_{n=1}^{L_r} \sum_{l=1}^{L_m} |\alpha_{m,n,l}|^2, \tag{7.35}$$

and when open-loop transmit diversity (space-time block code: STBC) is employed,

$$X_{ij} = \sum_{m=1}^{L_t} \sum_{n=1}^{L_r} \sum_{l=1}^{L_m} |\alpha_{m,n,l}|^2 / L_t, \tag{7.36}$$

where $\alpha_{m,n,l}$ represents the complex-valued channel gain due to multipath fading of the l^{th} path from transmit antenna branch m to receive antenna branch n. $|\alpha_{m,n,l}|$ can be subject to Rayleigh, Nakagami-m, Rice, or Nakagami-q fading statistics. Since X_{ij} is the sum of random variables $|\alpha_{m,n,l}|^2$, the PDF of X_{ij} can be obtained by the convolution of the PDF of each random variable. However, convolution is usually a complex operation; hence, by using the moment generating function (MGF), we can obtain the PDF of X_{ij} more easily than with convolution. Let $\phi_{X_{ij}}(s)$ and $\phi_{m,n,l}(s)$ be the MGF of X_{ij} and $|\alpha_{m,n,l}|^2$, respectively. If we assume that the multipath profile in each diversity branch has independent fading statistics, then the MGF of X_{ij} can be expressed as

$$\phi_{X_{ij}}(s) \simeq \prod_{m=1}^{L_t} \prod_{n=1}^{L_r} \prod_{l=1}^{L_m} \phi_{m,n,l}(s) \tag{7.37}$$

when closed-loop transmit diversity is employed, and

$$\phi_{X_{ij}}(s) = \prod_{m=1}^{L_t} \prod_{n=1}^{L_r} \prod_{l=1}^{L_m} \phi_{m,n,l}(s/L_t) \tag{7.38}$$

when open-loop transmit diversity is employed. Note that $\phi_{m,n,l}(s)$ can have different fading statistics in this model. The PDF of X_{ij} can be obtained from (7.37) or (7.38) through inverse Laplace transform, but, in general, for the general fading distributions, the closed form expression does not exist; hence, we have to use numerical methods to calculate the PDF of X_{ij} and the n^{th} moment of X_{i0} and $1/X_{ij}$ in (7.31) and (7.32) for the general fading distributions. The PDF of X_{ij} can be calculated by using the numerical inversion of Laplace transform proposed by Abate [36],

$$\begin{aligned} f_{X_{ij}}(x) &= L^{-1}[\phi_{X_{ij}}(s)] \\ &\simeq \frac{e^{A/2} 2^{-C}}{x} \sum_{k=0}^{C} \binom{C}{k} \left[\sum_{b=0}^{B+k} \frac{(-1)^b}{\delta_b} \Re \left\{ \phi_{X_{ij}} \left(\frac{A + 2\pi i b}{2x} \right) \right\} \right], \end{aligned} \tag{7.39}$$

where $\delta_b = \begin{cases} 2 & b = 0 \\ 1 & b = 1, 2, \ldots \end{cases}$, $\Re[\cdot]$ denotes the real part of complex argument, and the constants A, B, C are arbitrarily chosen to be 30, 18, and 24, respectively, to yield an accuracy of at least 10^{-7}. Then, the second expectations of (7.31) and (7.32) can be calculated by

$$\begin{aligned} E[X_{i0}^n] &= \int_0^\infty x^n f_{X_{i0}}(x) dx \\ &\simeq \int_0^\infty e^{A/2} 2^{-C} x^{n-1} \sum_{k=0}^{C} \binom{C}{k} \left[\sum_{b=0}^{B+k} \frac{(-1)^b}{\delta_b} \Re \left\{ \phi_{X_{i0}} \left(\frac{A + 2\pi i b}{2x} \right) \right\} \right] dx, \quad (7.40) \end{aligned}$$

where $\phi_{X_{i0}}(s) = L[\sum_1^{L_m} |\alpha_l|^2] = \prod_{l=1}^{L_m} \phi_l(s)$, and the third expectations can be calculated by

$$\begin{aligned} E\left[\frac{1}{X_{ij}^n} \right] &= \int_u^\infty \frac{1}{x^n} f_{X_{ij}}(x) dx \\ &\simeq \int_u^\infty \frac{e^{A/2} 2^{-C}}{x^{n+1}} \sum_{k=0}^{C} \binom{C}{k} \left[\sum_{b=0}^{B+k} \frac{(-1)^b}{\delta_b} \Re \left\{ \phi_{X_{ij}} \left(\frac{A + 2\pi i b}{2x} \right) \right\} \right] dx, \quad (7.41) \end{aligned}$$

where $u = 1/P_L$ with P_L being the upper limit of the transmit power of an MS. Even though perfect power control is assumed in our analysis, it is practical to impose a limit on the transmit power of an MS since MS can not transmit with infinite power. Also, in our analysis, X_{ij} becomes "1" in the case of slow power control, which compensate for the only long-term fading due to propagation loss and shadow fading, and $E[(1/X_{ij})^n]$ is not necessary to evaluate. Note that (7.40) and (7.41) can be applied to any general fading distributions to get the PDFs and the n^{th} moments of X_{i0} and $1/X_{ij}$.

7.3.3 Special case: Nakagami-m fading channels

For Nakagami-m fading distribution, $\phi_l(s)$ is given by

$$\phi_l(s) = \left(1 + \frac{\Omega_l}{m} s \right)^{-m}, \quad (7.42)$$

where Ω_l is the average power of the l^{th} multipath. Therefore, the MGF of X_{ij} can be expressed as, when the multipath fading is subject to Nakagami-m fading,

$$\phi_{X_{ij}}(s) = \prod_{l=1}^{L_m} \left(1 + \frac{\Omega_l}{m} s \right)^{-mL_tL_r}, \quad (7.43)$$

for the closed-loop transmit diversity, and

$$\phi_{X_{ij}}(s) = \prod_{l=1}^{L_m} \left(1 + \frac{\Omega_l}{mL_t}s\right)^{-mL_tL_r}, \tag{7.44}$$

for the open-loop transmit diversity. In (7.43) and (7.44), if mL_tL_r is an integer number, the PDF of X_j can be obtained in the closed form expression by the inverse Laplace transform through partial fraction expansion (PFE). Let $M = mL_tL_r$, which is an integer number, and $\lambda_l = \Omega_l/m$ for the closed-loop transmit diversity and $\lambda_l = \Omega_l/(mL_t)$ for the open-loop transmit diversity, then the MGF of X_j can be expanded as follows:

$$\phi_{X_{ij}}(s) = \prod_{l=1}^{L_m} (1+\lambda_l s)^{-M} = \sum_{l=1}^{L_m}\sum_{k=1}^{M} \frac{A_{l,k}}{(1+\lambda_l s)^k}, \tag{7.45}$$

where

$$A_{l,k} = \frac{1}{(-\lambda_l)^{n_0}} \sum_{n_1=0}^{n_0}\sum_{n_2=0}^{n_0-n_1}\cdots \sum_{n_{L_m}-2=0}^{n_0-n_1-\cdots-n_{L_m-3}} \prod_{i,u=1,i\neq l}^{L_m,L_m-1} \binom{M+n_u-1}{n_u} \frac{\lambda_i^{n_u}}{(1-\lambda_i/\lambda_l)^{M+n_u}}. \tag{7.46}$$

Then, the PDF of X_j is given by the inverse Laplace transform as follows:

$$\begin{aligned} f_{X_{ij}}(x) &= \sum_{l=1}^{L_m}\sum_{k=1}^{M} A_{l,k} f_l(x) \\ &= \sum_{l=1}^{L_m}\sum_{k=1}^{M} \frac{A_{l,k}}{\Gamma(k)} \left(\frac{1}{\lambda_l}\right)^k x^{k-1}\exp\left(-\frac{x}{\lambda_l}\right), \end{aligned} \tag{7.47}$$

where $\Gamma(a) = \int_0^\infty t^{a-1}e^{-t}dt$. Once the PDF is obtained, the n^{th} moment of X_{ij} and $1/X_{ij}$ can be calculated in closed form solutions as follows:

$$\begin{aligned} E[X_{ij}^n] &= \sum_{l=1}^{L_m}\sum_{k=1}^{M} \frac{A_{l,k}}{\Gamma(k)} \left(\frac{1}{\lambda_l}\right)^k \int_0^\infty x^{k+n-1}e^{-x/\lambda_l}ds \\ &= \sum_{l=1}^{L_m}\sum_{k=1}^{M} A_{l,k} \left(\frac{1}{\lambda_l}\right)^n \frac{\Gamma(k+n)}{\Gamma(k)}, \end{aligned} \tag{7.48}$$

and

$$E\left[\frac{1}{X_{ij}^n}\right] = \int_u^\infty \left(\frac{1}{x}\right)^n f_{X_j}(x)dx = \sum_{l=1}^{L_m}\sum_{k=1}^{M} \frac{A_{l,k}}{\Gamma(k)} \left(\frac{1}{\lambda_l}\right)^k \int_u^\infty x^{k-n-1}e^{-x/\lambda_l}dx$$

$$= \sum_{l=1}^{L_m} \left\{ \sum_{k=1}^{n} \frac{A_{l,k}}{\Gamma(k)} \left(\frac{1}{\lambda_l}\right)^k \frac{E_{n-k+1}(\frac{u}{\lambda_l})}{u^{n-k}} + \sum_{k=n+1}^{M} \frac{A_{l,k}}{\Gamma(k)} \left(\frac{1}{\lambda_l}\right)^n \Gamma\left(k-n, \frac{u}{\lambda_l}\right) \right\} \tag{7.49}$$

where $E_n(x) = x^{n-1}\int_x^\infty \frac{e^{-t}}{t^n}dt$ is the exponential integral function and $\Gamma(a,x) = \int_x^\infty t^{a-1}e^{-t}dt$ is the incomplete gamma function.

If $|\alpha_{i,j,l}|^2$ in (7.35) and (7.36) are correlated with each other and not necessarily identically distributed, that is, if there exist correlations between diversity branches such as antenna elements and rake fingers, the MGF of the sum of correlated random variables $|\alpha_{i,j,l}|^2$ can be written as

$$\phi_{X_{ij}}(s) = |I + sDC|^{-m} = \prod_{i=1}^{L_tL_rL_m} (1+\lambda_i s)^{-m}, \tag{7.50}$$

where the $L_tL_rL_m \times L_tL_rL_m$ diagonal matrix D is $D = \text{diag}(\Omega_1/m, \Omega_2/m, \ldots, \Omega_{L_tL_rL_m}/m)$ for the closed-loop transmit diversity and $D = \text{diag}(\Omega_1/mL_t, \Omega_2/mL_t, \ldots, \Omega_{L_tL_rL_m}/mL_t)$ for the open-loop transmit diversity, C denotes the positive definite matrix defined by $\sqrt{R_C}$ where R_C is the power correlation matrix between the diversity branches, and $\{\lambda_i\}_{i=1}^{L_tL_rL_m}$ are the eigenvalues of the matrix DC [79]. For correlated Nakagami-m channels with general fading index m, (7.50) can be inserted into (7.40) and (7.41) to calculate the n^{th} moment of X_{i0} and X_{ij}.

7.3.4 Average total interference from other-cell users

Considering voice users with voice activity factor ν, hexagonal cells with radius normalized to unity, and uniform density of mobile users with $\kappa = 2N/(3\sqrt{3})$ users per unit area, where N is the average number of users per cell, the n^{th} moment of the total intercell interference is [67], [70]

$$E\left[\left(\frac{I_{oc}}{S}\right)^n\right] = \nu\left\{\iint_{\overline{S}_0} E\left[\left(\frac{I_{oc}^{(i)}}{S}\right)^n_{\overline{S}_0}\right]\kappa dA_{\overline{S}_0} + \iint_{S_0} E\left[\left(\frac{I_{oc}^{(i)}}{S}\right)^n_{S_0}\right]\kappa dA_{S_0}\right\}. \tag{7.51}$$

Hence, the mean and variance can be written as, respectively,

$$E\left[\frac{I_{oc}}{S}\right] = \nu\left\{\iint_{\overline{S}_0} E\left[\left(\frac{I_{oc}^{(i)}}{S}\right)_{\overline{S}_0}\right]\kappa dA_{\overline{S}_0} + \iint_{S_0} E\left[\left(\frac{I_{oc}^{(i)}}{S}\right)_{S_0}\right]\kappa dA_{S_0}\right\}, \tag{7.52}$$

$$\text{var}\left[\frac{I_{oc}}{S}\right] = \nu\left\{\iint_{\overline{S}_0} E\left[\left(\frac{I_{oc}^{(i)}}{S}\right)^2_{\overline{S}_0}\right]\kappa dA_{\overline{S}_0} + \iint_{S_0} E\left[\left(\frac{I_{oc}^{(i)}}{S}\right)^2_{S_0}\right]\kappa dA_{S_0}\right\}$$

$$-\nu^2 \left\{ \iint_{\overline{S}_0} \left(E\left[\left(\frac{I_{oc}^{(i)}}{S} \right)_{\overline{S}_0} \right] \right)^2 \kappa dA_{\overline{S}_0} + \iint_{S_0} \left(E\left[\left(\frac{I_{oc}^{(i)}}{S} \right)_{S_0} \right] \right)^2 \kappa dA_{S_0} \right\}. \tag{7.53}$$

7.3.5 Intracell interference

Let us suppose that an i^{th} MS communicates with the zeroth BS. The transmit power P_T from the i^{th} MS to the zeroth BS will suffer the propagation loss of both long-term fading due to shadowing and short-term fading due to multipath. However, since the perfect power-controlled transmit power from the MS compensates for the signal variations due to the propagation and fading, the received signal at the zeroth BS appears to be the constant value of S. That is, the received signal at zeroth BS can be expressed as

$$P_R = P_T \cdot \frac{1}{r_{i0}^{\mu} 10^{\zeta_{i0}/10}} \cdot X_{i0} = S \tag{7.54}$$

On the other hand, in the case of slow power control, the received signal at the zeroth BS has still Rayleigh distribution as mentioned in the previous section. That is, (7.54) may be expressed as

$$P_R = \widetilde{P}_T \cdot \frac{1}{r_{i0}^{\mu} 10^{\zeta_{i0}/10}} \cdot X_{i0} = S \cdot X_{i0} \tag{7.55}$$

Now, let's suppose that an i^{th} MS is in the soft handoff. An MS outside the zeroth cell but within S_0 can communicate with the zeroth BS. Hence, the normalized instantaneous intra-cell interference may be expressed as

$$\left(\frac{I_{in}^{(i)}}{S} \right) = \phi_i \tag{7.56}$$

where ϕ_i is the indicator function that the i^{th} MS belongs to the j^{th} BS. That is,

$$\phi_i = \begin{cases} 1, & i \in BS_0 \\ 0, & i \notin BS_0 \end{cases} \tag{7.57}$$

and the probability that $\phi_i = 1$ is given by

$$P(\phi_i = 1) \quad = \quad \Pr\left(r_{i0}^{\mu} 10^{\zeta_{i0}/10} < \min_{j=1}^{Nc-1} \left\{ r_{ij}^{\mu} 10^{\zeta_{ij}/10} \right\} \right)$$

$$= \sum_{j=1}^{N_c-1} \int_{-\infty}^{\infty} \frac{e^{-z^2/2}}{\sqrt{2\pi}} \left[1 - Q\left(z + \frac{M_{ij} - M_{i0}}{\beta\sigma}\right)\right]$$
$$\times \prod_{k=1,k\neq j}^{N_c-1} \left(z + \frac{M_{ij} - M_{ik}}{b\sigma} + nb\beta\sigma\right) dz. \tag{7.58}$$

Then, the n^{th} moment to obtain the mean and variance is calculated as

$$E\left[\left(\frac{I_{in}^{(i)}}{S}\right)^n\right] = E\left[\phi_i^n\right] = \Pr\{\phi_i = 1\}. \tag{7.59}$$

On the other hand, in the case of slow power control, (7.56) may be expressed as

$$\left(\frac{I_{in}^{(i)}}{S}\right) = \phi_i \cdot \chi \ , \tag{7.60}$$

where $\chi = X_{i0}/E[X_{i0}]$, and the n^{th} moment of intra-cell interference for the slow power control becomes

$$E\left[\left(\frac{I_{in}^{(i)}}{S}\right)^n\right] = E\left[\phi_i^n\right] \cdot E\left[\chi^n\right]. \tag{7.61}$$

The n^{th} moment of the total intracell interference is

$$E\left[\left(\frac{I_{in}}{S}\right)^n\right] = \nu \iint_{S_0} E\left[\left(\frac{I_{in}^{(i)}}{S}\right)^n\right] \kappa dA_{S_0}. \tag{7.62}$$

Hence, the mean and variance of intracell interference can be written as, respectively,

$$E\left[\frac{I_{in}}{S}\right] = \nu \iint_{S_0} E\left[\frac{I_{in}^{(i)}}{S}\right] \kappa dA_{S_0}, \tag{7.63}$$

$$\text{var}\left[\frac{I_{in}}{S}\right] = \iint_{S_0} \left\{\nu E\left[\left(\frac{I_{in}^{(i)}}{S}\right)^2\right] - \nu^2 \left(E\left[\frac{I_{in}^{(i)}}{S}\right]\right)^2\right\} \kappa dA_{S_0}. \tag{7.64}$$

7.3.6 Total interference

Total interference consists of intercell interference and intracell interference from all MSs in the entire system. Hence, the mean and variance of the total interference are, respectively,

$$E\left[\frac{I}{S}\right] = E\left[\frac{I_{oc}}{S}\right] + E\left[\frac{I_{in}}{S}\right], \tag{7.65}$$

$$\text{var}\left[\frac{I}{S}\right] = \text{var}\left[\frac{I_{oc}}{S}\right] + \text{var}\left[\frac{I_{in}}{S}\right]. \tag{7.66}$$

7.3.7 Outage probability

In DS/CDMA cellular systems, since all users occupy the same frequency band and time allocation, outage occur when E_b/I_0 falls below a certain threshold γ_{th} which is required to maintain a specified QoS (quality of service). In this report, we consider two approaches to evaluate DS/CDMA cellular systems in terms of outage probability. One is the outage probability as a function of the number of users per cell, and the other is the outage probability as a function of the mobile transmit power margin.

A. Outage probability vs. the number of users per cell

Since the noise is dominated by interference from other users in DS/CDMA systems, the outage probability for a given user can be defined as

$$P_{outage} = \Pr\left(\frac{I}{S} > \chi \cdot \eta\right), \tag{7.67}$$

where $\eta = (W/R_b)/\gamma_{th}$ with W, the total bandwidth due to spreading, R_b, the information bit rate, and $\chi = 1$ when fast power control is employed and $\chi = X_j/E[X_j]$ when slow power control is employed. When fast power control is employed, compensation for multipath fading results in the occasional transmission of high power, which adds peaks of interference to the system by mobiles causing intercell interference, and resulting in a deviation from the central limit theorem. Hence, the distribution of the total interference is different from Gaussian, but can be approximated by a log-normal distribution [69], [70], [76]. Considering this and assuming all the cells in the entire system are uniformly loaded with the number of users N, and fast power control is employed, we can express the outage probability as

$$P_{outage,fast} = Q\left(\frac{\ln\eta - m_I}{\sigma_I}\right), \tag{7.68}$$

where

$$\sigma_I^2 = \ln(\sigma_{I/S}^2 + m_{I/S}^2) - 2\ln(m_{I/S}) \tag{7.69}$$

$$m_I = 0.5\ln(\sigma_{I/S}^2 + m_{I/S}^2) - \sigma_I^2 \tag{7.70}$$

where $m_{I/S} = E[I/S]$ and $\sigma^2_{I/S} = \text{var}[I/S]$. On the other hand, if slow power control is employed, χ is defined as $X_j/E[X_j]$, which models the signal variation due to the imperfect power control. Since the interference statistics for the slow power control is modeled as Gaussian random variable, the outage probability can be calculated as

$$P_{outage,slow} = \int_0^\infty Q\left(\frac{\chi \cdot \eta - m_{I/S}}{\sqrt{\sigma^2_{I/S}}}\right) f_\chi(\chi) d\chi \tag{7.71}$$

where $f_\chi(\chi) = E[X_j] \cdot f_{X_j}(E[X_j] \cdot \chi)$.

B. Outage probability vs. fade margin

Let us consider the outage probability as a function of the mobile transmit power margin. As mentioned before, the mobile transmit power is controlled so that the instantaneous received power at the base station is maintained at a certain level satisfying a required BER (bit error rate). However, the maximum transmit power of the mobile station is limited by the power amplifier. Therefore, in some cases such as severe fading environments, the instantaneous received power at the base station might not satisfy the required power level. We can define this occurrence as the outage rate (or probability). That is, we can simply define the outage probability as, assuming the mobile transmission power is limited to γ_{th},

$$P_{outage} = \Pr\{P_T > \gamma_{th}\} \tag{7.72}$$

where γ_{th} is the maximum mobile transmit power and P_T is

$$P_T = r_{ij}^\mu 10^{\zeta_{ij}/10} \frac{1}{X_{ij}}. \tag{7.73}$$

If we assume soft handoff, the outage probability can be expressed as

$$\begin{aligned} P_{outage} &= \sum_{j=0}^{N_c-1} \Pr\{P_T > \gamma_{th} | r_{ik}^\mu 10^{\zeta_{ik}/10} > r_{ij}^\mu 10^{\zeta_{ij}/10}, 0 \le k \le N_c - 1, k \ne j\} \\ &\times \Pr\{r_{ik}^\mu 10^{\zeta_{ik}/10} > r_{ij}^\mu 10^{\zeta_{ij}/10}\} \\ &= \Pr\left\{\min_{j=1}^{N_c-1}[r_{ij}^\mu 10^{\zeta_{ij}/10}] \frac{1}{X_{ij}} > \gamma_{th}\right\}. \end{aligned} \tag{7.74}$$

Hence, the outage probability that the threshold or the fade margin can not be met by a mobile at the basestation due to fading is

$$\begin{aligned} P_{outage} &= \Pr\left\{\min_{j=1}^{N_c-1}[r_{ij}^{\mu}10^{\zeta_{ij}/10}]\frac{1}{X_{ij}} > \gamma_{th}\right\} \\ &= \Pr\left\{\min_{j=1}^{N_c-1}[M_{ij}+b\xi_j] > \gamma_{th,dB} + X_{ij,dB} - a\xi\right\} \\ &= \prod_{j=0}^{N_c-1}\Pr\left\{\xi_j > \frac{\gamma_{th,dB}+X_{ij,dB}-a\xi-M_{ij}}{b}\right\} \\ &= \int_0^{\infty}\int_{-\infty}^{\infty}\prod_{j=0}^{N_c-1}Q\left(\frac{\gamma_{th,dB}+X_{ij,dB}-a\sigma z-M_{ij}}{b\sigma}\right)\frac{1}{\sqrt{2\pi}}e^{-z^2/2}dz f_{X_{ij}}(x)dx \quad (7.75) \end{aligned}$$

where $M_{ij} = 10\mu\log_{10}r_{ij}$, and a, b, σ, ξ, and ξ_j are defined in (7.3).

7.4 Numerical Results Analysis

Including short-term fading effect in the analysis of system capacity, as in (7.31) and (7.32), implies the system adopts fast power control which tracks signal variation due to multipath fading and shadowing. Perfect power control tracking multipath fading requires transmitting very high power occasionally to compensate fading loss when the user is in deep fading. This high power causes high interference to other users which are not power-controlled by the same base station, and decrease system capacity. If a limit is imposed on the transmission power, which is practical assumption since a mobile unit's transmission power is limited, the mobile user might not achieve the required target SIR, but other users will not suffer from the high interference [69]. Both increased outage probability due to the limit of the transmit power and decreased intercell interference have impact on system performance. Hence, in this work, we impose a limit on the transmit power at a mobile, which is assumed to be 20 dB throughout this work, assuming the mobile unit has enough power to compensate power loss due to distance and shadowing, and can completely compensate signal fluctuation due to multipath fading within the power limit with fast power control. In real systems, the power control is based on short-term average of signal-to-interference ratio, but for the analytical

tractability, instantaneous signal-to-interference strength power control is assumed for fast power control.

We investigate the effect of transmit diversity at handset, such as open-loop and closed-loop transmit diversity, in conjunction with receive diversity, on slow and fast power control, outage probability, relative other cell interference, and capacity. Also, we investigate the effect and the difference of slow power control with diversity techniques where slow power control can't compensate fading due to multipath fading but can compensate signal variation due to path loss and shadow fading. Hence, in slow power control, the gain achieved by spatial or path diversity for capacity improvement comes from flattening signal variation due to multipath. Slow and fast power control in this report actually represents upper and lower bounds on expected performance in real system.

The key model parameters considered in this report include:

- Order of spatial diversity - including both transmit and receive diversity
- Propagation channel models:
  - → Path loss and large scale fading channel propagation models
  - → Multipath fading models - different fading severities
  - → Pedestrian A and vehicular A multipath channel model
- Slow vs. fast power control
- 2-way soft handoff vs. 3-way soft handoff
- Impact of user distribution
- Impact of correlation between antenna elements and between resolvable paths

Table 7.2: System Parameters

System bandwidth (W)	1.25 MHz
Data rate (R_b)	8 Kbps
Voice activity (ν)	0.38
Target E_b/I_0	5.6 dB
Shadowing correlation between BSs	0.5
Log-normal shadowing	$\sigma = 8$ dB, $\mu = 4$
Soft Handoff (N_c)	3-way
Diversity order (M)	1,2,4,8
Transmit power margin (u)	20 dB

7.4.1 The effect of transmit diversity at handset in conjunction with receive diversity

In this section, we present the impact of spatial diversity techniques at handset on DS/CDMA reverse link capacity. The system parameters assumed throughout the rest of the chapter is summarized in Table 7.2.

Figure 7.4 provides a comparison of capacity for fast and slow power control with closed-loop transmit diversity techniques under pedestrian A channel model as described in the 3G standard specification, and Figure 7.5 shows capacity of the same system under the vehicular A channel model. Both cases employ 3-way soft handoff. In Figure 7.4 and Figure 7.5, γ_{th}, which is the required E_b/I_0 to achieve a given BER, is set to 5.6 dB for the sake of comparison for both slow and fast power control. For diversity techniques, the maximum spatial diversity order shown is 8 employing 2 transmit antenna and 4 receive antenna diversity with closed-loop diversity (CLTD) at the handset and MRC (Maximal Ratio Combining) at the base station. These results demonstrate a substantial benefit in using antenna (spatial) diversity techniques with respect to improved system capacity and outage probability. Here, system capacity is defined as the maximum number of users per cell achieving an outage

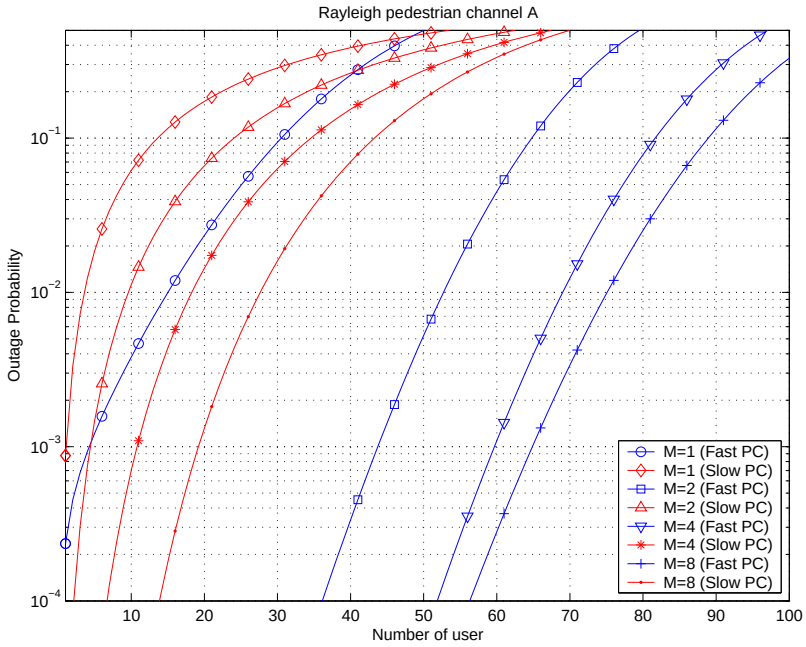

Figure 7.4: Capacity for slow and fast power control on pedestrian A channel with CLTD

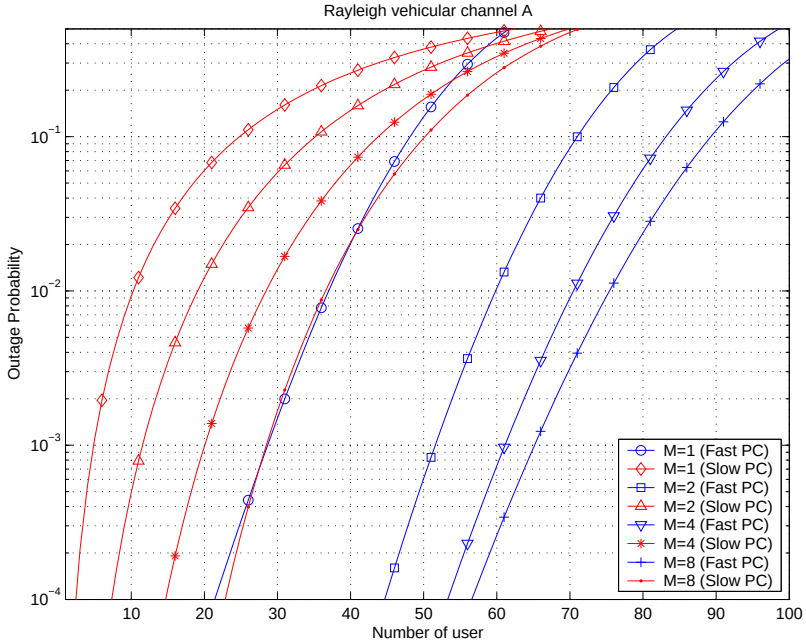

Figure 7.5: Capacity for slow and fast power control on vehicular A channel with CLTD

probability below 0.01. As shown in Figure 7.4, in the pedestrian A channel case, the capacity achieved is 9.5, 18, and 28 users for $M = 2$, 4, and 8, respectively, for slow power control, and 53, 69, and 75 users for $M = 2$, 4, and 8, respectively, for fast power control, where M is the total antenna (spatial) diversity order. Hence, there is an 89% and 194.7% capacity increase for slow power control when antenna diversity increases from 2 to 4 and 2 to 8, respectively. Also, there is a 30.2% and 41.5% capacity increase for fast power control. For the vehicular A channel, as shown in Figure 7.5, the capacity is 19, 28.5, and 37.5 users for $M = 2$, 4, and 8, respectively, for slow power control and 60, 71.5, 75.5 users for $M = 2$, 4, and 8, respectively, for fast power control. Hence, there is a 50% and 97.4% capacity increase for slow power control when antenna diversity increases from 2 to 4 and from 2 to 8, respectively. Also, there is a similar 19.2% and 25.8% capacity increase for fast power control. From these figures, it can be seen that systems employing fast power control achieve more capacity than those using slow power control under the same conditions, but relative performance gains achieved by adding higher order diversity are greater in systems employing slow power control as opposed to those using fast power control. Also, antenna (spatial) diversity has a more positive impact in pedestrian A channel environments as compared with vehicular A channel environments, since there is less path diversity available in pedestrian A channel environments than in vehicular A channel environments. Therefore, this suggests that system capacity is more sensitive to the variations in the received signal which have not been compensated completely by either power control or diversity processing than to total interference caused by occasional high power transmission from other users when fast power control is employed.

Figure 7.6 and Figure 7.8 show the capacity due to closed and open loop transmit diversity for systems using slow power control with 3-way soft handoff under pedestrian A and vehicular A channel environments, respectively. Figure 7.7 and Figure 7.9 also show the capacity due to closed and open loop transmit diversity for systems employing fast power control with 3-way soft handoff under pedestrian A and vehicular A channel models, respectively.

Clearly, transmit and receive diversity techniques, i.e., spatial diversity techniques, smooth the received signal, and reduce intercell interference by increasing the average signal power and reducing the signal variations, thereby reducing the required transmission power and occasional high power transmission "peaks". The reduced transmission power at handset and the flattened received power at the basestation lead to a system capacity increase.

As mentioned previously, spatial diversity improves system capacity through diversity combining and energy capturing. The former reduces signal variations at the receiver and the latter increases the average received signal power, both by combining replicas of the transmitted signal, providing an increase in the system capacity. In Figure 7.6 through Figure 7.9, OLTD denotes open-loop transmit diversity such as space time block code (STBC), CLTD denotes closed-loop transmit diversity, and m denotes the fading index in Nakagami-m fading model. Note that $m = 1$ is equivalent to Rayleigh fading. As seen in Figure 7.7 and Figure 7.9, CLTD outperforms OLTD due to energy capturing effect. However, for the slow power control case, as seen in Figure 7.6 and Figure 7.8, there is no difference between CLTD and OLTD. In our modeling, since slow power control does not track short term fluctuations of the received signal, it is assumed that slow power control compensates for only long term fading, which is shadow fading, and doesn't provide an energy capturing effect, but only diversity gain, which makes the probability that signals from each diversity branch will fade coherently, very small. Hence, in practical systems, due to the energy capturing effect, CLTD might perform better than OLTD in systems using slow power control. Therefore, the capacity increases using spatial diversity in Figure 7.6 and Figure 7.8 stem from reduced received signal fluctuations. From Figure 7.7 and Figure 7.9, it can be seen that a slower exponential decay in the power of subsequent multipath components results in more path diversity able to be exploited by the Rake receiver since the vehicular A channel performance is better than that in the pedestrian A channel. Hence, systems characterized by the pedestrian A channel achieve more substantial gains as the spatial diversity order increases than systems characterized by a vehicular A channel. As the spatial diversity order increases, the performance difference between the two models is reduced.

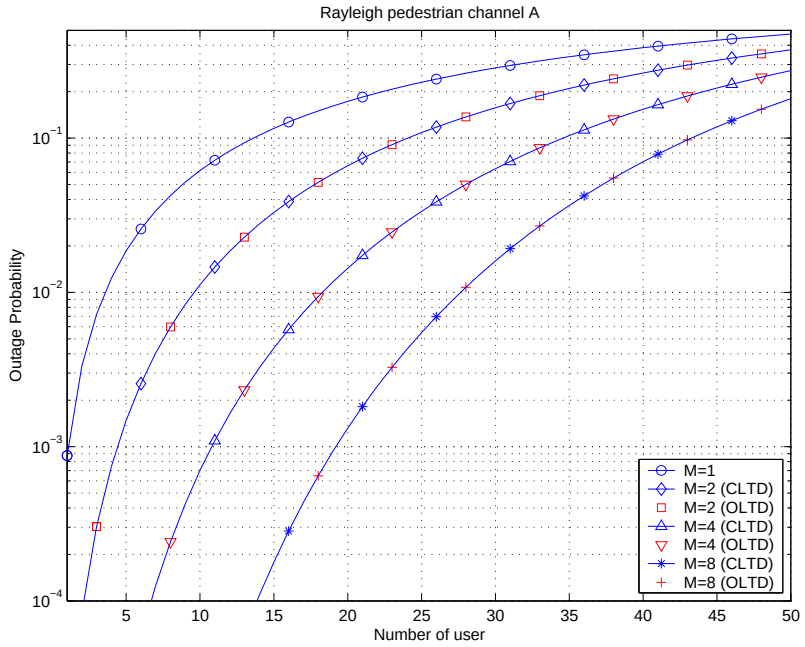

Figure 7.6: Capacity for slow power control on pedestrian A channel with CLTD and OLTD

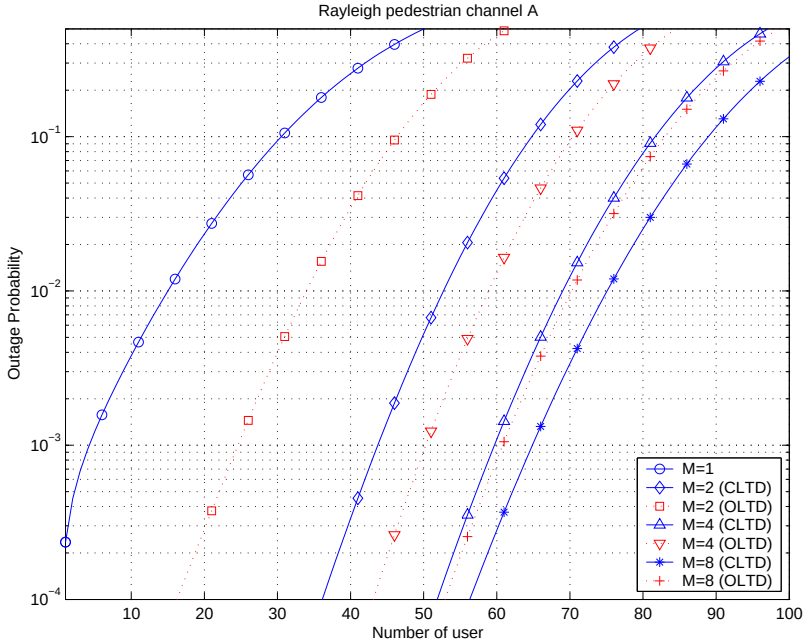

Figure 7.7: Capacity for fast power control on pedestrian A channel with CLTD and OLTD

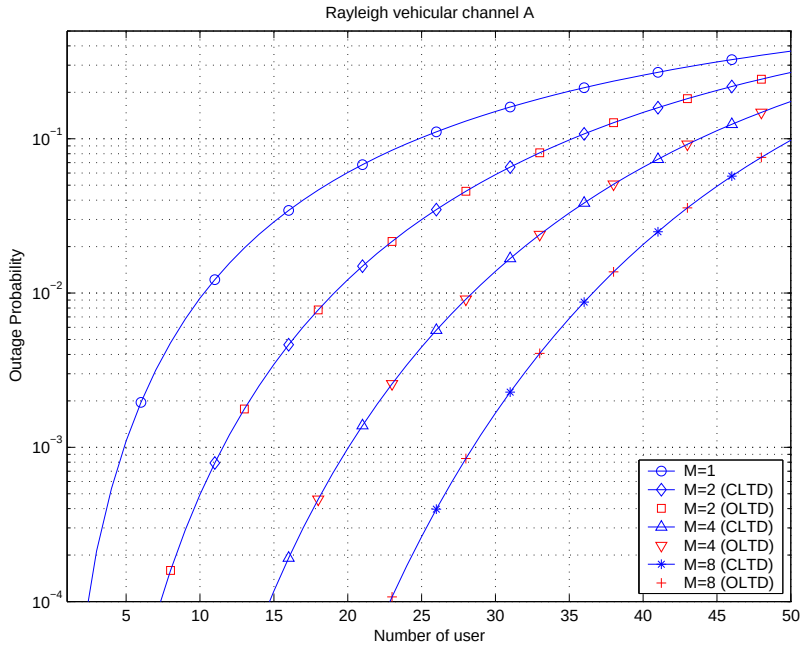

Figure 7.8: Capacity for fast power control on vehicular A channel with CLTD and OLTD

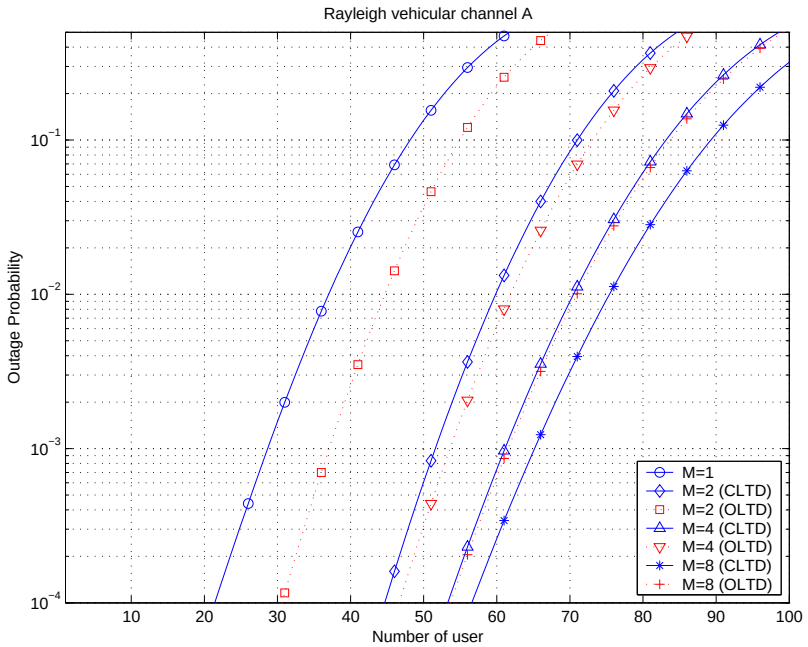

Figure 7.9: Capacity for fast power control on vehicular A channel with CLTD and OLTD

Figure 7.10 and Figure 7.11 show outage probability vs. fade margin for pedestrian A and vehicular A channels with 3-way soft handoff when the fade is varied from 0 dB to 20 dB. Regardless of whether or not transmit or receive diversity is used, the performance is always better in the vehicular A channel as expected since more path diversity is available for exploitation by the Rake receiver. In this report, we assume that all paths in the channel models are combined by the Rake receiver.

Figure 7.10 and Figure 7.11 clearly show that outage probability gets smaller as transmit and receive diversity order increases, and, hence, to maintain the same outage probability, a mobile user with transmit diversity used in conjunction with base station receive diversity requires less power margin, which can translate to a coverage increase. As seen in Figure 7.10, Figure 7.11, and Table 7.3, using transmit and receive diversity together can provide up to a 7.66 dB and 6.65 dB required fade margin reduction for the pedestrian A and vehicular A channels, respectively, for $P_{out} = 0.01$.

In our analysis, 2Tx1Rx CLTD (Closed-loop transmit diversity) is equivalent to 1Tx2Rx MRC (Maximal Ratio combining). Therefore, we consider 1Tx2Rx MRC as the baseline case for relative coverage comparison in Table 7.3. Since cell area is proportional to the square of the radius while propagation loss is proportional to the 4th power when a pathloss exponent of 4 is assumed, relative margins of 7.66 dB and 6.65 dB (in Table 7.3) represent a relative cell area increase of 2.42 and 2.15, or a reduction in the number of cells required. Figure 7.12 and Figure 7.13 show the outage probability as a function of othercell interference factor f, which is defined as $f \triangleq \frac{\text{average total interference from other-cell users}}{N} = \frac{E[I/S]}{N}$ where N is the average number of users per cell [67], [80], for pedestrian A and vehicular A channels, respectively, with $\mu = 4$, $\sigma = 8$ dB, and 3-way soft handoff. These figures are generated by changing the fade margin for outage probability and relative interference factor f by using (7.75) for outage probability, and (7.31), (7.32) for relative other cell interference factor f, increasing the fade margin by a 2 dB step size from 0 dB. Since (7.31), (7.32), and (7.75) are used to calculate the outage probability and relative other cell interference, fast power control is assumed for the calculation. Hence, as can be seen, increasing the power margin,

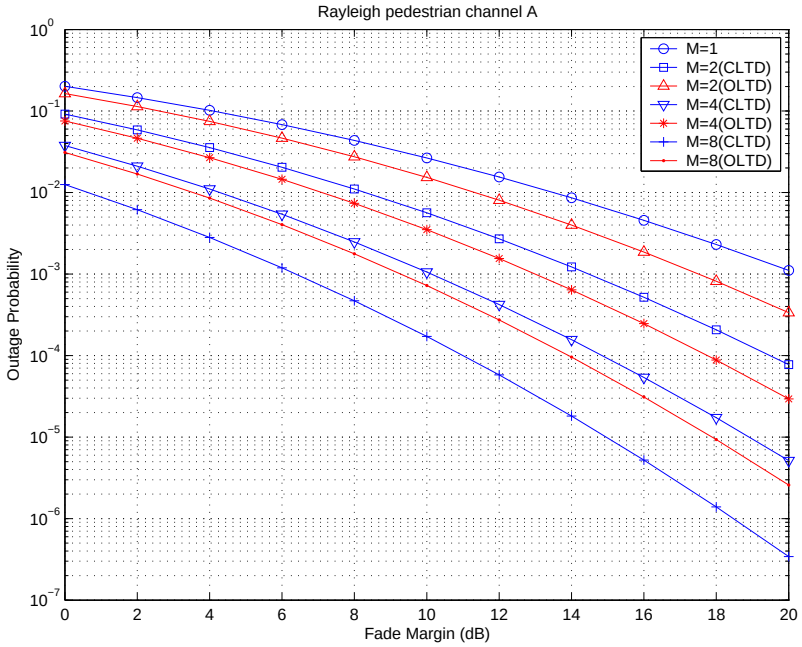

Figure 7.10: Outage probability vs. fade margin for fast power control on pedestrian A channel

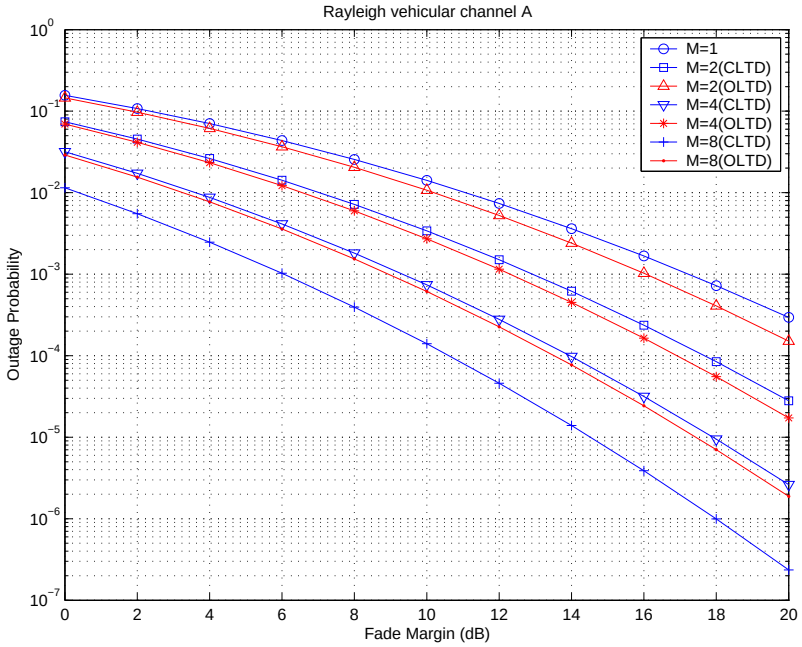

Figure 7.11: Outage probability vs. fade margin for fast power control on vehicular A channel

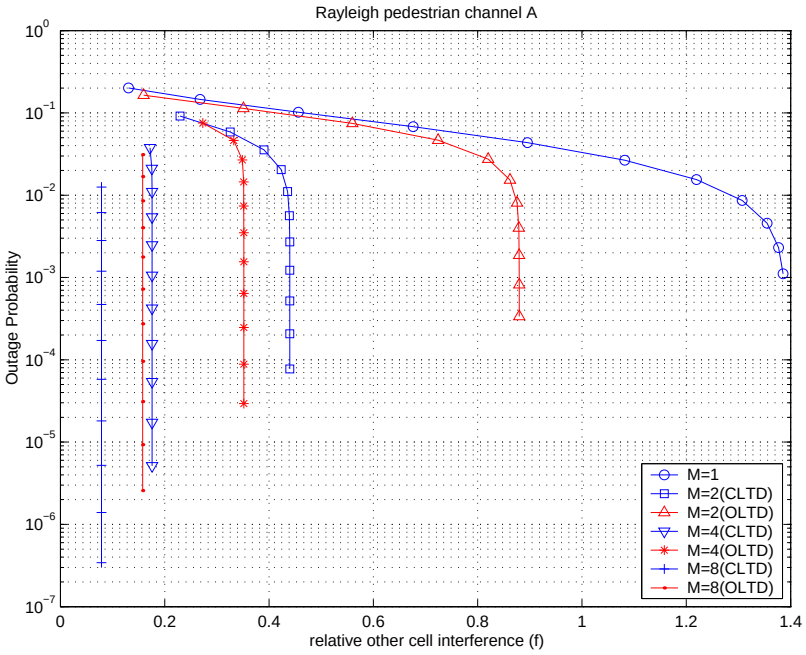

Figure 7.12: Outage probability vs. relative othercell interference factor for fast power control on pedestrian A channel

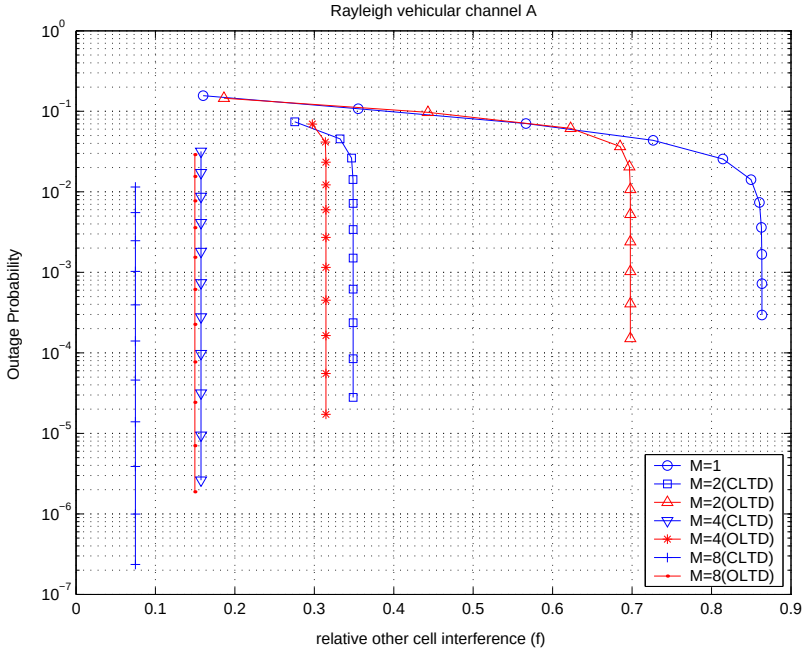

Figure 7.13: Outage probability vs. relative othercell interference for fast power control on vehicular A channel

Table 7.3: Relative margin and coverage for spatial diversity with 3-way soft handoff

Pedestrian A, $P_{out} = 10^{-2}$				Vehicular A, $P_{out} = 10^{-2}$			
	Fade Margin	Relative Margin	Relative Coverage		Fade Margin	Relative Margin	Relative Coverage
1Tx2Rx (MRC)	8.30 dB	0 dB	1	1Tx2Rx (MRC)	7.03 dB	0 dB	1
2Tx2Rx(OLTD)	7.10 dB	1.20 dB	1.15	2Tx2Rx(OLTD)	6.56 dB	0.47 dB	1.06
2Tx2Rx(CLTD)	4.28 dB	4.02 dB	1.59	2Tx2Rx(CLTD)	3.60 dB	3.43 dB	1.48
2Tx4Rx(OLTD)	3.54 dB	4.76 dB	1.73	2Tx4Rx(OLTD)	3.26 dB	3.77 dB	1.54
2Tx4Rx(CLTD)	0.64 dB	7.66 dB	2.42	2Tx4Rx(CLTD)	0.38 dB	6.65 dB	2.15

which is the maximum transmit power at the mobile handset, leads to an increase in other-cell interference due to fast power control, which results in high transmission power when a mobile user is in a deep fade. However, as diversity order increases, the received signal fluctuation decreases due to diversity gain, and results in a decrease in other-cell interference, translating to a capacity increase. At 1% outage probability, the relative other-cell interferences are 0.436 and 0.3488 for pedestrian A and vehicular A channels, respectively, when 1Tx2Rx MRC is used (from Figure 7.12 and Figure 7.13). When 2Tx2Rx CLTD is used, the f factors reduce to 0.1758 and 0.1573 for the pedestrian A and vehicular A channels, respectively. Since capacity is proportional to $1 + f$, using order 4 diversity gives a 22% and 16.5% capacity increase in the pedestrian A and vehicular A channels, respectively, under 3-way soft hand off and fast power control. Also, as can be seen in Figure 7.12 and Figure 7.13, the other-cell interference does not increase even with the fade margin increase when the diversity order is greater than or equal to 4. This is because the received signal variations are reduced by diversity gain, resulting in less occasional high transmit power necessary to compensate for multipath fading as previously explained. Note that there is a notable difference in the other-cell interference between pedestrian A and vehicular A channels when there is no antenna diversity, but the difference gets smaller as the antenna diversity order increases. This means that when there is insufficient path diversity to be exploited by the Rake receiver,

using antenna diversity can greatly increase not only the BER performance but the overall system capacity. Table 7.10 shows the other-cell interference factors for the pedestrian A channel with 3-way soft handoff (SHO) with a fade margin set to 20 dB. Table 7.11 shows the other-cell interference factors for the vehicular A channel with 3-way soft handoff (SHO) with a fade margin set to 20 dB. Table 7.6 shows the relative capacity improvement for pedestrian A channel and vehicular A channel when diversity order is increased and slow power control is employed, and Table 7.7 shows the relative capacity improvement when fast power control is employed. In both tables, the capacity was calculated by using (7.68) for fast power control case, (7.71) for slow power control case. From the figures comparing the capacity improvement for fast and slow power control, and Table 7.6 and Table 7.7, it seems that system capacity is more sensitive to variations in the received signal power which have not been compensated completely by either power control or diversity processing than to total interference caused by occasional high power transmission from other users. Table 7.8 shows the relative capacity improvement for pedestrian A and vehicular A channel with fast power control by using f factors. Note that estimating a system capacity using f factor can give more pessimistic gain than using (7.68) since f factor does not capture the reduction of the interference variance var$[I/S]$, which can affect the system capacity, when diversity techniques are used, while (7.68) captures the statistical characteristics of the intercell interference by using the first order (mean) and the second order (variance) statistics.

Table 7.4: f factors for pedestrian A channel with 3-way soft handoff and 20 dB fade margin

1Tx2Rx				2Tx2Rx (CLTD)				2Tx4Rx (CLTD)			
σ	$\mu = 3$	$\mu = 4$	$\mu = 5$	σ	$\mu = 3$	$\mu = 4$	$\mu = 5$	σ	$\mu = 3$	$\mu = 4$	$\mu = 5$
0	0.5886	0.3276	0.2264	0	0.2353	0.1309	0.0905	0	0.1056	0.0588	0.0406
2	0.6068	0.3381	0.2315	2	0.2426	0.1351	0.0925	2	0.1089	0.0607	0.0415
4	0.6472	0.3505	0.2355	4	0.2587	0.1401	0.0942	4	0.1161	0.0629	0.0423
6	0.7323	0.3801	0.2467	6	0.2927	0.1520	0.0986	6	0.1314	0.0682	0.0443
8	0.9101	0.4398	0.2677	8	0.3638	0.1758	0.1070	8	0.1633	0.0789	0.0480
10	1.3160	0.5744	0.3154	10	0.5260	0.2296	0.1261	10	0.2361	1.1030	0.0566
12	2.2546	0.8853	0.4420	12	0.9013	0.3539	0.1767	12	0.4045	0.1588	0.0793

Table 7.5: f factors for vehicualr A channel with 3-way soft handoff and 20 dB fade margin

1Tx2Rx				2Tx2Rx (CLTD)				2Tx4Rx (CLTD)			
σ	$\mu = 3$	$\mu = 4$	$\mu = 5$	σ	$\mu = 3$	$\mu = 4$	$\mu = 5$	σ	$\mu = 3$	$\mu = 4$	$\mu = 5$
0	0.4669	0.2599	0.1796	0	0.2106	0.1172	0.0810	0	0.1001	0.0557	0.0385
2	0.4813	0.2682	0.1836	2	0.2171	0.1210	0.0828	2	0.1032	0.0575	0.0394
4	0.5134	0.2780	0.1868	4	0.2316	0.1254	0.0843	4	0.1101	0.0596	0.0401
6	0.5809	0.3015	0.1957	6	0.2620	0.1360	0.0883	6	0.1245	0.0647	0.0420
8	0.7220	0.3489	0.2124	8	0.3256	0.1574	0.0958	8	0.1548	0.0748	0.0455
10	1.0439	0.4556	0.2502	10	0.4708	0.2055	0.1128	10	0.2238	1.0977	0.0536
12	1.7885	0.7022	0.3506	12	0.8066	0.3167	0.1581	12	0.3835	0.1506	0.0752

Table 7.6: Comparison of pedestrian A and vehicular A channel for slow power control with CLDT at 1 % P_{out} on Rayleigh fading for short-term faidng

Diversity Order	Ped A: capacity	% Gain	Veh A: capacity	% Gain
2	9.5		19	
4	18	89.5	28.5	50
8	27.5	189.5	36.5	92.1

Table 7.7: Comparison of pedestrian A and vehicular A channel for fast power control with CLDT at 1 % P_{out} on Rayleigh fading for short-term faidng

Diversity Order	Ped A: capacity	% Gain	Veh A: capacity	% Gain
2	53		60	
4	69	30.2	70.5	17.5
8	75	41.5	75.5	25.8

Table 7.8: Comparison of capacity gain based on f factors of pedestrian A and vehicular A channel for fast power control at 1 % P_{out} on Rayleigh fading

	Pedestrian A			Vehicular A		
Div. Order	f	$1+f$	% Gain	f	$1+f$	% Gain
2 MRC	0.4360	1.4360		0.3488	1.3488	
4 OLTD	0.3515	1.3515	6.3	0.3147	1.3147	2.6
4 CLTD	0.1758	1.1758	22.1	0.1573	1.1573	16.5
8 OLTD	0.1578	1.1578	24	0.1496	1.1496	17.3
8 CLTD	0.0789	1.0789	33.1	0.0748	1.0748	25.5

Key observations and effects for capacity

- Fast power control results in occasional high-power transmissions at handset necessary to combat fades. This results in increased other-cell interference, which decreases system capacity. If maximum handset transmit power is insufficient to overcome deep fades, the result is increased outage, which again decreases system capacity. On the other hand, fast power control reduces receive power variability at a desired basestation, which in turn permits a reduced fade margin. This will favorably impact system capacity by allowing handsets to transmit at a lower average power.

- Slow power control cannot compensate for fast fading. This effect results in a higher average transmit power, which increases inter-cell interference.

- Fast power control achieves greater capacity than slow power control for similar environments.

- Slow power control systems realize greater performance gains than fast power control systems, as a function of the order of the diversity. That is, the relative performance gains achieved by adding higher order diversity are greater in systems employing slow power control system than those achieved using fast power control.

- System capacity is more sensitive to variations in the received signal power which have not been compensated completely by either power control or diversity processing than to total interference caused by occasional high power transmission from other users.

- Spatial diversity processing (as opposed to path diversity processing) has a greater positive impact in the pedestrian A channel model as opposed to the vehicular channel model due to path diversity availability.

- Using transmit diversity at the handset in conjunction with receive diversity at the base station reduces other cell interference dramatically and reduces the variability of

the received signal, resulting in a significant capacity increase for both the slow and fast power control cases.

Key observations and effects for coverage

- As diversity order increases, the outage probability drops, resulting in a lower fade margin (or power margin) for a fixed outage probability.
- The lower power margin translates to a range and coverage improvement.
- The resultant power margins are lower (hence, better) for the vehicular A channel, as opposed to the pedestrian A channel, primarily due to the path diversity gain achieved with the rake receiver.

7.4.2 The effect of the number of multipaths combined by Rake receiver

In this section, to investigate the effect of multipath on system capacity and outage probability, an exponential power delay profile is defined as follows:

$$|\alpha_l|^2 = \frac{(1-e^{-\delta})e^{(1-l)\delta}}{1-e^{-L\delta}} E\left[\sum_{l=1}^{L} |\alpha_l|^2\right] \tag{7.76}$$

where $|\alpha_l|^2$ is the l^{th} squared path gain of exponential power delay profile, δ controls the delay spread, and L is the number of power delay profile components in the model. Table 7.9 shows the power delay profiles used to investigate the effect of path diversity on the system capacity in this section. The number of multipaths is assumed to be five in both the exponential A and B channels. Multipath components decay more quickly in exponential model A than exponential model B. As it can be seen in Figure 7.14, more capacity can be obtained in exponential B and vehicular A channel propagation environments since more path diversity is available, which can be exploited by the Rake receiver. Due to path diversity, received

Table 7.9: Channel models

Channel model	Average powers (dB)
Exponential A with $\delta = 2$	0, -8.69, -17.38, -26.15, -34.60
Exponential B with $\delta = 0.2$	0, -0.87, -1.74, -2.61, -3.47
Pedestrian A	0, -9.7, -19.2, -22.8
Vehicular A	0, -1, -9, -10, -15, -20

signal variation is reduced more in exponential B and vehicular A channel models than exponential A and pedestrian A channel models. Hence, less interference is created and better outage probability is achieved in exponential model B and vehicular A channel model. Figure 7.15 and Figure 7.16 show outage probability and relative interference factor f for the exponential power delay profile models, pedestrian A, and vehicular A channel models. From these figures, it can be seen that gains from path diversity increase system capacity and improve outage probability. However, comparing figures and tables in Section A and figures and tables in this section, no matter how many multipaths are available for path diversity, path diversity cannot provide better capacity and coverage than transmit diversity at the handset used in conjunction with receive diversity at the base station. Also, the f factor provided in [67] is a lower bound for the f factor when considering only path diversity and short term fading effects. However, employing spatial diversity results in a significantly lower f factor than the f factor presented in [67], when compared with the f factors presented in section A.

Key observations and effects

- A slower exponential decay in the power of subsequent multipath components results in more path diversity, which can be exploited by the Rake receiver. This reduces signal variability and other-cell interference, and improves the outage probability. Hence, higher capacity can be achieved in such multipath environments (see Figure 7.14).
- The original Viterbi model [67] (which did not include effects of multipath) predicted

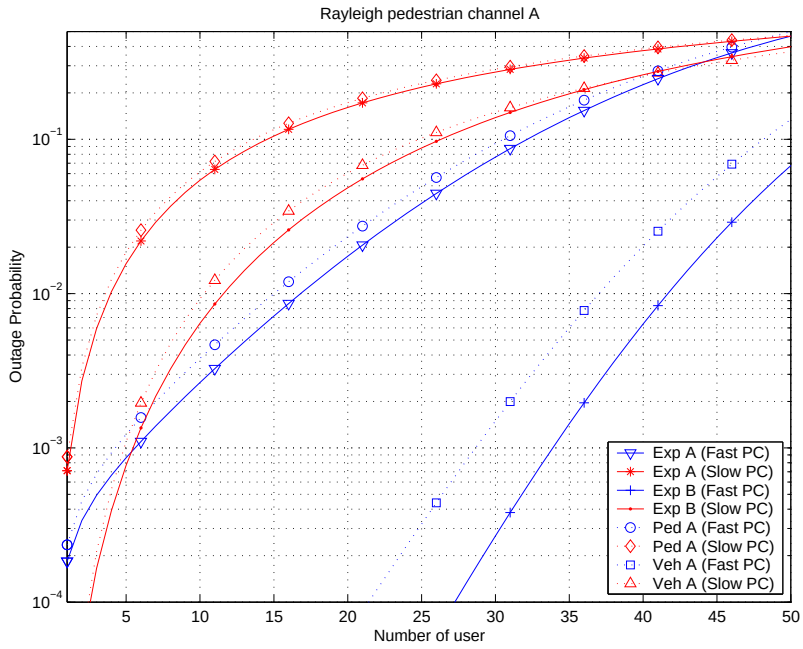

Figure 7.14: Capacity for slow and fast power control without spatial diversity using 3-way soft handoff

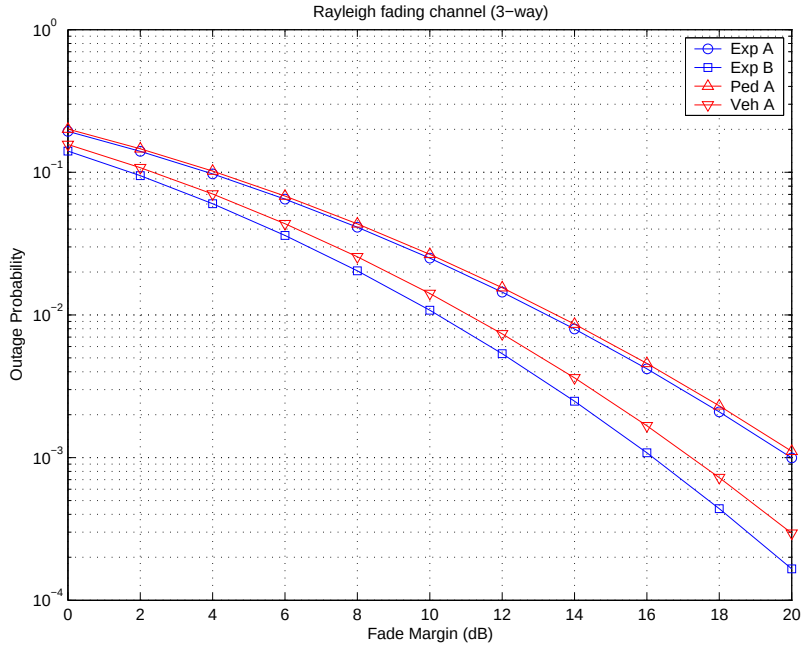

Figure 7.15: Outage probability without spatial diversity with fast power control 3-way soft handoff

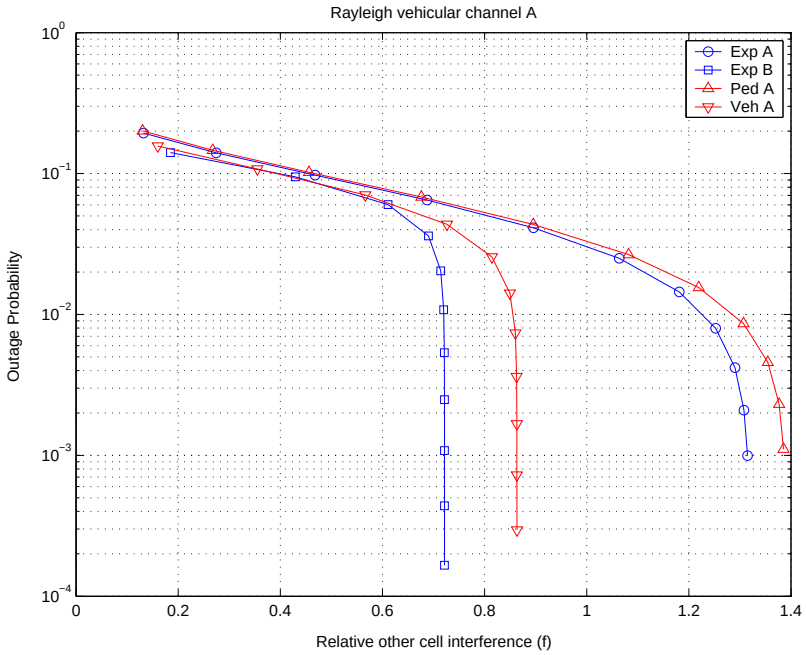

Figure 7.16: Outage probability vs. other-cell interference factor f without spatial diversity with fast power control and 3-way soft handoff

Table 7.10: f factors for exponential A and B channels with 3-way soft handoff and 20 dB fade margin

Exponential A				Exponential B			
σ	$\mu = 3$	$\mu = 4$	$\mu = 5$	σ	$\mu = 3$	$\mu = 4$	$\mu = 5$
0	1.7600	0.9795	0.6769	0	0.9656	0.5374	0.3714
2	1.8143	1.0108	0.6921	2	0.9955	0.5546	0.3797
4	1.9352	1.0480	0.7043	4	1.0618	0.5750	0.3864
6	2.1896	1.1366	0.7375	6	1.2014	0.6236	0.4047
8	2.7213	1.3150	0.8004	8	1.4931	0.7215	0.4392
10	3.9347	1.7173	0.9429	10	2.1589	0.9423	0.5174
12	6.7414	2.6469	1.3216	12	3.6988	1.4523	0.7251

Table 7.11: f factors for pedestrian A and vehicualr A channel with 3-way soft handoff and 20 dB fade margin

Pedestrian A				Vehicular A			
σ	$\mu = 3$	$\mu = 4$	$\mu = 5$	σ	$\mu = 3$	$\mu = 4$	$\mu = 5$
0	1.8544	1.0320	0.7132	0	1.1556	0.6431	0.4445
2	1.9116	1.0650	0.7292	2	1.1913	0.6637	0.4544
4	2.0390	1.1042	0.7420	4	1.2707	0.6882	0.4624
6	2.3070	1.1975	0.7771	6	1.4378	0.7463	0.4843
8	2.8672	1.3856	0.8434	8	1.7869	0.8635	0.5256
10	4.1458	1.8094	0.9935	10	2.5837	1.1277	0.6191
12	7.1029	2.7889	1.3925	12	4.4266	1.7381	0.8678

an inter-cell interference factor of 0.5697 under nominal channel conditions ($\mu = 4$ and $\sigma = 8$). This was essentially a lower-bound achieved through the exploitation of path diversity only. When multipath is taken into account with a 20 dB fade margin at the mobile handset, the f factor is considerably higher (0.7215 for exponential multipath profile B, 1.3150 for exponential multipath profile A, 1.3856 for pedestrian A channel, and 0.8635 for vehicular A channel). Hence, the early capacity models presented in the literature significantly underestimated the impact of multipath on inter-cell interference (see Table 7.10 and Table 7.11). Note also that spatial diversity processing is able to substantially reduce the elevated f factor, thereby achieving capacity performance gains in excess of what was originally believed possible.

7.4.3 The effect of fading statistics

In systems employing fast power control, reduced signal variation leads to reduced outage and interference, the interference caused by high power transmission to compensate fading loss, resulting in capacity increase. Reduced interference stems from increased average received power and less frequent high power transmissions. Also, in systems using slow power control, reduced received signal variation results in reduced outage, leading to capacity increase. In this section, we investigate the effect of fading statistics on system capacity and outage probability when transmit and receive diversity processing is employed. As the fading index m in the Nakagami-m fading environment increases, the signal variations due to multipath fading decrease. This will have impact on system capacity and outage probability, and also, on the gains achievable through diversity processing. In Figure 7.17 through Figure 7.42, fading index m for Nakagami-m fading is set to 0.5, 1, and 2. Note that $m = 1$ corresponds to Rayleigh fading. Also, capacity and other-cell interference are compared with Rayleigh and Ricean fading with the Ricean factor $K = 1$. When there is a strong specular or line-of-sight (LOS) component in the received signal with diffused signal by scatterers, the received signal variation reduces compared with diffused signal statistics such as Rayleigh.

It can be seen in the figures that as the diversity order increases, the performance differences between channels with different fading indices reduce. This is due to diversity gain reducing the received signal fluctuations. Hence, this suggests that the relative capacity gains achievable with spatial diversity processing diminish as the fading index increases, or equivalently, as the fading severity diminishes.

Key observations and effects

- The impact of different fading statistics gets smaller as spatial diversity order increases, as seen in Figure 7.17 through Figure 7.42.
- The introduction of spatial diversity lessens the performance sensitivity and degradation due to fade variability.
- The relative capacity and fade margin gains achievable with spatial diversity processing are greater in more severely fading multipath environments as seen in Figure 7.17, Figure 7.18, Figure 7.20, Figure 7.21, and Figure 7.35 through Figure 7.42

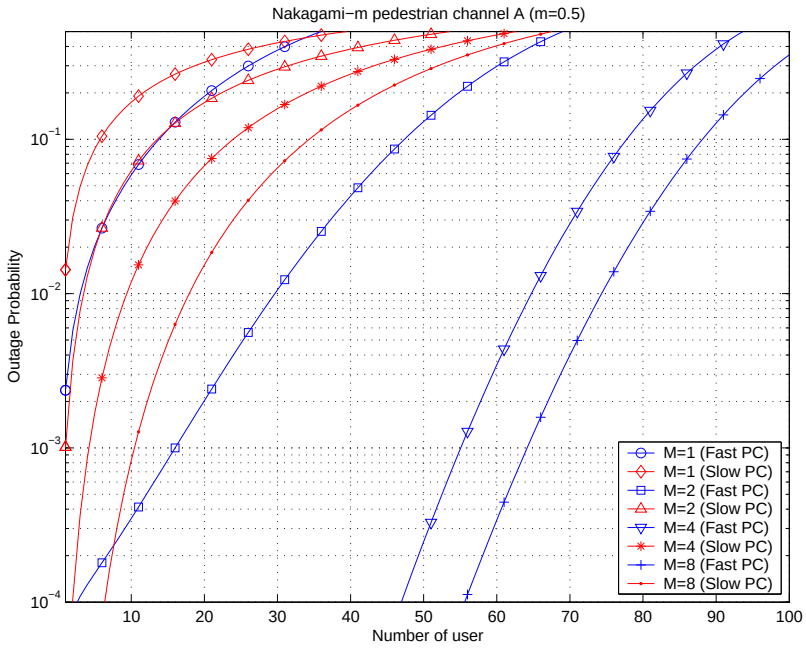

Figure 7.17: Capacity for pedestrian A channel with slow and fast power control, CLTD, $m = 0.5$, and 3-way soft handoff

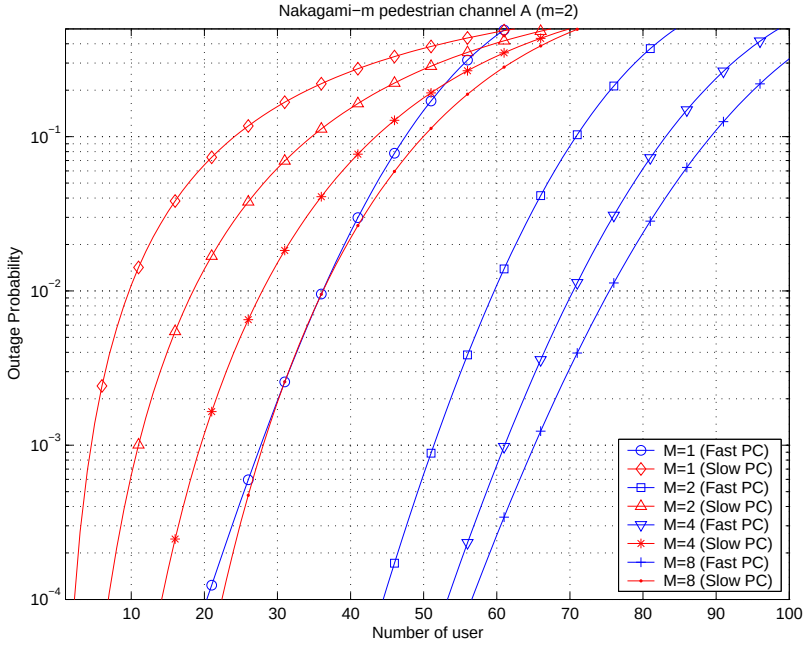

Figure 7.18: Capacity for pedestrian A channel with slow and fast power control, CLTD, $m = 2$, and 3-way soft handoff

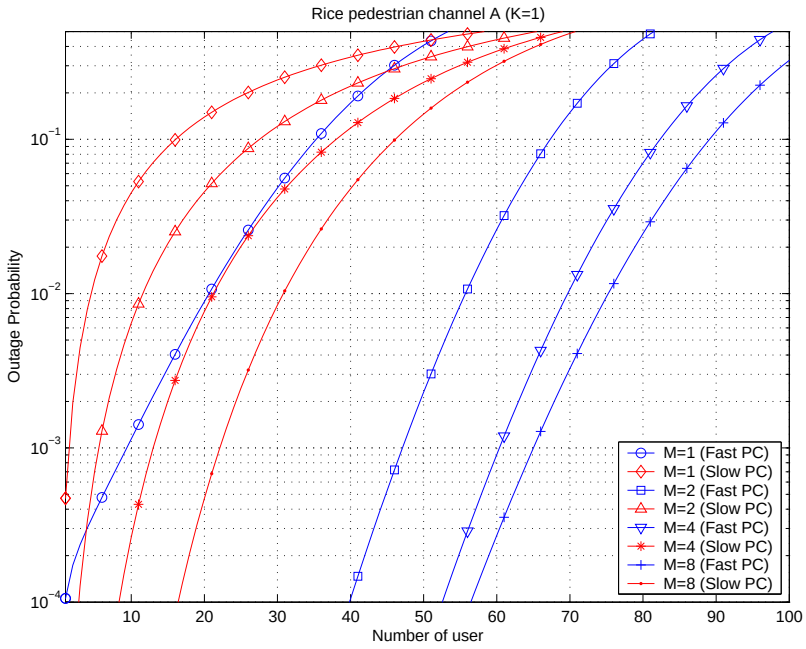

Figure 7.19: Capacity for pedestrian A channel with slow and fast power control, CLTD, $K = 1$, and 3-way soft handoff

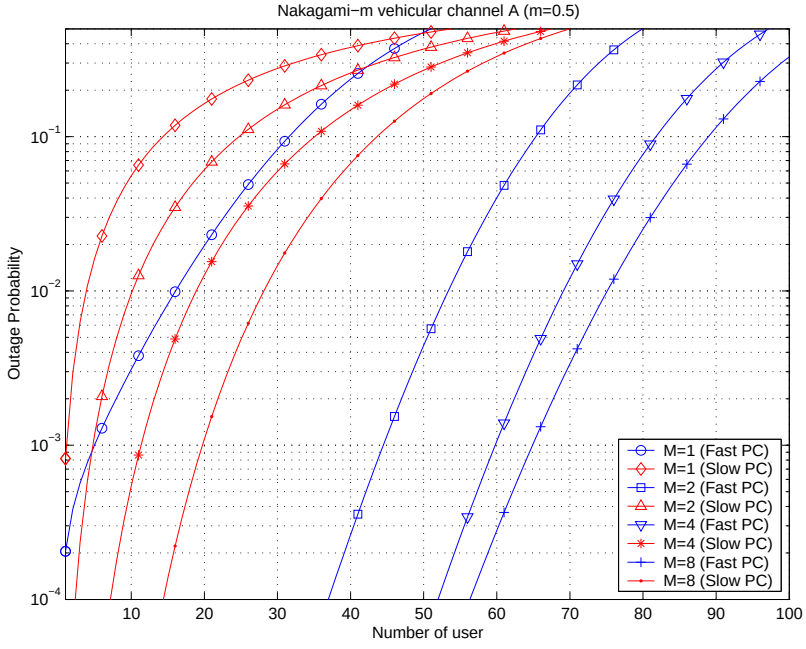

Figure 7.20: Capacity for vehicular A channel with slow and fast power control, CLTD, $m = 0.5$, and 3-way soft handoff

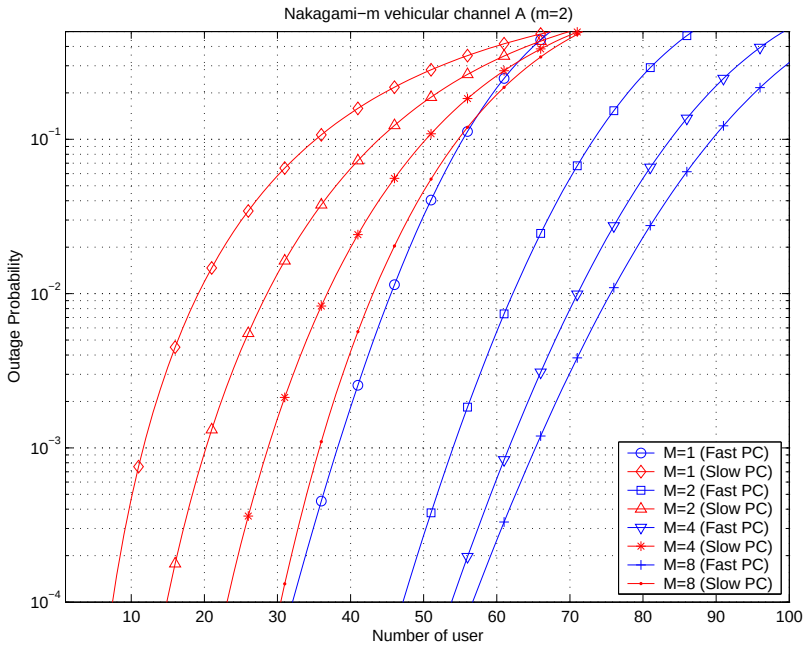

Figure 7.21: Capacity for vehicular A channel with slow and fast power control, CLTD, $m = 2$, and 3-way soft handoff

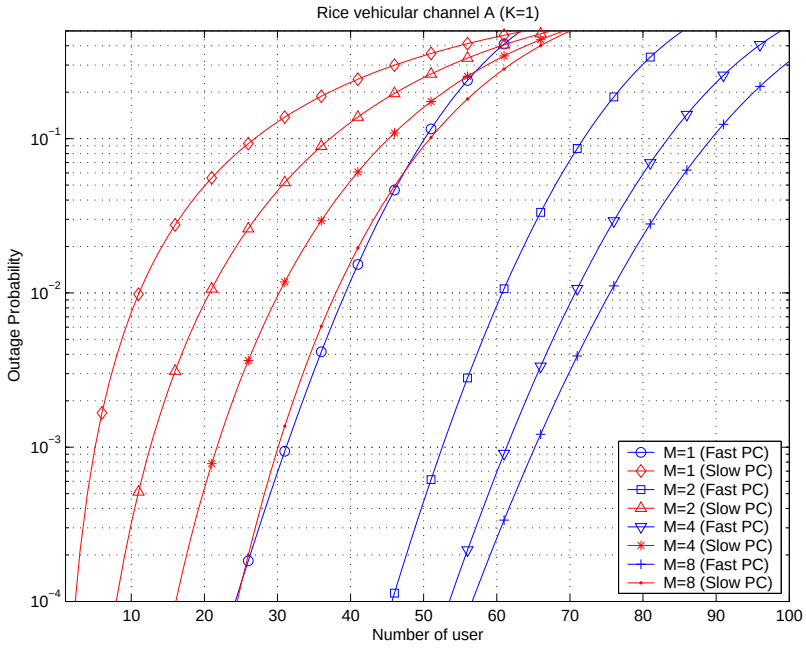

Figure 7.22: Capacity for vehicular A channel with slow and fast power control, CLTD, $K = 1$, and 3-way soft handoff

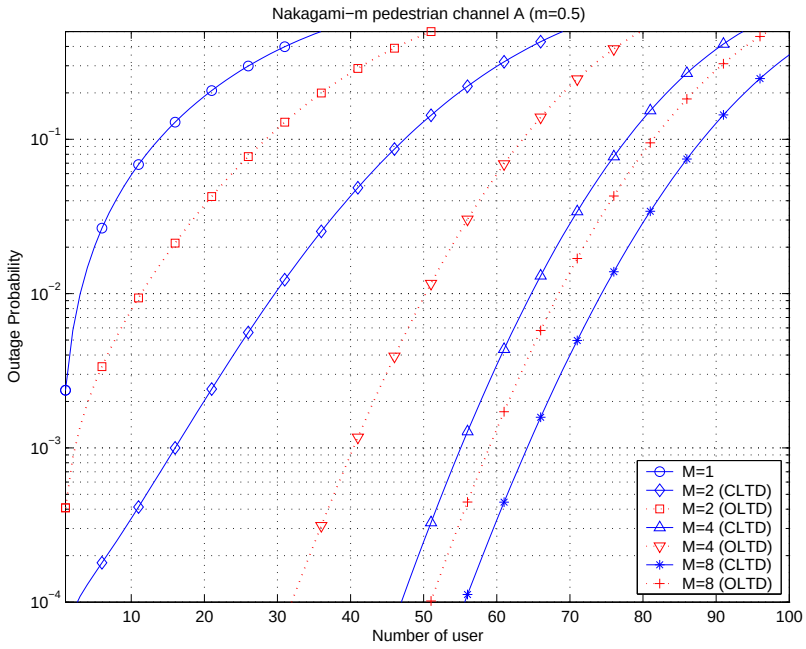

Figure 7.23: Capacity for pedestrian A channel with fast power control, $m = 0.5$, and 3-way soft handoff

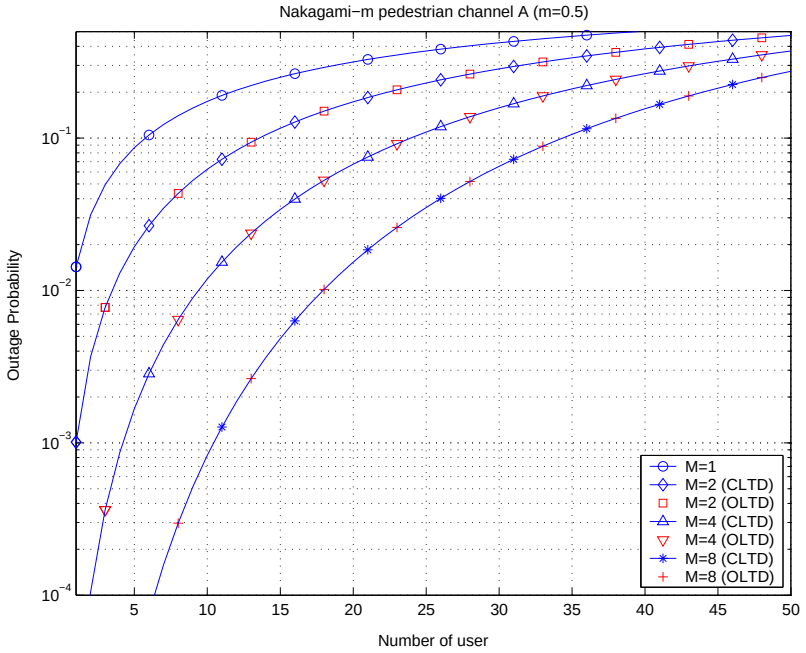

Figure 7.24: Capacity for pedestrian A channel with slow power control, $m = 0.5$, and 3-way soft handoff

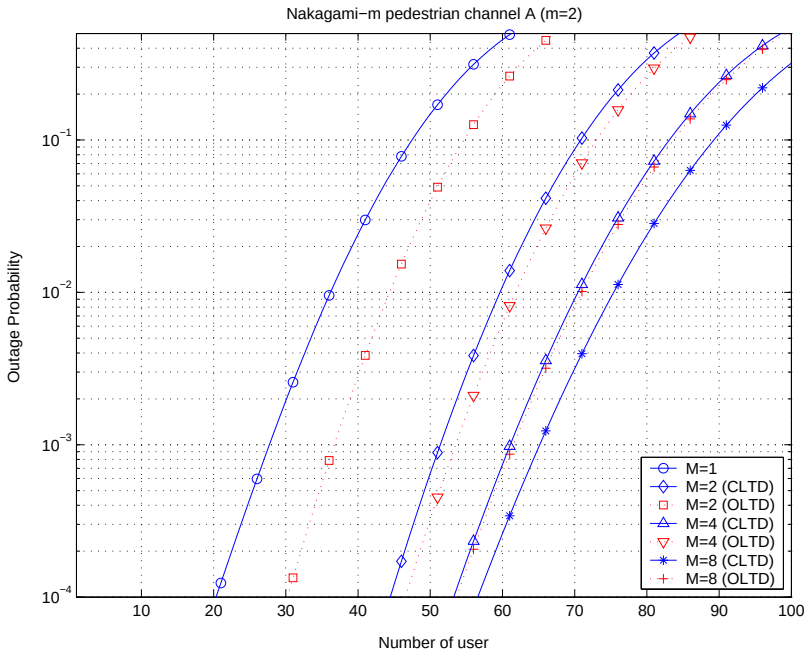

Figure 7.25: Capacity for pedestrian A channel with fast power control, $m = 2$, and 3-way soft handoff

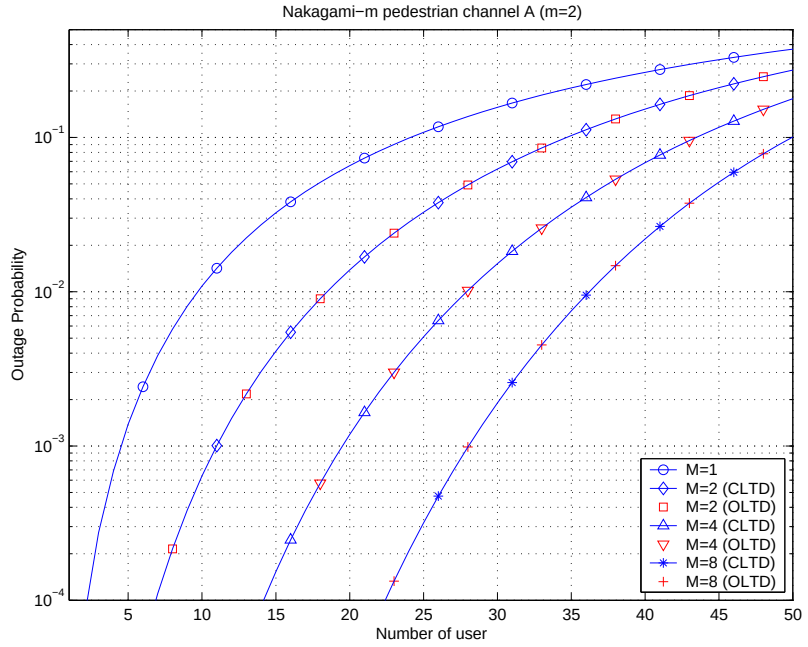

Figure 7.26: Capacity for pedestrian A channel with slow power control, $m = 2$, and 3-way soft handoff

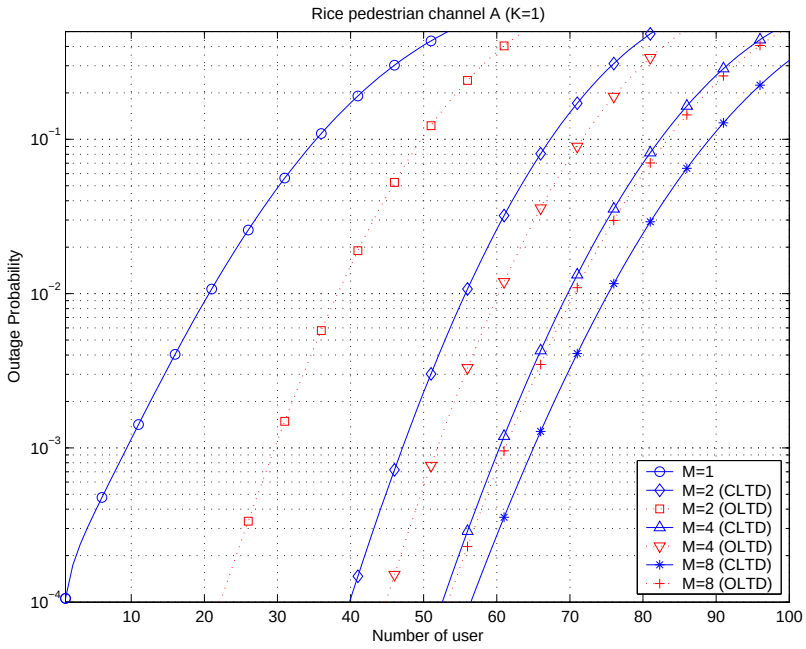

Figure 7.27: Capacity for pedestrian A channel with fast power control, $K = 1$, and 3-way soft handoff

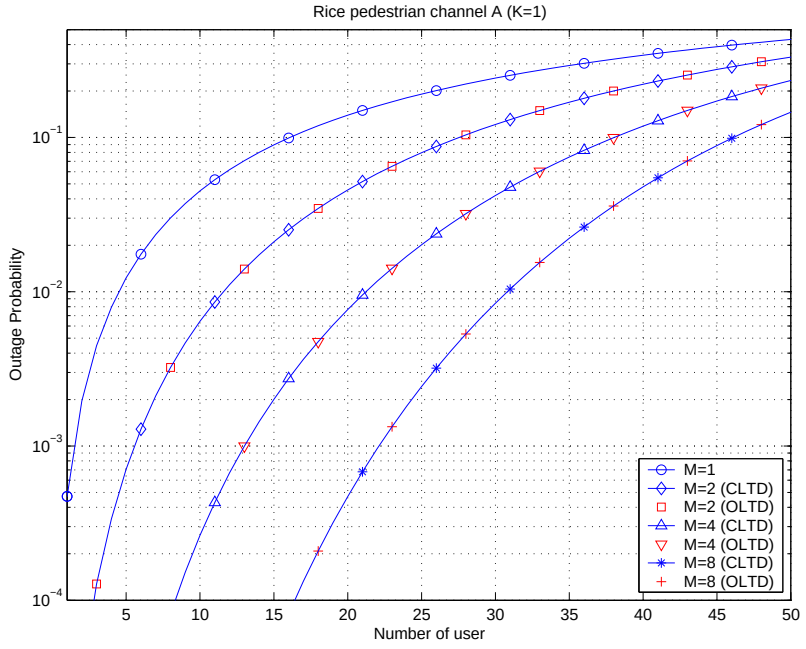

Figure 7.28: Capacity for pedestrian A channel with slow power control, $K = 1$, and 3-way soft handoff

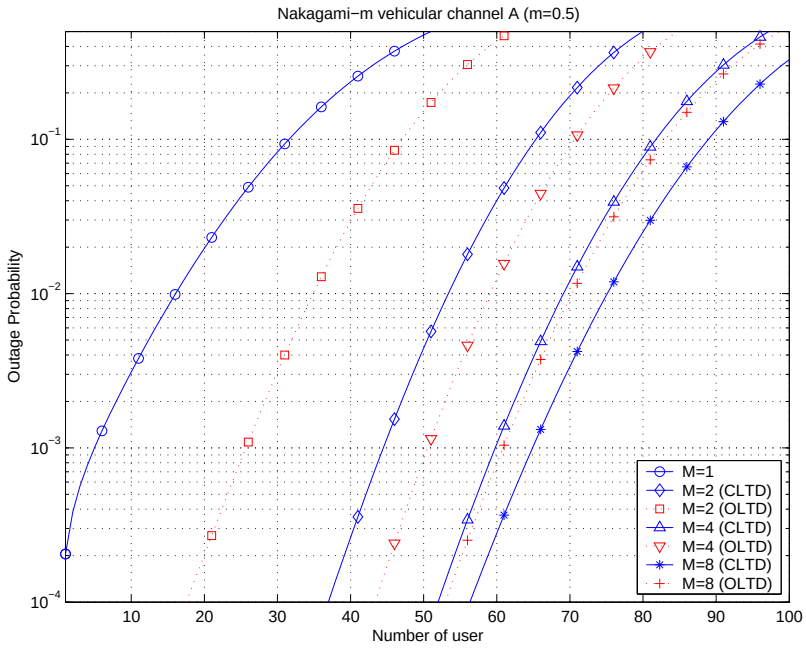

Figure 7.29: Capacity for vehicular A channel with fast power control, $m = 0.5$, and 3-way soft handoff

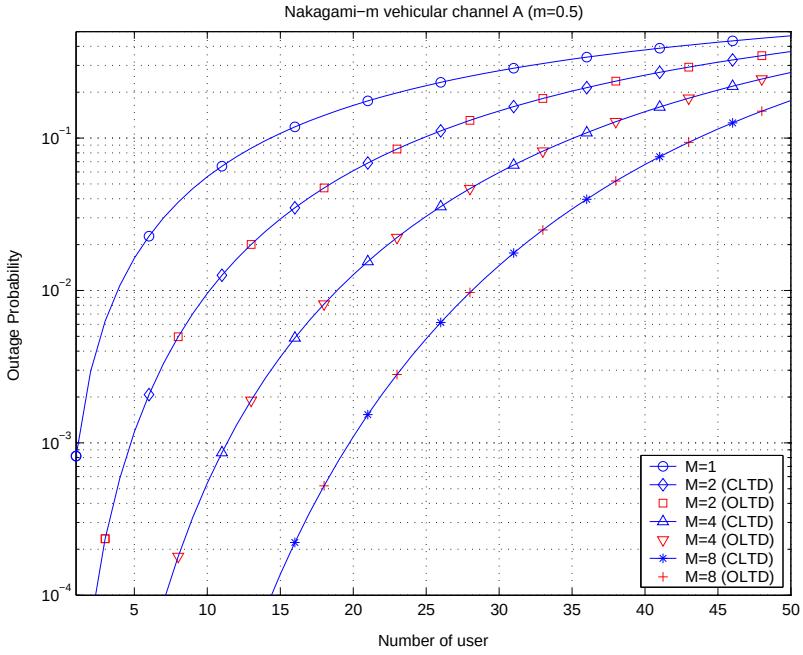

Figure 7.30: Capacity for vehicular A channel with slow power control, $m = 0.5$, and 3-way soft handoff

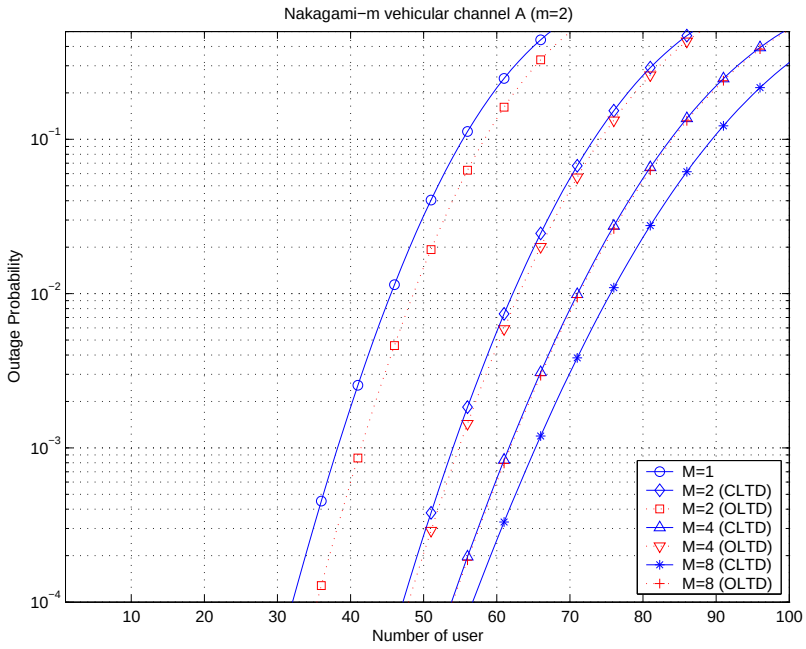

Figure 7.31: Capacity for vehicular A channel with fast power control, $m = 2$, and 3-way soft handoff

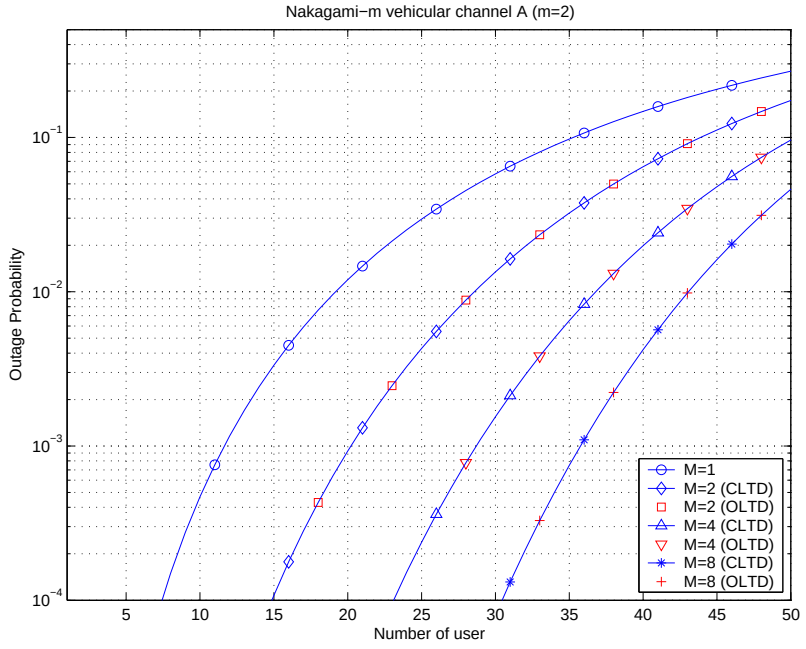

Figure 7.32: Capacity for vehicular A channel with slow power control, $m = 2$, and 3-way soft handoff

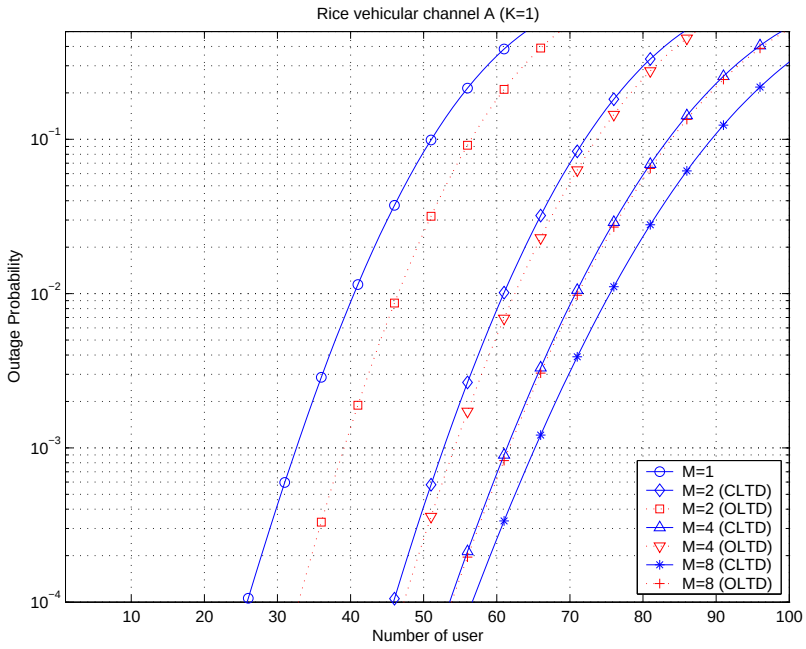

Figure 7.33: Capacity for vehicular A channel with fast power control, $K = 1$, and 3-way soft handoff

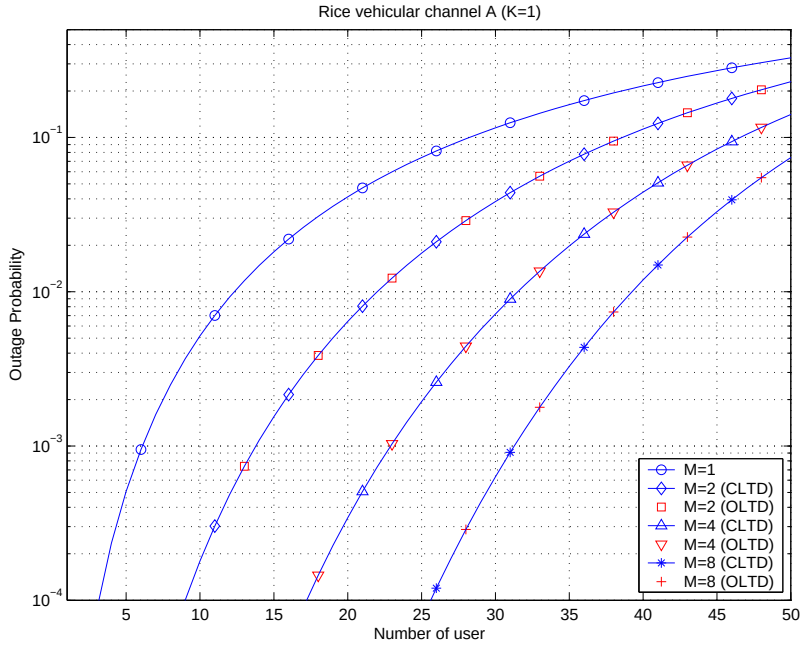

Figure 7.34: Capacity for vehicular A channel with slow power control, $K = 1$, and 3-way soft handoff

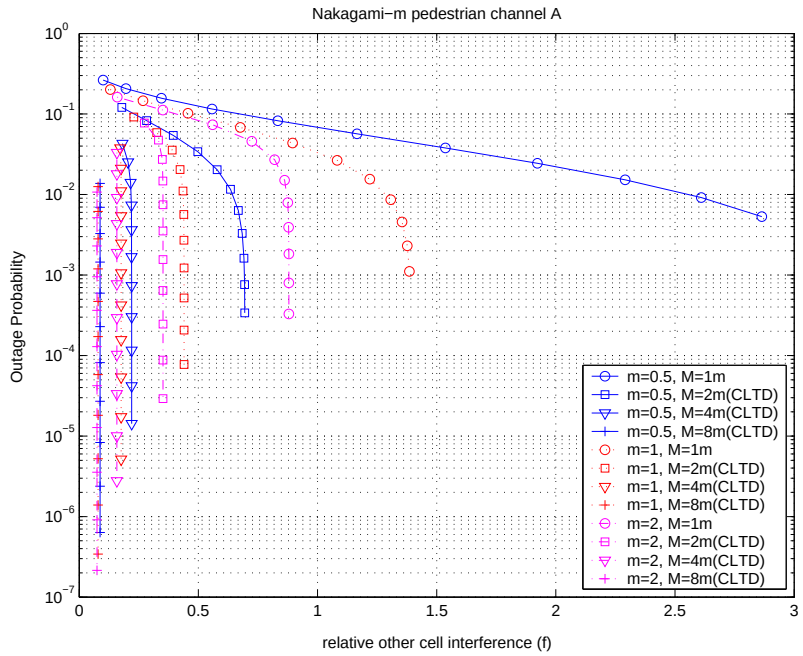

Figure 7.35: P_{out} and f factors for pedestrian A channel with different fading index $m = 0.5, 1$, and 2, and 3-way soft handoff

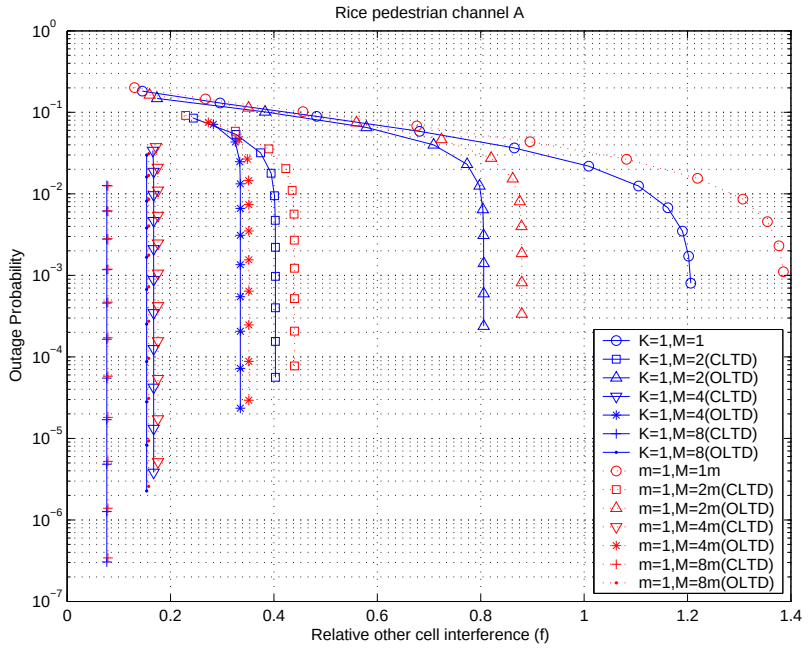

Figure 7.36: P_{out} and f factors for pedestrian A channel with different fading index $m = 1$ and $K = 1$, and 3-way soft handoff

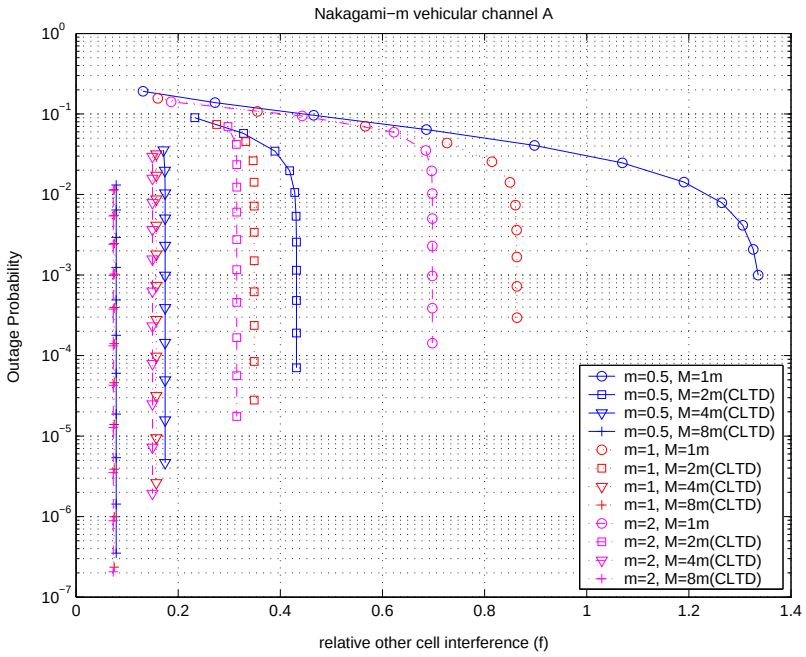

Figure 7.37: P_{out} and f factors for vehicular A channel with different fading index $m = 0.5, 1,$ and 2, and 3-way soft handoff

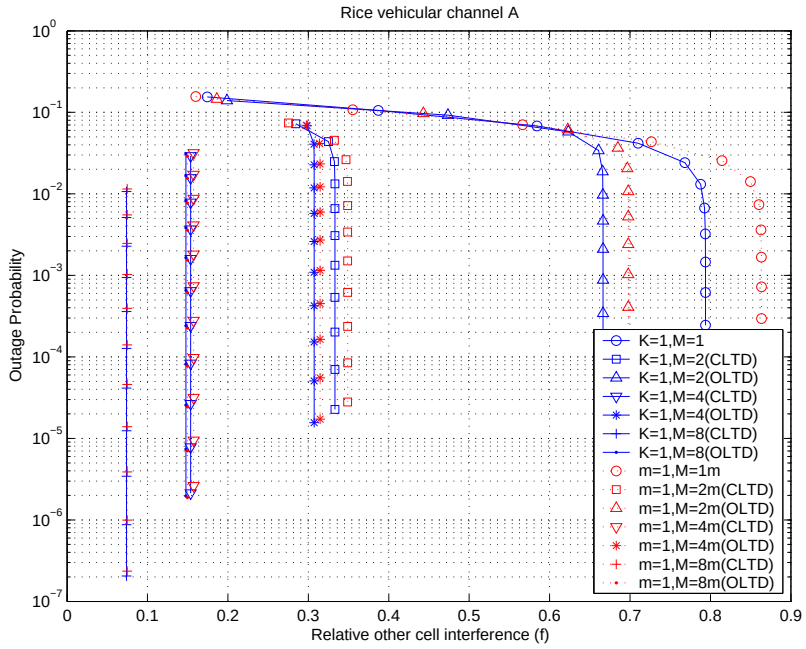

Figure 7.38: P_{out} and f factors for vehicular A channel with different fading index $m = 1$ and $K = 1$, and 3-way soft handoff

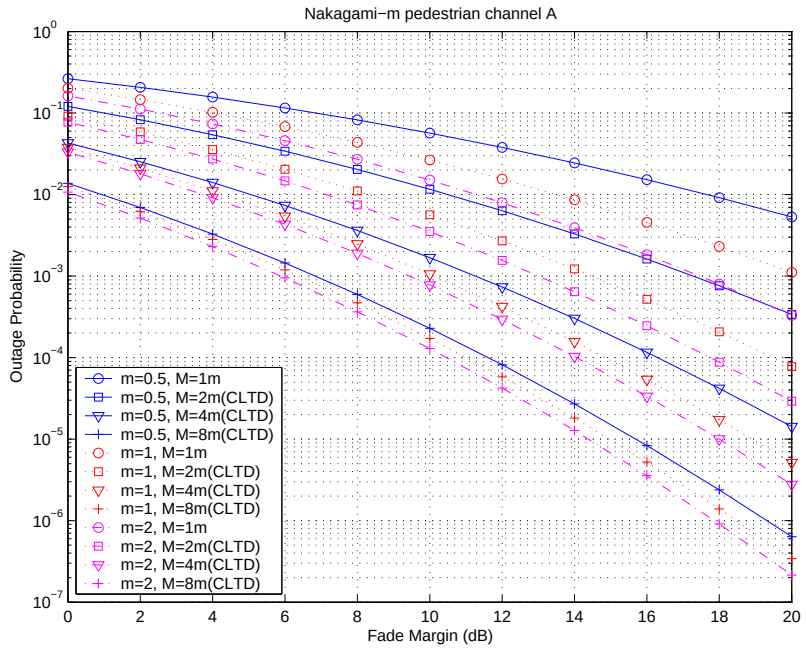

Figure 7.39: P_{out} and fade margin for pedestrian A channel with different fading index $m = 0.5, 1$, and 2, and 3-way soft handoff

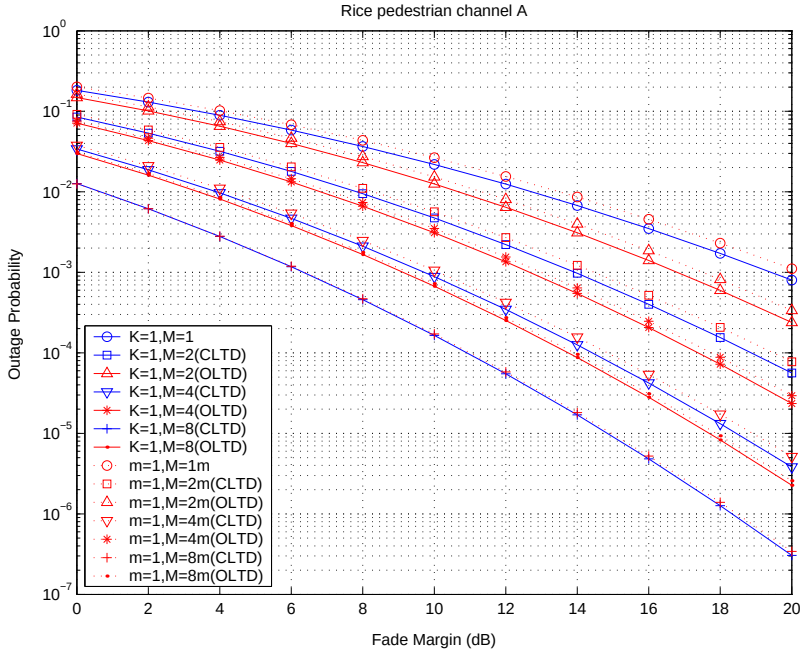

Figure 7.40: P_{out} and fade margin for pedestrian A channel with different fading index $m = 1$ and $K = 1$, and 3-way soft handoff

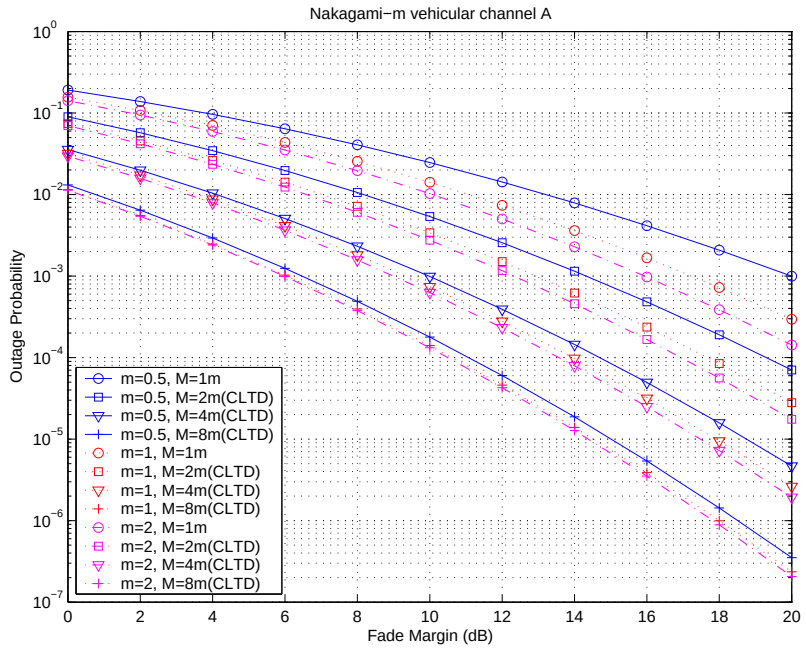

Figure 7.41: P_{out} and fade margin for vehicular A channel with different fading index $m = 0.5, 1$, and 2, and 3-way soft handoff

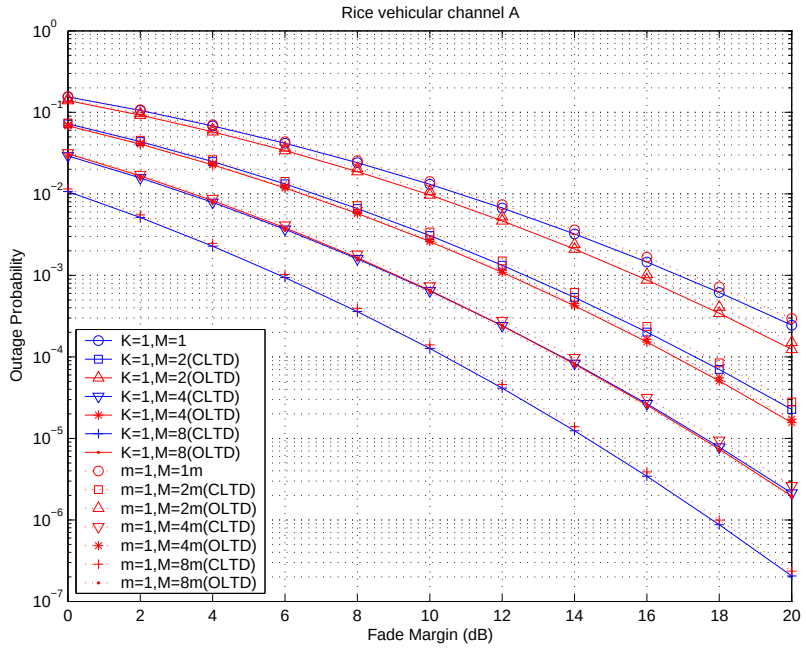

Figure 7.42: P_{out} and fade margin for vehicular A channel with different fading index $m = 1$ and $K = 1$, and 3-way soft handoff

Table 7.12: Capacity comparison for pedestrian A channel with different fading index employing slow power control and CLTD at P_{out}=0.01

	Pedestrian A channel capacity							
Div. Order	$m = 0.5$	% Gain	$m = 1$	% Gain	$m = 2$	% Gain	$K = 1$	% Gain
2	3.5		9.5		18.5		11.6	
4	9.5	171.4 %	18	89.5 %	28	51.4 %	21.23	83 %
8	18	414.3 %	27.5	189.5 %	36	94.6 %	30.8	165.5 %

Table 7.13: Capacity comparison for vehicular A channel with different fading index employing slow power control and CLTD at P_{out}=0.01

	Vehicular A channel capacity							
Div. Order	$m = 0.5$	% Gain	$m = 1$	% Gain	$m = 2$	% Gain	$K = 1$	% Gain
2	10		19		28.5		20.72	
4	19	90 %	28.5	50 %	37	29.8 %	30.23	45.9 %
8	28	180 %	36.5	92.1 %	43	50.9 %	38	83.4 %

Table 7.14: Capacity comparison for pedestrian A channel with different fading index employing fast power control and CLTD at P_{out}=0.01

	Vehicular A channel capacity							
Div. Order	$m = 0.5$	% Gain	$m = 1$	% Gain	$m = 2$	% Gain	$K = 1$	% Gain
2	30		53		60		55.71	
4	65	116.7 %	69	30.2 %	70.5	17.5 %	69.7	25.1 %
8	74.5	148.3 %	75	41.5 %	75.5	25.8 %	75.25	35.1 %

Table 7.15: Capacity comparison for vehicular A channel with different fading index employing fast power control and CLTD at P_{out}=0.01

	Vehicular A channel capacity							
Div. Order	$m = 0.5$	% Gain	$m = 1$	% Gain	$m = 2$	% Gain	$K = 1$	% Gain
2	53.5		60		62		60.75	
4	69	29 %	70.5	17.5 %	71	14.5 %	70.72	16.4 %
8	75	40.2 %	75.5	25.8 %	76	22.6 %	75.6	24.4 %

Table 7.16: Relative margin and coverage for spatial diversity on pedestrian A channel with different fading index, fast power control, CLTD, and 3-way soft handoff

Pedestrian A channel									
	$m = 0.5$			$m = 1$			$m = 2$		
Diversity Order	Fade Margin	Relative Margin	Relative Coverage	Fade Margin	Relative Margin	Relative Coverage	Fade Margin	Relative Margin	Relative Coverage
1Tx2Rx	10.5 dB	0 dB	1	8.3 dB	0 dB	1	7.14 dB	0 dB	1
2Tx2Rx	5.05 dB	5.45 dB	1.87	4.28 dB	4.02 dB	1.59	3.73 dB	3.41 dB	1.48
2Tx4Rx	0.925 dB	9.575 dB	3.01	0.64 dB	7.66 dB	2.42	0.2 dB	6.94 dB	2.22

Table 7.17: Relative margin and coverage for spatial diversity on vehicular A channel with different fading index, fast power control, CLTD, and 3-way soft handoff

Vehicular A channel									
	$m = 0.5$			$m = 1$			$m = 2$		
Diversity Order	Fade Margin	Relative Margin	Relative Coverage	Fade Margin	Relative Margin	Relative Coverage	Fade Margin	Relative Margin	Relative Coverage
1Tx2Rx	8.17 dB	0 dB	1	7.03 dB	0 dB	1	6.59 dB	0 dB	1
2Tx2Rx	4.11 dB	4.06 dB	1.6	3.6 dB	3.43 dB	1.48	3.32 dB	3.27 dB	1.46
2Tx4Rx	0.76 dB	7.41 dB	2.35	0.38 dB	6.65 dB	2.15	0.33 dB	6.26 dB	2.1

Table 7.18: Other-cell interference factor f and relative gain for pedestrian A with fast power control at $P_{out} = 0.01$

Pedestrian A								
Diversity	$m = 0.5$		$m = 1$		$m = 2$		$K = 1$	
Order	f	% Gain	f	% Gain	f	% Gain	f	% Gain
2	0.643		0.436		0.3515		0.4006	
4	0.2173	35 %	0.1758	22.1 %	0.1578	16.7 %	0.1675	20 %
8	0.0877	51.1 %	0.0789	33.1 %	0.0749	25.7 %	0.077	30 %

Table 7.19: Other-cell interference factor f and relative gain for vehicular A with fast power control at $P_{out} = 0.01$

Vehicular A								
Diversity	$m = 0.5$		$m = 1$		$m = 2$		$K = 1$	
Order	f	% Gain	f	% Gain	f	% Gain	f	% Gain
2	0.4286		0.3488		0.3147		0.3332	
4	0.1744	21.6 %	0.1573	16.5 %	0.1496	14.4 %	0.1536	15.6 %
8	0.0787	32.4 %	0.0748	25.5 %	0.0730	22.5 %	0.0739	24.1 %

7.4.4 The effect of the number of cells involved in a soft handoff

As it is shown in [67], soft handoff increases system capacity and coverage. As the number of cells involved in soft handoff increases, the macrodiversity gain increases, resulting in less interference, hence, leading to a capacity increase. This can be observed in Figure 7.43 through Figure 7.54.

Key observations and effects

- As antenna diversity order increases, the performance difference between 2-way soft handoff and 3-way handoff diminishes. In other words, the benefits accrued from 3-cell macrodiversity are lessened as the antenna diversity order increases.
- Relative capacity gains from antenna diversity are more pronounced in those cases in which soft handoffs are limited to 2-cells, rather than 3 cells.

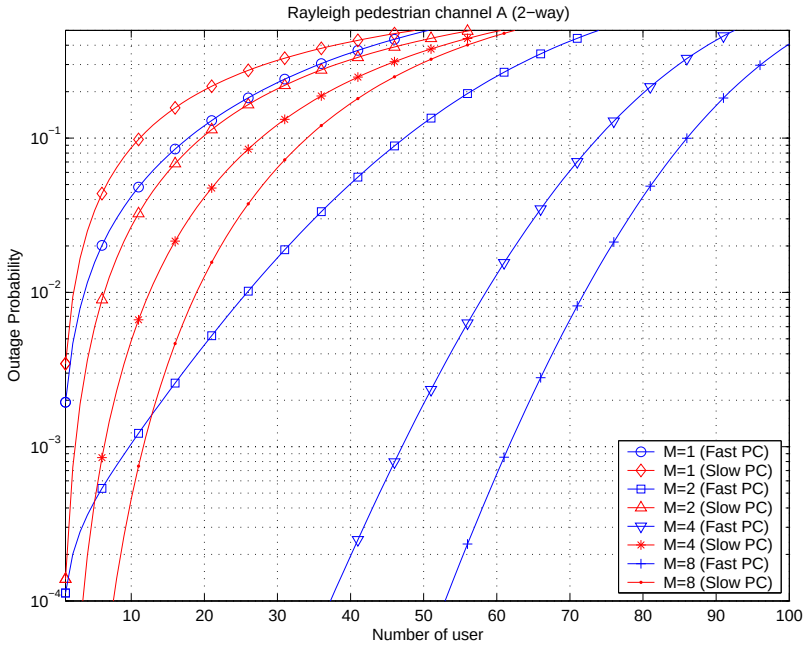

Figure 7.43: Capacity for pedestrian A channel with CLTD and 2-way soft handoff

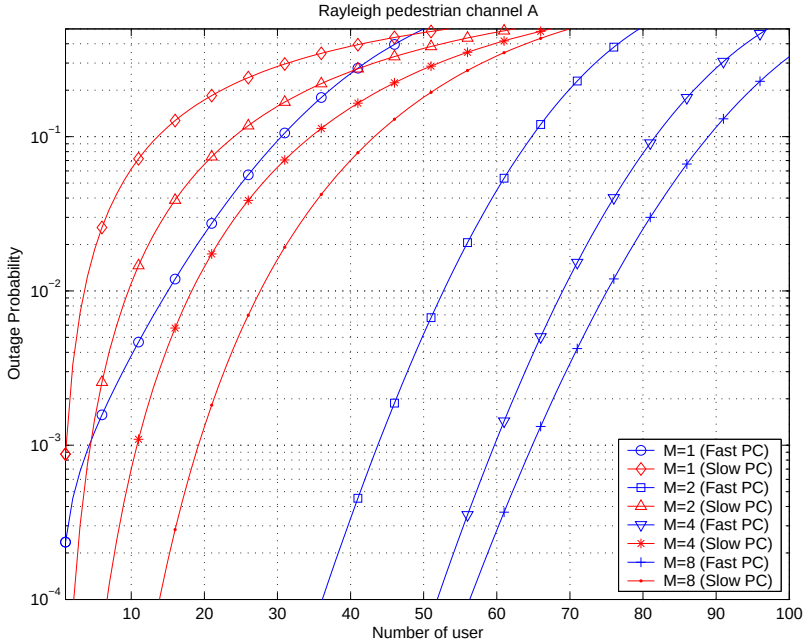

Figure 7.44: Capacity for pedestrian A channel with CLTD and 3-way soft handoff

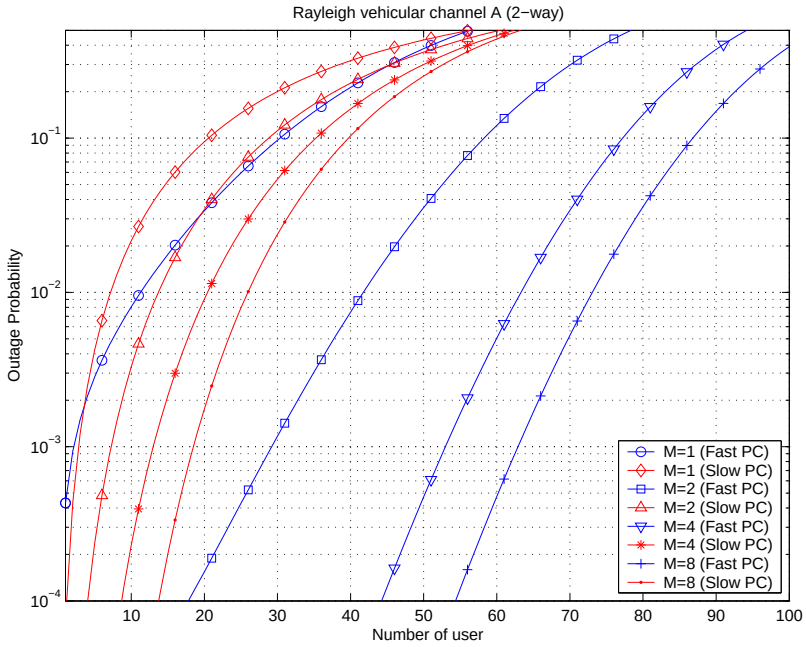

Figure 7.45: Capacity for vehicular A channel with CLTD and 2-way soft handoff

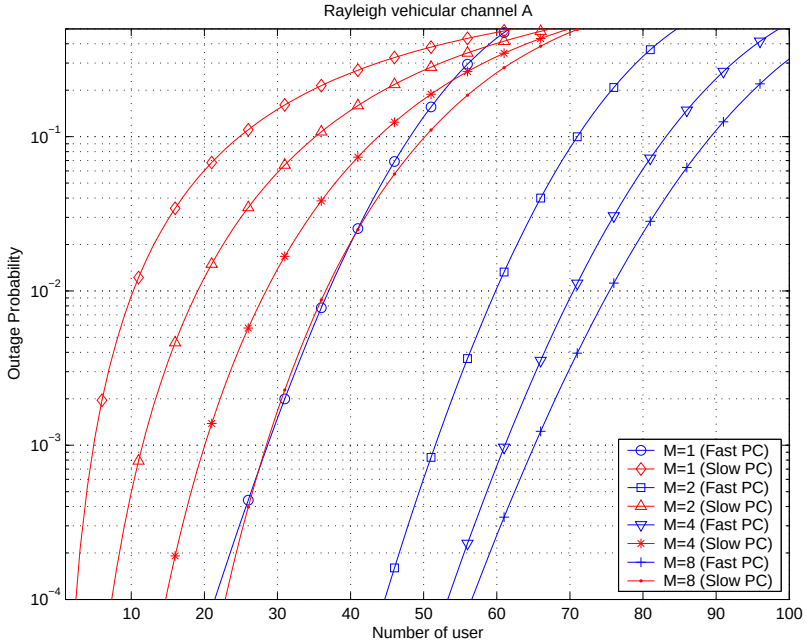

Figure 7.46: Capacity for vehicular A channel with CLTD and 3-way soft handoff

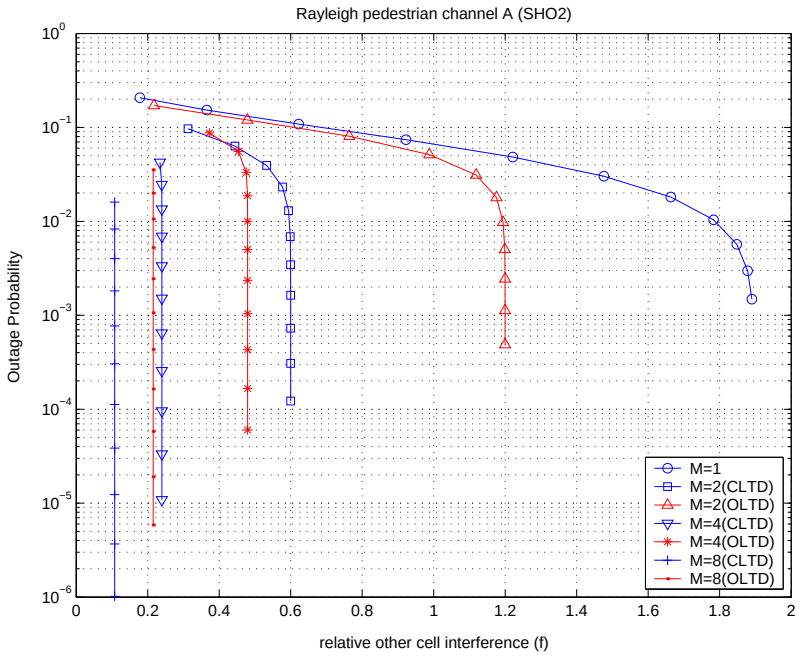

Figure 7.47: Other-cell interference factor f for pedestrian A channel with fast power control and 2-way soft handoff

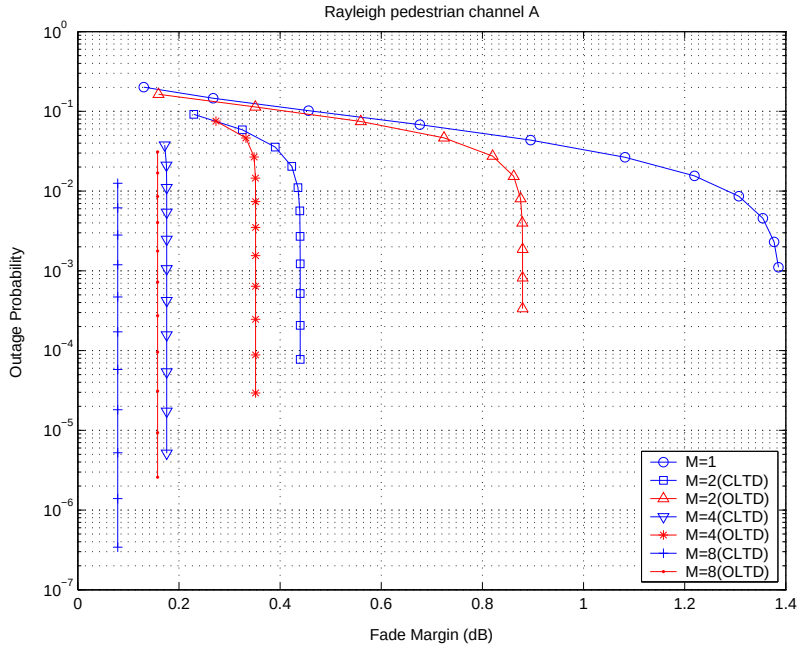

Figure 7.48: Other-cell interference factor f for pedestrian A channel with fast power control and 3-way soft handoff

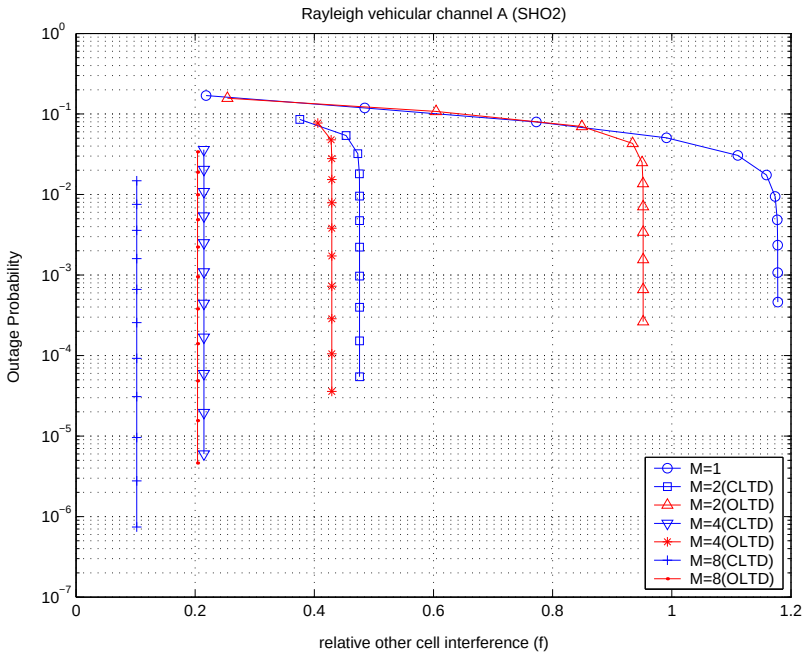

Figure 7.49: Other-cell interference factor f for vehicular A channel with fast power control and 2-way soft handoff

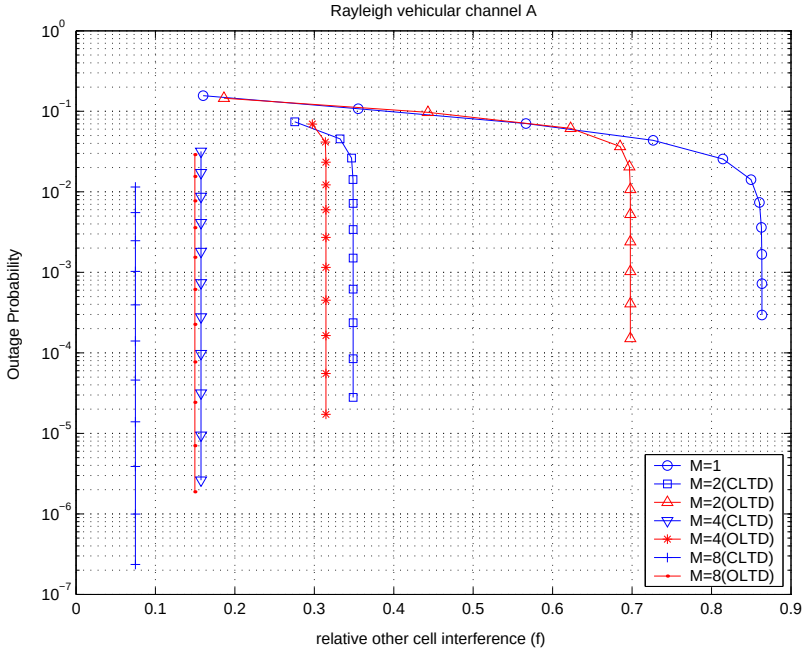

Figure 7.50: Other-cell interference factor f for vehicular A channel with fast power control and 3-way soft handoff

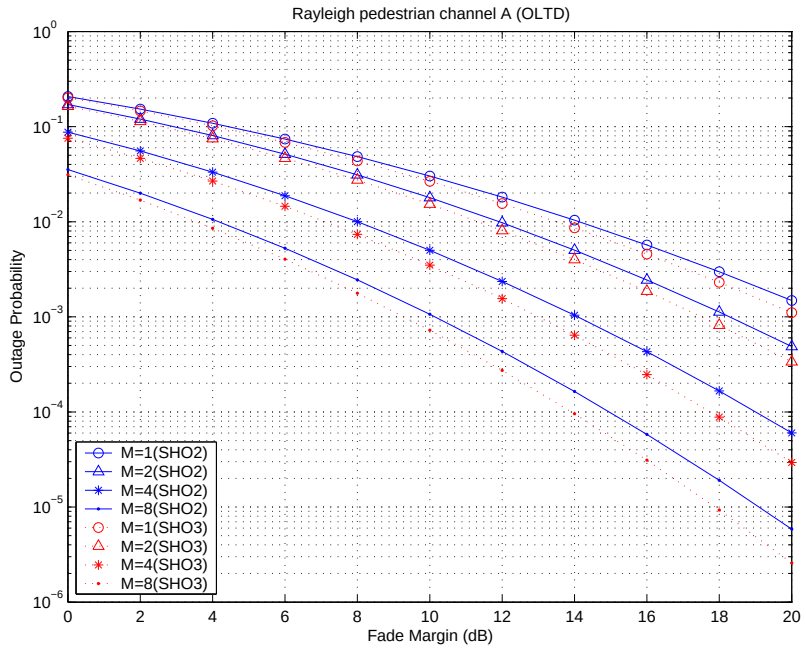

Figure 7.51: Outage probability vs. fade margin for pedestrian A channel with OLTD and fast power control

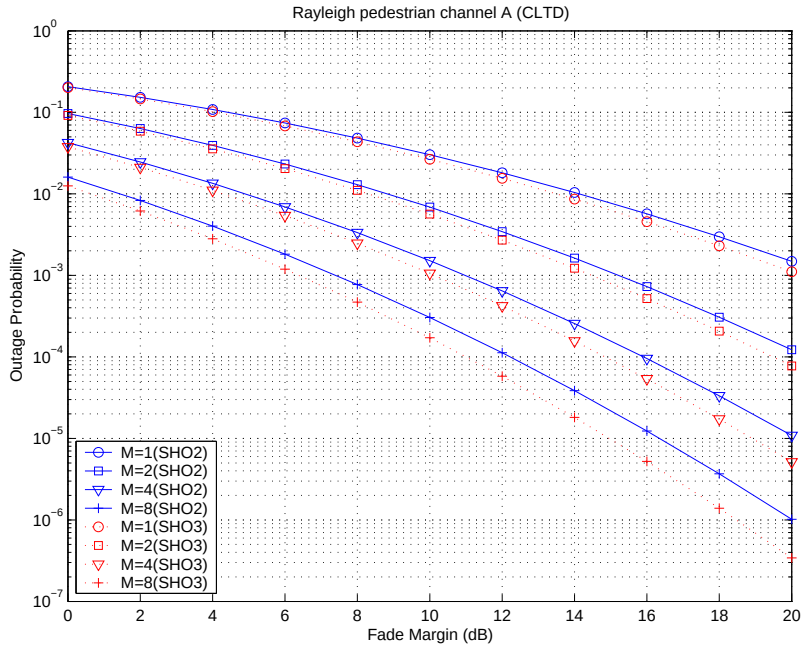

Figure 7.52: Outage probability vs. fade margin for pedestrian A channel with CLTD and fast power control

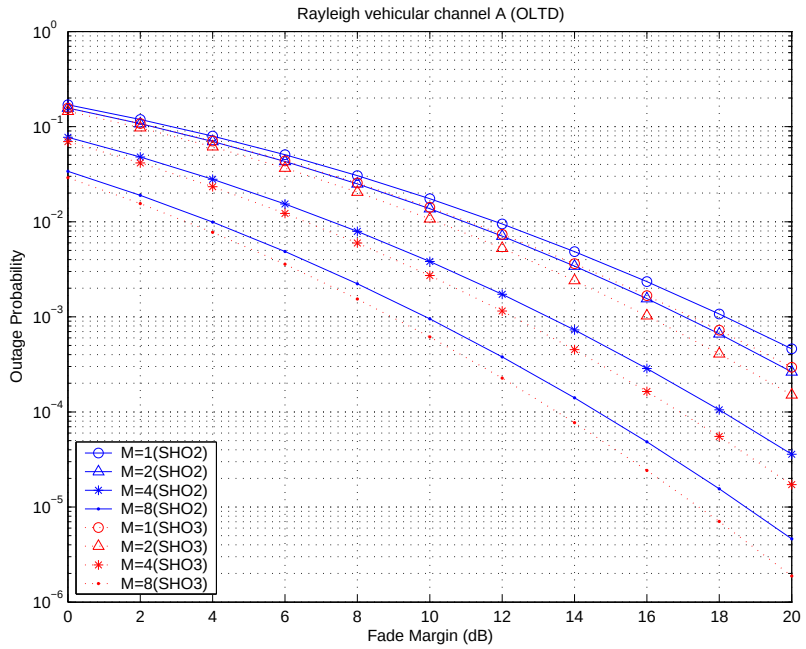

Figure 7.53: Outage probability vs. fade margin for vehicular A channel with OLTD and fast power control

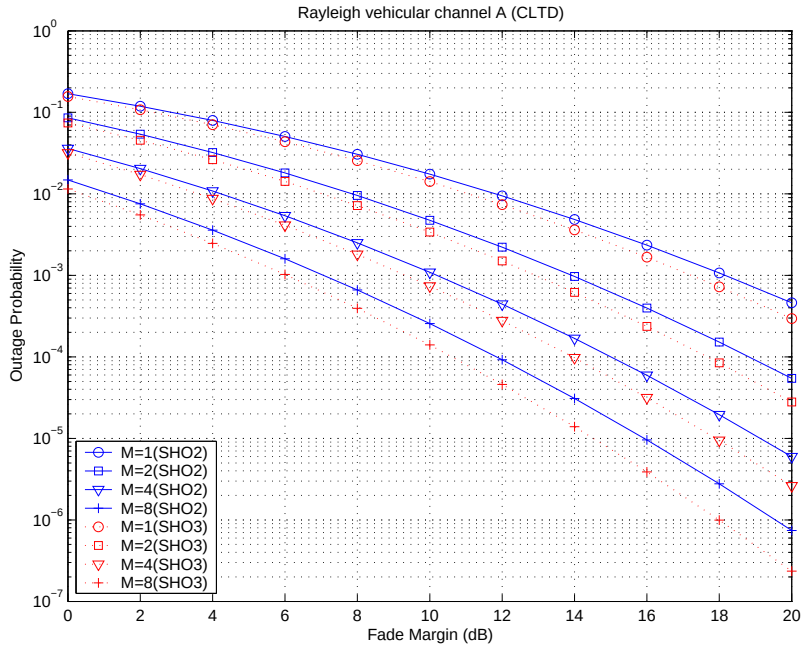

Figure 7.54: Outage probability vs. fade margin for vehicular A channel with CLTD and fast power control

Table 7.20: Capacity improvement of 2-way and 3-way SHO with slow power control

Pedestrian A channel capacity					
Div. order	SHO2	% Gain	SHO3	% Gain	SHO2 → SHO3 % Gain
2	6.3		9.5		50.8 %
4	12.5	98.4 %	18	89.5 %	44 %
8	18.9	200 %	27.5	189.5 %	45.5 %

Table 7.21: Capacity improvement of 2-way and 3-way SHO with fast power control

Pedestrian A channel capacity					
Div. order	SHO2	% Gain	SHO3	% Gain	SHO2 → SHO3 % Gain
2	25.85		53		105.3 %
4	58.5	126.3 %	69	30.2 %	15.2 %
8	72	178.5 %	75	41.5 %	4.2 %

Table 7.22: Capacity improvement of 2-way and 3-way SHO with slow power control

Vehicular A channel capacity					
Div. order	SHO2	% Gain	SHO3	% Gain	SHO2 → SHO3 % Gain
2	13.7		19		38.7 %
4	20.4	48.9 %	28.5	50 %	39.7 %
8	26	89.8 %	36.5	92.1 %	40.4 %

Table 7.23: Capacity improvement of 2-way and 3-way SHO with fast power control

Vehicular A channel capacity					
Div. order	SHO2	% Gain	SHO3	% Gain	SHO2 → SHO3 % Gain
2	41.7		60		43.9 %
4	63.3	51.8 %	70.5	17.5 %	10.2 %
8	73.1	75.3 %	75	25.8 %	2.6 %

Table 7.24: f factor comparison of 2-way and 3-way SHO for pedestrian A channel with fast power control

Pedestrian A							
	SHO2			SHO3			SHO2 → SHO3
Div. order	f	$1+f$	% Gain	f	$1+f$	% Gain	% Gain
2 MRC	0.5960	1.5960		0.4360	1.4360		11.1 %
4 OLTD	0.4796	1.4796	7.9 %	0.3515	1.3515	6.3 %	9.5 %
4 CLTD	0.2398	1.2398	28.7 %	0.1758	1.1758	22.1 %	5.4 %
8 OLDT	0.2153	1.2153	31.3 %	0.1578	1.1578	24 %	5.0 %
8 OLTD	0.1080	1.1080	44 %	0.0789	1.0789	33.1 %	1.6 %

Table 7.25: f factor comparison of 2-way and 3-way SHO for vehicular A channel with fast power control

Vehicular A							
	SHO2			SHO3			SHO2 → SHO3
Div. order	f	$1+f$	% Gain	f	$1+f$	% Gain	% Gain
2 MRC	0.4760	1.4760		0.3488	1.3488		9.4 %
4 OLTD	0.4293	1.4293	3.3 %	0.3147	1.3147	2.6 %	8.7 %
4 CLTD	0.2146	1.2146	21.5 %	0.1573	1.1573	16.5 %	5.0 %
8 OLDT	0.2041	1.2041	22.6 %	0.1496	1.1496	17.3 %	4.7 %
8 OLTD	0.1021	1.1021	33.9 %	0.0748	1.0748	25.5 %	2.5 %

Table 7.26: Comparison of relative coverage of 2-way and 3-way SHO with fast power control

Pedestrian A								
	SHO2			SHO3			SHO2 → SHO3	
Diversity Order	Fade Margin	Relative Margin	Relative Coverage	Fade Margin	Relative Margin	Relative Coverage	Relative Margin	Relative Coverage
MRC	8.82 dB	0 dB	1.00	8.3 dB	0 dB	1.00	0.52 dB	1.06
4 OLTD	8 dB	0.82 dB	1.10	7.1 dB	1.20 dB	1.15	0.9 dB	1.11
4 CLTD	4.89 dB	3.93 dB	1.57	4.28 dB	4.02 dB	1.59	0.61 dB	1.07
8 OLTD	4.16 dB	4.66 dB	1.71	3.54 dB	4.76 dB	1.73	0.62 dB	1.07
8 CLTD	1.42 dB	7.40 dB	2.34	0.64 dB	7.66 dB	2.42	0.78 dB	1.09

Table 7.27: Comparison of relative coverage of 2-way and 3-way SHO with fast power control

Vehicular A								
	SHO2			SHO3			SHO2 → SHO3	
Diversity Order	Fade Margin	Relative Margin	Relative Coverage	Fade Margin	Relative Margin	Relative Coverage	Relative Margin	Relative Coverage
MRC	7.86 dB	0 dB	1.00	7.03 dB	0 dB	1.00	0.83 dB	1.10
4 OLTD	7.3 dB	0.56 dB	1.07	6.56 dB	0.47 dB	1.06	0.74 dB	1.09
4 CLTD	4.23 dB	3.63 dB	1.52	3.60 dB	3.43 dB	1.48	0.63 dB	1.08
8 OLTD	3.97 dB	3.89 dB	1.56	3.26 dB	3.77 dB	1.54	0.71 dB	1.09
8 CLTD	1.16 dB	6.70 dB	2.16	0.38 dB	6.65 dB	2.15	0.78 dB	1.09

7.4.5 The effect of user distribution

In the previous sections, we assumed a uniform user distribution throughout the cell. In this section, we investigate the impact of various user distributions on the system. Three cases are considered including (1) users are uniformly distributed in the region $0.5 < r < 1$, (2) users are uniformly distributed in the region $0 < r < 0.5$, or (3) users are uniformly distributed throughout the cell, where r is the distance from the mobile to its serving base station. The cell radius is assumed to be one without loss of generality. The intent of this analysis is to model user concentrations around cell boundaries, user concentrations near the base station, and uniform user distributions throughout the cell.

Figure 7.55 and Figure 7.57 show outage probability for the pedestrian A and vehicular A channels with both slow and fast power control, and with 3-way handoff when users are concentrated around the cell boundaries. As can be seen in the figures, the capacity of a system with users distributed in the outer ring of a cell is less than that observed for cases in which users are concentrated around the base station, that is, uniformly distributed in the inner ring (Figure 7.56 and Figure 7.58) and users are uniformly distributed throughout the cell. This can be seen in Figure 7.4, Figure 7.5, Figure 7.55, Figure 7.57, Figure 7.56, and Figure 7.58. Since users distributed in the outer ring of a cell region are distanced from the desired base station, those users create more interference to other cell users as they attempt to compensate for fading and propagation losses; Therefore, a system loaded with users relatively close to the cell boundaries experiences increased interference, as required to achieve the same outage probability (Figure 7.65, Figure 7.66, Figure 7.67, and Figure 7.68). Also, in terms of outage and coverage, since a mobile on a boundary represents the worst case [67], as more users are close to the boundary, outage probability performance degrades and the coverage reduces even though there is a soft handoff macrodiversity gain as seen in Figure 7.69, Figure 7.70, Figure 7.71, Figure 7.72.

Key observations and effects

- Compared to either a uniform distribution of users throughout the cell or a concentration of users around the base station, capacity decreases when users concentrate near cell boundaries due to increased interference from other cells to compensate for fading and path loss.

- Spatial diversity has a more pronounced impact on users concentrated near the cell boundaries as compared with the cases where users are uniformly distributed throughout the cell or concentrated around the base station.

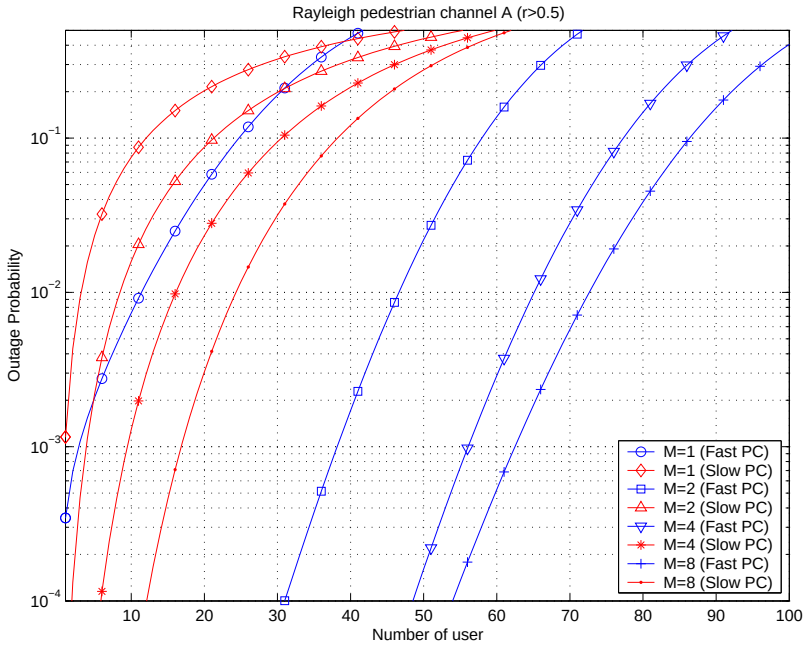

Figure 7.55: Capacity for pedestrian A channel with CLTD when $r > 0.5$

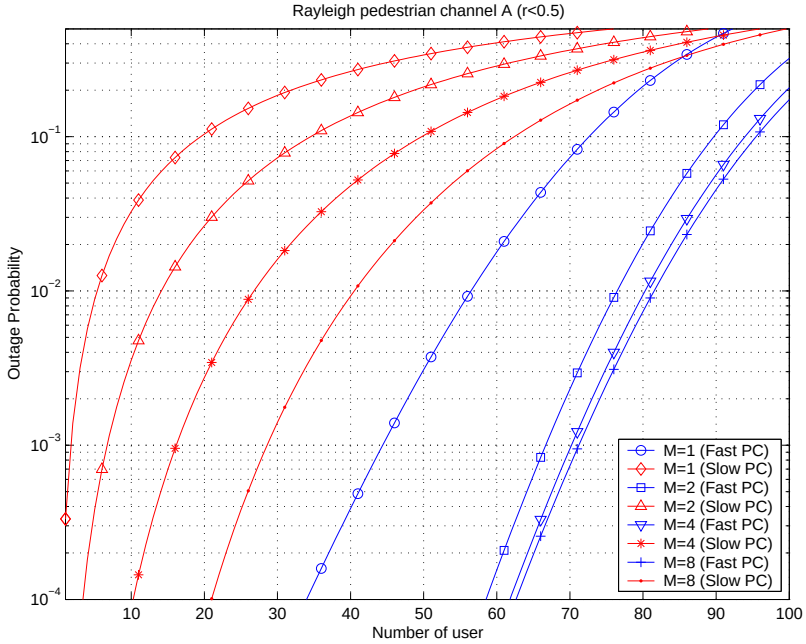

Figure 7.56: Capacity for pedestrian A channel with CLTD when $r < 0.5$

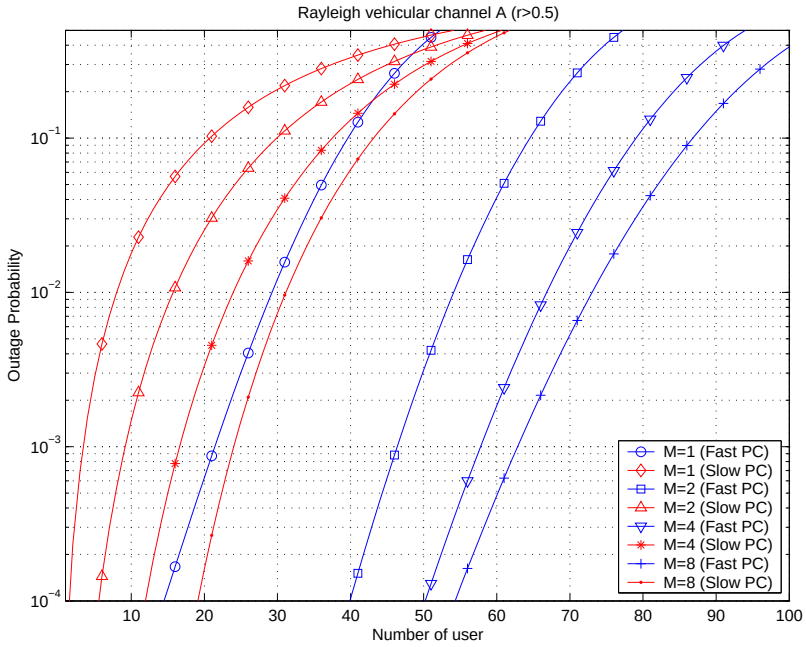

Figure 7.57: Capacity for vehicular A channel with CLTD when $r > 0.5$

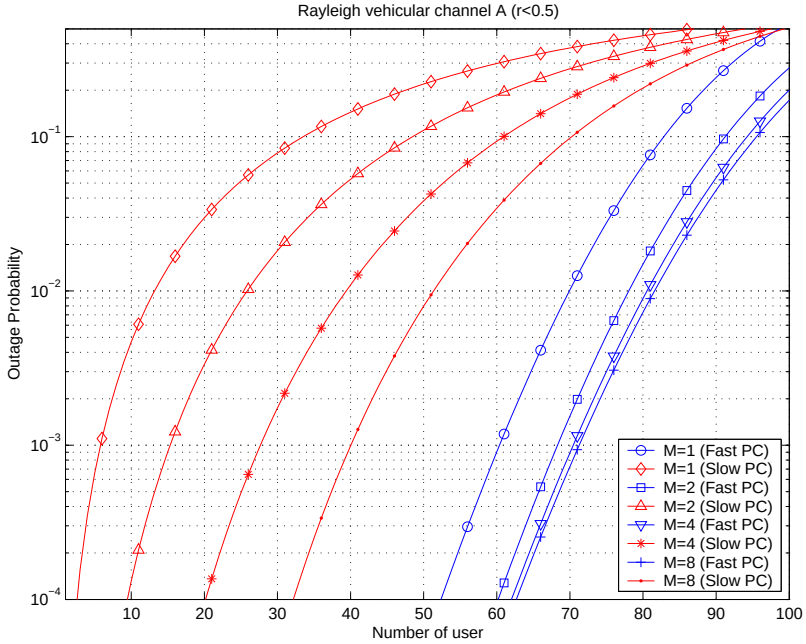

Figure 7.58: Capacity for vehicular A channel with CLTD when $r < 0.5$

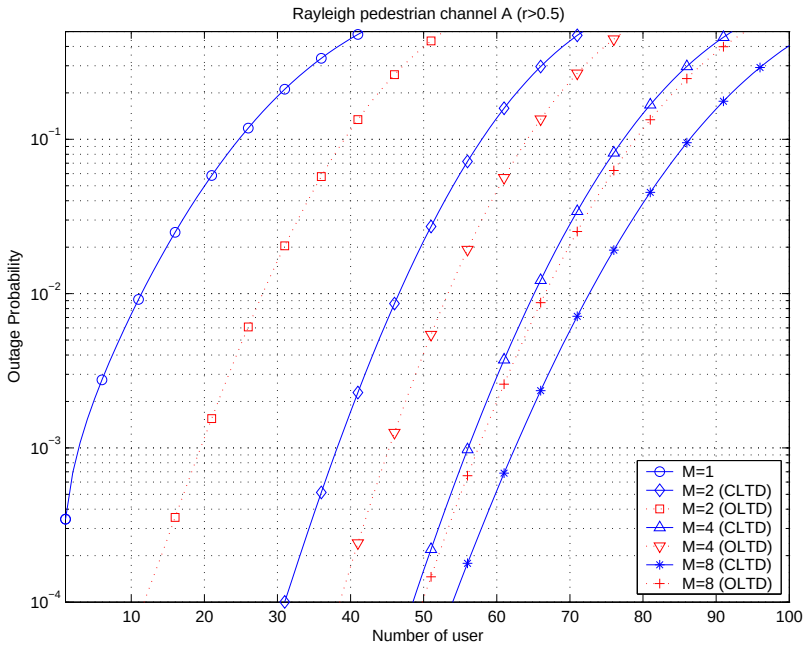

Figure 7.59: Capacity for pedestrian A channel with fast power control, CLTD, and OLTD when $r > 0.5$

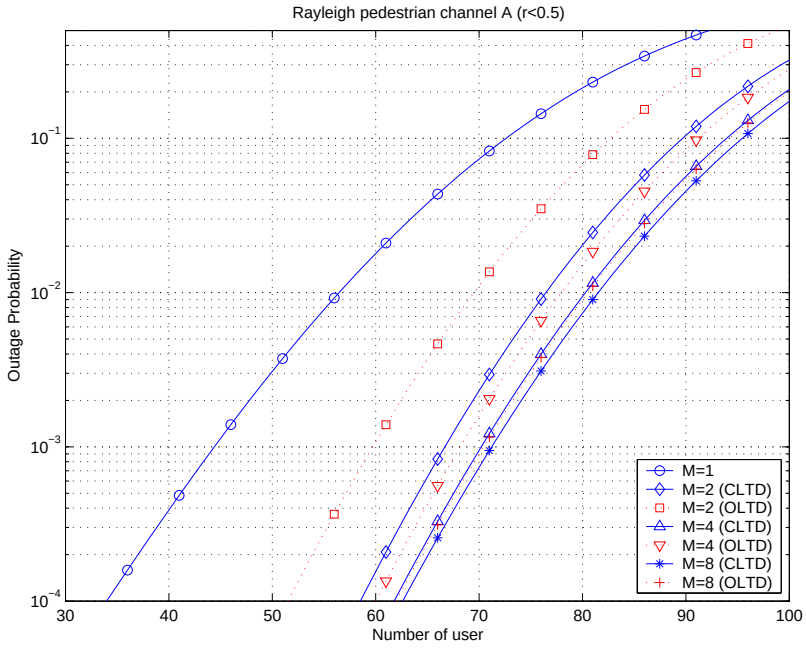

Figure 7.60: Capacity for pedestrian A channel with fast power control, CLTD, and OLTD when $r < 0.5$

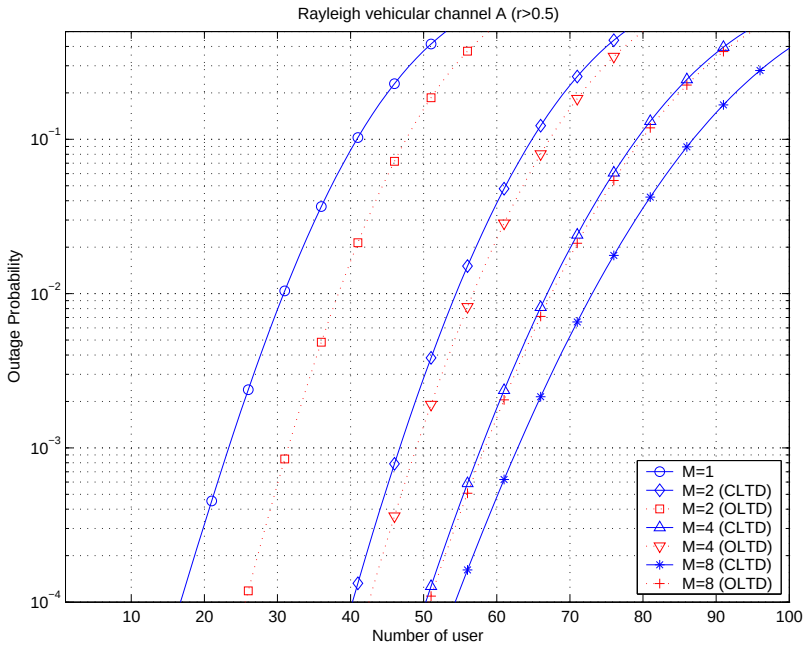

Figure 7.61: Capacity for vehicular A channel with fast power control, CLTD, and OLTD when $r > 0.5$

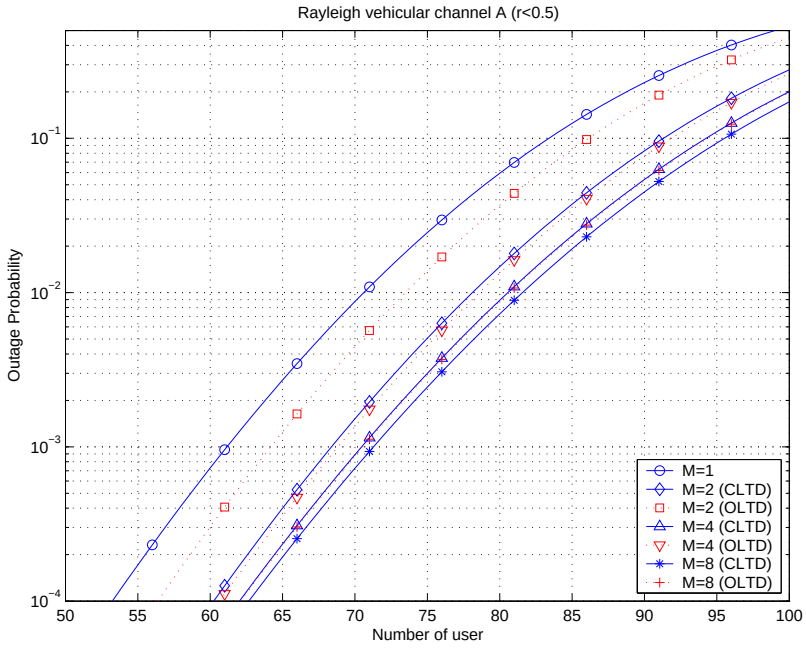

Figure 7.62: Capacity for vehicular A channel with fast power control, CLTD, and OLTD when $r < 0.5$

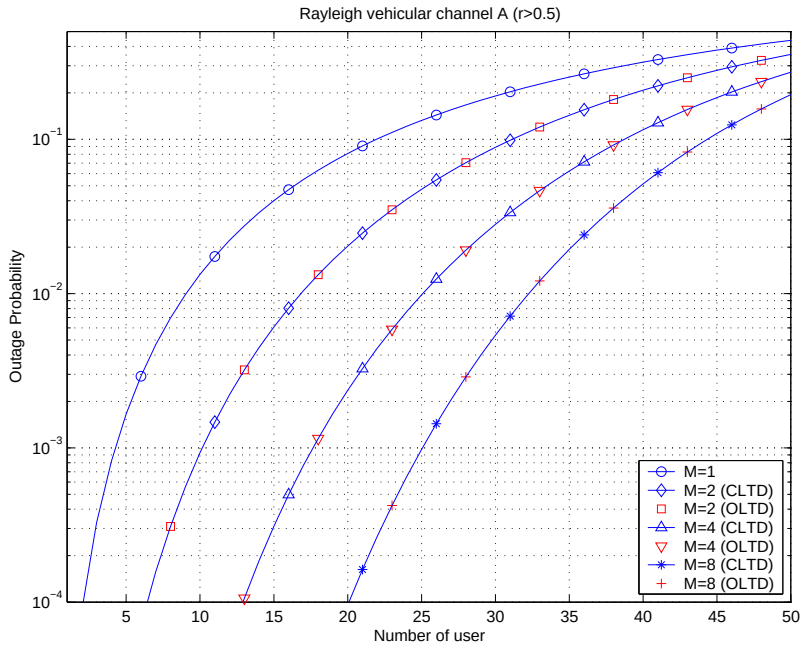

Figure 7.63: Capacity for vehicular A channel with slow power control, CLTD, and OLTD when $r > 0.5$

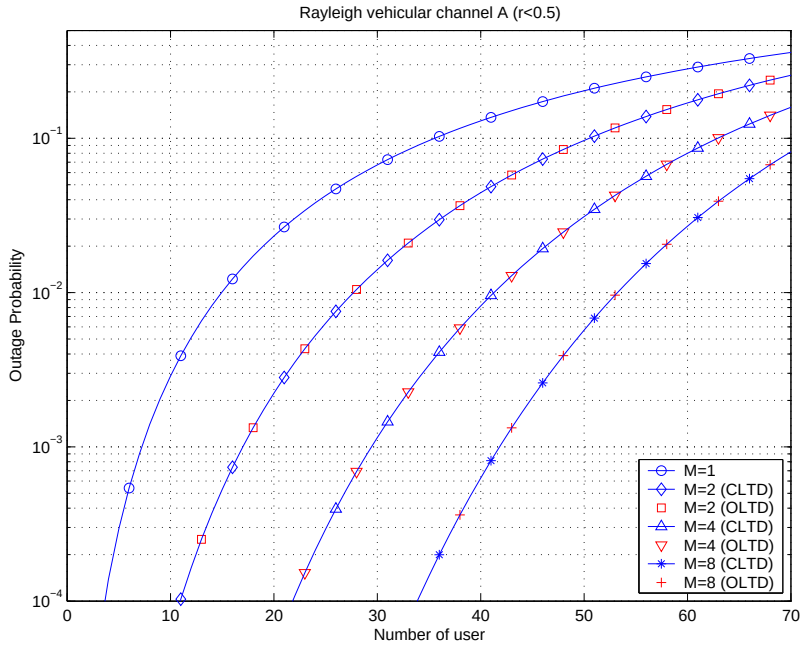

Figure 7.64: Capacity for vehicular A channel with slow power control, CLTD, and OLTD when $r < 0.5$

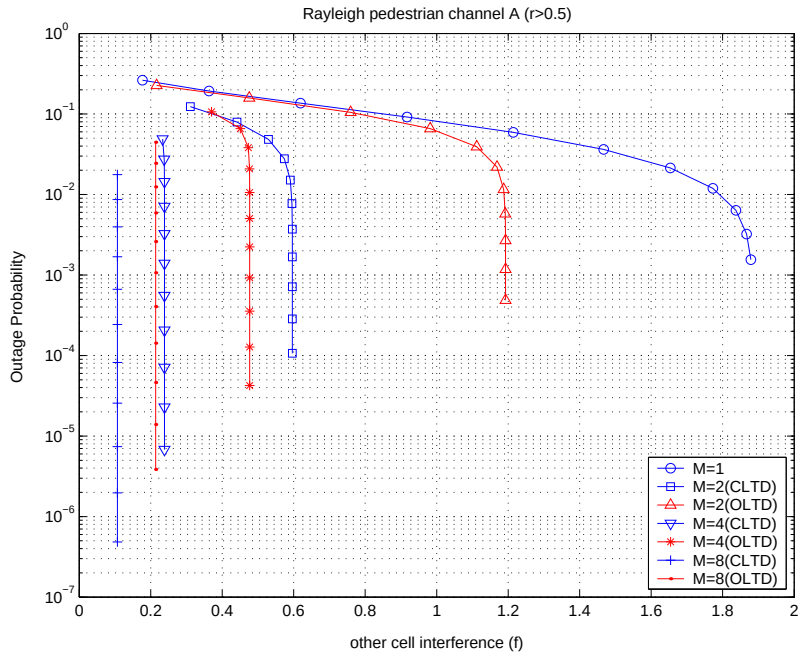

Figure 7.65: Other-cell interference factor f for pedestrian A channel with fast power control, CLTD, and OLTD when $r > 0.5$

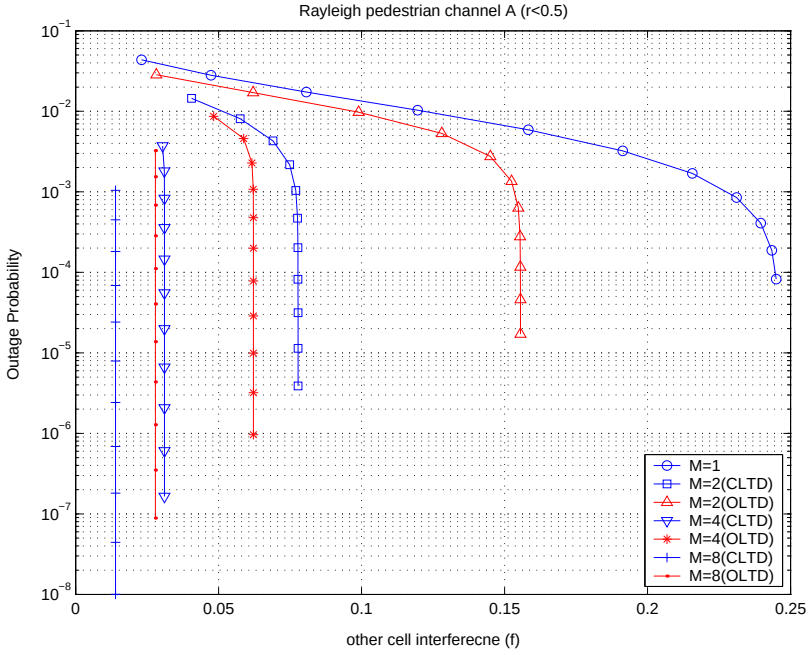

Figure 7.66: Other-cell interference factor f for pedestrian A channel with fast power control, CLTD, and OLTD when $r < 0.5$

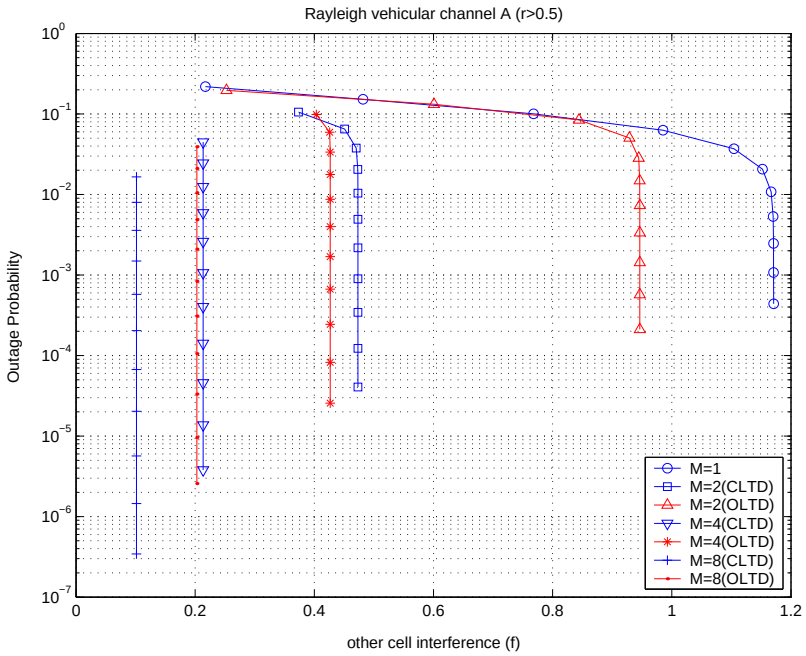

Figure 7.67: Other-cell interference factor f for vehicular A channel with fast power control, CLTD, and OLTD when $r > 0.5$

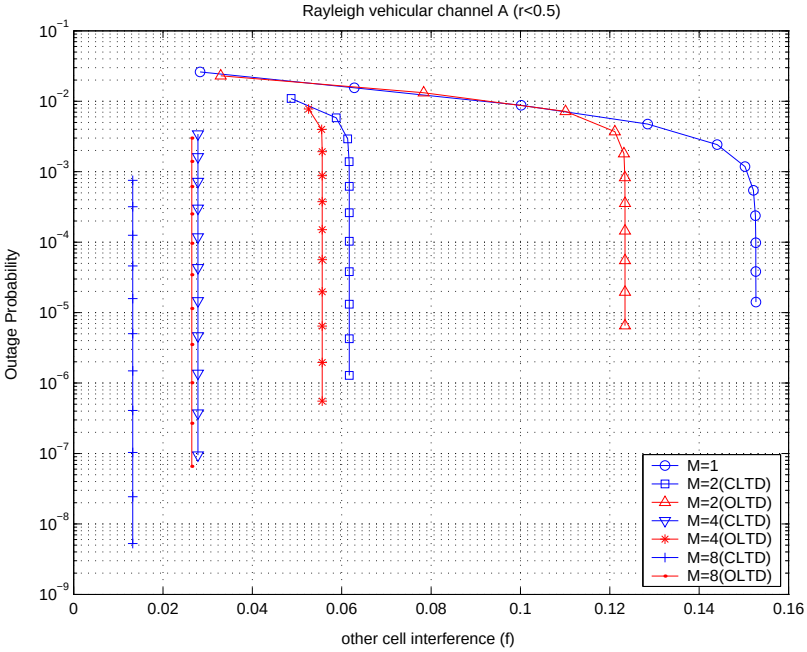

Figure 7.68: Other-cell interference factor f for vehicular A channel with fast power control, CLTD, and OLTD when $r < 0.5$

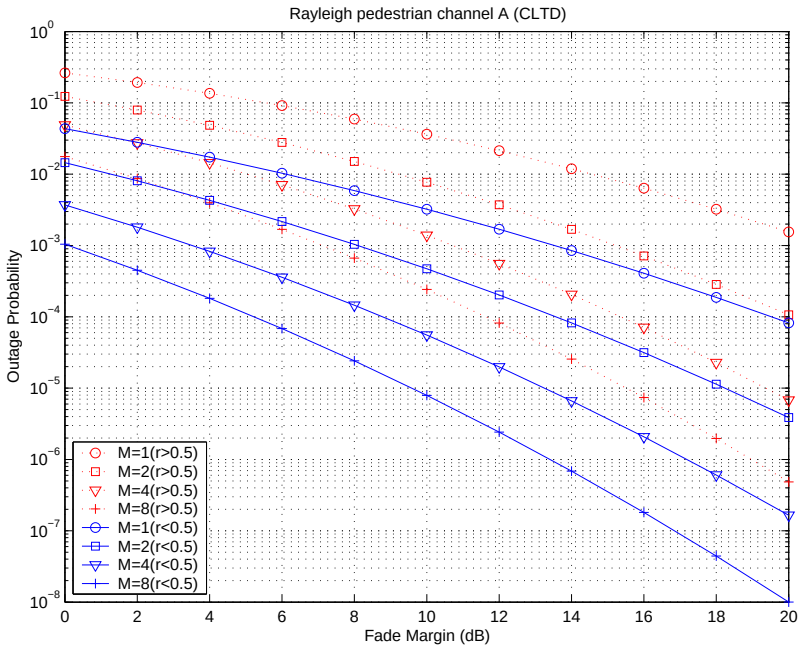

Figure 7.69: Outage probability vs. fade margin for pedestrian A channel with fast power control and CLTD

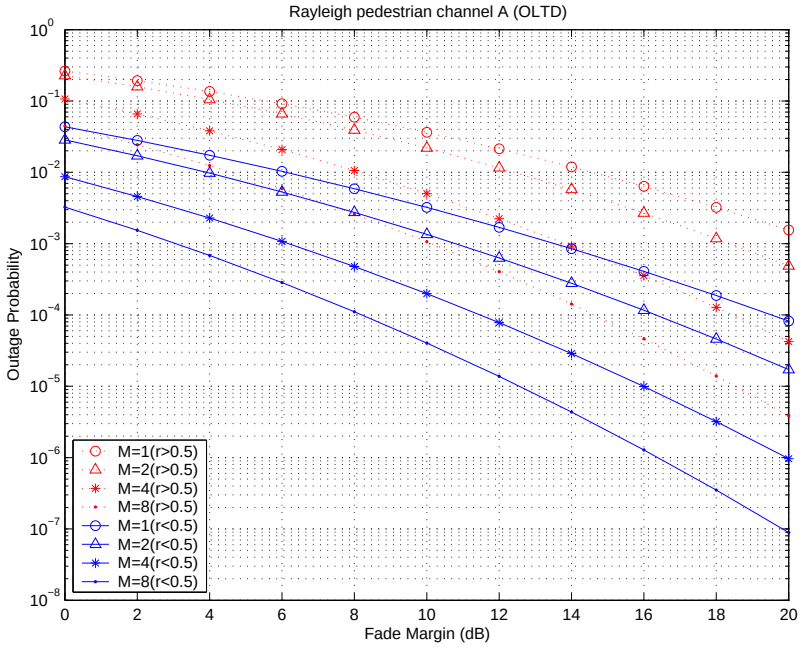

Figure 7.70: Outage probability vs. fade margin for pedestrian A channel with fast power control and OLTD

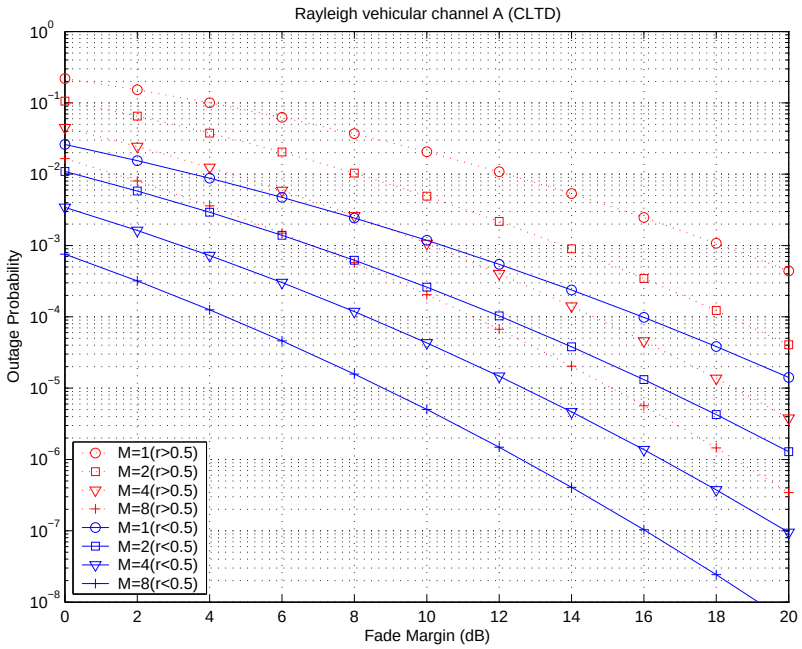

Figure 7.71: Outage probability vs. fade margin for vehicular A channel with fast power control and CLTD

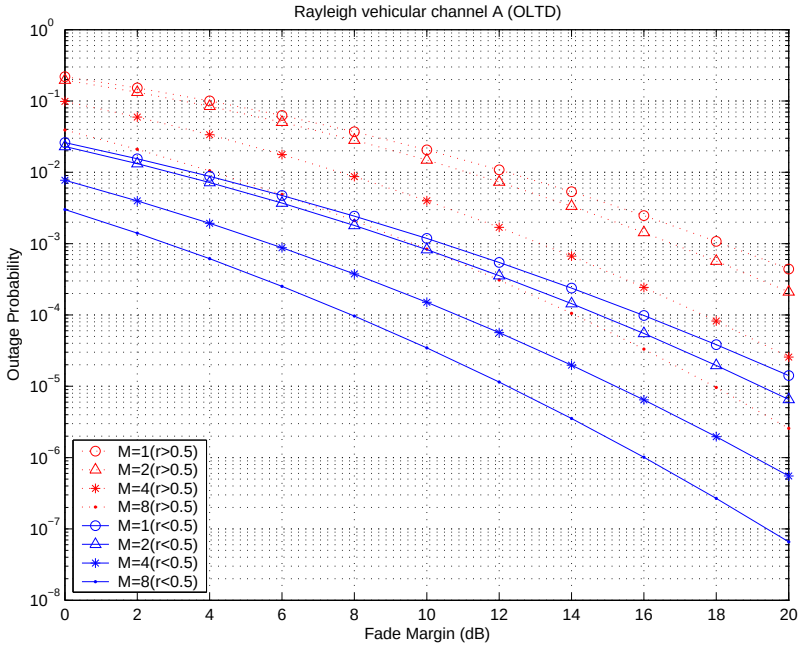

Figure 7.72: Outage probability vs. fade margin for vehicular A channel with fast power control and OLTD

Table 7.28: Capacity gain for different user distributions with slow power control

	Pedestrian A channel capacity					
Div. Order	$r < 0.5$	% Gain	uniform	% Gain	$r > 0.5$	% Gain
2	14.1		9.5		8.5	
4	26.8	90.1 %	18	89.5 %	16.1	89.4 %
8	40.5	187.2 %	27.5	189.5 %	24.3	185.9 %

Table 7.29: Capacity gain for different user distributions with fast power control

	Pedestrian A channel capacity					
Div. Order	$r < 0.5$	% Gain	uniform	% Gain	$r > 0.5$	% Gain
2	76.5		53		46.6	
4	80.3	5.0 %	69	30.2 %	65.1	39.7 %
8	81.5	6.5 %	75	41.5 %	72.6	55.8 %

Table 7.30: Capacity gain for different user distributions with slow power control

	Vehicular A channel capacity					
Div. Order	$r < 0.5$	% Gain	uniform	% Gain	$r > 0.5$	% Gain
2	25.8		19		15.7	
4	39.4	52.7 %	28.5	50 %	24	52.9 %
8	51.4	99.2 %	36.5	92.1 %	31.2	98.7 %

Table 7.31: Capacity gain for different user distributions with fast power control

	Vehicular A channel capacity					
Div. Order	$r < 0.5$	% Gain	uniform	% Gain	$r > 0.5$	% Gain
2	78.1		60		54.1	
4	80.6	3.2 %	70.5	17.5 %	66.8	23.5 %
8	81.6	4.5 %	75	25.8 %	73	34.9 %

Table 7.32: Other-cell interference factor f for different user distribution on pedestrian A with fast power control

Pedestrian A Channel									
	$r < 0.5$			uniform			$r > 0.5$		
Div. Order	f	$1+f$	% Gain	f	$1+f$	% Gain	f	$1+f$	% Gain
2 MRC	0.0514	1.0514		0.4360	1.4360		0.5934	1.5934	
4 OLTD	0.0437	1.0437	0.7 %	0.3515	1.3515	6.3 %	0.4767	1.4767	7.9 %
4 CLTD	0.0227	1.0227	2.8 %	0.1758	1.1758	22.1 %	0.2383	1.2383	28.7 %
8 CLTD	0.0239	1.0239	2.7 %	0.1578	1.1578	24 %	0.2141	1.2141	31.2 %
8 CLTD	0.0118	1.0118	3.9 %	0.0789	1.0789	33.1 %	0.1070	1.1070	43.9 %

Table 7.33: Other-cell interference factor f for different user distribution on vehicular A with fast power control

Vehicular A Channel									
	$r < 0.5$			uniform			$r > 0.5$		
Div. Order	f	$1+f$	% Gain	f	$1+f$	% Gain	f	$1+f$	% Gain
2 MRC	0.0501	1.0501		0.3488	1.3488		0.4731	1.4731	
4 OLTD	0.0467	1.0467	0.3 %	0.3147	1.3147	2.6 %	0.4267	1.4267	3.3 %
4 CLTD	0.0246	1.0246	2.5 %	0.1573	1.1573	16.5 %	0.2134	1.2134	21.4 %
8 CLTD	0.0254	1.0254	2.4 %	0.1496	1.1496	17.3 %	0.2029	1.2029	22.5 %
8 CLTD	0.0118	1.0118	3.8 %	0.0748	1.0748	25.5 %	0.1015	1.1015	33.7 %

7.4.6 Impact of correlation between spatial diversity branches and between multipaths

So far it has been assumed that the signals from each spatial diversity branch are not correlated each other. In this section, not only correlation between antenna branches, but also correlation between multipaths in channel models is considered to investigate the impact of correlation on system capacity. Correlation between antenna diversity branches is assumed to be 0.7, and inter-path correlation is assumed to be 0.3. As can be seen in Figure 7.73 and Figure 7.74, in a system employing slow power control, correlation has a more severe negative impact. As described in the previous section, system capacity is more sensitive to received signal variations; the variations of the received signal is a lot less reduced through spatial diversity processing due to the correlation between the branches. Antenna diversity achieves a performance improvement by reducing the probability that each branch will experience correlated fading and by increasing the average received signal power. Therefore, since there is a correlation between diversity branches, there is now more variation in the received signal power as compared with the uncorrelated case, and a reduced average received signal power, which both lead to a capacity loss. Even though there is a correlation between diversity branches, there is still a capacity increase in systems using fast power control as diversity order increases, due to the energy capturing capability of the spatial (antenna) diversity technique.

Key observations and effects

- Inter-path correlation and antenna diversity branch correlation have more negative impact on a system employing slow power control than a system using fast power control since system capacity is more sensitive to received signal variations.
- Even though there exist correlations between antenna diversity branches, using antenna diversity provides a performance benefit to systems using fast power control in terms

of capacity, outage probability and interference.

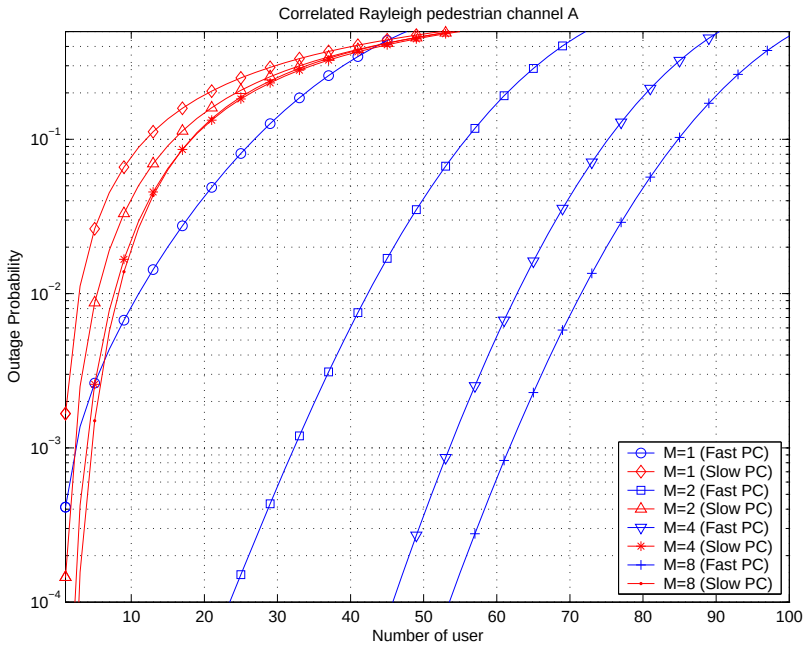

Figure 7.73: Capacity for pedestrian A channel with correlated Rayleigh fading, CLTD, and 3-way soft handoff

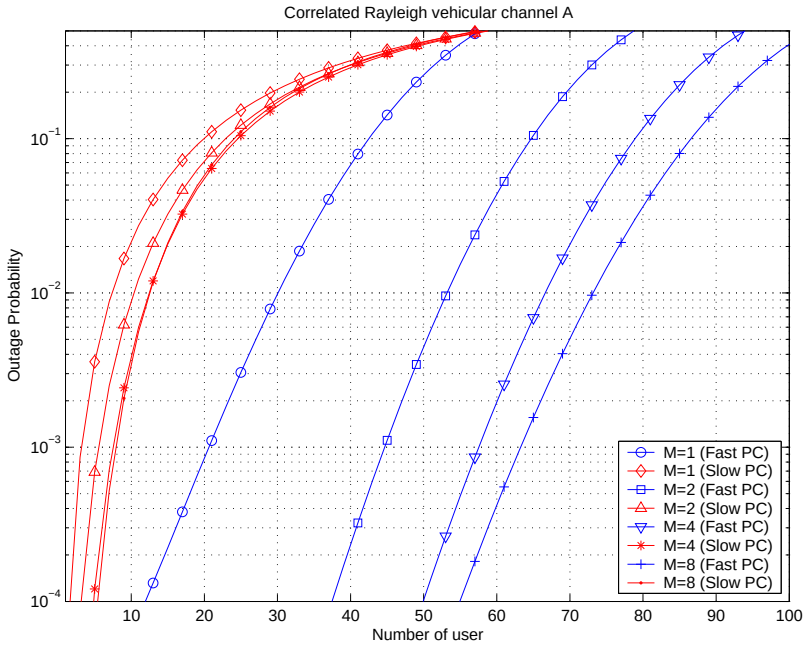

Figure 7.74: Capacity for vehicular A channel with correlated Rayleigh fading, CLTD, and 3-way soft handoff

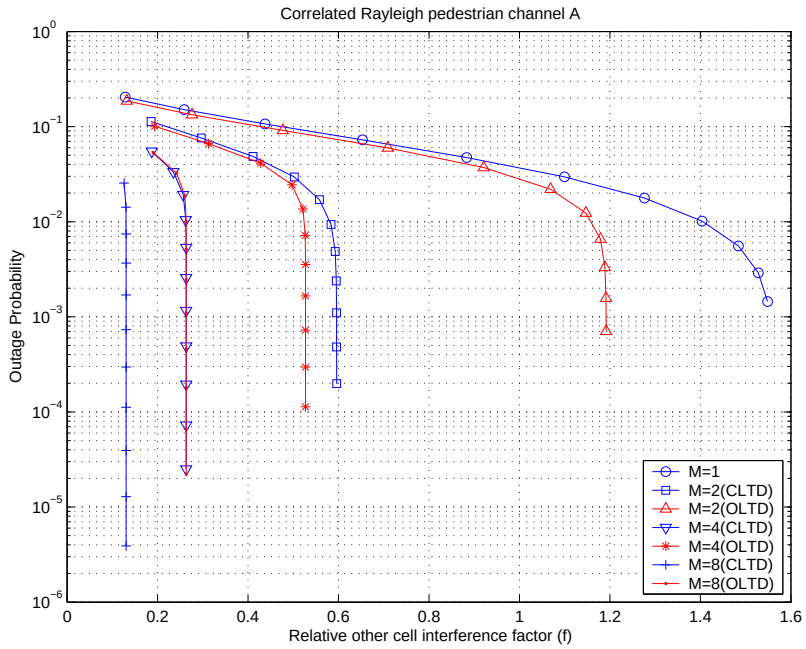

Figure 7.75: Other-cell interference factor f for pedestrian A channel with correlated Rayleigh fading, fast power control, and 3-way soft handoff

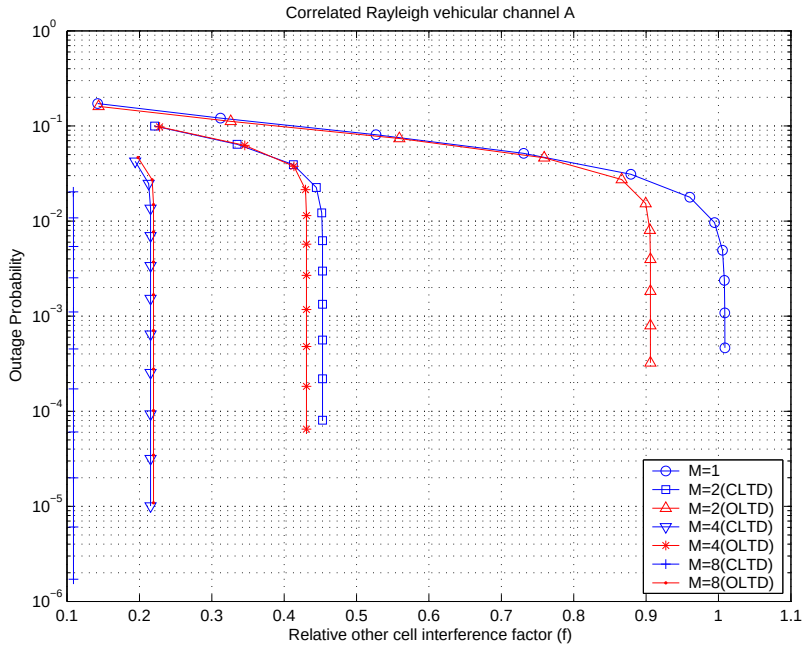

Figure 7.76: Other-cell interference factor f for vehicular A channel with correlated Rayleigh fading, fast power control, and 3-way soft handoff

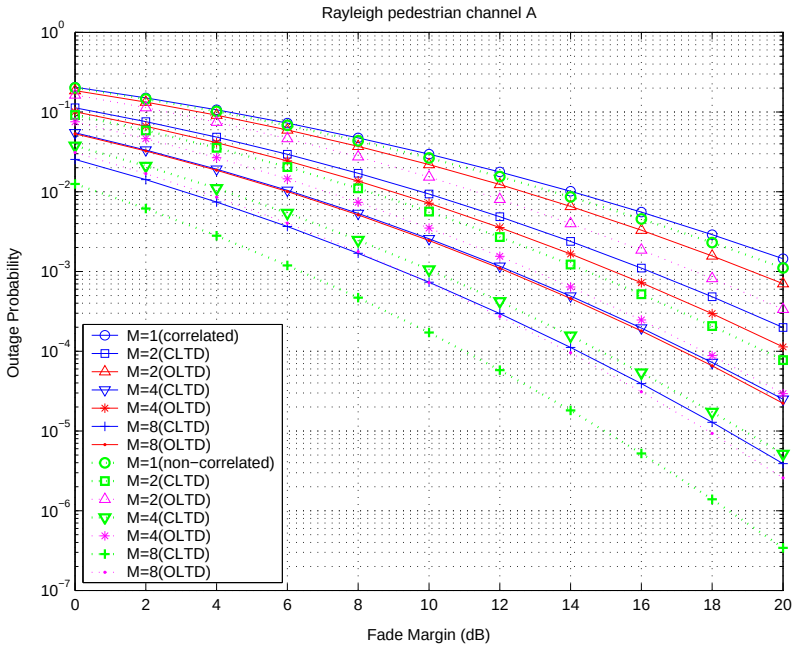

Figure 7.77: Outage vs. fade margin for pedestrian A channel with correlated Rayleigh fading, fast power control and 3-way soft handoff

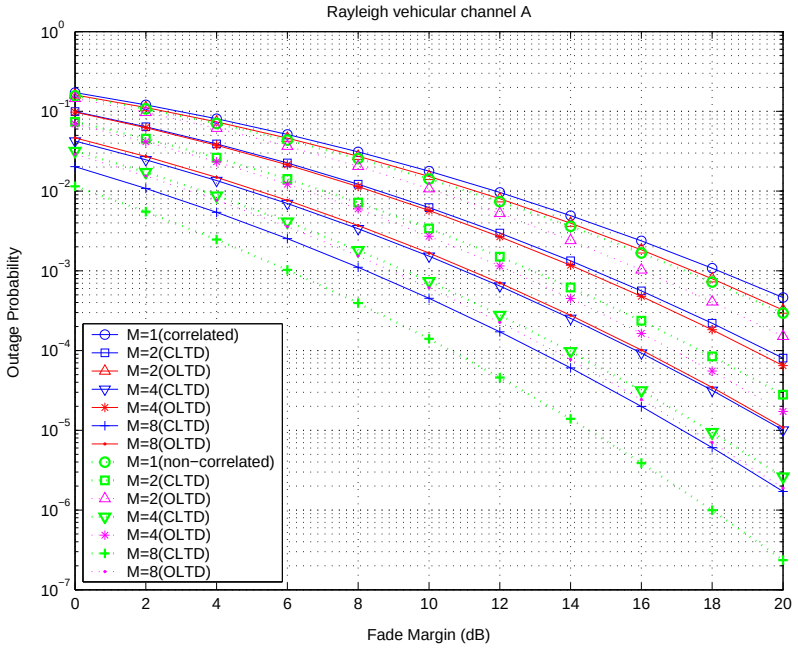

Figure 7.78: Outage vs. fade margin for vehicular A channel with correlated Rayleigh fading, fast power control, and 3-way soft handoff

Table 7.34: Capacity gain for pedestrian A channel with Rayleigh fading through spatial diversity using CLTD

Pedestrian A channel capacity								
	Slow power control				Fast power control			
Div. order	Uncorrelated	% Gain	Correlated	% Gain	Uncorrelated	% Gain	Correlated	% Gain
2	9.5		5.3		53		42.4	
4	18	89.5 %	7.7	45.3 %	69	30.2 %	62.8	48.1 %
8	27.5	189.5 %	8.3	56.6 %	75	41.5 %	71.5	68.6 %

Table 7.35: Capacity gain for vehicular A channel with Rayleigh fading through spatial diversity using CLTD

Vehicular A channel capacity								
	Slow power control				Fast power control			
Div. order	Uncorrelated	% Gain	Correlated	% Gain	Uncorrelated	% Gain	Correlated	% Gain
2	19		10.4		60		53.2	
4	28.5	50 %	12.5	20.2 %	70.5	17.5 %	66.6	25.2 %
8	36.5	92.1 %	12.6	21.2 %	75	25.8 %	73.2	37.6 %

Table 7.36: f factors on pedestrian A channel with Rayleigh fading in a system using fast power control with fade margin 20 dB

Pedestrian A channel						
	Uncorrelated			Correlated		
Div. order	f	$1+f$	% Gain	f	$1+f$	% Gain
2 MRC	0.4360	1.4360		0.5809	1.5809	
4 OLTD	0.3515	1.3515	6.3 %	0.5239	1.5239	3.7 %
4 CLTD	0.1758	1.1758	22.1 %	0.2626	1.2626	25.2 %
8 OLTD	0.1578	1.1578	24 %	0.2632	1.2632	25.2 %
8 CLTD	0.0789	1.0789	33.1 %	0.1303	1.1303	39.9 %

Table 7.37: f factors on vehicular A channel with Rayleigh fading in a system using fast power control with fade margin 20 dB

Vehicular A channel						
	Uncorrelated			Correlated		
Div. order	f	$1+f$	% Gain	f	$1+f$	% Gain
2 MRC	0.3488	1.3488		0.4522	1.4522	
4 OLTD	0.3147	1.3147	2.6 %	0.4308	1.4308	1.5 %
4 CLTD	0.1573	1.1573	16.5 %	0.2153	1.2153	19.5 %
8 OLTD	0.1496	1.1496	17.3 %	0.2194	1.2194	19.1 %
8 CLTD	0.0748	1.0748	25.5 %	0.1088	1.1088	31.0 %

Table 7.38: Comparison of relative coverage of uncorrelated and correlated Rayleigh pedestrian A channel with fast power control

Pedestrian A						
	Uncorrelated			Correlated		
Diversity Order	Fade Margin	Relative Margin	Relative Coverage	Fade Margin	Relative Margin	Relative Coverage
MRC	8.3 dB	0 dB	1.00	9.78 dB	0 dB	1.00
4 OLTD	7.1 dB	1.20 dB	1.15	8.97 dB	0.81 dB	1.10
4 CLTD	4.28 dB	4.02 dB	1.59	6.13 dB	3.65 dB	1.52
8 OLTD	3.54 dB	4.76 dB	1.73	6.02 dB	3.76 dB	1.54
8 CLTD	0.64 dB	7.66 dB	2.42	3.09 dB	6.69 dB	2.16

Table 7.39: Comparison of relative coverage of uncorrelated and correlated Rayleigh vehicular A channel with fast power control

Vehicular A						
	Uncorrelated			Correlated		
Diversity Order	Fade Margin	Relative Margin	Relative Coverage	Fade Margin	Relative Margin	Relative Coverage
MRC	7.03 dB	0 dB	1.00	8.59 dB	0 dB	1.00
4 OLTD	6.56 dB	0.47 dB	1.06	8.38 dB	0.21 dB	1.02
4 CLTD	3.60 dB	3.43 dB	1.48	4.92 dB	3.67 dB	1.53
8 OLTD	3.26 dB	3.77 dB	1.54	5.20 dB	3.39 dB	1.48
8 CLTD	0.38 dB	6.65 dB	2.15	2.22 dB	6.37 dB	2.08

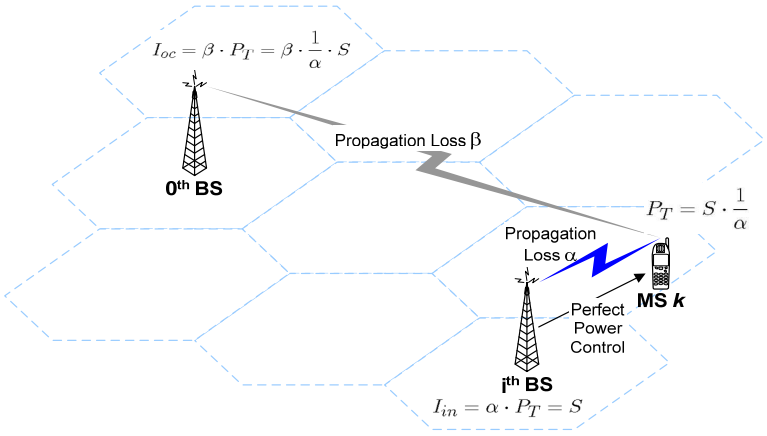

Figure 7.79: System model

7.5 CDMA System Level Simulation

The objective of the system level simulation is not only to verify the previous analysis results, but also to estimate the capacity by introducing various degradation factors which are difficult (if it is not impossible) to be modeled in the analytical framework. The system level simulation can be further utilized for analyzing the impact of various communication algorithms on the system capacity. In this section, we briefly describe cdma2000 system level simulator, and present simulation results in the next section.

7.5.1 Specification

System model for the system level simulation is basically the same as the system model described in Figure 7.79. To validate the analysis results, most system parameters of the simulation are set to the same as those of analytical framework in the previous section. Table 7.40 shows the basic specification of the system level simulator currently implemented. Note that in the system level simulator, the number of cells and the number of users/cell

Table 7.40: Specification of system level simulator

Parameters	Specification
Number of cells	Up to 37 corresponding to 3-tier of hexagonal cells
Number of users/cell	Only limited by memory allocation
Cell radius	Normalized to 1 (no dimension)
Sector/cell	No sectorization
Antenna gain	Omni-directional
Supporting handoff	Hard handoff/3-way soft handoff
Voice activity	0.38 (ON-OFF traffic / Flexible data rate based on the standard specified Markov chain probability)
Propagation loss	Multipath Rayleigh fading channel, Log-normal shadowing, and path loss
Channel model	ITU-R channel model
MS transmit diversity	Up to 2 antennas - optimum /equal gain combining
BS receive diversity	Up to 4 antennas - maximal ratio combining
Multipath combining	Maximal ratio combining of all possible multipath / resolvable multipath based on link level simulator
Power control	Channel inversion / fixed step power control based on the received signal strength
Mobile Velocity	3 120 Km/h

are critical factors for the memory allocation. Even though the maximum number of cells are 37 corresponding to 3-tier of hexagonal cells, all simulation results in this report are performed with 19 cells (corresponding to 2-tier of hexagonal cells) due to the simulation time increase from the large memory allocation which usually generates large paging files. Also, the maximum number of users/cell is set to 100.

7.5.2 Simulation flow

The basic flow of the system level simulation is as follows. First, all BSs are placed on the center of each cell and the specified number of MSs per cell are uniformly dropped in each

cell. For the soft handoff, each MS determines the BS, which provides the least average attenuation to communicate with. Then, each MS in the entire system is power controlled by each BS to which it is connected. The reference power for the power control is assumed to be '1'. For every simulation turn, which corresponds to 1.25ms power control unit, the power control function calculates the received signal power attenuated by the long-term and short-term propagation losses, compares it with the reference power and updates the transmit power of MS. After updating all MSs' transmit power, total interference is calculated by collecting transmit powers from all the mobile stations to the zeroth BS, taking into account the signal power attenuation by propagation loss. In the flowchart and the simulation code, the measurement of total interference and power control is performed in the same function. The collected total interference is compared with the reference value for determining the system outage. The main flowchart is shown in Figure 7.80.

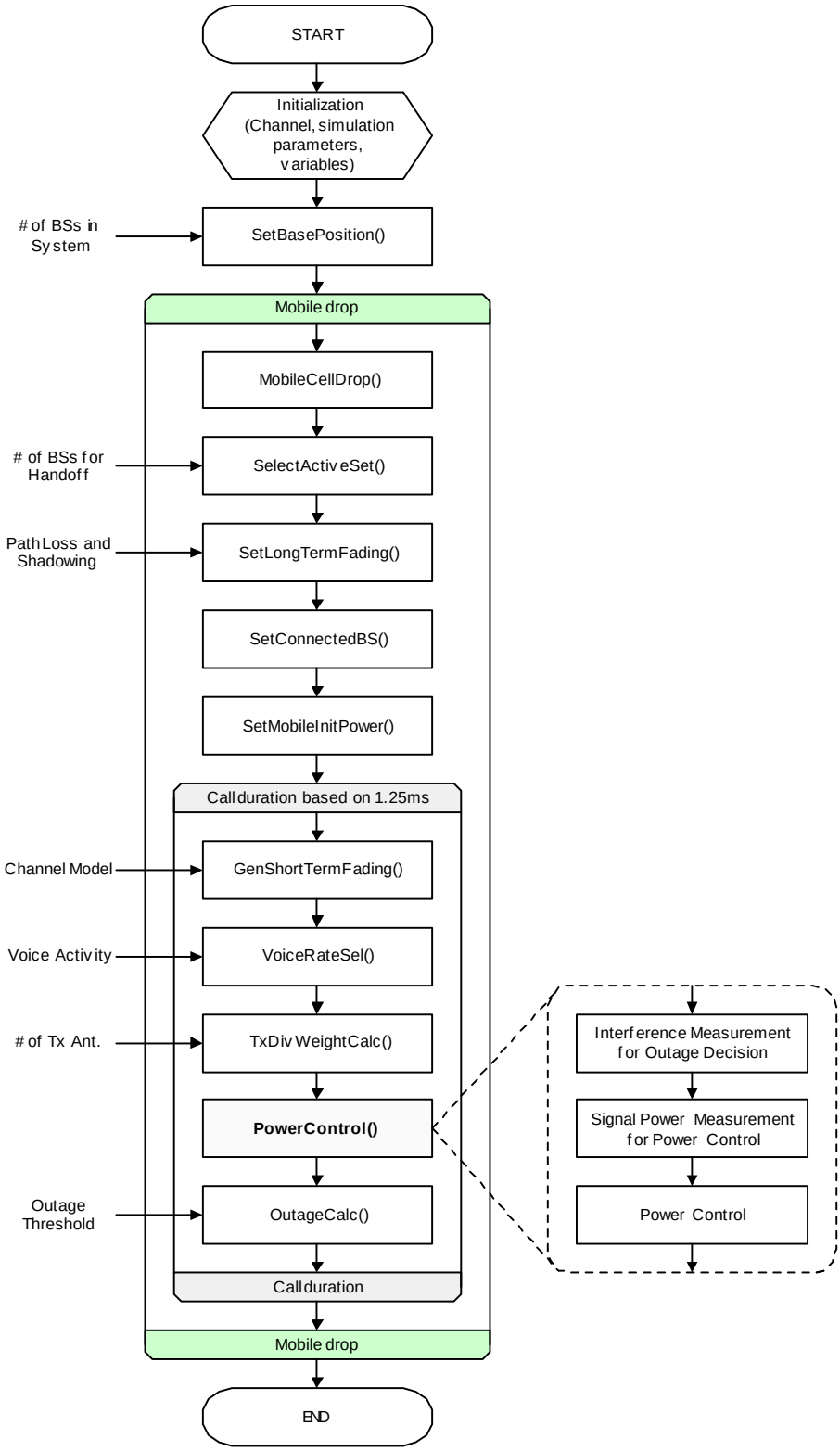

Figure 7.80: Flow chart of system simulator

7.5.3 Calculation of received signal power

The received signal power calculation is different according to whether the transmit diversity is applied or not. The received signal power with receive diversity only is calculated as

$$P_R = P_T \cdot \alpha \cdot \beta \cdot \sum_{i=1}^{L_r} \sum_{j=1}^{L_m} |h_{i,j}|^2 \tag{7.77}$$

where P_T is the transmit power of mobile station, α is the voice activity, β represents the long-term propagation loss and $h_{i,j}$ is the short-term fading channel response of j^{th} multipath component at i^{th} receive antenna with L_m multipaths and L_r receive antennas. On the other hand, the received signal power with both receive diversity and transmit diversity is calculated as

$$P_R = P_T \cdot \alpha \cdot \beta \cdot \sum_{i=1}^{L_r} \sum_{j=1}^{L_m} |h_{i,j,1} \cdot w_1 + h_{i,j,2} \cdot w_2|^2 \tag{7.78}$$

where w_1 and w_2 are the weight vectors for two transmit antennas, and $h_{i,j,1}$ and $h_{i,j,2}$ are the short-term fading channel response of the j^{th} multipath component at the i^{th} receive antenna corresponding to the first and second transmit antenna, respectively. The transmit weight vectors, w_1 and w_2 will be obtained based on maximizing the received signal power at the receiver. However, in calculating the received signal power for the power control, voice activity is not applied (that is, always $\alpha = 1$ in calculating the received signal power) for the proper power control operation when the voice is deactivated. The voice activity is applied only to the total interference measurement for checking the system outage.

On the other hand, when the resolvable multipath combining is enabled, the fractional multipath components among L_m multipath components will be combined. The resolvable multipath components are determined by the sampling resolution of the receiver and are the same as those implemented in the link simulator. The resolvable multipath components for pedestrian channel A and vehicular channel A are shown in Table 7.41. Note that the resolvable multipath combining is also applied to the intracell interference measurement since we have assumed that the intracell interference is not changed in terms of its mean. However, in the intracell interference measurement, all possible multipaths are taken into account.

Table 7.41: Resolvable multipath components for pedestrian and vehicular channel A

Channel model	Resolvable multipath	Total number of multipath
Pedestrian channel A	1 (1^{st} path only)	4
Vehicular channel A	4 (1^{st}, 2^{nd}, 4^{th}, 6^{th} paths)	6

7.5.4 Total interference measurement

Interference measurement will be different between intercell interference and intracell interference based on the assumption in the analytical framework. Intercell interference is calculated as

$$I_{oc} = \sum_{i=1}^{N} \sum_{j=1, j \notin BS_0}^{K} \left(P_{T(i,j)} \cdot \alpha_{i,j} \cdot \beta_{i,j} \cdot \sum_{k=1}^{L_m} |h_{i,j,k}|^2 \right) \tag{7.79}$$

where N and K are the number of base-stations in the entire system and the number of users in a cell, respectively, $P_{T(i,j)}$, $\alpha_{i,j}$ and $\beta_{i,j}$ are the transmit power, voice activity factor, and long-term propagation loss of the j^{th} user in the i^{th} cell, respectively, and represents the short-term fading channel response of the k^{th} multipath component for the j^{th} user in the i^{th} cell. On the other hand, the intracell interference with the receive diversity only is calculated as

$$I_{in} = \sum_{i=1}^{N} \sum_{j=1, j in BS_0}^{K} \left(P_{T(i,j)} \cdot \alpha_{i,j} \cdot \beta_{i,j.} \sum_{k=1}^{L_r} \sum_{l=1}^{L_m} |h_{i,j,k,l}|^2 \right) \tag{7.80}$$

where $h_{i,j,k,l}$ represents the short-term fading channel response of the l^{th} multipath component at the k^{th} receive antenna for the j^{th} user in the i^{th} cell. The intracell interference with both the receive diversity and transmit diversity is calculated as

$$I_{in} = \sum_{i=1}^{N} \sum_{j=1, j in BS_0}^{K} \left(P_{T(i,j)} \cdot \alpha_{i,j} \cdot \beta_{i,j} \sum_{k=1}^{L_r} \sum_{l=1}^{L_m} |h_{i,j,k,l,1} \cdot w_{i,j,1} + h_{i,j,k,l,2} \cdot w_{i,j,2}|^2 \right) \tag{7.81}$$

where $h_{i,j,k,l,1}$ and $h_{i,j,k,l,2}$ are the short-term fading channel responses of the l^{th} multipath component at the k^{th} receive antenna for the j^{th} user in the i^{th} cell, corresponding to the

first and second transmit antenna, respectively, and $w_{i,j,1}$ and $w_{i,j,2}$ are the antenna weights of the first and second transmit antenna, respectively, for the j^{th} user in the i^{th} cell. The total interference is the sum of I_{in} and I_{oc} calculated by Equation (7.79), (7.79), and (7.81). Then, the total interference is directly compared with the reference value for deciding the system outage without normalization, since the reference value for the power control is set to '1'.

7.6 Simulation Results

In this section, we present a set of simulation results which can show the impact of transmit diversity technique at handset in conjunction with receive diversity on the reverse link DS/CDMA system capacity under practical scenarios. First, we verify the validity of both simulation and analytical results by comparing the simulation results with the analytical results obtained under the same condition. Then, we present several simulation results with practical scenarios such as feedback delay and errors, resolvable multipath combining, transmit power constraint, imperfect power control and so on, and compare them with the basic results without errors.

Figure 7.81 shows the simulation results for pedestrian channel A model, where the mobile velocity is assumed to be '3 Km/h' and power control is performed by changing the transmit power of mobile station in the unit of 0.5 dB step size according to the received signal power. All multipath components in the channel model are combined in the simulations for the sake of comparison with the analytical results: note that in the analytical analysis, all the multipaths are combined at the receiver. The dotted lines represent the analytical results, and the solid lines are the simulation results. While the simulation results with the receive-diversity-only match well with the analytical result, the simulation results with the transmit diversity show more deviation from the analytical result due to the increased number of multipath components as compared with 1-path Rayleigh fading channel model.

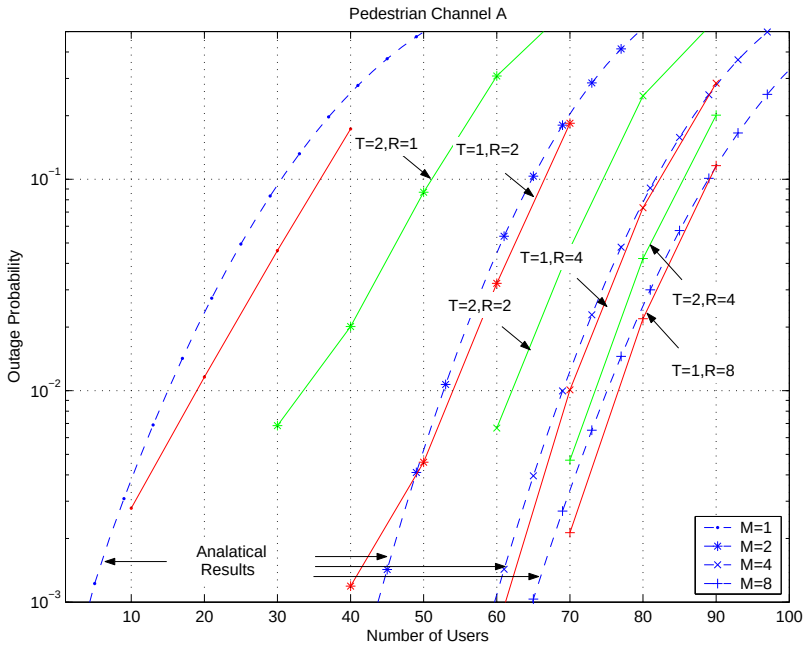

Figure 7.81: Outage probabilities vs. the number of users per cell in the pedestrian channel A with all multipaths combined

Since two dimensional transmit weight vector tries to exploit higher dimension in signal space to maximize the signal-to-noise ratio at the receiver, the actual performance gain of using transmit diversity deviates from analytical estimates as the number of diversity branches and resolvable multipaths increases. However, these differences are reduced when the receiver combines only resolvable multipath components. Typically, in pedestrian channel A, there is only one resolvable multipath among four multipaths in the channel model.

The simulation results for the case that the receiver combines only resolvable multipaths are shown in Figure 7.82. Just as before, the dotted lines are the analytical results where all the multipaths in the pedestrian channel A model are combined. Since the resolvable multipath component is only '1' in pedestrian channel A, the trends of outage probability are very similar to that in 1-path Rayleigh fading channel. The performance difference between the simulation results and the analytical results is due to the partial energy combining at the receiver in the simulations, while the analytical results is based on combining all possible

Table 7.42: System capacity with resolvable multipath combining in pedestrian channel A

Diversity		T=2, R=1	T=1, R=2	T=2, R=2	T=1, R=4	T=2, R=4	T=1, R=8
Number	All m-path	33.5	54	62.1	70	73.4	76.6
of users	Resolvable	39	39	66	68.5	74	76.5

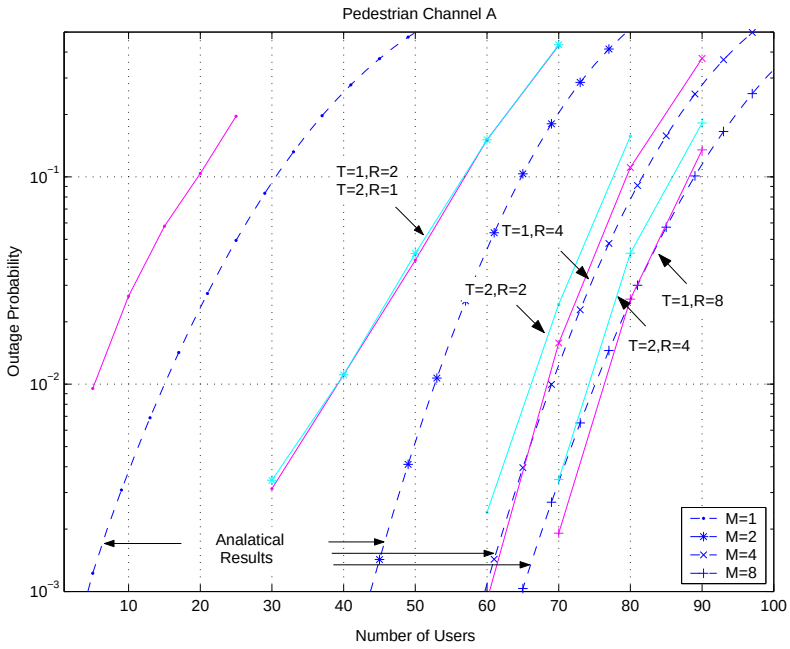

Figure 7.82: Outage probabilities vs. the number of users per cell in pedestrian channel A with the resolvable multipath combining

multipaths. The system capacity achieved by resolvable multipath combining is shown in Table 7.42. When transmit diversity is employed, we observe that the system capacity for the case where only resolvable multipaths are combined (Figure 7.82) slightly increases as compared with the system capacity for the case of all possible multipath combining (Figure 7.81). The reason is that the chosen principal eigenvector for the transmit weight vector does not fully exploit the channel structure as the number of multipaths increases, resulting in less efficient power transfer.

Table 7.43: System capacity with estimation error and resolvable multipath combining in pedestrian channel A

Diversity		T=2, R=1	T=1, R=2	T=2, R=2	T=1, R=4	T=2, R=4	T=1, R=8
Number	w/o error	39	39	66	68.5	74	76.5
of users	with error	37	38	62	63.5	69.7	71

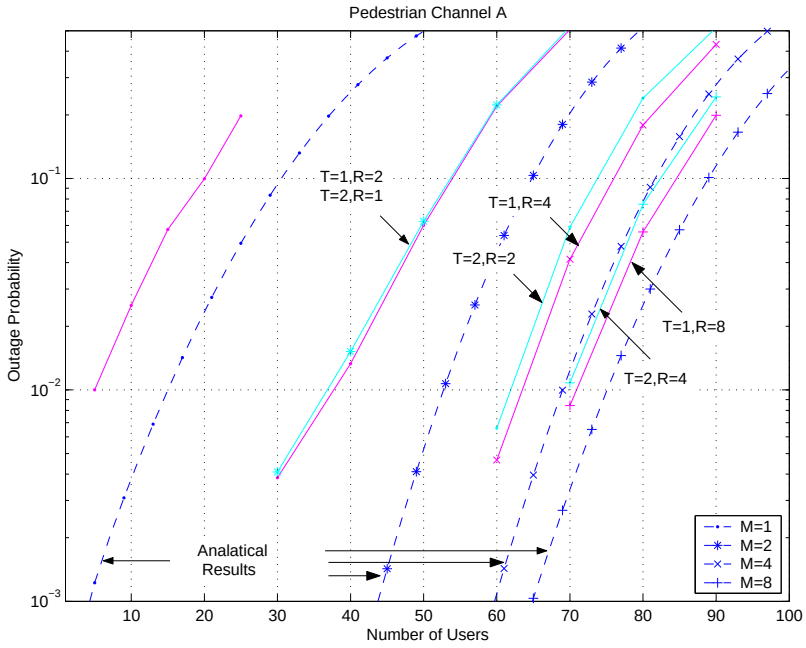

Figure 7.83: Outage probabilities vs. the number of users per cell in the pedestrian channel A with the resolvable multipath combining and feedback error

Figure 7.83 shows the outage probabilities in pedestrian channel A with the feedback delay and error. The analytical results, which combine all available multipaths without any errors, are plotted in the dotted lines as a reference for comparison. Two power control groups' (PCGs') feedback delay of power control command and transmit weight vector are assumed, and error of power control command is assumed to be 10%. However, it is assumed that there is no error in transmit weight vector command. Due to the feedback delay, it is observed that there is small difference even between 'T=2, R=1' and 'T=1, R=2'

Table 7.44: System capacity with equal gain transmit diversity

Diversity		T=2, R=1	T=2, R=2	T=2, R=4
Number	MRC	37	62	69.7
of users	EGC	33.5	59.5	69

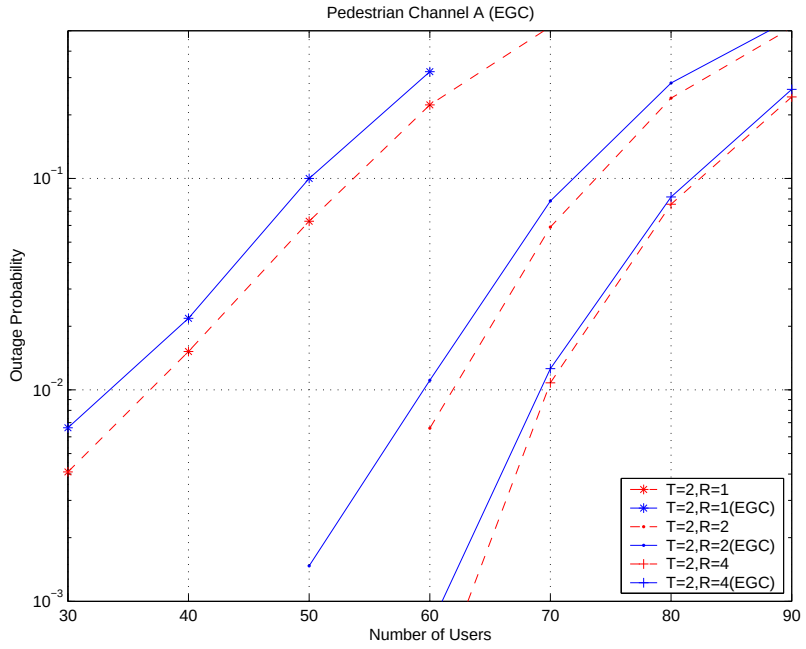

Figure 7.84: Outage probabilities vs. the number of users per cell in the pedestrian channel A with equal gain transmit diversity

cases. Without feedback delay, the outage probability of them is the same as shown in Figure 7.82. In addition, the feedback error of power control causes some degradation of outage probability as compared to the outage probability without feedback error. The system capacities, achieved with feedback delay and error, are summarized in Table 7.43.

For a suboptimum transmit diversity, equal gain transmit diversity, in which only phase information of fading channel is used to calculate transmit antenna weights, is also considered for performance comparisons. Equal gain transmit diversity technique is known to be simple yet effective when the amount of feedback information is limited, since only phase

information is fed back into transmitter reducing the feedback information. Nevertheless, equal gain transmit diversity achieves comparable performance as compared with maximal ratio combining type (also called transmit adaptive array (TxAA) in WCDMA). The simulation results with the equal gain transmit diversity are shown in Figure 7.84. Just as before, pedestrian channel A model is assumed and mobile velocity is set to 3 Km/h. Equal gain transmit diversity is denoted by EGC and plotted in the solid line. As a reference, the optimum transmit diversity, in which both channel gain and phase information are used, is also presented in the dotted line. It is observed that the outage probabilities of equal gain transmit diversity is slightly degraded as compared with those of optimum transmit diversity. In addition, the amount of degradation is observed to decreases, as diversity order increases. Table 7.44 summarizes the achievable capacity by equal gain diversity. As a reference, the capacities of optimum transmit diversity are also shown (denoted by 'MRC') in the table.

Another performance degradation of transmit diversity can come from antenna correlation. Generally, antenna correlation depends on antenna configurations and channel propagation environments. In practice, there can be some amount of correlation depending on channel environment even for the same antenna spacing. So, we need to evaluate the impact of correlation on the performance of transmit diversity technique. Figure 7.85 shows the outage probabilities vs. the number of users in pedestrian channel A for several correlation coefficients between two transmit antennas. We have assumed that base-station antenna elements experience uncorrelated fading. It is observed that when there are only two transmit

Table 7.45: System capacity for optimum transmit diversity with correlated transmit diversity

Diversity		T=2, R=1	T=1, R=2	T=2, R=2	T=1, R=4	T=2, R=4	T=1, R=8
Number	$\rho = 0.0$	36.8	38	61.9	63.5	69.7	71
of users	$\rho = 0.3$	33.5	38	59.6	63.5	70.1	71
per cell	$\rho = 0.7$	26	38	56.2	63.5	69.7	71

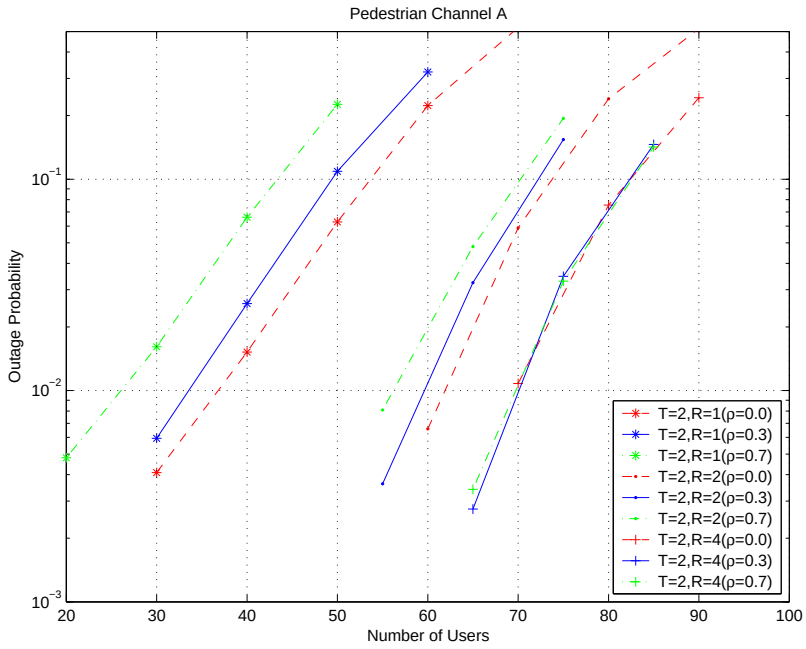

Figure 7.85: Outage probabilities vs. the number of users per cell in the pedestrian channel A with correlations between transmit antennas

antennas without receive diversity, the impact of correlation is relatively larger than when there are multiple receive antennas with two transmit antennas. Furthermore, as the receive diversity order increases, the impact of correlation between two transmit antennas decreases. We can expect that there is less impact of correlation between two transmit antennas on the performance when the number of uncorrelated receive antenna elements are greater than the number of transmit antennas. For several correlation coefficients between two transmit antennas, the achievable capacity by optimum transmit diversity are summarized in Table 7.45.

So far, we have considered the cases where the feedback rate is fast enough to compensate for the channel variation. However, just as any kind of closed loop system inherently suffers from severe performance degradation when the feedback rate cannot follow input variation, closed transmit diversity technique also will experience some degree of performance degradation when the channel variation is faster than the feedback rate of transmit weight vector.

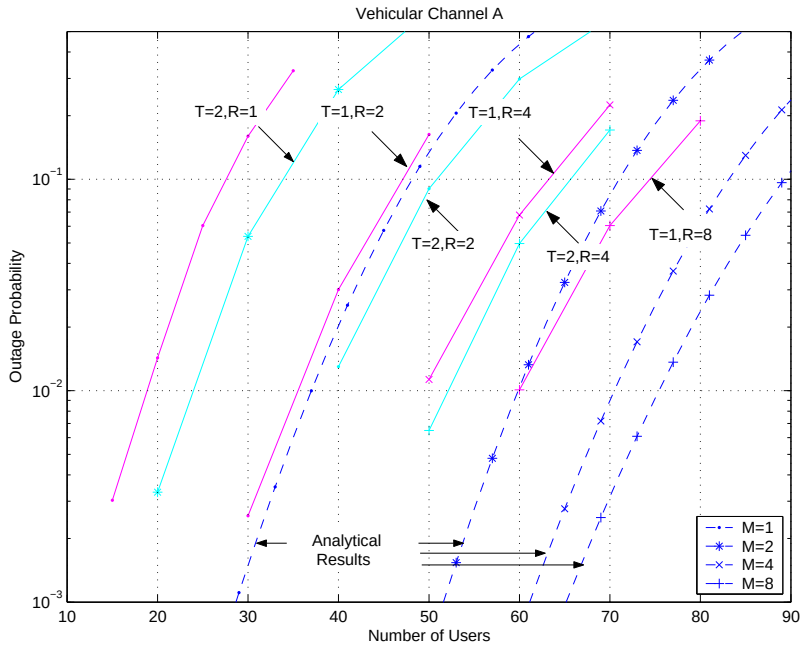

Figure 7.86: Outage probabilities vs. the number of users per cell in the vehicular channel A with feedback errors

Figure 7.86 shows the outage probabilities in vehicular channel A. The mobile velocity for the vehicular channel is assumed to be 30 Km/h. Furthermore, it is assumed that only resolvable multipaths are combined. As a reference, the dotted lines indicate the analytical results where the mobile velocity is not taken into account and all possible multipaths are combined. Due to the power control error from the feedback delay by high mobility and multipath component powers which are not captured, the performance degradations from the analysis results are observed to be large even in the receive-diversity-only cases. These feedback delay and irresolvable multipath components also further deteriorate the performance of closed-loop transmit diversity. So, the performance of the system employing closed-loop transmit diversity is closer to that of the system not employing closed-loop transmit diversity. However, there are still small performance improvements by multiple transmit antennas and these improvements will be more pronounced if the channel coding is taken into account.

In Figure 7.87, the impact of correlation between two transmit antennas on the capacity

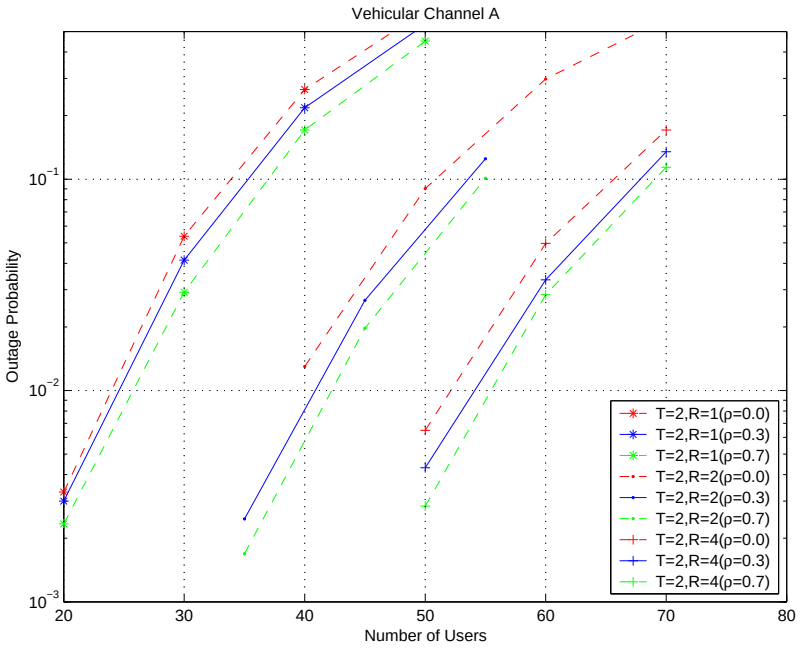

Figure 7.87: Outage probabilities vs. the number of users per cell in the vehicular channel A with correlations between transmit antennas

is evaluated in vehicular channel A environment. Mobile velocity is assumed to be 30 Km/h. Different from the corresponding results of pedestrian environment shown in Figure **??**, it is observed that system capacity improves as the correlation coefficient becomes large. Due to the increased number of multipaths in vehicular channel as compared with pedestrian channel, the eigenspread of composite channel matrix to calculate transmit antenna weight vector increases, resulting in less efficient power transfer through the channel since the cho-

Table 7.46: System capacity for optimum transmit diversity with correlations between transmit antennas

Diversity		T=2, R=1	T=1, R=2	T=2, R=2	T=1, R=4	T=2, R=4	T=1, R=8
Number	$\rho = 0.0$	23.1	35.5	36.8	49.2	52.3	60
of users	$\rho = 0.3$	24.6	35.5	40.9	49.2	54.1	60
per cell	$\rho = 0.7$	25.8	35.5	42.2	49.2	55.5	60

Table 7.47: System capacity depending on the penetration ratio of MSs equipped with transmit diversity in systems under pedestrian channel

% of MS with TxD		T=2, R=1	T=1, R=2	T=2, R=2	T=1, R=4	T=2, R=4	T=1, R=8
Number	R=2	37.7	39.9	43.5	47.7	54.4	61.9
of users	R=4	63.5	64.1	65.0	66.1	67.9	69.5

sen principal eigenvector for the transmit weight vector does not fully exploit the channel structure due to eigenspread. On the other hand, correlated transmit antennas has an effect of reducing the spread of eigenvalues of the channel space. Hence, performance of transmit antennas improves as the correlation between transmit antennas increases in vehicular channel environment. For an extreme case that the correlation between transmit antennas is '1', the rank of channel space reduces to '1' and closed loop transmit diversity will behave like directional beam-forming, from which array gain can be exploited. Thus, when there are several dominant multipath components, transmit beam-forming technique with receive diversity will provides better performance than transmit diversity in conjunction with receive diversity. The achievable capacity by optimum transmit diversity with correlated transmit antennas is summarized in Table 7.48.

Up to now, it has been assumed that all MSs in the system are equipped with the same order of transmit diversity. However, different from receive diversity at BS, transmit diversity at MS will not be implemented in all MSs at the initial deployment stage. Thus, it is required to estimate the capacity improvement when parts of MSs in the system are equipped with transmit diversity, which is not easy to do in the analysis. Figure 7.88 shows the system capacity based on 10^{-2} outage probability according to the different penetration ratio of MSs equipped with transmit diversity technique in pedestrian channel environment. It is observed that the improvement of capacity by transmit diversity at MS is slow at the initial deployment. However, as observed at two receive antenna case, the trend of improvement shows exponential increment. For four receive antenna, the improvement by transmit

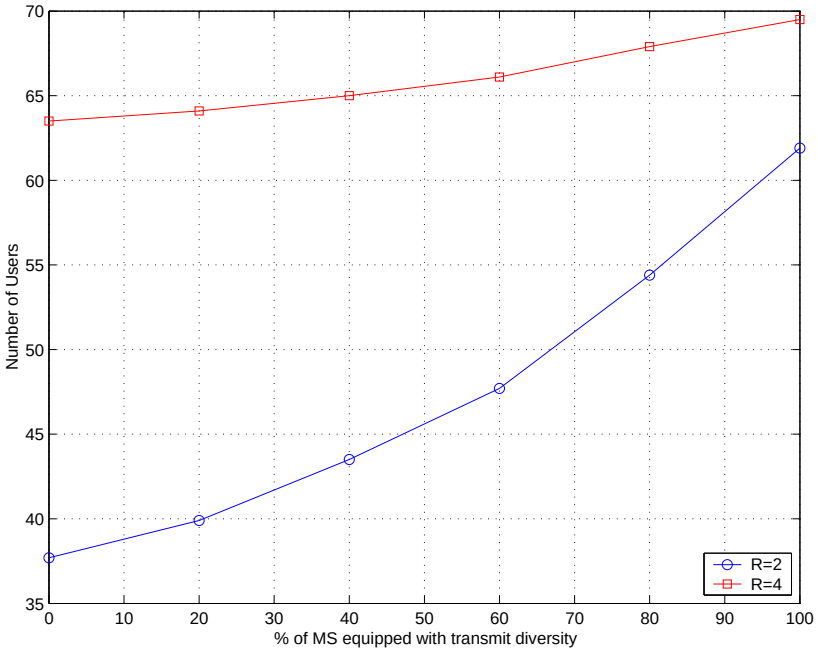

Figure 7.88: Outage probabilities vs. different penetration ratio of MSs equipped with transmit diversity

diversity is not so significant because channel is already flatten enough by four receive diversity. Nevertheless, transmit diversity still provide additional capacity improvement by presenting energy capturing effect with two transmit antennas.

More practically, we can consider various channel environments at the same time; all MSs are not in the same channel environment. Figure 7.89 shows the outage probabilities vs. the number of users in heterogeneous channel environments, where a half of MSs are in

Table 7.48: System capacity in heterogenous channel environments

Diversity		T=2, R=1	T=1, R=2	T=2, R=2	T=1, R=4	T=2, R=4	T=1, R=8
Number	Veh only	24	35.5	38.5	49.2	52.1	60
of users	Ped (50%)	29.2	37.7	48.4	56.6	60.8	67
per cell	Ped only	37	38	62	63.5	69.7	71

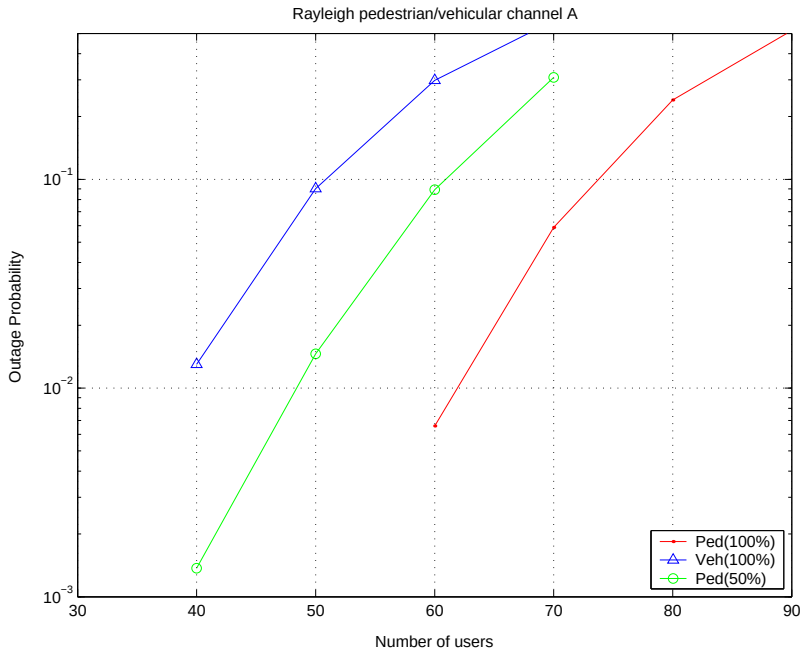

Figure 7.89: Outage probabilities vs. the number of users per cell in heterogeneous channel environments

pedestrian channel and the others are in vehicular channel environment. Mobile velocity for the pedestrian channel is assumed to be 3 Km/h and that for the vehicular channel is assumed to be 30 Km/h. For diversity order, 'T=2, R=2' case is considered. It is observed that system capacity is significantly degraded in heterogeneous channel environment as compared with the environments where all the MSs are in pedestrian channel. However, the relative improvement of system capacity by each diversity order still remains as shown in Table 7.48.

7.7 Chapter summary

A general mathematical framework to evaluate the impact of transmit and receive diversity processing on the capacity, outage probability, and coverage of the reverse link of a DS/CDMA system, and the analysis results obtained from it are presented in this chapter. By using this analytical approach, it is observed that transmit diversity at the handset used in conjunction with receive diversity at the base station can significantly improve system capacity, outage probability, and coverage. Key observations from this study include:

- Using transmit diversity at the handset in conjunction with receive diversity at the base station reduces other-cell (intercell) interference dramatically and reduces the variability of the received signal, resulting in a significant capacity increase for both the slow and fast power control cases;
- Antenna diversity has a greater positive impact on a system operating in environments in which the available path diversity is small;
- The impact of fade variability is reduced with respect to the system capacity and outage probability, as the antenna diversity order increases ;
- The gain achievable through spatial diversity processing diminishes as the fading index increases, or equivalently, as the fading severity diminishes;
- When users are not uniformly distributed in a cell, particularly in those cases in which users are concentrated near cell boundaries, the system capacity and outage probability degrade and the relative performance gain due to antenna diversity increases;
- Systems employing fast power control achieve greater capacity than those employing slow power control when evaluated under the same conditions; However, the relative capacity increase is greater for slow power control when the antenna diversity order is increased;

- System capacity is more sensitive to variations in the received signal which have not been compensated completely by either power control or diversity processing;
- Increased inter-path correlation and branch correlation reduces system capacity and increases the outage probability;
- Inter-path correlation and antenna diversity branch correlation have a more negative impact on systems employing slow power control than systems using fast power control.

Also, the system level simulator for the reverse link DS/CDMA cellular system has been developed to validate the analytical results and to evaluate the impact of several practical implementation issues on the system capacity. As practical implementation issues, the followings have been taken into account and evaluated.

- Imperfect power control: it includes the feedback delay and error of power control command. Its impact on the system capacity are taken into account along with feedback delay of transmit weight vector and resolvable multipath combining. It is observed that their impacts are bigger in the vehicular channel than in the pedestrian channel.
- Feedback delay of transmit weight vector
- Resolvable multipath combining
- Mobile velocity: for closed-loop transmit diversity technique, mobile velocity is a critical factor which causes performance degradation. In vehicular channel environment, mobile velocity of 30 Km/h cause severe degradations of system capacity as compared with the system capacity of receive-diversity only for the same diversity order. Mobile velocity also degrades the power control performance, which is why the performance of receive diversity only deviates from the result where both transmit and receive diversity are employed for the same order of diversity.
- Equal gain transmit diversity: when the amount of feedback is constrained, equal gain transmit diversity, which is sub-optimum, can be considered to be used. As

compared with the performance of the optimum transmit diversity, its performance is slightly degraded. However, it provides a comparable performance to optimum transmit diversity, and also the performance gap between them decreases as receive diversity order increases.

- Correlated transmit antennas: correlated transmit antennas are another source degrading the performance of transmit diversity. However, as the eigenspread of composite channel matrix increases, correlated antennas provide array gain in conjunction with diversity gain at the receiver, resulting in better performance than that of a system which tries to exploit transmit diversity.

Chapter 8

Conclusions

This dissertation presents analytical framework, which can facilitate the analysis and design of wireless communication systems with antenna arrays and provide insights on parametric investigation for optimizing system design. The MGF (CHF) of random variables (RVs), which can be the output of diversity combiner or detected signal statistics, or represent interference statistics, expedites the characterization of statistical characteristics of digital communication systems when it is hard to get a closed-form solution of probability density function (PDF). In this dissertation, we have applied the framework not only to physical layer performance analysis, but also to the investigation of the impact of transmit diversity technique on the reverse link DS/CDMA system capacity. It is important to see the interactions between different layers in protocol stacks since as wireless communication systems evolve, more sophisticated algorithms in different layers are implemented, and it is not possible to evaluate and predict system behavior by evaluating algorithms in protocol stacks in an isolated way. The capacity increase in the reverse link DS/CDMA system employing transmit diversity techniques, which we have investigated in chapter 7, comes from the interaction between diversity technique (physical layer algorithm) and power control (medium access control (MAC) layer algorithm). This is a good case study where one can see how physical layer algorithms impact on system level performance. The key to exploiting algorithms in

different layers in wireless communication protocol stacks is understanding the cross-layer interactions. This is the future direction to take, and analytical solution in physical layer can serve as a base parameter to investigate higher layer protocols.

Also, although we have mainly focused on investigating the performance of spatial diversity techniques in this dissertation, the framework we have explored can be extended to the analysis and design of wireless communication systems using the general idea of exploiting multiple input multiple output in systems. Among them, if we name a few, the following might be a good research direction to take: distributed MIMO system (cooperative diversity among distributed wireless units in wireless networks), antenna selection problem (efficient joint selection of transmit and receive antennas) in wireless MIMO system, and opportunistic routing protocol which tries to exploit wireless channel information in packet routing.

Appendix A

Recursive Integration Formula

Define the definite integral $I(a,b,c)$ as

$$I(a,b,c) = \int_0^\infty y^{2a-1} e^{-by^2-cy} dy = e^{\frac{c^2}{4b}} \int_0^\infty y^{2a-1} e^{-b\left(y+\frac{c}{2b}\right)^2} dy \tag{A.1}$$

where $2a$ is a positive integer, b is a positive real number while c may assume any complex number values. Using the variable substitution $u = \sqrt{b}\left(y + \frac{c}{2b}\right)$ and $dy = du/\sqrt{b}$, (A.1) can be restated as

$$I(a,b,c) = e^{\frac{c^2}{4b}} \left(\frac{1}{\sqrt{b}}\right)^{2a} \int_{c/(2\sqrt{b})}^\infty \left(u - \frac{c}{2\sqrt{b}}\right)^{2a-1} e^{-u^2} du \tag{A.2}$$

Since $2a$ is a positive integer, we can expand the power term using binomial series expansion as

$$\begin{aligned} I(a,b,c) &= e^{\frac{c^2}{4b}} \left(\frac{1}{\sqrt{b}}\right)^{2a} \int_{c/(2\sqrt{b})}^\infty \sum_{i=0}^{2a-1} \binom{2a-1}{i} u^i \left(-\frac{c}{2\sqrt{b}}\right)^{2a-1-i} e^{-u^2} du \\ &= e^{\frac{c^2}{4b}} \left(\frac{1}{\sqrt{b}}\right)^{2a} \sum_{i=0}^{2a-1} \binom{2a-1}{i} \left(-\frac{c}{2\sqrt{b}}\right)^{2a-1-i} \int_{c/(2\sqrt{b})}^\infty u^i e^{-u^2} du \end{aligned} \tag{A.3}$$

If we define an auxiliary function $H_i(z) = (-z)^{2a-1-i} e^{z^2} \int_z^\infty u^i e^{-u^2} du$, (A.3) can be expressed concisely as

$$I(a,b,c) = \left(\frac{1}{\sqrt{b}}\right)^{2a} \sum_{i=0}^{2a-1} \binom{2a-1}{i} H_i\left(\frac{c}{2\sqrt{b}}\right) \tag{A.4}$$

It is also interesting to note that $H_i(z)$ satisfies the following recursive formula:

$$H_{i+2}(z) = (-1)^{2a-1-i}\left(\frac{1}{2}\right)z^{2a-2} + \left(\frac{1}{2}\right)(i+1)z^{-2}H_i(z), \qquad i \geq 0 \tag{A.5}$$

where $\begin{cases} H_0(z) = (-1)^{2a-1}z^{2a-1}e^{z^2}\left(\frac{\sqrt{\pi}}{2}\right)\mathrm{erfc}(z), & i=0 \\ H_1(z) = (-1)^{2a-2}\left(\frac{1}{2}\right)z^{2a-2}, & i=1 \end{cases}$

The validity of (A.5) can be readily shown through integration by parts of the integration term $\int_z^\infty u^i e^{-u^2}du$. Let $dv = u^i du$, then $H_i(z)$ can be expressed as

$$\begin{aligned} H_i(z) &= (-z)^{2a-1-i}e^{z^2}\left[-\frac{1}{i+1}z^{i+1}e^{-z^2} + \frac{2}{i+1}\int_z^\infty u^{i+2}e^{-u^2}du\right] \\ &= -\frac{1}{i+1}(-1)^{2a-1-i}z^{2a} + (-z)^2\frac{2}{i+1}H_{i+2}(z) \end{aligned} \tag{A.6}$$

Rearranging (A.6) leads to (A.5).

Appendix B

Closed Form Expression for the Definite Integral Containing x^{ν} and $e^{-\beta x^2}$

In this appendix, we will derive a closed-form solution for the definite integral of the form

$$\int_0^{\infty} x^{\nu-1} e^{-\beta x^2} dx. \tag{B.1}$$

Using [42, Eq. (3.462.1)], we can immediately get

$$\int_0^{\infty} x^{\nu-1} e^{-\beta x^2} dx = (2\beta)^{-\nu/2} \Gamma(\nu) D_{-\nu}(0) \tag{B.2}$$

where $D_p(z)$ is parabolic cylinder function, and from [42, Eq. (9.240)], $D_{-\nu}(0)$ can be given by

$$D_{-\nu}(0) = 2^{-\nu/2} \frac{\sqrt{\pi}}{\Gamma\left(\frac{1+\nu}{2}\right)} {}_1F_1\left(\frac{\nu}{2}, \frac{1}{2}, 0\right). \tag{B.3}$$

Since ${}_1F_1(a, b, z)$ is defined as

$$\begin{aligned} {}_1F_1(a, b, z) &= 1 + \frac{az}{b} + \frac{(a)_2}{(b)_2}\frac{z^2}{2!} + \cdots + \frac{(a)_n}{(b)_n}\frac{z^n}{n!} + \cdots \\ &= \sum_{n=0}^{\infty} \frac{(a)_n}{(b)_n}\frac{z^n}{n!}, \end{aligned} \tag{B.4}$$

we can calculate ${}_1F_1(a, b, 0)$ for any arbitrary values of a and b, and the result is

$$ {}_1F_1(a, b, 0) = 1. \tag{B.5}$$

Therefore, using (B.3) and (B.5), we can obtain a closed-form solution of (B.1) as follows:

$$\int_0^\infty x^{\nu-1} e^{-\beta x^2} dx = (2\sqrt{\beta})^{-\nu} \sqrt{\pi} \frac{\Gamma(\nu)}{\Gamma\left(\frac{1+\nu}{2}\right)}. \tag{B.6}$$

Appendix C

Closed Form Expression for the Definite Double Integral Consisting of Exponentials, Powers, and Trigonometric Functions

In this appendix, we will derive closed-form solutions for the double integrals of the form

$$\frac{1}{\pi}\int_0^{\theta_U}\int_0^{\infty} x^{\alpha} h(\theta) e^{-h(\theta)x} dx d\theta, \tag{C.1}$$

and

$$\frac{2}{\pi}\int_0^{\theta_U}\int_0^{\infty} x^{2\alpha+1} h(\theta) e^{-h(\theta)x^2} dx d\theta, \tag{C.2}$$

where

$$h(\theta) = \begin{cases} \frac{\sin^2\theta_c}{\sin^2\theta} \\ \frac{\sin^2\theta_c}{1+\cos\theta_c\cos\theta} \end{cases} \tag{C.3}$$

and α is integer.

First, we will derive a closed-form solution for (C.1) when $h(\theta) = \frac{\sin^2\theta_c}{\sin^2\theta}$. Using variable

substitution $\frac{\sin^2\theta_c}{\sin^2\theta}x = u$, we can get

$$\begin{aligned}\frac{1}{\pi}\int_0^{\theta_U}\int_0^{\infty} x^{\alpha}\frac{\sin^2\theta_c}{\sin^2\theta}e^{-\frac{\sin^2\theta_c}{\sin^2\theta}x}dxd\theta &= \frac{1}{\pi}\int_0^{\theta_U}\int_0^{\infty}\left(\frac{\sin^2\theta_c}{\sin^2\theta}\right)^{-\alpha}u^{\alpha}e^{-u}dud\theta \\ &= \frac{1}{\pi}\Gamma(1+\alpha)\int_0^{\theta_U}\left(\frac{\sin^2\theta_c}{\sin^2\theta}\right)^{-\alpha}d\theta \\ &= \frac{1}{\pi}\frac{\Gamma(1+\alpha)}{\sin^{2\alpha}\theta_c}\int_0^{\theta_U}\sin^{2\alpha}\theta d\theta. \end{aligned} \tag{C.4}$$

Let $I_s(\alpha,\theta_U) = \int_0^{\theta_U}\sin^{2\alpha}\theta d\theta$. Then, using [42, Eq. (2.513.1)], we can obtain that

$$I_s(\alpha,\theta_U) = \frac{1}{2^{2\alpha}}\binom{2\alpha}{\alpha}\theta_U + \frac{(-1)^{\alpha}}{2^{2\alpha-1}}\sum_{k=0}^{\alpha-1}(-1)^k\binom{2\alpha}{k}\frac{\sin((2\alpha-2k)\theta_U)}{2\alpha-2k}. \tag{C.5}$$

Using (C.5) in (C.4), we have a closed-form solution for (C.1) when $h(\theta) = \frac{\sin^2\theta_c}{\sin^2\theta}$

$$\frac{1}{\pi}\int_0^{\theta_U}\int_0^{\infty} x^{\alpha}\frac{\sin^2\theta_c}{\sin^2\theta}e^{-\frac{\sin^2\theta_c}{\sin^2\theta}x}dxd\theta = \frac{1}{\pi}\frac{\Gamma(1+\alpha)}{\sin^{2\alpha}\theta_c}I_s(\alpha,\theta_U). \tag{C.6}$$

Secondly, when $h(\theta) = \frac{\sin^2\theta_c}{1+\cos\theta_c\cos\theta}$, using variable substitution $\frac{\sin^2\theta_c}{1+\cos\theta_c\cos\theta}x = u$ in (C.1) and subsequently letting $\theta = 2\varphi$, we can get

$$\begin{aligned}&\frac{1}{\pi}\int_0^{\theta_U}\int_0^{\infty} x^{\alpha}\frac{\sin^2\theta_c}{1+\cos\theta_c\cos\theta}e^{-\frac{\sin^2\theta_c}{1+\cos\theta_c\cos\theta}x}dxd\theta \\ &= \frac{1}{\pi}\int_0^{\theta_U}\int_0^{\infty}\left(\frac{\sin^2\theta_c}{1+\cos\theta_c\cos\theta}\right)^{-\alpha}u^{\alpha}e^{-u}dud\theta \\ &= \frac{1}{\pi}\frac{\Gamma(1+\alpha)}{\sin^{2\alpha}\theta_c}\underbrace{\int_0^{\theta_U}(1+\cos\theta_c\cos\theta)^{\alpha}d\theta}_{I_V(\alpha,\theta_U,\theta_c)} \\ &= \frac{1}{\pi}\frac{\Gamma(1+\alpha)}{\sin^{2\alpha}\theta_c}\underbrace{\int_0^{\theta_U/2}(1+\cos\theta_c\cos 2\varphi)^{\alpha}2d\varphi}_{I_V(\alpha,\theta_U,\theta_c)}. \end{aligned} \tag{C.7}$$

Using trigonometric identity $\cos 2\varphi = 2\cos^2\varphi - 1$ in $I_V(\alpha,\theta_U,\theta_c)$, we can rewrite $I_V(\alpha,\theta_U,\theta_c)$ as

$$I_V(\alpha,\theta_U,\theta_c) = \int_0^{\theta_U/2}[(1-\cos\theta_c) + 2\cos\theta_c\cos^2\varphi]^{\alpha}2d\varphi, \tag{C.8}$$

and applying binomial theorem, we can get

$$I_V(\alpha,\theta_U,\theta_c)=\sum_{k=0}^{\alpha}\binom{\alpha}{k}2^{k+1}\cos^k\theta_c[1-\cos\theta_c]^{\alpha-k}\underbrace{\int_0^{\theta_U/2}\cos^{2k}\varphi d\varphi}_{I_c(k,\theta_U/2)}. \tag{C.9}$$

Using [42, Eq. (2.513.3)] for $I_c(k,\theta_U/2)$, we can obtain

$$I_c(k,\theta_U/2)=\frac{1}{2^{2k+1}}\binom{2k}{k}\theta_U+\frac{1}{2^{2k-1}}\sum_{l=0}^{k-1}\binom{2k}{l}\frac{\sin\left(\frac{(2k-2l)\theta_U}{2}\right)}{2k-2l}. \tag{C.10}$$

Therefore, $I_V(\alpha,\theta_U,\theta_c)$ can be expressed as

$$I_V(\alpha,\theta_U,\theta_c)=\sum_{k=0}^{\alpha}\binom{\alpha}{k}2^{k+1}\cos^k\theta_c[1-\cos\theta_c]^{\alpha-k}I_c(k,\theta_U/2) \tag{C.11}$$

In (C.7), if we use trigonometric identity $\cos 2\varphi = 1-2\sin^2\varphi$ in $I_V(\alpha,\theta_U,\theta_c)$ and apply binomial theorem subsequently, we can express $I_V(\alpha,\theta_U,\theta_c)$ differently from (C.11) as

$$I_V(\alpha,\theta_U,\theta_c)=\sum_{k=0}^{\alpha}\binom{\alpha}{k}(-1)^k2^{k+1}\cos^k\theta_c[1+\cos\theta]^{\alpha-k}\int_0^{\theta_U/2}\sin^{2k}\varphi d\varphi. \tag{C.12}$$

Hence,

$$I_V(\alpha,\theta_U,\theta_c)=\sum_{k=0}^{\alpha}\binom{\alpha}{k}(-1)^k2^{k+1}\cos^k\theta_c[1+\cos\theta_c]^{\alpha-k}I_s(k,\theta_U/2). \tag{C.13}$$

If $0\leq\theta_U/2\leq\pi/2$, then using variable substitution $\sin^2\varphi=y$, we can get

$$\begin{aligned}\int_0^{\theta_U/2}\sin^{2k}\varphi d\varphi &= \int_0^{\sin^2(\theta_U/2)}y^k\frac{dy}{2\sqrt{y}\sqrt{1-y}}\\ &= \frac{1}{2}\int_0^{\sin^2\theta_U/2}y^{k-\frac{1}{2}}(1-y)^{-\frac{1}{2}}dy\\ &= \frac{1}{2}B_{\sin^2(\theta_U/2)}\left(k+\frac{1}{2},\frac{1}{2}\right),\end{aligned} \tag{C.14}$$

where $B_{\sin^2(\theta_U/2)}\left(k+1\frac{1}{2},\frac{1}{2}\right)$ is the incomplete Beta function defined as

$$B_b(t_1,t_2)=\int_0^b y^{t_1-1}(1-y)^{t_2-1}dy. \tag{C.15}$$

Therefore,

$$I_V(\alpha,\theta_U,\theta_c)=\begin{cases}\sum_{k=0}^{\alpha}\binom{\alpha}{k}2^{k+1}\cos^k\theta_c[1-\cos\theta_c]^{\alpha-k}I_c(k,\theta_U/2), & \text{any } \theta_U \text{ values}\\ \sum_{k=0}^{\alpha}\binom{\alpha}{k}(-1)^k2^{k+1}\cos^k\theta_c(1+\cos\theta_c)^{\alpha-k}I_s(k,\theta_U/2), & \text{any } \theta_U \text{ values}\\ \sum_{k=0}^{\alpha}\binom{\alpha}{k}(-1)^k2^k\cos^k\theta_c(1+\cos\theta_c)^{\alpha-k}B_{\sin^2(\theta_U/2)}\left(k+\frac{1}{2},\frac{1}{2}\right), & \text{if } 0\leq\theta_U/2\leq\pi/2\end{cases} \tag{C.16}$$

Using (C.16) in (C.7), we have a closed-form solution for (C.1) when $h(\theta)=\frac{\sin^2\theta_c}{1+\cos\theta_c\cos\theta}$ as

$$\frac{1}{\pi}\int_0^{\theta_U}\int_0^{\infty}x^{\alpha}\frac{\sin^2\theta_c}{1+\cos\theta_c\cos\theta}e^{-\frac{\sin^2\theta_c}{1+\cos\theta_c\cos\theta}x}dxd\theta=\frac{1}{\pi}\frac{\Gamma(1+\alpha)}{\sin^{2\alpha}\theta_c}I_V(\alpha,\theta_U,\theta_c). \tag{C.17}$$

Thirdly, in a similar way for deriving closed-form solutions for (C.1), closed-form solutions for (C.2) can be derived. When $h(\theta)=\frac{\sin^2\theta_c}{\sin^2\theta}$, applying (B.6) to (C.2) and subsequently using (C.5) gives

$$\begin{aligned}\frac{2}{\pi}\int_0^{\theta_U}\int_0^{\infty}x^{2\alpha+1}\frac{\sin^2\theta_c}{\sin^2\theta}e^{-\frac{\sin^2\theta_c}{\sin^2\theta}x^2}dxd\theta &= \frac{2^{-(2\alpha+1)}}{\sqrt{\pi}}\frac{\Gamma(2\alpha+2)}{\Gamma\left(\frac{2\alpha+3}{2}\right)}\int_0^{\theta_U}\left(\frac{\sin^2\theta_c}{\sin^2\theta}\right)^{-\alpha}d\theta\\ &= \frac{2^{-(2\alpha+1)}}{\sqrt{\pi}}\frac{\Gamma(2\alpha+2)}{\Gamma\left(\frac{2\alpha+3}{2}\right)}\frac{I_s(\alpha,\theta_U)}{\sin^{2\alpha}\theta_c}.\end{aligned} \tag{C.18}$$

Finally, when $h(\theta)=\frac{\sin^2\theta_c}{1+\cos\theta_c\cos\theta}$, also applying (B.6) to (C.2) and subsequently using (C.16) gives

$$\begin{aligned}&\frac{2}{\pi}\int_0^{\theta_U}\int_0^{\infty}x^{2\alpha+1}\frac{\sin^2\theta_c}{1+\cos\theta_c\cos\theta}e^{-\frac{\sin^2\theta_c}{1+\cos\theta_c\cos\theta}x^2}dxd\theta\\ &=\frac{2^{-(2\alpha+1)}}{\sqrt{\pi}}\frac{\Gamma(2\alpha+2)}{\Gamma\left(\frac{2\alpha+3}{2}\right)}\int_0^{\theta_U}\left(\frac{\sin^2\theta_c}{1+\cos\theta_c\cos\theta}\right)^{-\alpha}d\theta\\ &=\frac{2^{-(2\alpha+1)}}{\sqrt{\pi}}\frac{\Gamma(2\alpha+2)}{\Gamma\left(\frac{2\alpha+3}{2}\right)}\frac{I_V(\alpha,\theta_U,\theta_c)}{\sin^{2\alpha}\theta_c}.\end{aligned} \tag{C.19}$$

Bibliography

[1] S. M. Alamouti, "Simple transmit diversity technique for wireless communications," *IEEE Journal on Selected Areas in Communications*, vol. 16, pp. 1451-1458, October 1998.

[2] L. C. Godara, "Application of antenna arrays to mobile communiations-Part I: Performance improvement, easilbility, and system considerations," *Proc. IEEE,* vol. 85, pp. 1029-1060, July 1997.

[3] L. C. Godara, "Application of antenna arrays to mobile communications-Part II: Beamforming and diretion-of-arrival considerations," *Proc. IEEE,* vol. 85, pp. 1193-1245, Aug. 1997.

[4] M.-S. Alouini, A. Bastami, and E. Ebbini, "Outage probability of cellular mobile radio systems with successive interference cancellation," in *Proc. Asilomar Conf. Signals, Systems, Computers,* 1999, pp. 192-196.

[5] M. O. Hasna and M.-S. Alouini, "Performance evaluation of cellular mobile radio systems with successive cochannel interference cancellation," in *Proc. IEEE Vehicular Technology Conf.,* Fall 2000, pp. 1506-1513.

[6] A. Annamalai and V. Srivastava, "Outage probability of cellular mobile radio systems employing a selective cochannel interference cancellation scheme," in *IEEE VTS 54th Vehicular Technology Conf.,* vol. 1, Fall 2001, pp. 492-496.

[7] A. Annamalai and V. Srivastava, "Outage probability of cellular mobile radio systems employing a selective cochannel interference cancellation scheme," in *J. Wireless Commun.,* vol. 2, pp. 421-438, 2002.

[8] R. Mostafa, A. Annamalai, and J. H. Reed, "Performance evaluation of cellular mobile radio systems with interference nulling of dominant interferers," *IEEE Trans. Commun.,* vol. 52, No.2, Feb. 2004, pp.326-335.

[9] G. Safraz and A. Annamalai, "Performance evaluation of cellular mobile radio systems with successive cancellation of non-identically distributed cochannel interferers in a Rayleigh fading environment," *IEEE WCNC,* 2003, vol. 1, pp.579-584.

[10] R. Vaughan and W. Venables, "Permanant expressions for order statistic densities," *Royal Statistical Society Journal*, vol. 34, No. 2, pp. 308-310, 1972.

[11] A. Annamalai, C. Tellambura, and V. K. Bhargava, "Simple and accurate methods for outage analysis in cellular mobile radio systems-a unified approach," *IEEE Trans. Commun.,* vol. 49, pp. 303-316, Feb. 2001.

[12] M. Abramovitz and I. A. Stegun, *Handbook of Mathematical Functions*, New York: Dover, 1972.

[13] J. Gil-Pelaez, "Note on the inversion theorem," *Biometrika*, vol. 38, pp. 481-482, 1951.

[14] R. Prasad, *Universal Wireless Personal Communications,* Boston, MA: Artech House, 1998.

[15] D. G. Brennan, "Linear diversity combining techniques," *Proc. IRE*, Vol. 47, pp. 1075-1102, June 1959.

[16] N. C. Beaulieu, "Introduction to 'Linear diversity combining techniques'," *Proc. IEEE*, Vol. 91, No. 2, pp. 328-330, Feb. 2003.

[17] Annamalai, C. Tellambura and V. K. Bhargava, "Equal gain diversity receiver performance in wireless channels," *IEEE Trans Commun.*, Vol. 48, No. 10, pp. 1732-1745, Oct. 2000.

[18] B. Dietrich, K. Dietze, J. R. Nealy, and W. L. Stutzman, "Spatial, polarization, and pattern diversity for wireless handheld terminals," *IEEE Trans. On Antennas and Propagations*, Vol. 49, No. 9, pp. 1271-1281, Sep. 2001.

[19] Annamalai, V. Ramanathan and C. Tellambura, "Analysis of equal-gain diversity receiver in correlated fading channels," *Proc. IEEE VTC, Fall 2002*, Vol. 4, pp. 2038-2041.

[20] R. Mallik, M. Win, and J. Winters, "Performance of dual diversity predetection EGC in correlated Rayleigh fading with unequal SNRs," *IEEE Trans. Commun.*, Vol. 50, pp. 1041-1044, Jul 2002.

[21] C. Iskander and P. Mathiopoulos, "Performance of M-QAM with coherent equal-gain combining in correlated Nakagami-m fading," *Electronics Letters*, Vol. 39, No. 1, pp. 141-142, Jan. 2003.

[22] C. Iskander and P. Mathiopoulos, "Performance of dual-branch coherent equal-gain combining in correlated Nakagami-m fading," *Electronics Letters*, Vol. 39, No. 15, pp. 1152-1154, Jul. 2003.

[23] G. Karagiannidis, D. A. Zogas, S. A. Kotsopoulos, "BER performance of dual predetection EGC in correlative Nakagami-m fading," *IEEE Trans. Comm.,* Vol. 52, No.1, pp. 50-53, Jan. 2004.

[24] V. Ramanathan and A. Annamalai, "Analysis of equal gain diversity receivers in correlated Rayleigh fading channels," *IEEE Comm. Letters*, Vol. 8, No.6, pp. 362-364, June 2004.

[25] S. Gaur and A. Annamalai, "Moment generating function based performance evaluation of two branch equal gain combining diversity receivers over correlated Nakagami-m fading channels," *to appear in IEEE. Trans. on Vehicular Technology,* 2005.

[26] S. Gaur and A. Annamalai, "Analysis of dual-diversity coherent equal gain combining in non-indepedent and non-identical Nakagami-m channels," *to appear in the Wiley Journal on Wireless Communications and Mobile Computing,* 2005.

[27] G. Karagiannidis, "Moment-based approach to the performance analysis of equal gain diversity in Nakagami-m fading," *IEEE Trans. Comm.,* Vol. 52, No. 5, pp. 685-690, May 2005.

[28] Y. Chen and C. Tellambura, "Equal gain combiner performance in equally-correlated Rayleigh fading channels," *IEEE PACRIM '03*, Aug. 2003, pp. 98-101.

[29] Y. Chen and C. Tellambura, "Performance of L-branch diversity combiner in equally correlated Rician fading channels," *Proc. IEEE Globecom,* pp. 3379-3383, 2004.

[30] Y. Chen and C. Tellambura, "Distribution functions of selection combiner output in equally correlated Rayleigh, Rician, and Nakagami-m fading channels," *IEEE Trans. Comm.,* Vol. 52 No. 11, pp. 1948-1956, November 2004.

[31] H. Suzuki, "A statistical model for urban multipath propagation," *IEEE Trans. Commun.,* vol. 25, pp. 673-680, July 1977.

[32] H. Aulin, "Characteristics of a digital radio channel," *IEEE Trans. Veh. Technol.,* vol. 30, pp 45-53, May 1981.

[33] W. Braun and U. Dersch, "Physical mobile radio channel model," *IEEE Trans. Veh. Technol.,* vol. 40, pp. 472-482, 1991.

[34] M. Nakagami, "The m-distribution – a general formula of intensity distribution of rapid fading," in *Statistical Methods in Radio Wave Propagation*, W. G. Hoffman, Ed. New York: Pergamon, 1960.

[35] V. A. Aalo, "Performance of maximal-raito diversity systems in a correlated Nakagami-fading environment," *IEEE Trans. Commun.*, Vol. 43, No. 8, pp. 2360-2369, Aug. 1995.

[36] J. Abate and W. Whitt, "Numerical inversion of Laplace transforms of probability distribution," *ORSA J. Computing*, vol. 7, no. 1, pp.36-43, Winter 1995.

[37] Y. Ko, M. Alouini, and M. K. Simon, "Outage probability of diversity systems over generalized fading channels," *IEEE Trans. Comm.,* vol. 48, No. 11, pp.1783-1787, Nov. 2000.

[38] C. W. Helstrom, "Computing the distribution of sums of random sine waves and of Rayleigh-distributed random variables by saddle-point integration," *IEEE Trans. Comm.,* vol. 45, No. 11, pp.1487-1494, Nov. 1997.

[39] C. W. Helstrom, "Analysis of avalanche diode receivers by saddle-point integration," *IEEE Trans. Comm.,* vol. 40, No. 8, pp.1327-1338, Aug. 1992.

[40] P. R. Krishnaiah and M. M. Rao, "Remarks on a multivariate Gamma distribution," *American Mathematical Monthly,* Vol. 68, pp. 342-346, Apr. 1961.

[41] R. K. Mallik and M. Z. Win, "Analysis of hybrid selection/maximal-ratio combining in correlated Nakagami fading," *IEEE Trans. Comm.,* Vol. 50, No. 8, pp. 1372-1383, Aug. 2002.

[42] Gradshteyn and I. Ryzhik, *Table of Integrals, Series and Products*, Academic Press, 1995.

[43] Q. T. Zhang, "A decomposition technique for efficient generation of correlated Nakagami fading channels," *IEEE JSAC,* Vol. 18, No. 11, pp. 2385-2392, Nov. 2000.

[44] N. Kong, T. Eng, and L. B. Milstein, "A selection combining scheme for RAKE receivers," *Proc. IEEE ICUPU 1995,* pp. 426-430, Nov. 1995.

[45] M. K. Simon and M. Alouini, "An MGF-based performance analysis of generalized selection combining over Rayleigh fading channels," *IEEE Trans. Comm.,* Vol. 48, No. 3, pp. 401-415, Mar. 2000.

[46] A. Annamalai, G. Deora, and C. Tellambura, "Unified error probability analysis for generalized selection diversity in Rician fading channels," *Proc. IEEE VTC 2002,* pp. 2042-2046, May 2002.

[47] Y. Ma and S. Pasupathy, "Efficient performance evaluation for generalized selection combining on generalized fading channels," *IEEE Trans. Wireless Comm.,* Vol. 3, No. 1, pp. 29-34, Jan. 2004.

[48] A. Annamalai, G. Deora, and C. Tellambura, "Theoretical diversity improvement in GSC(N,L) receiver with nonidentical fading statistics," *IEEE Trans. Comm.,* vol. 53, pp. 1027-1035, June 2005.

[49] A. I. Sulyman and M. Kousa, "Bit error rate performance of a generalized diversity selection combining scheme in Nakagami fading channels," *Proc. IEEE WCNC 2000,* Vol. 3, pp. 1080-1085, Sept. 2000.

[50] L. Yue, "Analysis of generalized selection combining techniques," *Proc. IEEE VTC 2000-Spring,* Vol. 2, pp. 1191-1195, May 2000.

[51] M. K. Simon and M. Alouini, "Performance analysis of generalized selection combining with threshold test per branch (T-GSC)," *IEEE Trans. Veh. Technol.,* Vol. 51, No. 5, pp. 1018-1029, Sep. 2002.

[52] A. Annamalai, G. Deora, C. Tellambura, "Unified analysis of generalized selection diversity with normalized threshold test Per branch," *Proc. IEEE WCNC 2003,* Vol. 2, pp. 752-756, March 2003.

[53] X. Zhang and N. C. Beaulieu, "Threshold-based hybrid selection/maximal-ratio combining over generalized fading channels," *Proc. IEEE GLOBECOM 2004,* Vol. 1, pp. 462-468, Dec. 2004.

[54] G. L. Turin, F. D. Clapp, T. L. Johnston, S. B. Fine, and D. Lavry, "A statistical model of urban multipath propagation," *IEEE Trans. Veh. Technol.,* Vol. 21, pp. 1-9, Feb. 1972.

[55] A. S. Bajwa, "UHF wideband statistical model and simulation of mobile radio multipath propagation effects," *Proc. Inst. Elect. Eng.,* Vol. 132, pt. F, pp. 327-333, Aug. 1985.

[56] X. Zhang and N. C. Beaulieu, "SER of threshold-based hybrid selection/maximal-ratio combining in equicorrelated Nakagami fading," *IEEE Comm. Letters,* Vol. 8, No. 9, pp. 552-554, September 2004.

[57] Y. Chen and C. Tellambura, "A new generalized selection combining scheme and its performance over fading channels," *Proc. IEEE WCNC 2004,* pp. 926-931, Mar. 2004.

[58] C. Tellambura, A. Mueller, and V. K. Bhargava, "Analysis of M-ary phase-shift-keying with diversity reception for land mobile satellite channels," *IEEE Trans. Veh. Technol.*, Vol. 46, pp. 910-922, Nov. 1997.

[59] M. K. Simon and M. Alouini, "A unified approach to the performance analysis of digital communication over generalized fading channels," *Proc. IEEE*, Vol. 86, No. 9, pp. 1860-1877, Sep. 1998.

[60] S. Stein "Fading Channel Issues in System Engineering," *IEEE JASC,* pp. 68-69, Feb. 1987.

[61] J. G. Proakis, *Digital Communications,* 3rd ed. New York: McGraw-Hill, 1995.

[62] M. K. Simon and M. Alouini, "A unified approach to the performance analysis of digital communication over generalized fading channels," *Proc. IEEE*, Vol. 86, No. 9, pp. 1860-1877, Sep. 1998.

[63] P. R. Krishnaiah and M. M. Rao, "Remarks on a multivariate Gamma distribution," *American Mathematical Monthly,* Vol. 68, pp. 342-346, Apr. 1961.

[64] Z. Wang and G. B. Giannakis, "A simple and general parametrization quantifying performance in fading channels," *IEEE Trans. Communications,*, Vol. 51, pp. 1389-1398, Aug. 2003.

[65] Y. Ma, Z. Wang, and S. Pasupathy, "Asymptotic gains of generalized selection combining," *Proc. IEEE VTC 2003-Fall,* pp. 3149-3153, Oct. 2003.

[66] K. S. Gilhousen, I. M. Jacobs, R. Padovani, A. J. Viterbi, L. A. Weaver, Jr., and C. E. Wheatley III, "On the capacity of a cellular CDMA system," *IEEE Trans. Vehicular Technology*, vol. 40, pp. 303-312, May 1991.

[67] A. J. Viterbi, A. M. Viterbi, K. S. Gilhousen, and E. Zehavi, "Soft handoff extends CDMA cell coverage and increases reverse link capacity," *IEEE JSAC*, vol. 12, pp. 1281-1288, Oct. 1994.

[68] John Y. Kim and Gordon L. Stüber, "CDMA soft handoff analysis in the presence of power control error and shadowing correlation," *IEEE Trans. Wireless Comm.*, vol. 1, pp. 245-255, April 2002.

[69] Bassam Hashem and Elvino S. Sousa, "Reverse link capacity and interference statistics of a fixed-step power-controlled DS/CDMA system under slow multipath fading," *IEEE Trans. Communications*, vol. 47, pp. 1905-1912, Dec. 1999.

[70] Juan M. Romero-Jerez et al., "Interference statistics of cellular DS/CDMA systems with base station diversity under multipath fading," *IEEE Trans. Wireless Comm.*, vol. 2, pp. 1109-1113, Nov. 2003.

[71] Duk Kyung Kim and Fumiyuki Adachi, "Theoretical analysis of reverse link capacity for an SIR-based power-controlled cellular CDMA system in a multipath fading environment," *IEEE Trans. Vehicular Technology*, vol. 50, pp. 452-464, Mar. 2001.

[72] Bassam Hashem and Elvino S. Sousa, "On the cvapacity of cellular DS/CDMA systems under slow Rician/Rayleigh-Fading channels," *IEEE Trans. Vehicular Technology*, vol. 49, pp. 1752-1759, September 2000.

[73] Y. Li, "Reverse link capacity and coverage improvement using mobile transmit diversity," Magnolia Broadband Technical Report, March 2003.

[74] A. A. Abu-Dayya and N. C. Beaulieu, "Micro- and macrodiversity NCFSK (DPSK) on shadowed Nakagami-fading channels," *IEEE Trans. Communications*, vol. 42, pp. 2693-2702, Sep. 1994.

[75] A. A. Abu-Dayya and N. C. beaulieu, "Microdiversity on Rician fading channels," *IEEE Trans. Communications*, vol. 42, pp. 2258-2267, June 1994.

[76] S. Ariyavisitakul and L. Chang, "Signal and interference statistics of a CDMA system with feedback power control," *IEEE Trans. Communications*, vol. 41, pp. 1626-1634, Nov. 1993.

[77] M. Sandell, "Analytical analysis of transmit diversity in WCDMA on fading multipath channels," *PIMRC' 99*.

[78] Qiang Shen and Witold A. Krzymien, "The effect of fading on the Erlang capacity of the IS-95 CDMA cellular system," *IEEE International Conference on Communications*, vol.3, pp. 1829-1833, June 1996.

[79] M. Alouini, A. Abdi, and M. Kaveh, "Sum of gamma variates and performance of wireless communication systems over Nakagami-fading channels," *IEEE Trans. Veh. Technology*, vol. 50, pp. 1471-1480, November, 2001.

[80] A. J. Viterbi, A. M. Viterbi, and E. Zehavi, "Ohter-cell interference in cellular power-controlled CDMA," *IEEE Trans. Comm.*, vol. 42, pp. 1501-1504, Feb./Mar./Apr., 1994.

Vita

Kyung Kyoon Bae was born and raised in Seoul, Korea. He received his Bachelor of Science degree in electrical engineering from Yonsei university, Seoul, Korea, in 1993, and his Master of Science degree in electrical engineering from Virginia Tech, Blacksburg, VA, in 1998. Currently, Kyung is a Ph.D. candidate at the Mobile and Portable Radio Research Group (MPRG), Virginia Tech, working in the area of the performance analysis of array processing with Prof. William Tranter and Prof. A. Annamalai. His research interests are multiple input multiple output (MIMO) system and the interaction between physical layer and higher layer algorithms on protocol stack.